GLUTATHIONE-RESPONSIVE SUPERPARAMAGNETIC IRON OXIDE (Fe₃O₄) NANOPARTICLES FOR THE MAGNETIC HYPERTHERMIA AND CHEMOTHERAPY

THESIS SUBMITTED TO

D. Y. PATIL EDUCATION SOCIETY (DEEMED TO BE UNIVERSITY), KOLHAPUR



FOR THE DEGREE OF

IN
PHYSICS

BY

Miss. NADIYA NIYAZAHMAD PATEL

M. Sc.

Prof. RAGHUNATH S. PATIL

M. Sc., Ph. D.

PROFESSOR,
CENTRE FOR INTERDISCIPLINARY RESEARCH,
D. Y. PATIL EDUCATION SOCIETY
(DEEMED TO BE UNIVERSITY),
KOLHAPUR- 416 006, MAHARASHTRA, (INDIA)

2025

GLUTATHIONE-RESPONSIVE SUPERPARAMAGNETIC IRON OXIDE (Fe₃O₄) NANOPARTICLES FOR THE MAGNETIC HYPERTHERMIA AND CHEMOTHERAPY

A THESIS SUBMITTED TO

D. Y. PATIL EDUCATION SOCIETY (DEEMED TO BE UNIVERSITY), KOLHAPUR



FOR THE DEGREE OF

DOCTOR OF PHILOSOPHY

IN

PHYSICS

UNDER THE FACULTY OF

INTERDISCIPLINARY STUDIES

BY

MISS. NADIYA NIYAZAHMAD PATEL

M.Sc.

UNDER THE SUPERVISION OF

PROF. RAGHUNATH S. PATIL

M.Sc., Ph.D.

CENTRE FOR INTERDISCIPLINARY RESEARCH,
D. Y. PATIL EDUCATION SOCIETY (DEEMED TO BE UNIVERSITY),

KOLHAPUR - 416006

2025

DECLARATION

I am Miss. Nadiya Niyazahmad Patel, hereby declare that the thesis "GLUTATHIONE-RESPONSIVE SUPERPARAMAGNETIC IRON OXIDE (Fe₃O₄)NANOPARTICLES FOR THE MAGNETIC HYPERTHERMIA AND CHEMOTHERAPY" submitted for the degree of Doctor of Philosophy (Ph.D.) in Physics, under the faculty of Interdisciplinary studies of the D. Y. Patil Education Society (Deemed to be University), Kolhapur under the guidance of Prof. Raghunath S. Patil, Centre for Interdisciplinary Research (CIR), D. Y. Patil Education Society (Deemed to be University), Kolhapur, is completed and written by me. This thesis has not been made before the basis for the award of any other higher education institute in India or any other country to the best of my knowledge. Further, I declare that I have not violated any of the provisions under the Copyright and Piracy/Cyber/IPR Act amended from time to time.

Research Student

Miss. Nadiya Niyazahmad Patel

Place: Kolhapur

Date: 24/03/2025

CERTIFICATE OF GUIDE

This is to certify that the thesis entitled "GLUTATHIONE-RESPONSIVE **SUPERPARAMAGNETIC IRON** OXIDE (Fe₃O₄) NANOPARTICLES FOR THE MAGNETIC **HYPERTHERMIA** CHEMOTHERAPY" which is being submitted herewith for the degree of Doctor of Philosophy (Ph.D.) in Physics, Faculty of Interdisciplinary Studies, under the guidance of Prof. Raghunath S. Patil, Centre for Interdisciplinary Research (CIR), D. Y. Patil Education Society (Deemed to be University), Kolhapur, is the result of original research work completed by Miss. Nadiya Niyazahmad Patel under my supervision and guidance and to the best of my knowledge and belief, the work embodied in this thesis has not formed earlier for the basis of award of any degree or similar title of this or any other University or examining body.

Place: Kolhapur

Date: 24/03/2025

Forwarded through,

Prof. Dr. C. D. Lokhande
Dean and Research Director,
Centre for Interdisciplinary Research
D.Y. Patil Education Society
(Deemed to be University),
Kolhapur - 416006

Research Guide

Prof. Dr. Raghunath S. Patil

Professor

Centre for Interdisciplinary Research D.Y. Patil Education Society (Deemed to be University), Kolhapur – 416006

ABSTRACT

Nanoparticle-based therapies have garnered significant interest in cancer treatment due to their potential for targeted drug delivery and enhanced therapeutic efficacy. The present study emphasizes the synthesis of Magnetite (Fe₃O₄) nanoparticles by chemical coprecipitation method and their subsequent functionalization with Poly Ethylene Glycol (PEG) and Glutathione (GSH) to improve biocompatibility and facilitate targeted drug delivery and hyperthermia study. To evaluate the structural, morphological, and chemical characteristics of the synthesized particles, characterization techniques such as X-Ray Diffraction (XRD), Dynamic Light Scattering (DLS), zeta potential (ζ-potential), Scanning Electron Microscopy (SEM), Transmission Electron Microscopy (TEM), and Fourier-Transform Infrared Spectroscopy (FTIR) were used. The magnetic properties of synthesized nanoparticles were analyzed using a Vibrating Sample Magnetometer (VSM). The results show that the synthesized nanoparticles are superparamagnetic, with saturation magnetization (Ms) values of approximately 50 to 49 emu g ¹ at room temperature over the field of 15 kOe. The magnetic induction study shows that the synthesized magnetic nanoparticles reach therapeutic temperature (42–45°C) during the first 10 minutes of exposure to an Alternating Current (AC) magnetic field. When Doxorubicin (DOX) was loaded on PEG coated Magnetite- Fe₃O₄ and GSH coated Magnetite- Fe₃O₄ nanoparticles, a maximum drug entrapment capacity was observed after 48 hours of loading. UV-visible spectroscopy was used to assess the in vitro drug releases. The results show that extracellular GSH spiking facilitates higher drug release under acidic conditions (pH-4.5) than PEG. This extensive study highlights the potential of Magnetite- Fe₃O₄, PEG coated Magnetite- Fe₃O₄, and GSH-coated Magnetite- -Fe₃O₄ nanoparticles as promising agents for targeted cancer treatment and offers insightful information for clinical translation. Furthermore, the cytotoxic effects of nanoparticles were studied on fibroblast cell lines (L929) and Breast cancer cell lines (MDA-MB-231) using a 3- (4, 5-dimethythiazol-2-yl) - 2, 5-diphenyl tetrazolium bromide (MTT) cell viability assay. The findings show that the synthesized nanoparticles are minimally harmful to healthy cells (L929) but display dose-dependent cytotoxicity toward cancer cells (MDA-MB-231). Also, the hemolysis assay was used to evaluate the impact of synthesized particles on the red blood cell membrane, preventing lysis under stress conditions.

ACKNOWLEDGEMENT

Completing my PhD work marks my significant achievement, and I am proud of my dedication and perseverance that took me through this academic journey. The work presented in this thesis would not have been possible without my close association with many people who were always there when I needed them the most. I take this opportunity to acknowledge them and extend my sincere gratitude for helping me to make this thesis a possibility.

I embrace the opportunity to express my deep sense of gratitude to my guide *Prof. Raghunath S. Patil* for his constant guidance, valuable suggestions, and kind encouragement during my association with his research group. His encouragement, constant support, intellectual stimulation, perceptive guidance, immensely valuable ideas, and suggestions from the initial to the final level enabled me to develop an understanding of the subject. He has cultivated in me a deep sense of curiosity, critical thinking, planning, execution of the plan, approaching challenges in resilience, and making a meaningful impact in my chosen field. His suggestions will remain with me as an inexhaustible source of scientific learning throughout my life.

I would like to express my gratitude to the President *Dr. Sanjay D. Patil*, Vice -President *Mr. Satej D. Patil*, Hon'ble Vice-chancellor *Dr. R. K. Sharma*, Registrar *Dr. V. V. Bhosale and* the Controller of Examinations *Mr. Abhay Joshi* for their inspiration and constant support. I would like to express sincere gratitude to *Prof. Dr. C. D. Lokhande*, Dean and Research Director, CIR for his time-to-time insightful feedback and valuable suggestions during these years. I am especially thankful to *Dr. Vishwajeet M. Khot*, for encouraging, supporting, and valuable suggestions during my research work. My special thanks to *Dr. M. G. Joshi* (HOD, SCRM & MBT), *Dr. U. M. Patil*, *Dr. J. L. Gunjakar*, *Dr. S. B. Patil*, *Dr. P. P. Pawar*, *Dr. Shivaji Kashate*, *Dr. Walmiki Koli*, *Dr. Ashwini Jadahav*, *Dr. Arpita Pandey-Tewari*, *and Dr. Rajni Bansode* for their guidance, cooperation, and empathy. I am thankful to the wonderful teaching and nonteaching staff of CIR for their cooperation. I am grateful to *Mr. Manohar S. Lad*, *Ms. Najiya R. Mulla*, *Ms. Tamseen M. Nejkar*, *Ms. Pronoti Kamble*, *Ms. Ayesha T. Maner*, *Mr. Matin A. Patel*, and all my colleagues for always being there and bearing with me during all times in my wonderful days of Ph.D.

My heartfelt thanks to my beloved father *Mr. Niyazahmad T. Patel* and my mother *Ms. Mahjabee N. Patel* for their love, affection, and support during every moment of my life. I am thankful to my younger brother *Mr. Umer N. Patel*, my nieces *Ms. Safiya A. Patel*, *Ms. Fatima A. Patel* and *Ayesha* for becoming my all-time stress buster. I am immensely grateful to my sisters and brothers for supporting me both emotionally and financially: my love and gratitude for them can hardly be expressed in words.

I gratefully acknowledge the D. Y. Patil Education Society, Kolhapur for providing me with the necessary funding and fellowship to pursue research work. I am also thankful to Malhotra Weikfield Foundation, Pune for financial support. This list of acknowledgments can only capture a small fraction of the people who supported my work. I send my deep thanks to all.

Place: Kolhapur ~ Nadiya Patel

LIST OF PATENTS, PUBLICATIONS, AND ATTENDED CONFERENCES

Patents granted/published (04):

- 1. A process for making magnetite (Fe₃O₄) nanoparticles for Hyperthermia application. Prof. R. S. Patil, **Ms. N. N. Patel**, Dr. V. M. Khot, Prof. C. D. Lokhande [Filed Date-14-7-23, Application Number-202321047466] [Published-06-10-23].
- 2. A process for making magnetite (Fe₃O₄) nanoparticles for Hyperthermia application. Prof. R. S. Patil, **Ms. N. N. Patel**, Dr. V. M. Khot, Prof. C. D. Lokhande [Filed Date-27-7-23, Application Number-202321050633] [Published-06-10-23].
- 3. A process for making Glutathione (GSH) conjugate magnetite (Fe₃O₄) nanoparticles for Biomedical application. Prof. R. S. Patil, **Ms. N. N. Patel**, Ms. N. R. Mulla, Ms. T. M. Nejkar, Dr. V. M. Khot, Prof. C. D. Lokhande [Filed Date-04-07-24, Application Number-202421051342] [Published 06-09-2024].
- 4. Chemical synthesis of Iron-doped Manganese oxide thin film electrode for energy storage application. Prof. R. S. Patil, Ms. N. R. Mulla, **Ms. N. N. Patel**, Ms. T. M. Nejkar, Dr. U. M. Patil, Prof. C. D. Lokhande [Filed Date-1-11-24, Application Number-202421083712] [Published 13-12-2024].

Articles in International journals (04):

- 1. **Nadiya N. Patel**, Najiya R. Mulla, Vishwajeet M Khot, Raghunath S. Patil. Anticancer activity of surface functionalized magnetite (Fe₃O₄) nanoparticles-effect of polymer coating. Emergent Materials. 207 (3) (2024)1071-80. [I.F. 4.8- Published].
- 2. **Nadiya N. Patel**, Vishwajeet M. Khot, Raghunath S. Patil, Efficient elimination of pathogens using iron oxide-based magnetic nanoparticles, Chemical Papers. 78 (6) (2024) 3857-69 [I.F. 2.2- Published].
- 3. **Nadiya N. Patel**, Vishwajeet M Khot, Raghunath S. Patil. Optimization of Magnetite Nanoparticles for Magnetic Hyperthermia: Correlation with Physicochemical Properties and Cation Distribution. ChemistrySelect. 9 (40) (2024) e202403034. [I.F. 1.9-Published].
- 4. Najiya R. Mulla, **Nadiya N. Patel**, Sharddha B. Bhosale, Umakant M. Patil, Raghunath S. Patil. Morphologically tuned MnO₂ thin film electrodes prepared by growth kinetic dependent SILAR approach for high-performance extrinsic pseudocapacitors. Journal of Alloys and Compounds. 1006 (2024) 176261. [I.F. 5.8-Published].

Conference/seminar/workshop participation & presentations (09):

- 1. Participated in the 9-day Research Methodology Workshop organized by Internal Quality Assurance Cell & Research Guidance Cell from 21st February to 5th March 2022 at D. Y. Patil Education Society (Deemed to be University), Kolhapur.
- 2. Presented a poster on 28 th February 2022, in DYANSHODH 2022, organized by the Centre for Interdisciplinary Research (CIR), D. Y. Patil Education Society (Deemed to be university), Kolhapur.
- 3. Participated in the structural & morphological characterization using sophisticated instruments under the scheme of STUTI supported by DST, Ministry of Science and Technology New Delhi from 12th to 18th September 2022 held at SAIF-DST-CFC center, Shivaji University, Kolhapur.
- 4. Presented a poster paper at the International Conference on Advance Materials Synthesis, Characterization, and Application (AMSCA Mavericks-2022) held at the Department of Physics, Savitribai Phule Pune University, Pune from 18th to 20th October 2022.
- 5. Presented a poster at "DNYANSHODH-2023(search for knowledge)" on 9th March 2023 organized by the Centre for Interdisciplinary Research (CIR), D.Y. Patil Education Society (Deemed to be university), Kolhapur.
- 6. Presented a poster at "One day International Conference on "Recent Trends in Fabrication of Nanomaterials and Their Applications (ICRTFNA-2023)", 15th March 2023 organized by Rajarshi Chhatrapati Shahu College Kolhapur. (1st Rank in Poster Presentation).
- 7. Poster Presentation at an international conference on "Advanced Materials Synthesis, Characterization and Applications (AMSCA -2023) Organized by the Department of Physics (SPPU), Pune. 21st to 24th November 2023.
- 8. Oral Presentation at an International Conference on Nanotechnology Addressing the Convergence of Materials Science, Biotechnology, and Medical Science (IC-NACMBM- 2024) Organized by CIR, D. Y. Patil Education Society Kolhapur. 12th to 14th February 2024.
- 9. Participated in PM-USHA sponsored National Workshop on "Density Functional Theory of Material Scientist 2024 (NDSFTMS-2024) organized by the Department of Physics, Shivaji University, Kolhapur.23rd to 24th September 2024.

CONTENT

Title	Page No.
CHAPTER 01: INTRODUCTION	[1-22]
1.1 Introduction	
1.2 Nanoparticles (NPs)	
1.3 Magnetic Nanoparticles (MNPs)	
1.4 Magnetic Oxide Nanoparticles	
1.5 Statement of Problem	
1.6 Objectives of the Study	
References	
CHAPTER 02: MAGNETIC NANOPARTICLES	[23-48]
(MNPS) FOR CANCER THERAPIES:	
THEORETICAL ASPECTS	
2.1 Introduction to Cancer and Related Therapies	
2.2 Cancer Tumor Microenvironment	
2.3 Nanoparticles for Cancer Tumor Treatment	
2.4 Magnetic Hyper Thermia (MHT) Therapy	
2.5 Literature Review on MNPs used for MHT and	
Chemotherapy	
References	
CHAPTER 03: EXPERIMENTAL TECHNIQUES	[49-88]
3.1 Introduction	2
3.2 Synthesis of MNPs by Chemical Co-Precipitation	
Method	
3.3 Surface Functionalization	
3.4 Characterization of Magnetic Nanoparticles	
3.5 Biocompatibility Study	
References	
CHAPTER 04: SYNTHESIS, CHARACTERIZATION,	[89-104]
AND MAGNETIC HYPERTHERMIA STUDY OF	
MAGNETITE- Fe ₃ O ₄ NANOPARTICLES	
4.1 Introduction	
4.2 Experimental	
4.3 Results and Discussion	
4.4 Conclusions	
References	
CHAPTER 05: SYNTHESIS, CHARACTERIZATION,	[105-126]
MAGNETIC HYPERTHERMIA, AND	
CHEMOTHERAPY STUDY OF PEG COATED	
MAGNETITE- Fe ₃ O ₄ NANOPARTICLES	
5.1 Introduction	
5.2 Experimental	
5.3 Results and Discussion	
5.4 Conclusions	
References	

CHAPTER 06: SYNTHESIS, CHARACTERIZATION,	[127-146]
MAGNETIC HYPERTHERMIA, AND	
CHEMOTHERAPY STUDY OF GSH COATED	
MAGNETITE- Fe ₃ O ₄ NANOPARTICLES	
6.1 Introduction	
6.2 Experimental	
6.3 Results and Discussion	
6.4 Conclusions	
References	
CHAPTER 07: SUMMARY AND CONCLUSIONS	
7.1 Summary	[147-148]
7.2 Conclusions	
CHAPTER 08: RECOMMENDATIONS	[149]

LIST OF FIGURES

Sr. No	Title		
	Chapter-01		
1.1	Size comparison.	01	
1.2	Types of nanomaterials (0D, 1D, 2D, and 3D).	02	
1.3	Biomedical applications of MNPs.	03	
1.4	Schematic representation of a) diamagnetic, b) paramagnetic, and c) ferromagnetic materials in the presence and absence of magnetic field.	04	
1.5	Hysteresis loops of magnetic materials.	05	
1.6	Domain splitting and reduction in demagnetizing energy of hexagonal and cubic crystals: effects on magnetic field and domain creation.	07	
1.7	Domain wall- The rotation of magnetic moments through a 180°.	08	
1.8	Comparative stability of multi-domain and single-domain magnetic states.	09	
1.9	Size-dependent coercivity for MNPs.	10	
1.10	Field-dependent magnetization in Magnetite- Fe ₃ O ₄ NPs: anisotropy along easy, medium, and hard axes.	11	
	Chapter-02		
2.1	Presentation of Tumor Micro Environment (TME).	24	
2.2	Mechanisms of passive and active targeting in drug delivery: EPR effect and receptor-mediated approaches.	30	
2.3	Schematic of the first prototype of the Magnetic Fluid Hyperthermia (MFH) therapy System.	33	
2.4	Magnetic Hyper Thermia (MHT) using MNPs.	34	
2.5	Hysteresis loop of a multi-domain ferromagnetic materials.	35	
2.6	Magnetic loss mechanisms in single-domain magnetic nanoparticles: (a) Neel relaxation and (b) Brownian relaxation.	37	
	Chapter-03		
3.1	Synthesis of nanoparticles by coprecipitation method.	51	
3.2	Nucleation and growth of MNPs based on the La Mer model.	52	
3.3	Factors affecting the coprecipitation method.	53	
3.4	(1) Elimination of hydrophobic nanoparticles and (2) Coated hydrophilic nanoparticles in blood circulation.	55	
3.5	Need of surface functionalization for biomedical applications.	56	
3.6	Surface functionalization of MNPs.	58	
3.7	Schematic representation of Zeta potential.	59	
3.8	Core-shell configurations of magnetic composite nanomaterials.	62	
3.9	Hysteresis loop for soft and hard magnetic materials.	69	
3.10	(a) schematic of X-ray diffractometer and (b) XRD of Magnetite- Fe ₃ O ₄ nanoparticles.	72	

3.11	(a) Schematic of an FTIR spectrometer and (b) FTIR spectrum of Magnetite- Fe ₃ O ₄ nanoparticles.	73		
3.12	(a) Schematic of scanning electron microscope and (b) SEM images of Magnetite- Fe ₃ O ₄ particles.	75		
3.13	(a) Optical configuration of the Zetasizer and (b) Zeta potential for Magnetite- Fe ₃ O ₄ nanoparticles.			
3.14	(a) Optical configuration of Dynamic Light Scattering (DLS) and (b) DLS of Magnetite- Fe ₃ O ₄ nanoparticles.	77		
3.16	Experimental setup for MHT.	78		
3.17	(a) Principle of VSM and (b) VSM analysis of IONPs.	79		
3.18	Various assays (methods) to assess biocompatibility: (a) Cell Viability, (b) Cytotoxicity, and (c) Hemolysis.	80		
3.19	MTT assay to study cell viability and cell toxicity of nanoparticles.	81		
	Chapter-04			
4.1	XRD patterns of Hematite- α-Fe ₂ O ₃ (sample I ₁) and Magnetite- Fe ₃ O ₄ (samples I ₂ , I ₃ , and I ₄) nanoparticles.	92		
4.2	TE micrographs of Magnetite- Fe ₃ O ₄ (sample I ₂) nanoparticles at different magnifications.	92		
4.3	SE Micrographs of samples I ₂ , I ₃ , and I ₄ at 2000X and 40000X.	93		
4.4	EDX profile of samples I ₂ , I ₃ , and I ₄ .	93		
4.5	1 1			
4.6	Hydrodynamic diameter of IONPs.			
4.7	Zeta potential value of IONPs (Inset: enlarge view of zeta potential scale from -70 to +10 mV).			
4.8	Magnetization versus magnetic field curves of samples I ₂ , I ₃ , and I ₄ .	97		
4.9	Langevin fit for sample I ₂ .	97		
4.10	Temperature Vs Time variation for: (A) I ₂ , (B) I ₃ , and (C) I ₄ .	98		
4.11	(a) Histogram of cell viability percentage and (b) The microscopy pictures of the L929 cell line.	100		
4.12	(a) Histogram of cytotoxicity percentage and (b)The microscopy pictures of the MDA MB 231 cell line.	101		
4.13	(a) Hemolysis percentage of Magnetite- Fe ₃ O ₄ nanoparticles and (b) the photographs of RBC suspensions (1) Positive control (Triton x-100), (2) Negative Control (saline), and (3) Test sample.	102		
	Chapter-05			
5.1	(a) XRD patterns of Magnetite- Fe ₃ O ₄ (P0) nanoparticles and PEG coated Magnetite- Fe ₃ O ₄ (P1, P2, P3, and P4) nanoparticles and (b) enlarged view of (311) peak.			
5.2	TE micrographs of PEG coated Magnetite- Fe ₃ O ₄ (sample P1) nanoparticles at different magnifications.	110		
5.3	SE Micrographs of Magnetite- Fe ₃ O ₄ nanoparticles (sample P0) and PEG-coated Magnetite- Fe ₃ O ₄ nanoparticles (samples P1 and P4) at 2000X and 40000X magnifications.	110		
5.4	FTIR spectra of Magnetite- Fe ₃ O ₄ (sample P0) nanoparticles, PEG, and PEG coated Magnetite- Fe ₃ O ₄ (samples P1 to P4) nanoparticles.	112		

5.5	Hydrodynamic diameter of PEG coated Magnetite- Fe ₃ O ₄ nanoparticles (Sample P1).	113			
5.6	Zeta potential value of PEG coated Magnetite- Fe ₃ O ₄ nanoparticles (sample P1) by DLS technique (Inset: enlarge view of zeta potential scale from -70 to +10 mV).	113			
5.7	Magnetization versus magnetic field curves of Magnetite- Fe ₃ O ₄ (sample P0) and PEG-coated Magnetite- Fe ₃ O ₄ (samples P1 and P4) nanoparticles.	114			
5.8	Temperature Vs Time variation for PEG coated Magnetite- Fe ₃ O ₄ (P1) nanoparticles.	116			
5.9	(a) Ultraviolet absorption spectroscopy of DOX and (b) Calibration curve of DOX.	117			
5.10	Drug release percentage of the DOX loaded Magnetite- Fe ₃ O ₄ nanoparticles and PEG coated Magnetite- Fe ₃ O ₄ nanoparticles at different pH: (a) pH-4.5, (b) pH-6.8, and (c) pH-7.4.	119			
5.11	(a) Histogram of cytotoxicity percentage and (b) The microscopy pictures of the L929 cell line.	120			
5.12	(a) Histogram of cytotoxicity percentage and (b) The microscopy pictures of the MDA MB 231 cell line.	121			
5.13	Hemolysis percentage of Triton X-100 (positive control) and PEG coated Magnetite-Fe ₃ O ₄ nanoparticles.	122			
	Chapter-06				
6.1	Synthesis of (a) Magnetite- Fe ₃ O ₄ nanoparticles and (b) GSH-coated Magnetite-Fe ₃ O ₄ nanoparticles.	129			
6.2	XRD patterns of Magnetite- Fe ₃ O ₄ nanoparticles and GSH coated Magnetite- Fe ₃ O ₄ nanoparticles.	131			
6.3	TE micrographs of GSH coated Magnetite-Fe ₃ O ₄ nanoparticles at different magnifications.	131			
6.4	SE Micrographs of GSH coated Magnetite-Fe ₃ O ₄ nanoparticles at 2000X and 40000X.	132			
6.5	FTIR spectra of Magnetite- Fe ₃ O ₄ nanoparticles, GSH, and GSH coated Magnetite- Fe ₃ O ₄ nanoparticles.	133			
6.6	Hydrodynamic diameter of GSH coated Magnetite- Fe ₃ O ₄ nanoparticles.	134			
6.7	Zeta potential value of GSH coated Magnetite- Fe_3O_4 nanoparticles (Inset: enlarge view of zeta potential scale from -60 to +10 mV).	135			
6.8	Magnetization versus magnetic field curves of Magnetite-Fe ₃ O ₄ nanoparticles and GSH coated Magnetite- Fe ₃ O ₄ nanoparticles.	135			
6.9	Temperature Vs Time variation for Magnetite- Fe ₃ O ₄ and GSH coated Magnetite- Fe ₃ O ₄ nanoparticles.	137			
6.10	Drug release percentage of the DOX loaded Magnetite- Fe ₃ O ₄ nanoparticles and GSH coated Magnetite-Fe ₃ O ₄ nanoparticles at different pH: (a) pH-4.5, (b) pH-6.8, and (c) pH-7.4.	139			
6.11	(a) Histogram of cell viability percentage and (b) The microscopy pictures of the L929 cell line.	140			
6.12	(a) Histogram of cell viability percentage and (b) The microscopy pictures of the MDA MB 231 cell line.				
6.13	Hemolysis percentage of GSH coated Magnetite- Fe ₃ O ₄ nanoparticles.	142			

LIST OF CHART

Sr. No	. No Title	
	Chapter-02	
2.1	Graphical overview of cancer therapies.	23
	Chapter-03	
3.1	Two-step approach for the synthesis of MNPs/ carbon nanomaterials.	67
3.2	Different techniques used for characterization of MNPs.	71
3.3	Different types of cytotoxicity and cell viability assays.	80

LIST OF TABLES

Sr. No	Page No.	
	Chapter-01	
1.1	Physical and magnetic properties of iron oxide nanoparticles.	14
	Chapter-02	
2.1	Literature review of MNPs for MHT and chemotherapy.	44
	Chapter-04	
4.1	Weight percentages of the Fe and O atoms in the samples I_2 , I_3 , and I_4 from EDX profile.	94
4.2	Saturation magnetization (Ms) and Coercivity (Hc) values of samples I ₂ , I ₃ , and I ₄ .	97
4.3	SAR and ILP values for samples I ₂ , I ₃ , and I ₄ for different magnetic field strengths.	99
	Chapter-05	
5.1	Optimized preparative parameters for the synthesis of Magnetite- Fe_3O_4 nanoparticles.	107
5.2	Variation of PEG concentration with Magnetite- Fe ₃ O ₄ nanoparticles.	107
5.3	Saturation magnetization (Ms) and Coercivity (Hc) of Magnetite-Fe ₃ O ₄ (sample P0) nanoparticles and PEG coated Magnetite-Fe ₃ O ₄ (samples P1 and P4) nanoparticles.	115
5.4	SAR and ILP values for PEG coated Magnetite- Fe ₃ O ₄ (sample P1) nanoparticles for different magnetic field strengths.	116
5.5	Drug release percentage of DOX loaded Magnetite- Fe ₃ O ₄ nanoparticles (sample P0) and PEG coated Magnetite- Fe ₃ O ₄ nanoparticles (sample P1) at different pH values.	119
	Chapter-06	
6.1	Literature for the synthesis of surface functionalized Magnetite-Fe ₃ O ₄ nanoparticles and their biomedical applications.	128
6.2	Magnetic properties of Magnetite- Fe ₃ O ₄ and GSH coated Magnetite- Fe ₃ O ₄ nanoparticles from VSM analysis.	136
6.3	SAR and ILP values for GSH coated Magnetite- Fe ₃ O ₄ nanoparticles.	137
6.4	Drug release percentage of DOX loaded Magnetite- Fe ₃ O ₄ nanoparticles and GSH coated Magnetite- Fe ₃ O ₄ nanoparticles at different pH values.	138

LIST OF ABBREVIATIONS

Full form	Abbreviations
1, 1-Diphenyl-2, Picryl-Hydrazyl	DPPH
3-(4, 5-dimethythiazol-2-yl)-2, 5-diphenyl tetrazolium bromide	MTT
3-aminopropyltriethyloxysilane	APTES
Adenosine triphosphate	ATP
Alternating current	AC
Alternating current magnetic field	ACMF
Alternating magnetic field	AMF
Arterial embolization hyperthermia	AEH
Atom transfers radical polymerization	ATRP
Bis[3-(triethoxysilyl) propyl] tetrasulfde	BTES
Cancer-associated fibroblasts	CAFs
Carboxymethyl cellulose	CMC
Cetrimonium bromide	CTAB
Chemo Dynamic Therapy	CDT
Conduction band	CB
Curcumin	CUR
Deoxyribonucleic acid	DNA
Derjaguin, Landau, Verwey, and Overbeek	DLVO
dichlorophenol	DCP
Dimethyl sulfoxide	DMSO
Direct injection hyperthermia	DIH
Double distilled water	DDW
Doxorubicin	DOX
Drug delivery system	DDS
Dynamic light scattering	DLS
Eddy current	ED
Endothelial cells	ECs
Energy-dispersive X-ray spectrometer	EDX
Enhanced Permeability and Retention	EPR
European medicines agency	EMA
Fluorouracil	FU
Fluorouracil	FU
Folic acid	FA
Food and drug administration	FDA
Fourier transform infrared spectroscopy	FTIR
Full width at half maxima	FWHM
Glutathione	GSH
Graphene oxide	GO
GSH peroxidase	GPXs
GSH-S-transferases	GSTs
Gum arabic	GA
Human red blood cell	HRBC
Human umbilical vein endothelial cells	HUVEC
Hyaluronidase	HAase
Intracellular hyperthermia	IH
Intravenous	IV
Intrinsic loss power	ILP
Iron oxide nanocubes	IONCs
Iron oxide nanoparticles	IONPs
Joint Committee on Powder Diffraction Standards	JCPDS

Layer by Layer	LBL
layered transition metal dichalcogenides	LTMDs
lithium manganese iron phosphate	LFMP
Localised surface plasmon resonance	LSPR
Lonidamine	LND
Magnetic field	MF
Magnetic fluid hyperthermia	MFH
Magnetic hyperthermia	MHT
Magnetic iron oxide nanoparticles	MIONPs
Magnetic nanoparticles	MNPs
Magnetic resonance imaging	MRI
Matrix metalloproteinases	MMPs
-	MOF
Metal-organic frameworks Monophysical phagocyte system	MPS
Mononuclear phagocyte system	
Nanoparticles	NPs
Oleylamine	OA
One-dimensional	1D
Permeability and retention	EPR
Phosphate-buffered saline	PBS
Poly (acrylic acid)	PAA
Poly (ethylene imine)	PEI
Poly (lactic acid)	PLA
Poly (methacryloyloxyethyl phosphorylcholine)	MPC
Poly (vinyl alcohol)	PVA
Poly(N-isopropylacrylamide)	PNIPAAm
Polycaprolactone	PCL
Polydispersity index	PDI
Polyethylene glycol	PEG
Positron emission tomography	PET
Reactive oxygen species	ROS
Reduced graphene oxide	RGO
Reticuloendothelial system	RES
Reverse addition-fragmentation chain transfer polymerization	RAFTP
Saturation magnetization	Ms
Scanning electron microscopy	SEM
Specific absorption rate	SAR
Specific loss power	SLP
Superparamagnetic iron oxide nanoparticles	SPIONs
Surface-enhanced Raman scatting	SERS
Tetraoxylsilane	TEOS
Three-dimensional	3D
Transmission electron microscopy	TEM
Triethyloxysilane, trimethoxysilane meracaprtrophyl	MPTES
triethyloxysilane	
Tumor microenvironment	TME
Two-dimensional	2D
Upconversion	UC
Valence band	VB
Vibrating sample magnetometer	VSM
Vinylethoxysaline	VTEOS
World health organization	WHO
X-ray diffraction	XRD
Zero-dimensional	0D
Zeta potential	ζ-potential
Zem potentiai	5-potentiai

CHAPTER-01 INTRODUCTION

INDEX

Sr.No		Title		
1.1	Introd	ntroduction		
1.2	Nanop	oarticles (NPs)	01
1.3	Magn	etic Nano	particles (MNPs)	02
	1.3.1	Types o	f Magnetism / Magnetic Properties	04
		1.3.1.1	Diamagnetism	04
		1.3.1.21	Paramagnetism	04
		1.3.1.3 1	Ferromagnetism	05
	1.3.2	Exception	onal Features of MNPs	06
		1.3.2.1	Finite Size Effect	06
			1.3.2.1.1 Single Domain State	06
			1.3.2.1.2 Superparamagnetism	08
			1.3.2.1.3 Coercivity	10
		1.3.2.2	Anisotropy	11
			1.3.2.2.1 Shape-Dependent Magnetic Properties	11
			1.3.2.2.2 Surface Effects	11
1.4	Magn	etic Oxid	e Nanoparticles	12
	1.4.1	Hematit	$e(\alpha-Fe_2O_3)$	12
	1.4.2	Maghen	nite $(\gamma - Fe_2O_3)$	13
	1.4.3	Magneti	ite (Fe ₃ O ₄)	13
1.5	Staten	nent of Pr	oblem	15
1.6	Objec	bjectives of the Study		16
	Refere	ences		18

1.1 Introduction:

The term nanotechnology was first presented in 1959 by American scientist and Nobel Prize winner Richard Feynman. Feynman delivered a talk titled "There's Plenty of Room at the Bottom" at the California Institute of Technology (Caltech) at the American Physical Society's annual conference [1]. In 1974, a scientist from Japan named Norio Taniguchi used the term "nanotechnology" first time, defining as "the processing of separation, consolidation, and deformation of materials by one atom or one molecule"[2]. The Greek word "nano," means "dwarf" or "very small," is used to refer anything that is one thousand millionth of a meter (10-9 m). The terms "nanoscience" and "nanotechnology" refer to the study of structures and molecules on nanoscales, or between 1 and 100 nm. The "nanotechnology" is the technology that uses this knowledge to create machines and other real-world items [3]. Here, special techniques allow for developing novel applications in nanoscale science, engineering, and technology, including as imaging, modeling, measuring, and matter formation. Materials that have been structured at the nanoscale to provide new or unusual characteristics are called nanomaterials. They are separated into four categories: nanotubes, nanopowder, nanoparticles (NPs), and nanocrystals [4]. A comparison of size is shown in Fig.1.1.

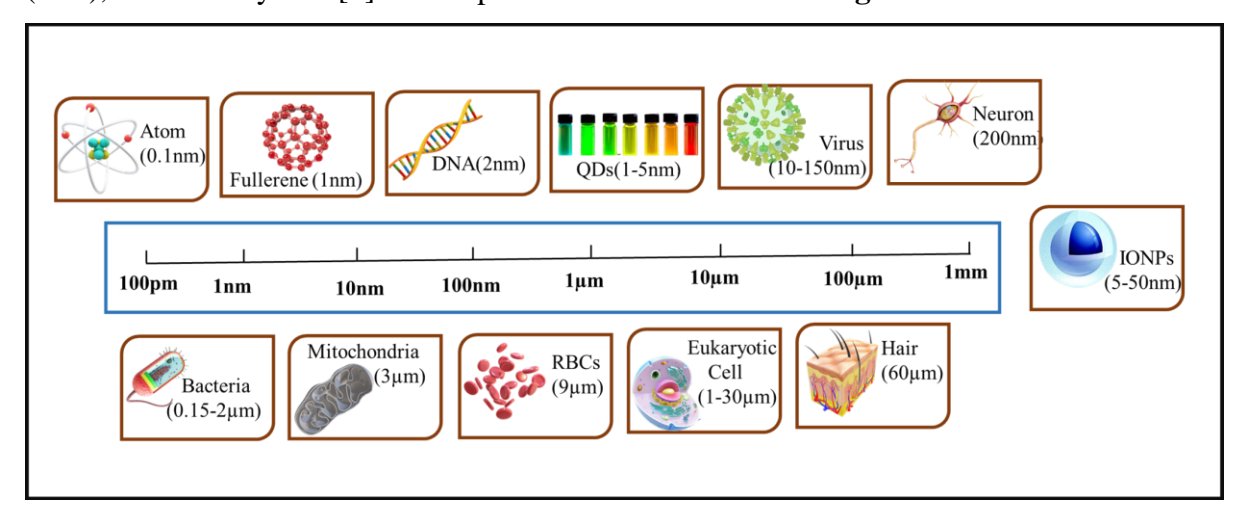


Fig.1.1: Size comparison.

The size of nanomaterials has considerable impact on its electrical properties, magnetic behavior, catalytic activities, medicinal efficacy, etc. This is due to their large specific surface area. Nanomaterials have several uses in the fields of electronics, agriculture, and the environment.

1.2 Nanoparticles (NPs):

Various types of nanomaterials can be synthesized using plethora of techniques (methods). NPs exhibit size and shape-dependent properties. These materials can be classified as zero-dimensional (0D), one-dimensional (1D), two-dimensional (2D), or three-dimensional

(3D) based on their general form as shown in **Fig.1.2**. Nanomaterials are either compact (interacting nanoscale-sized units that repeat as structural components) materials or nano dispersions (homogeneous media like vacuum, gas, liquid, or solid with separated nanosized inclusions). Nanomaterials have distinct physicochemical properties in contrast to bulk materials due to their nanoscale size which opens up a wide range of new uses [5].

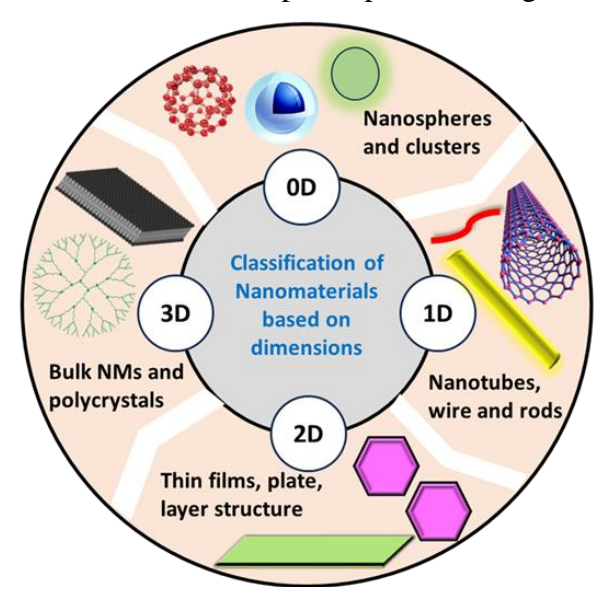


Fig.1.2: Types of nanomaterials (0D, 1D, 2D, and 3D).

Core-shell NPs are generally composed of three layers: (a) the surface layer, which can be modified with small molecules, metal ions, surfactants, and other polymers; (b) The shell layer, which differs chemically from the core; and (c) the core, which is the main component of the NP. Because of these remarkable qualities of surface functionalization or coating, researchers in a variety of disciplines have shown a great deal of interest in these materials [4]. Properties of NPs like biocompatibility, antibacterial and anti-inflammatory activities, tumor targeting, efficient drug administration, bioavailability, bioactivity, and bio-absorption have stimulated their use in biotechnology and applied microbiology [5,6].

1.3 Magnetic Nanoparticles (MNPs):

Magnetic NPs (MNPs) exhibit magnetic properties useful in number of applications. Magnetic materials are utilized in hard drives, videotapes, sensors, motors, and generators [7,8]. The atomic basis of magnetic properties originates from the spin and orbital motion of electrons in an atom. Spin and angular momentum produce magnetic moment. The resultant magnetic moment is by L-S or J-J coupling.

In 1778, Austrian physician Franz Anton Mesmer developed ideas on magnetic fluids and suggested the first medical use of MNPs to humans [9]. He maintained the impact of imperceptible "universal fluids" on the human body (following Newtonian notions of "aether"

connected to tides and gravitational forces) and put out his theory of "animal magnetism," which became well-known across Europe. Mesmerism, a therapy mostly based on hypnotism, has led to an ongoing stream of scientific studies as well as "supernatural" quack medicine. With the development of reliable methods for synthesizing biocompatible MNPs, the idea of aiming magnetic nanospheres inside microscopic living things gathered strength and eventually materialized. MNPs are similar in size to subcellular structures or Deoxyribonucleic Acid (DNA), hence this field has opened the possibility of cell separation techniques that use magnets as external driving forces. Similarly, new breakthroughs in the chemistry of attaching biological units to MNP surfaces and particle surface engineering have offered fascinating new pathways for highly selective drug delivery vectors [10].

However, in vivo applications include complex issues about how a living thing reacts to foreign objects injected into the body (such as drug-particle complexes). Practical experiment must address the issue of immunological responses caused by the invading nanoparticles within the host, particularly from the Reticuloendothelial System (RES). for example, the design of Drug Delivery System (DDS) (by using particles loaded with a monoclonal antibody) need the complete immunological study before administration [11].

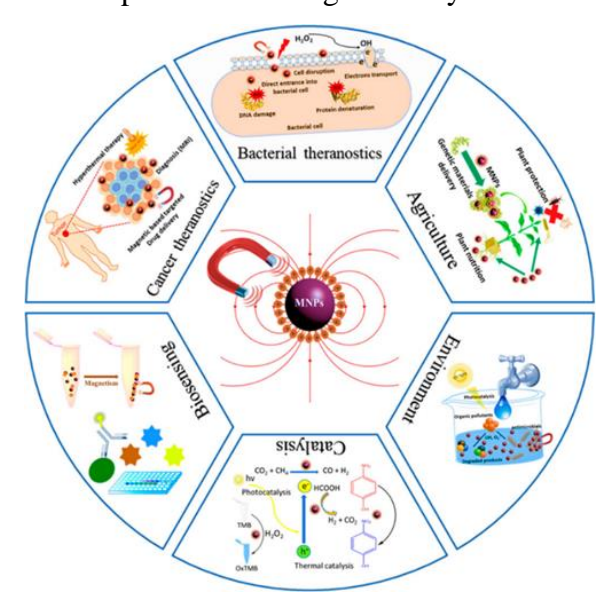


Fig.1.3: Biomedical applications of MNPs [6].

The following physical concepts drive the applications of MNPs in biomedical field:

- **a.** To implant MNPs remotely into organs or tissues, the Magnetic Field (MF) gradients must be controlled, i.e. the application of a magnetic force surrounding the targeted region is used. (Examples: Magnetic separation used for DNA sequencing, magnetic implants, and targeting).
- **b.** The use of magnetic moment of MNPs to disrupt proton nuclear resonance (for example, as a contrast medium in Magnetic Resonance Imaging (MRI)).

c. Generation of heat using magnetic nanometric particles due to magnetic losses (magnetic hyperthermia). **Fig.1.3** displays several uses of MNPs in the biological field.

1.3.1 Types of Magnetism / Magnetic Properties:

Particles with mass and electric charge (protons, electrons, holes, positive and negative ions) move in response to electric and MFs. An electrically charged particle in rotation produces a magnetic dipole, also known as a magneton. The magnitude and direction of any MF produced by an object, such as a magnet, are measured by the magnetic dipole moment. The magnetization (M) of a magnetic material in an external MF is measured in terms of its susceptibility (χ) and permeability (μ) which are related by **Equation 1.1**,

Magnetic materials are classed as diamagnetic, paramagnetic, or ferromagnetic based on how they respond to external MFs [12].

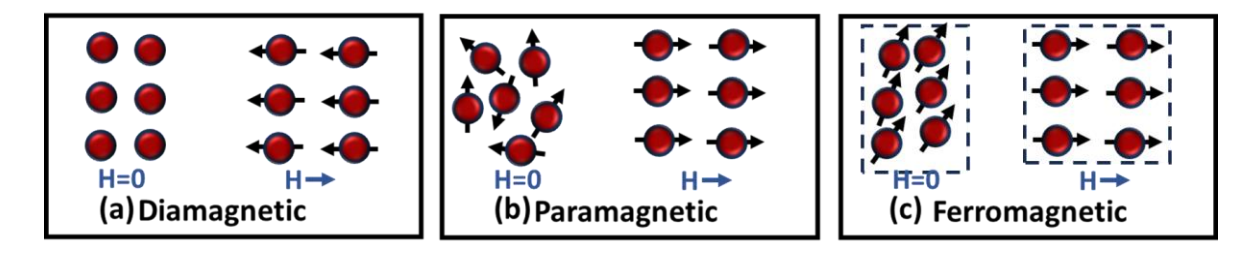


Fig.1.4: Schematic representation of **(a)** Diamagnetic, **(b)** Paramagnetic, and **(c)** Ferromagnetic materials in the presence and absence of magnetic field.

1.3.1.1 Diamagnetism:

In diamagnetic materials, dipoles are either missing or oriented arbitrarily in the absence of an MF (**Fig.1.4** (a)). In the presence of a MF, diamagnetic materials align itself in the opposite direction of the applied field, resulting in low and negative susceptibility values (- 10^{-6} to -10^{-3}) [13]. The spins revert to their initial positions and lose their magnetic characteristics when external field is removed. Quartz (SiO₂), wood, water, copper, silver, and most biological molecules are examples of diamagnetic materials. Diamagnetic materials have filled electronic subshells, i.e. no unpaired electrons [12].

1.3.1.2 Paramagnetism:

Paramagnetic materials exhibit a weak MF parallel to external MF. Magnetic dipoles present in paramagnetic materials in presence and absence of external MF are shown in **Fig.1.4** (**b**) which align only when an external MF is applied and vanish when the MF is removed [13]. The value of susceptibility varies between 10⁻⁵ to 10⁻³ in the presence of extrarenal MF [12].

1.3.1.3 Ferromagnetism:

Ferromagnetic materials are highly magnetic and have a positive susceptibility. In the absence of an external MF, the magnetic moments of an array of atoms align in the same direction to form a domain. Hence, they have net magnetic moment as shown in **Fig.1.4** (c). The value of susceptibility is positive and varies between 1 to 10000 under the influence of MF. Ferromagnetic materials are further divided into ferrimagnetic and antiferromagnetic materials. MNPs have a magnetic moment that is rapidly aligned in the direction of an external field and zero when there is no external field, similar to paramagnetic materials. This phenomenon happens at the blocking temperature, and paramagnetic materials become superparamagnetic [13]. This property allows them to maintain colloidal stability, which makes them useful for biological applications [12].

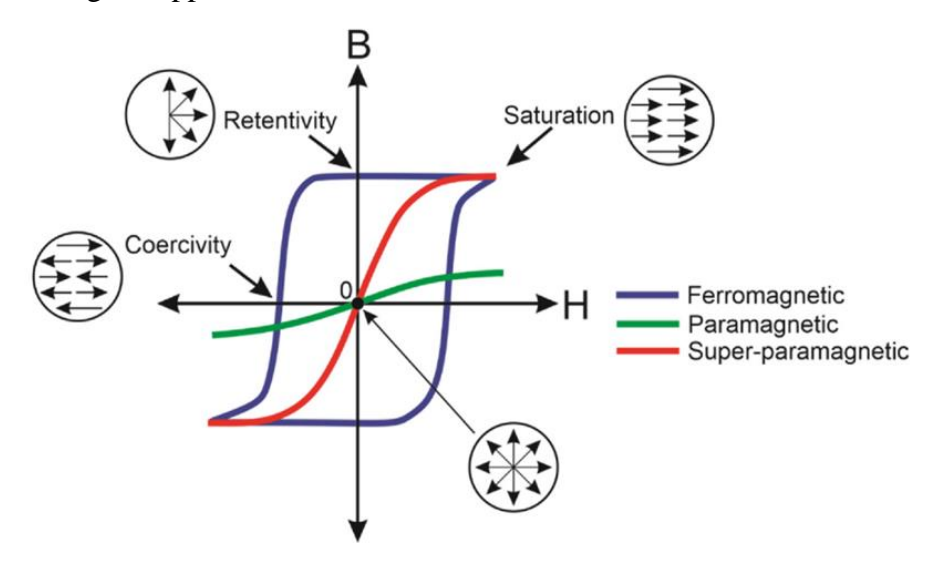


Fig.1.5: Hysteresis loops of magnetic materials [13].

When the external field is removed, superparamagnetic NPs lose their magnetism and become non-attractive to one another, which reduces the amount of nanoparticle aggregation. Furthermore, because of their high sensitivity to applied MFs, superparamagnetic NPs give greater control over how their magnetic characteristics are applied [13]. Magnetization saturation happens in an applied MF when all magnetic dipoles align in the same direction. This characteristic makes them useful in MRI and for the administration of drugs. Fig.1.5 shows the particular magnetization (B-H) curves for magnetic materials showing the saturation magnetization (Ms), remanent magnetization (M_r), and coercivity (H_c). Where the saturation magnetization (Ms) is the highest induced magnetization, remanent magnetization (M_r) is the residual induced magnetization after the removal of an applied field, and coercivity (H_c) is the strength of an external coercive field necessary to bring the magnetization to zero. The responses of superparamagnetic NPs (Violet line (sigmoid curve), paramagnetic NPs (Green

line), and ferromagnetic NPs (Blue line) are also shown in the same image [13].

A particle of a ferromagnetic material, as predicted by Frenkel and Dorfman, consists of a single magnetic domain smaller than a critical particle size. Kittel developed the first preliminary estimations of critical particle sizes. A spherical sample of a typical ferromagnetic material has an estimated radius of 15 nm. These monodomain ferromagnetic particles have magnetic moment of the order of millions of Bohr magnetons [13].

1.3.2 Exceptional Features of MNPs:

When MNPs are smaller than the single domain limit (20 nm for iron oxide), superparamagnetism is observed. Below Curie temperature, ferromagnetic or ferrimagnetic materials break into the single domain from the multi-domain and behave as superparamagnetic. The intriguing features of the MNPs are listed below,

1.3.2.1 Finite Size Effect:

To accurately incorporate the size-dependent magnetic features, the dimensions at the nanoscale must be carefully controlled. Synthesis of MNPs with particle size ranges between 6-15 nm was executed through the controlled growth of synthesized monodispersed MNPs [14]. This was done to synthesize MNPs with the specified size distributions of their constituent particles. The grain size of the MNPs has a direct influence on saturation magnetization (Ms) because of the size effect [15]. The magnetic anisotropy of the tiny nanoparticle has a very high value; but, as the particle size approaches an average of 8 nm, it drops off dramatically and continues to diminish until it approaches the value of bulk Fe₃O₄ [16]. The finite size effect has following outcomes:

- A) Single Domain,
- B) Superparamagnetism, and
- C) Coercivity.

1.3.2.1.1 Single Domain State:

The domain walls in multidomain ferromagnetic particles divide the region of uniform magnetization [17]. The applied field must be greater than the demagnetizing field to maintain a saturated condition. After the field has been removed, the particle breaks into domains as a result of the magnetostatic energy associated with the saturated state, which lowers the saturation magnetization (Ms) value. If the particle size is decreased below the critical volume, more energy is needed to develop a domain wall than is needed to maintain a single domain state [18]. A single-domain particle is always saturated by definition when all of its volumes spontaneously magnetize in one direction parallel to an applied field. The critical diameter of

the particle depends on the nature of material and is up to 20 nm. This critical diameter can be calculated using **Equation 1.2**. The value of critical diameter (d_c) is different for different materials and applicable only to spherical and non-interacting or non-aggregate particles.

 k_{eff} = Anisotropy constant,

A=Exchange constant, and

 μ_o =Vacuum permeability.

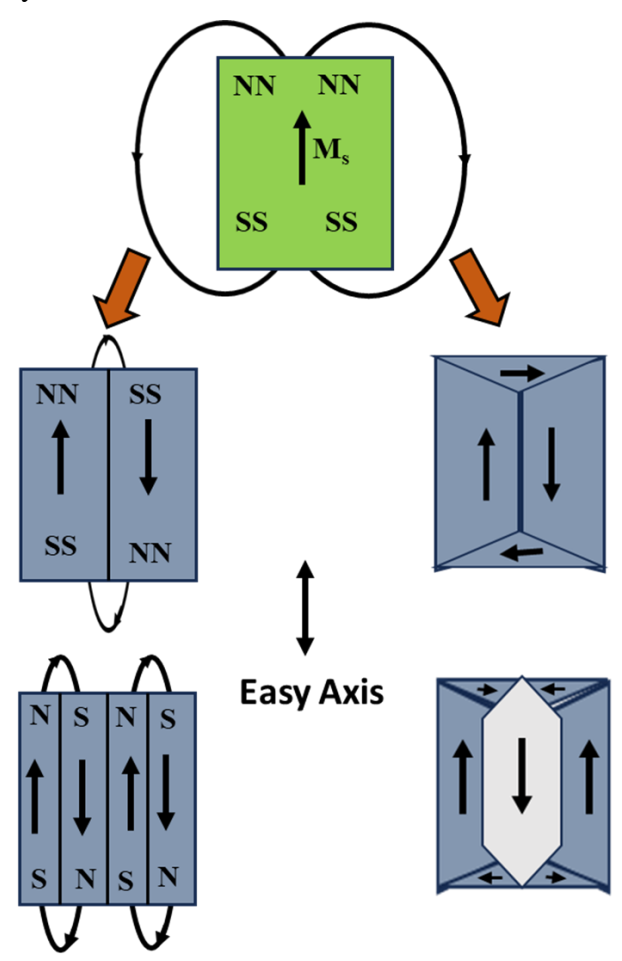


Fig.1.6: Domain splitting and reduction in demagnetizing energy of hexagonal and cubic crystals: effects on magnetic field and domain creation.

A substantial fraction of the magnetic moments pointing in the same direction combine to form a magnetic domain in a ferromagnetic material. Every atomic dipole in a domain is pointing in the same direction. The domains inside a material can be thought of as tiny magnets. To minimize the energy of the system, ferromagnetic materials tend to fragment into domains that relate them in a way that minimizes the overall energy of a material. As illustrated in **Fig.1.6**, a single domain in a hexagonal crystal can split into two smaller, oppositely aligned

domains. This process can be repeated until splitting into additional domains which do not result in a favorable energy decrease because energy must be generated and maintained in the transition region between domains, or domain walls. The splitting of domain can also happen in cubic crystals when the domains follow the directions of easy axes and are perpendicular to one another. This minimizes the energy of the system with the same effect. Based on the crystallographic structure or easy axis, the magnetic moment rotates by 90° or 180° in various directions across domain walls. This occurs due to adverse changes in magnetic moment directions and the ability of a wall to share the 90° or 180° difference in spin alignments between domains.

Fig.1.7 depicts the enlarged representation of domains in various orientations, although the domains flip by discrete angles in a limited region known as the domain walls. Anisotropy and exchange interaction mostly determine the fixed width of domain walls.

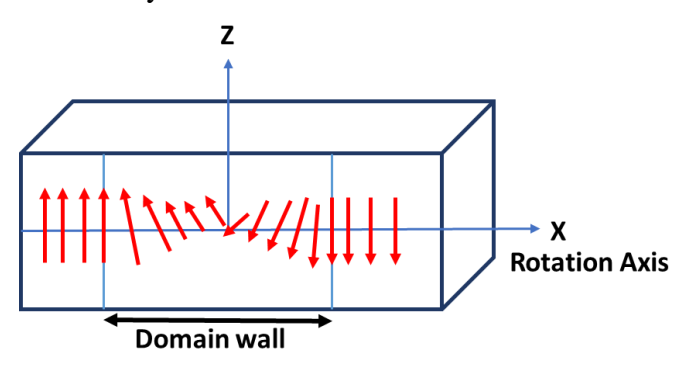


Fig.1.7: Domain wall - The rotation of magnetic moments through 180°.

1.3.2.1.2 Superparamagnetism:

The typical diameter of MNPs is up to 100 nm, if this size is reduced below 20 nm, i.e. critical diameter, then they are superparamagnetic in nature. Superparamagnetism is explained by the behavior of well-isolated single-domain particles as shown in **Fig.1.8**.

The magnetic anisotropy energy, which is responsible for retaining the magnetic moment along a certain axis, may be utilized to determine the dependence of magnetic qualities on different directions and can be expressed as in the form of **Equation 1.3** as follows,

$$E(\theta) = K_{eff}V\sin^2\theta \qquad(1.3)$$
 where,

V = Particle volume,

 K_{eff} =anisotropy constant, and

 θ = Angle between magnetization and easy axis.

Also, Thermal energy (E_T) at temperature (T) is given by **Equation 1.4**

$$E_T = k_B T \qquad \dots \dots \dots (1.4)$$

where,

*K*_B=Boltzmann Constant

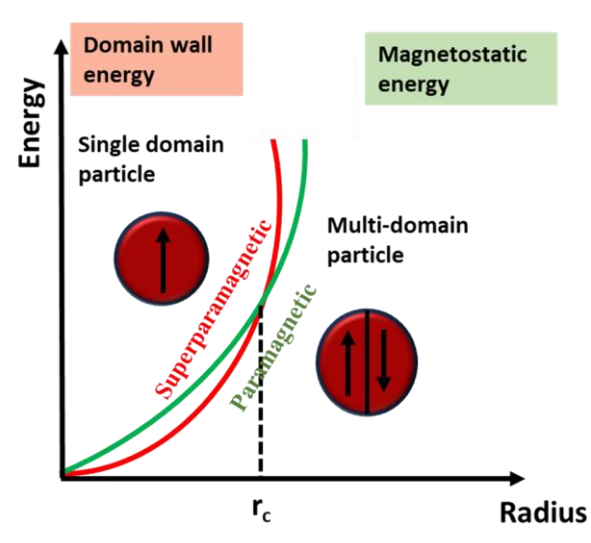


Fig.1.8: Comparative stability of multi-domain and single-domain magnetic states.

As particle size decreases, particles become superparamagnetic at that size, the thermal energy of particles is more than the anisotropy energy [i.e. $E(\Theta) < E_T$ or $KVsin^2(\Theta) < K_BT$] which easily flips the magnetization value revealing no hysteresis. A blocked state is attained when the relaxation time (τ) exceeds the characteristics measurement time (τ_m), that is, when $\tau > \tau_m$. The temperature separating these two zones is known as blocking temperature (TB), and is calculated using **Equation 1.5**. The blocking temperature is affected by the applied MF, effective anisotropy constant, particle size, and experimental measuring time.

$$T_B = \frac{\kappa_{eff}}{30\kappa_B} \tag{1.5}$$

where,

 T_B = Blocking temperature,

 K_{eff} =anisotropy constant, and

*K*_B=Boltzmann Constant.

The large magnetic particle contains multiple domain structures where domain walls separate uniform magnetization. A single-domain particle has homogeneous magnetization and uniform spin orientation. Superparamagnetic materials are either ferrimagnetic or ferromagnetic that align their magnetic moments parallel to the direction of an external MF but as the external MF is removed, they return to their initial direction [19,20].

The B-H loop does not show hysteresis for MNPs with superparamagnetic properties because of reversible forward-backward magnetization curves, zero magnetization at zero applied field, and no residual magnetism seen after the MF was removed, as shown in **Fig.1.5**.

It depends on the particle size, the applied MF, and the effective anisotropy constant [21,22]. Relaxation of magnetization can be determined by the two different mechanisms. 1) Neel Mechanism and 2) Brownian Mechanism.

Neel Relaxation time (τ_N) can be obtained using **Equation 1.6**,

Where $E_a=K_{eff}$. V is the energy barrier that divides two energy levels between magnetization states (up and down), K_{β} is the Boltzmann constant, and t_0 is the pre-exponential factor related to an attempt time, of the order of 10^{-9} - 10^{-12} s.

The Brownian relaxation time (τ_B) is obtained using **Equation 1.7**,

where,

 η = Viscosity of media,

 V_h = Hydrodynamic volume, and

 r_h = Hydrodynamic diameter.

1.3.2.1.3 Coercivity:

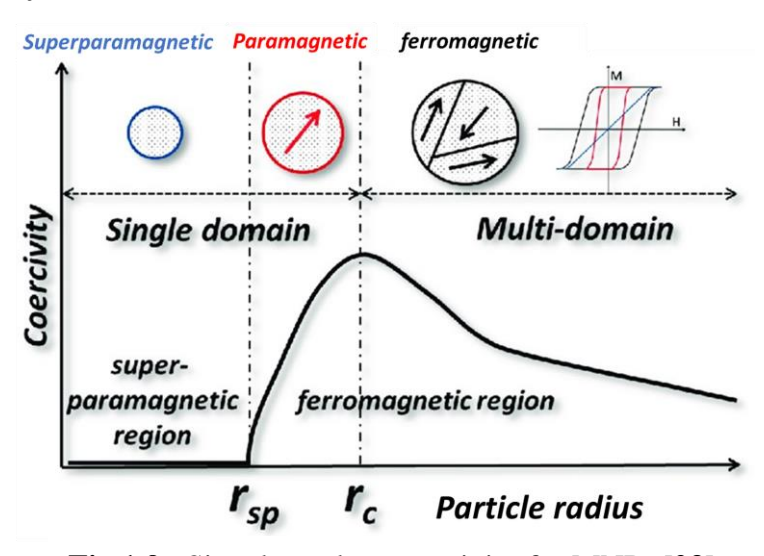


Fig.1.9: Size-dependent coercivity for MNPs [23].

Coercivity varies with particle size, shown in **Fig.1.9**. Coercivity is zero for the particles showing superparamagnetic behavior. Prior to declining with particle size in the ferromagnetic zone, the coercivity rises with particle size and reaches its highest value in the paramagnetic region [23].

1.3.2.2 Anisotropy:

Variation in magnetic properties with the direction within the material is called magnetic anisotropy. **Fig.1.10**. shows field-dependent magnetization in Magnetite-Fe₃O₄ NPs.

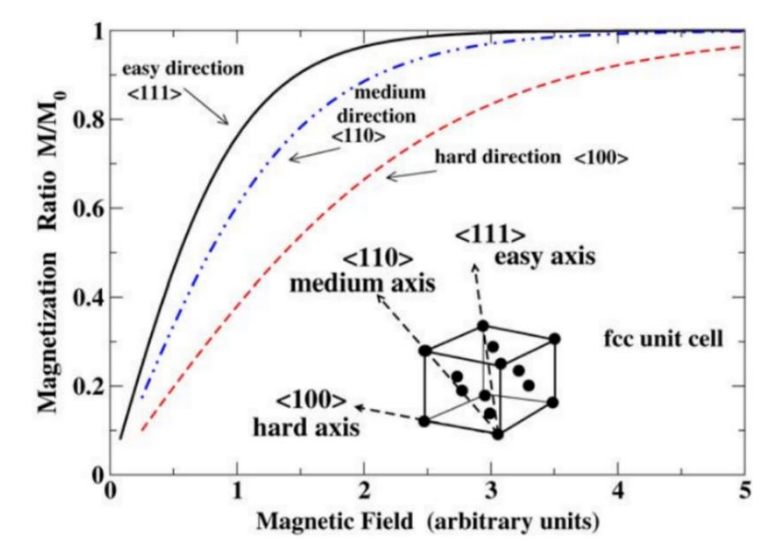


Fig.1.10. Field-dependent magnetization in Magnetite- Fe₃O₄ NPs: anisotropy along easy, medium, and hard axes [24].

Three crystallographic axes are defined in case of Magnetite- Fe₃O₄ MNPs (inverse spinel structure), easy axis along [111], medium axis along [110] and hard axis along [100]. As the external MF strengthens, the magnetization increases until it reaches saturation. Saturation is achieved for the easy axis with a little external MF strength [24].

1.3.2.2.1 Shape-Dependent Magnetic Properties:

The magnetic properties of MNPs depend on their shape. For example, nanoparticles with quasi-cubic shapes have higher saturation magnetization (Ms) values. If the particles are perfectly spherical (isotropic), they are magnetized equally in all directions under the applied MF. In contrast, non-spherical particles are easier to magnetize along their easy axis due to a phenomenon known as shape anisotropy [24].

1.3.2.2.2 Surface Effects:

As the size of the NPs decreases, most of their atoms act like surface atoms, making surface and interface effects more noticeable-

- 1. Surface coating influences the magnetic characteristics of MNPs. However, in some circumstances, a clear correlation between the magnetic core and the surface coating has been observed. There is now no substantial correlation that can be established because of the complex and system-specific magnetic response of the system to an inert coating (organic ligands) [25,26].
- 2. Coating of MNPs significantly alters their magnetic characteristics. This results from new

and novel composites showing biassed nanostructures with varied blocking temperature [27-30].

1.4 Magnetic Oxide Nanoparticles:

Metal oxides particles of nanoscale that show magnetic properties are called magnetic oxide nanoparticles. Among the different MNPs, iron oxide nanoparticles (IONPs) have garnered the most attention due to their, magnetic properties, easy synthesis method [31-37], tunable size and structure [38-41], intrinsic catalytic activity [42-45], good biocompatibility [46-50], availability of surface modification [51-55], physical and chemical stability, environmental safety, and low toxicity [56]. The basic features of magnetic iron oxide nanoparticles (MIONPs) render them appropriate for a diverse array of biological applications. Some of these applications include serving as a contrast agent in MRI [8], separation and identification of cells [57,58], hyperthermia therapy [59], and administration of drugs [60].

Iron oxide is a naturally occurring compound found in a wide variety of forms; in nature, there are roughly 16 different phases, among them Hematite- α -Fe₂O₃, Maghemite- γ -Fe₂O₃, and Magnetite- Fe₃O₄ are relatively abundant and show temperature-induced phase changes. They are utilized in magnetic fluids, catalysis, magnetic data recording and storage media, magnetic paper, and environmental protection in addition to biotechnology and biomedicine. Recently IONPs have been used for MRI, Magnetic Hyper Thermia (MHT), magnetic medication administration, and cell separation [61].

1.4.1 Hematite (α -Fe₂O₃):

Hematite is the most stable n-type semiconductor and iron oxide at room temperature. The band gap 2.2 eV allows the conduction band (CB) to be made up of empty d-orbitals of ferric ions (Fe³⁺), while the valence band (VB) is made up of occupied 3d crystal field orbitals of Fe³⁺ ions mixed with some O 2p nonbonding orbitals [62]. Hematite- α -Fe₂O₃ has a rhombohedral crystal structure with a hexagonal unit cell with lattice parameters of a = 0.5034 nm and c = 1.375 nm. The structure of Hematite- α -Fe₂O₃ is a sixfold ring created by a hcp array of O ions aligned along [001] direction. The Fe³⁺ ion occupies two-thirds of an octahedral site that is constrained by a nearly perfect hexagonal closed-packed oxygen lattice. It exhibits an antiferromagnetic order for temperatures lower than the Neel temperature (955 K). Because of its inexpensive cost and great corrosion resistance, Hematite- α -Fe₂O₃ is widely utilized in pigment, gas sensors, and catalysts. It is also used as a starting material in the production of Magnetite- Fe₃O₄ and Maghemite- γ -Fe₂O₃ [63-65].

1.4.2 Maghemite $(\gamma - \text{Fe}_2\text{O}_3)$:

Maghemite- γ - Fe₂O₃ is an n-type semiconductor with a band gap of 2 eV. It is categorized as ferrimagnetic oxide and has a high Neel temperature of 950 K and a net magnetic moment of 2.5 μ B per formula unit. 32 O²⁻ ions, 21 (1/3) Fe³⁺ ions, and 2 (1/3) vacancies are present in the cubic unit cell of Maghemite- γ - Fe₂O₃ with lattice parameter a=0.834 nm. Tetrahedral sites are occupied by eight cations, while the remaining cations are arranged at random along octahedral sites [66-68]. When Magnetite- Fe₃O₄ is exposed to oxygen, it undergoes a transformation resulting in the formation of Maghemite- γ - Fe₂O₃. Fe³⁺ ions are only consistently dispersed in roughly two-thirds of the sites, leaving the other sites vacant. Crystal centers are also oxidized to Fe³⁺ by the passage of Fe²⁺ ions inside the crystal. Two sites that are filled with Fe³⁺ ions are followed by one empty site [69,70].

1.4.3 Magnetite (Fe₃O₄):

Magnetite- Fe₃O₄ is a densely packed material along the [111] direction with a face-centered cubic inverse spinel structure supported by 32 O²⁻ ions. Magnetite- Fe₃O₄ has both trivalent (Fe³⁺) and divalent (Fe²⁺) iron ions inside of its structure with a lattice parameter of a=0.839 nm [71,72]. Fe³⁺ ions occupy tetrahedral sites and are surrounded by four oxygen atoms, while a mixture of Fe²⁺/Fe³⁺ ions occupy the octahedral site and are surrounded by six oxygen atoms. This structure is expressed as: Fe³⁺ (tetrahedral-A) Fe²⁺ Fe³⁺ (Octahedral-B) O₄ [73-75]. While Fe²⁺ ions in B sites contribute to macroscopic ferromagnetic properties, Fe³⁺ ions in A and B sites are coupled antiferromagnetically [76]. Magnetite- Fe₃O₄ easily goes through a Maghemite- γ- Fe₂O₃ phase transition at room temperature (Equation 1.8).

$$[Fe_8^{3+}]_t \ [Fe_8^{2+} \ Fe_8^{3+}]_o \ O_{32} \xrightarrow{Oxidation} [Fe_8^{3+}]_t \ [Fe_{5.32 \equiv 2.67}^{2+} \ Fe_8^{3+}]_o \ O_{32}$$
(1.8)

Magnetite

where,

t=Tetrahedral,

o=Octahedral, and

■=Vacancy.

Magnetite- Fe₃O₄ may act as both an n- and p-type semiconductor when added with divalent ions such as Co, Mn, Zn, etc. As these divalent ions can replace some or all of its Fe²⁺ ions. When the material is held in an external MF, the spin magnetic moments assigned to the Fe³⁺ ions dispersed in octahedral locations align parallelly, whereas those assigned to the Fe³⁺ ions placed in tetrahedral positions align oppositely, which causes an antiparallel coupling. This is because Fe³⁺ ions are dispersed in tetrahedral locations but in the opposite direction.

and both sets of spin magnetic moments are aligned with them. Because of this, the spin moments of all of the Fe^{3+} ions that are present in Magnetite- Fe_3O_4 cancel each other, and as a consequence, it does not show any magnetic properties as they do not contribute to the total magnetization of material. The overall magnetization of Magnetite- Fe_3O_4 may be due to aligned spin magnetic moments of Fe^{2+} ions in the external field direction.

Table 1.1 describes the physical and magnetic properties of Hematite- α -Fe₂O₃, Maghemite- γ -Fe₂O₃, and Magnetite- Fe₃O₄.

Table 1.1: Physical and magnetic properties of iron oxide nanoparticles.

	Oxide		
Property	Hematite	Maghemite	Magnetite
Molecular Formula	α-Fe ₂ O ₃	γ-Fe ₂ O ₃	Fe ₃ O ₄
Density(g/cm ³)	5.26	4.87	5.18
Melting Point	1350	-	1583-1597
Magnetism	Weakly ferromagnetic/Anti ferromagnetic	Ferrimagnetic	Ferrimagnetic/ paramagnetic
Crystallography	raphy Hexagonal, Rhombohedral		Cubic
Curie Temperature (K)	956	820-986	858
Saturation magnetization (Ms) at 300 K [A·m²/kg].	0.3	60–80	92–100
Lattice parameter (nm)	a = 0.5034; c = 1.375; (hexagonal); a = 0.5427; $\alpha = 55.3^{\circ}$ (rhombohedral)	a = 0.83474 (cubic); b = 0.8347; c = 2.501 (tetragonal)	a = 0.8396
Colour	Red	Reddish-brown	Black

Superparamagnetic iron oxide NPs (SPIONs) are IONPs that are smaller than 20 nm and show superparamagnetic behavior [69]. Among these MNPs, SPIONs have adaptable qualities such as high saturation magnetization (Ms), high magnetic susceptibility, low coercivity (Hc), slow oxidation, low toxicity, and retaining magnetism even in the absence of an external MF as compared to other MNPs [77]. There are several potential biological

applications for SPIONs, including gene therapy, MRI, hyperthermia, stem cell tracking, tissue healing, manipulation of cell organelles, specific targeted drug delivery, and early diagnosis of diabetes and inflammatory cancer [78-82].

Spinel Ferrite Nanoparticles:

Nanocrystalline spinel ferrites have undergone extensive research owing to their potential applications in microwave absorbers, high-density recording systems, chemical sensors, imaging, permanent magnets, high-frequency devices, ferrofluid technology, and biomedical applications [83]. Oxygen atoms are packed closely together in spinel ferrite complexes, exhibiting tetrahedral and octahedral sublattices. In the compound structure, M²⁺ (M = Fe, Co, Mg, Ni, etc.) and Fe³⁺ are organized at two different crystallographic sites (A and B) with tetrahedral and octahedral oxygen coordination respectively. Normal spinel is the structure that results when 16 B sites are filled by Fe³⁺ and 8 A sites are filled by M²⁺ cations. In inverse spinel structure, M²⁺ ions exclusively occupy the B site whereas Fe³⁺ ions randomly occupy both A and B sites. The majority of spinel has a mixed (partially inverse) structure because both M²⁺ and Fe³⁺ cations are present on both A and B sites and the cation distribution is mixed [84].

Magnetic ferrite NPs with inverse spinel structures have garnered a lot of interest due to their possible use as ferrofluids. Hydrophilic ferrofluids are mostly employed in medical applications, such as the treatment and detection of medical problems, while hydrophobic fluids with scattered MNPs are being used in applications like rotating shaft seals and loudspeakers [85]. Ferrite NPs have been seen to exhibit spin canting, metastable cation distribution, core/shell structure, and superparamagnetism at the nanoscale. These phenomena depend upon several variables like anisotropy, surface morphology, composition, grain size, and interparticle interactions. The electrical and magnetic properties of ferrites can be affected by the distribution of cations between tetrahedral and octahedral sites. The distribution can be regulated by the synthesis method and circumstance [86].

1.5 Statement of Problem:

Cancer has been recognized as a major health issue worldwide. Cancer is a biological disease that develops when cell division becomes uncontrollable. This disease continues to spread, even though various cancer treatments have been developed. Surgery, chemotherapy, and radiation therapy are still the most popular cancer treatments, but with inevitable and severe side effects. Therefore, alternative therapies that are more efficient and as effective are needed. Magnetic Hyper Thermia (MHT) can be a promising cancer therapy. In 2011, hyperthermia

therapy received clinical approval in Europe for the treatment of glioblastoma and clinical trials for prostate cancer and brain tumors [87]. It is a treatment that kills the cancerous cell by elevating temperature to a therapeutic temperature range of 42-45 °C with minimal damage to healthy cells thus limiting the side effects (As the temperature range between 42 and 45 °C is considered to be the hyperthermia temperature and recognized as the most effective in the field of oncology). Whereas the temperature above 56°C kills the normal health cells.

The technical challenge with hyperthermia is heating the targeted tumor area to the desired temperature without injuring adjacent healthy tissue. To overcome this, MNPs have been used as thermos seeds. In this technique, MNPs are injected into the specific tumor site and external Alternating Magnetic Field (AMF) is applied to produce heat (hyperthermia). IONPs are the most often probed magnetic nanomaterial for hyperthermia because of their biocompatibility, ease of surface modification, and high stability. The effect of hyperthermia and chemotherapy helps to enhance the therapeutic effect with minimal side effects and cancer cell death (cell apoptosis). Thus, using IONPs (Magnetite- Fe₃O₄) one can achieve cancer cell death due to hyperthermia.

The present work aims to synthesize biocompatible superparamagnetic IONPs (Magnetite- Fe₃O₄ nanoparticles) for MHT and chemotherapy. In MHT, NPs can elevate the temperature of tumor cells to hyperthermia threshold temperature (42-45°C) with minimal damage to healthy cells. The present work is focused on synthesis of SPIONs by chemical method with desired physicochemical properties (particle size, shape, magnetic saturation value, nontoxicity, biocompatibility) and its characterization using different characterization techniques such as X-ray Diffraction (XRD), Scanning Electron Microscopy (SEM), Fourier Transform Infrared spectroscopy (FTIR), Vibrating Sample Magnetometers (VSM), and Biocompatibility studies. The preparative parameters are optimized in such a way that they provide desired hyperthermia effect.

Title of the thesis: Glutathione-responsive superparamagnetic iron oxide (Fe₃O₄) nanoparticles for the magnetic hyperthermia and chemotherapy.

1.6 Objectives of the Study:

- 1. Synthesis and characterizations of superparamagnetic iron oxide (Fe₃O₄) by chemical method.
- 2. Synthesis of Poly Ethylene Glycol (PEG) coated Superparamagnetic Iron Oxide (Fe₃O₄) Nanoparticle (SPIONS) and their characterizations.

- 3. Synthesis of GSH coated Superparamagnetic Iron Oxide (Fe₃O₄) Nanoparticle (SPIONS) and their characterizations.
- 4. Magnetic Hyperthermia and Chemotherapy study of PEG coated, and GSH coated superparamagnetic iron oxide (Fe₃O₄) nanoparticles (SPIONs).

References:

- 1. Feynman R. There's plenty of room at the bottom. Reson J Sci Educ. 16 (9) (2011) 890-905.
- 2. Guin M and Singh N. Nanomaterials: Overview and Historical Perspectives. Emerging Nanomaterials and Their Impact on Society in the 21st Century. 135 (2023) 1-22.
- 3. Bayda S, Adeel M, Tuccinardi T, Cordani M, Rizzolio F. Molecules. 25 (1) (2019) 112-27.
- 4. Khan I, Saeed K, Khan I. Arab. J. Chem. 12 (7) (2019) 908-31.
- 5. Amendola V, Meneghetti M. Phys. Chem. Chem. Phys. 11 (20) (2009) 3805-21.
- Ali A, Shah T, Ullah R, Zhou P, Guo M, Ovais M, Tan Z, Rui Y. Front. Chem. 9 (2021) 629054-79.
- 7. Colombo M, Carregal-Romero S, Casula M, Gutiérrez L, Morales M, Böhm I, Heverhagen J, Prosperi D, Parak W. Chem. Soc. Rev. 41 (11) (2012) 4306-34.
- 8. Lu A, Salabas E, Schüth F. Angew. Chem. Int. Ed. 46 (8) (2007) 1222-44.
- 9. Donaldson I. Acc. Chem. Res. 98 (12) (2005) 572-75.
- 10. Kievit F and Zhang M. Acc. Chem. Res. 44 (10) (2011) 853-62.
- 11. Pathak Y and Thassu D. Drugs and Pharmaceutical Science Series. informa healthcare USA. 191 (67) (2009) 1-30.
- 12. Yadollahpour A and Rashidi S. Orient J Chem. 31 (1) (2015) 25-30.
- 13. Kolhatkar A, Jamison A, Litvinov D, Willson R, Lee T. Int. J. Mol. Sci. 14 (8) (2013) 15977-6009.
- 14. Park J, Joo J, Kwon S, Jang Y, Hyeon T. Angew. Chem. 46 (25) (2007) 4630-60
- 15. Xuan S, Wang Y, Yu J, Cham-Fai Leung K. Chem. Mat. 21 (21) (2009) 5079-87.
- Demortiere A, Panissod P, Pichon B, Pourroy G, Guillon D, Donnio B. Bégin-Colin S. Nanoscale. 3 (1) (2011) 225-32.
- 17. Pradhan P, Giri J, Samanta G, Sarma H, Mishra K, Bellare J, Banerjee R, Bahadur D. J Biomed Mater Res B Appl Biomater. 81 (1) (2007) 12-22.
- 18. Salunkhe A, Khot V, Pawar S. Curr. Top. Med. Chem. 14 (5) (2014) 572-94.
- 19. Bajpai O, Setua D, Chattopadhyay S. J. Res. Updates Polym. Sci. 3(4) (201) 184-204.
- Tombácz E, Turcu R, Socoliuc V, Vékás L. Biochem. Biophys. Res. Commun. 468 (3) (2015) 442-53.
- 21. Wu W, Xiao X, Zhang S, Li H, Zhou X, Jiang C. Nanoscale Res. Lett. 4 (8) (2009) 926-31.
- 22. Zhang L and Zhang Y. J. Magn. Magn. Mater. 321 (5) (2009) 15-20.
- 23. Kalubowilage M, Janik K, Bossmann S. Appl. Sci. 9 (14) (2019) 2927-44.
- 24. Senoy T and Anantharaman M. (Doctoral dissertation, Cochin University of Science & Technology) (2009).
- 25. Cruz-Montoya E and Rinaldi C. J. Polym. Sci. Part B, Polym. Phys. 49 (16) (2011) 1163-72.
- 26. Obaidat I, Mohite V, Issa B, Tit N, Haik Y. Cryst. Res. Technol. 44 (5) (2009) 489-94.

- 27. Nogués J, Sort J, Langlais V, Skumryev V, Suriñach S, Muñoz J, Baró M. Phys. Rep. 422 (3) (2005) 65-117.
- 28. Skumryev V, Stoyanov S, Zhang Y, Hadjipanayis, G, Givord D, Nogues J. Nature. 423 (6942) (2003) 850-53.
- 29. Martinez-Boubeta C, Balcells L, Monty C, Martinez B. J Phys Condens Matter. 22 (2) (2009) 026004-11.
- 30. Huber D. Small. 1 (5) (2005) 482-501.
- 31. Wang H, Kou X, Zhang J, Li J. Bull. Mater. Sci. 31 (2008) 97-100.
- 32. Shubayev V, Pisanic II T, Jin S. Adv. Drug Deliv. Rev. 61 (6) (2009) 467-77.
- 33. Wang X, Zhuang J, Peng Q, Li Y. Nature. 437 (7055) (2005) 121-24.
- 34. Xu Z, Shen C, Hou Y, Gao H, Sun S. Chem. Mat. 21 (9) (2009) 1778-80.
- 35. Suh S, Yuet K, Hwang D, Bong K, Doyle P, Hatton T. J. Am. Chem. Soc. 134 (17) (2012) 7337-43.
- 36. Ling D, Lee N, Hyeon T. Acc. Chem. Res. 48 (5) (2015) 1276-85.
- 37. Orza A, Wu H, Xu Y, Lu Q, Mao H. ACS Appl. Mater. Interfaces. 9 (24) (2017) 20719-27.
- 38. Feld A, Weimer A, Kornowski A, Winckelmans N, Merkl J, Kloust H, Zierold R, Schmidtke C, Schotten T, Riedner M, Bals S. ACS nano.13 (1) (2018) 152-62.
- 39. Hu M, Belik A, Imura M, Yamauchi Y. J. Am. Chem. Soc. 135 (1) (2013) 384-91.
- 40. Chai Y, Feng F, Li Q, Yu C, Feng X, Lu P, Yu X, Ge M, Wang X, Yao L. J. Am. Chem. Soc. 141 (8) (2019) 3366-70.
- 41. Tanaka S, Kaneti Y, Bhattacharjee R, Islam M, Nakahata R, Abdullah N, Yusa S, Nguyen N, Shiddiky M, Yamauchi Y, Hossain M. ACS Appl. Mater. Interfaces. 10 (1) (2018) 1039-49.
- 42. Wu H, Lee D, Tufa L, Kim J, Lee J. Chem. Mat. 31 (7) (2019) 2263-68.
- 43. Tan B, Zhao H, Wu W, Liu X, Zhang Y, Quan X. Nanoscale. 9 (47) (2017) 18699-710.
- 44. Feng L, Xie R, Wang C, Gai S, He F, Yang D, Yang P, Lin J. Acs Nano. 12 (11) (2018) 11000-12.
- 45. Yu J, Zhao F, Gao W, Yang X, Ju Y, Zhao L, Guo W, Xie J, Liang XJ, Tao X, Li J. ACS nano. 13 (9) (2019) 10002-14.
- 46. Han Y, Ouyang J, Li Y, Wang F, Jiang J. ACS Appl. Mater. Interfaces. 12 (1) (2019) 288-97.
- 47. Long M, Pan Y, Lin H, Hedstrom L, Xu B. J. Am. Chem. Soc. 133 (26) (2011) 10006-09.
- 48. Reddy L, Arias J, Nicolas J, Couvreur P. Chem. Rev. 112 (11) (2012) 5818-78.
- 49. Liu G, Gao J, Ai H, Chen X. Small. 9 (9-10) (2013) 1533-45.
- 50. Arami H, Khandhar A, Liggitt D, Krishnan K. Chem. Soc. Rev. 44 (23) (2015) 8576-607.
- 51. Zanganeh S, Hutter G, Spitler R, Lenkov O, Mahmoudi M, Shaw A, Pajarinen J, Nejadnik H, Goodman S, Moseley M, Coussens L. Nat. Nanotechnol. 11 (11) (2016) 986-94.

- 52. Lattuada M and Hatton T. Langmuir. 23 (4) (2007) 2158-68.
- 53. Huang H, Hu S, Chian C, Chen S, Lai H, Chen Y. J. Mater. Chem. 22 (17) (2012) 8566-73.
- 54. Liu Y, Chen T, Wu C, Qiu L, Hu R, Li J, Cansiz S, Zhang L, Cui C, Zhu G, You M. J. Am. Chem. Soc..136 (36) (2014) 12552-55.
- 55. Fu J, He L, Xu W, Zhuang J, Yang X, Zhang X, Wu M, Yin Y. Chem Commun. 52 (1) (2016) 128-31.
- 56. Liu B, Deng X, Xie Z, Cheng Z, Yang P, Lin J. Adv. Mater. 29 (36) (2017) 1604878-88.
- 57. Mashhadi Malekzadeh A, Ramazani A, Tabatabaei Rezaei S, Niknejad H. J. Colloid Interface Sci. 490 (2017) 64-73.
- 58. Gu H, Xu K, Xu C, Xu B. Commun. 9 (2006) 941-49.
- 59. Lin R, Li, Y, MacDonald T, Wu H, Provenzale J, Peng X, Huang J, Wang L, Wang A, Yang J. Colloids Surf. B Biointerfaces. 150 (2017) 261-70.
- 60. Zhang Z and Song S. Biomater. 106 (2016) 13-23.
- 61. Saikia C, Das M, Ramteke A, Maji T. Int. J. Biol. Macromol. 93 (2016) 1121-32.
- 62. Ganapathe L, Mohamed M, Mohamad Yunus R, Berhanuddin D. Magnetochemistry. 6 (4) (2020) 68-104.
- 63. Shen S, Lindley S, Chen X, Zhang J. Energy Environ. Sci. 9 (9) (2016) 2744-75.
- 64. Wu C, Yin P, Zhu X, OuYang C, Xie Y. J.Phys. Chem. B. 110 (36) (2006) 17806-12.
- 65. Shokouhimehr M, Piao Y, Kim J, Jang Y, Hyeon T. Angew. Chem. Int. Ed. 46 (37) (2007) 7039-43.
- 66. Noqta O, Aziz A, Usman I, Bououdina M. J. Supercond. Nov. Magn. 32 (2019) 779-95.
- 67. Sheng-Nan S, Chao W, Zan-Zan Z, Yang-Long H, Venkatraman S, Zhi-Chuan X. Chin Phys B. 23 (3) (2014) 037503-23.
- 68. Pullar R. Prog. Mater. Sci. 57 (7) (2012)1191-334.
- 69. Dronskowski R. Adv. Funct. Mater. 11 (1) (2001) 27-29.
- 70. Grau-Crespo R, Al-Baitai A, Saadoune I, De Leeuw N. J Phys Condens Matter. 22 (25) (2010) 255401-20.
- 71. Palanisamy S and Wang Y. Dalton Trans. 48 (26) (2019) 9490-515.
- 72. Kaur P, Aliru M, Chadha A, Asea A, Krishnan S. Int. J. Hyperth. 32 (1) (2016) 76-88.
- 73. Nguyen M, Tran H, Xu S, Lee T. Appl. Sci.11 (23) (2021) 11301-34.
- 74. Ju S, Cai T, Lu H, Gong C. J. Am. Chem. Soc. 134 (33) (2012) 13780-86.
- 75. Wu W, Wu Z, Yu T, Jiang C, Kim W. Sci. Technol. Adv. Mater.16 (2) (2015) 02351-95.
- Mantovan R, Lamperti A, Georgieva M, Tallarida G, Fanciulli M. J.Phys. D. Appl. Phys. 43
 (6) (2010) 065002-27.
- 77. Lee J, Jang J, Choi J, Moon S, Noh S, Kim J, Kim J, Kim I, Park K, Cheon J. Nat. Nanotechnol. 6 (7) (2011) 418-22.

- 78. Mahmoudi M, Simchi A, Imani M, Shokrgozar M, Milani A, Häfeli U. Stroeve P. Colloids Surf. B: Biointerfaces. 75 (1) (2010) 300-9.
- 79. Gupta A and Gupta M. Biomaterials. 26 (18) (2005) 3995-4021.
- 80. Sonvico F, Mornet S, Vasseur S, Dubernet C, Jaillard D, Degrouard J, Hoebeke J, Duguet E, Colombo P, Couvreur P. Bioconjugate Chem. 16 (5) (2005) 1181-88.
- 81. Dobson J. Gene therapy.13 (4) (2006) 283-87.
- 82. Jendelová P, Herynek V, Urdzíková L, Glogarová K, Kroupová J, Andersson B, Bryja V, Burian M, Hájek M, Syková E. J. Neurosci. Res. 76 (2) (2004) 232-43.
- 83. Nikam D, Jadhav S, Khot V, Bohara R, Hong C, Mali S, Pawar S. RSC Adv. 5 (3) (2015) 2338-45.
- 84. Manohar A, Vijayakanth V, Vattikuti S, Manivasagan P, Jang E, Chintagumpala K, Kim K. ACS Appl. Nano Mater. 5 (4) (2022) 5847-56.
- 85. Kim J, Kim S, Kim Y. J. Nanosci. Nanotechnol. 14 (11) (2014) 8739-44.
- 86. Khot V, Salunkhe A, Phadatare M, Thorat N, Pawar S. J. Phys. D: Appl. Phys. 46 (5) (2012) 055303-13.
- 87. Mahmoudi K, Bouras A, Bozec D, Ivkov R, Hadjipanayis C. Int. J. Hyperthermia. 34(8) (2018)1316-28.

CHAPTER-02

MAGNETIC NANOPARTICLES

(MNPs) FOR CANCER THERAPIES:

THEORETICAL ASPECTS

INDEX

Sr.No		Title	Page No.
2.1	Introdu	ction to Cancer and Related Therapies	23
2.2	Cancer	Tumor Microenvironment	24
2.3	Nanopa	articles for Cancer Tumor Treatment	25
	2.3.1	Photothermal Therapy	27
	2.3.2	Chemotherapy/ Drug Delivery	28
		2.3.2.1 Targeted Drug Delivery	29
	2.3.3	Hyperthermia Therapy	31
		2.3.3.1 Modes of Hyperthermia	31
2.4	Magnet	tic Hyper Thermia (MHT) Therapy	33
	2.4.1	Eddy Current Loss	35
	2.4.2	Hysteresis Loss	35
	2.4.3	Relaxation Loss	36
		2.4.3.1 Neel Relaxation Mechanism	36
		2.4.3.2 Brownian Relaxation Mechanism	37
	2.4.4	Parameters for Efficient MHT Application	38
		2.4.4.1 Size and Nature of MNPs	38
		2.4.4.2 Uniform and Controlled Heating	38
		2.4.4.3 Biocompatibility	39
		2.4.4.4 Colloidal Stability	39
		2.4.4.5 High Specific Absorption Rate (SAR)	40
		2.4.4.6 Frequency of Applied AMF	41
2.5	Literatu	are Review on MNPs used for MHT and Chemotherapy	41
	Referen	nces	45

2.1 Introduction to Cancer and Related Therapies:

Cancer is a biological disease that arises when cell division becomes uncontrolled and is also one of the major reasons for mortality in the world. According to the American Cancer Society's 2024 global cancer statistics report, 20 million cases were detected in 2022, and by 2050, the number is predicted to reach 35 million worldwide. Over the past five to six decades, there has been no change in the number of cancer deaths despite the discovery of new drugs and treatment combinations, even though nearly 2,00,000 mouse experiments, two million scientific publications completed, and an annual spending of approximately 15 billion US dollars invested worldwide [1]. Thus, a new cancer diagnosis and therapy is desperately needed.

There are two types of cancer treatments: conventional therapies and non-conventional therapies. Conventional cancer therapies include surgery, radiation therapy, chemotherapy, immunotherapy, and hormone therapy, which are now in use either alone or in combination with other conventional therapies, on the basis of kind of cancer and the stage of the disease. In many cases of localized cancer, surgery is curative where all or almost all malignant tissues can be removed. It is still the most successful conventional treatment for solid tumors. The objective of surgery is to eliminate as much of the tumor as feasible [2]. Hyperthermia is a nonconventional therapy that is being used in conjunction with other conventional therapies.

Types of cancer treatment Conventional Therapy Nonconventional Therapy Local **Systemic Photothermal** Hyperthermia

Chart 2.1 shows a graphical overview of cancer therapies.

Photodynamic Therapy Treatment Therapy Therapy Radiation Harmonal Monoclonal-Radioactive Chemotherapy Surgery **Therapy** therapy therapy material **Phase** Phase specific nonspecific

Chart 2.1: Graphical overview of cancer therapies.

The magnetic properties of Magnetic Nanoparticles (MNPs) are crucial in coining the therapies. The significant contributions have come from a range of pioneering researchers starting from Franz Mesmer, Gilchrist to Andrew Jorden. These researchers shaped the area significantly from the point of theoretical understanding. In parallel, several applications are investigated which are based on fundamental properties of MNPs such as sensing, and heating.

2.2 Cancer Tumor Microenvironment:

When cells divide more often than they should or when they do not undergo programmed cell death, aberrant cell proliferation results, which causes tumors. Tumors are classified as either benign or malignant. Malignant tumors are the most dangerous kinds of tumors because they can spread rapidly, infect surrounding tissues, and spread to other regions of the body, resulting in serious conditions that, if left untreated, can be fatal. Tumors are not only a collection of cancer cells; rather, it is a heterogeneous combination of resident and invasive host cells, extracellular matrix, and secreted substances. Microscopic analysis of solid tumors highlights the intricate complexity of cancer by demonstrating the Tumor Micro Environment (TME). It is a highly structured ecosystem with non-malignant cells along with cancer cells, all of which are embedded in a modified extracellular matrix that is vascularized as shown in Fig.2.1 [3].

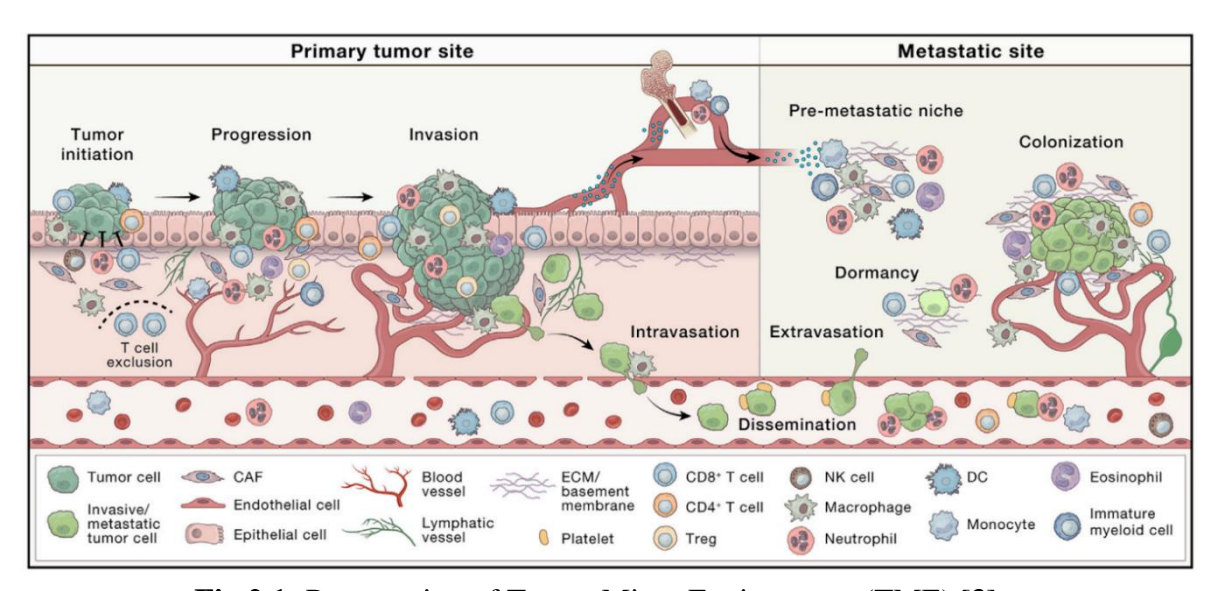


Fig.2.1: Presentation of Tumor Micro Environment (TME) [3].

TME development is a complex and dynamic system. The composition of the TME varies depending on the kind of cancer, but extracellular matrix, stromal cells, immune cells, and blood vessels are all common. It is proposed that the "TME is an active promoter of cancer progression, not just a silent bystander."

During the early stages of tumor formation, cancer cells and components of the TME form a dynamic and mutual relationship that aids cancer cell survival, local invasion, and metastatic dissemination [4]. Various types of cells, such as adipocytes and neurons, Endothelial Cells (ECs), immune cells, and Cancer-Associated Fibroblasts (CAFs), comprise the TME which vary according to the tissue. To survive, cancer cells can change their environment, employing fibroblasts to get the growth factors needed for their development and

replication. Soluble factors are released when adjacent endothelial cells interact with tumor cells, and these factors drive angiogenic processes.

Tumor cells evade immune destruction by producing immunosuppressive cytokines and losing tumor antigen expression, making them invisible to the immune system. These mechanisms create an immunosuppressive TME, which reprograms normal immune cells to support tumor growth and progression. Effective therapies must account for the complex role of the TME in tumor development and progression.

2.3 Nanoparticles for Cancer Tumor Treatment:

The conditions of TME that trigger the therapy for improved results with minimum side effects are acidic pH, endogenous hydrogen peroxide (H₂O₂), over-expressed enzymes, hypoxia due to limited oxygen supply, excess Glutathione (GSH -g-glutamyl-cysteinyl-glycine tripeptide), and Reactive Oxygen Species (ROS) generation, etc.

a) pH-Responsive:

The acidic pH of tumor tissues and/or endocytic vesicles like endosomes and lysosomes has been considered to be a suitable internal trigger for the regulated release of anticancer drugs. Extracellular pH values in tumors were compared to those in the blood and healthy tissues (pH 7.4). ranged from 6.0 to 7.2. Furthermore, fast acidification occurs during endocytosis due to a proton inflow. Endosomes and lysosomes have intracellular pH values of 5.0-6.0 and 4.0-5.0, respectively. The acidic pH of the tumor media is also regarded as an appropriate trigger for selectively destroying cancer cells. Many acid-responsive drug delivery nanoplatforms have recently been developed based on the acidic pH level within the tumor. These nano drugs are stable in normal tissues; however, the acidic pH of the TME activates them, causing them to release the drugs at tumor locations [4].

b) GSH Responsive:

The most abundant thiol in mammalian cells is a g-glutamyl-cysteinyl-glycine tripeptide (GSH), which plays an essential part in the primary biological processes. In intracellular environment, GSH concentrations are between 0.5-10 mM where as it is 2-20 mM in the blood or extracellular matrix. Drugs can be trained to release intracellularly by taking advantage of this significant difference between the exterior environment and the intracellular cytosol. More importantly, compared to healthy tissues, tumor tissue substantially reduces a hypoxic state, with intracellular GSH contents at least fourfold higher than those in normal cells. The considerable different GSH concentrations between normal and tumor cells is crucial for tumor-specific drug delivery [4].

Liposomes, polymerases, polymeric nanogels, micelles, dendrimers, protein nanocapsules, and Nanoparticles (NPs) are examples of redox-responsive nanocarriers that have been used to provide sensitivity to the intracellular reduction potential for the burst release of conjugated or encapsulated drugs into tumor cells. The polymer-drug linkage for intra- or intermolecular conjugation, side chain, backbone, or cross-linker of the materials used to make nanocarriers can all contain characteristic disulfide (S–S) bonds. The disulfide bond is extremely stable in the extracellular environment when GSH levels are low. It tends to be quickly cleaved by a GSH-mediated thiol-disulfide exchange mechanism in a reducing intracellular environment, though, which might lead to the release of drug and the destruction of nanocarrier [4].

c) ROS Responsive:

Research has demonstrated that cancer cells consistently produce higher quantities of ROS than normal cells. These ROS are produced by neoplastic transformation and are derived from by-products of aerobic metabolism, which include superoxide, hydroxyl radicals, and hydrogen peroxide. It is possible to increase the sensitivity of ROS-responsive drug carriers for site-specific drug release. One excellent source of potent oxidizing hydroxyl radicals (• OH) is the Fenton reaction, which occurs when H₂O₂ and an iron catalyst come together. Iron Oxide Nanoparticles (IONPs) are used as an efficient donor of Fe²⁺ in the acidic TME to accomplish a localized Fenton reaction for effective drug release. It is interesting to note that high-efficiency therapies are made possible by the • OH produced by the localized Fenton reaction without the need for external energy [4].

d) Enzyme Responsive:

For most metabolic processes, enzymes are important macromolecular biological catalysts. The deregulation of enzyme expression or enzyme dysfunction is linked to the pathophysiology of several illnesses, including cancer. Enzyme-responsive nanosystems for anticancer drug delivery have been developed to deliver anticancer drugs on demand. This is accomplished by adding particular moieties that are preferentially identified and destroyed by enzymes that are overexpressed in extracellular or intracellular tumor environments as compared to normal tissues. Matrix Metalloproteinases (MMPs), hyaluronidase (HAase), and cathepsin B are the most often researched cancer-associated enzymes functioning as advantageous triggers [4].

Because of the inherent qualities of MNPs, they drew a lot of attention among the wide range of nanoscale materials being researched for biological applications [5]. The size range of

nanoparticles is 1 to 100 nanometers and is smaller or comparable to the sizes of genes (2 nm broad and 10-100 nm long), proteins (5-50 nm), viruses (20-450 nm), and cells (10-100 μ m). This suggests that they can be in close contact with a biological entity. Secondly, due to magnetic properties, they can be controlled using external magnetic/electric fields. This ability for "action at a distance," combined with the penetration of magnetic fields through human tissue, unlocks numerous applications for transferring or immobilizing magnetically tagged biological entities or MNPs. This allows to deliver a payload, like an anticancer drug, or a group of radioactive atoms, to a target within the tumor.

MNPs must possess the following qualities to be utilized in biomedical applications: a suitable hydrodynamic diameter, a high saturation magnetization (Ms), small core size, and mono dispersity, biocompatibility, and nontoxicity over the period of degradation.

The usage of single or multicore iron oxide ensures colloidal stability by preventing nonspecific adsorption of biomolecules and serving as anchors and spacers. Effectiveness in a biomedical application is partially based on the superparamagnetic behavior of MNPs. Along with electronic and catalytic applications, MNPs are most widely used for biomedical purposes such as hyperthermia, a contrast agent for Magnetic Resonance Imaging (MRI), labeling and storing of the cells, cell transfection, Positron Emission Tomography (PET), tissue-specific drug/gene delivery system, or combination of two or more of them. Some of the applications of MNPs are,

2.3.1 Photothermal Therapy:

Photothermal therapy involves elevating the temperature of tumor cells over 42°C. To accomplish this, laser light must be applied to the cells, converting the energy of the radiation into heat. The radiation used falls within the near-infrared region (heat radiation). To increase the efficiency and selectivity of energy-to-heat transfer, a photothermal agent that absorbs light should be administered into the tumor. Elemental NPs like gold, silver, carbon, and dyes act as excellent photothermal agents in tumor therapy. These nanoparticles can be utilized alone or in conjunction with other materials. MNPs have a significant theoretical constraint when utilized alone because of their low molar absorption coefficient in the near-infrared spectrum. This issue can be resolved by carefully arranging the nanoparticles into clusters. Under these circumstances, the suggested radiation is more effectively absorbed and the energy is converted to heat more effectively than in individual nanoparticles. However, it may also be constructed as a medicinal system, where a medicine connected to the MNPs is released in a regulated way by the heat created by the nanoparticles when they are exposed to infrared light [6].

2.3.2 Chemotherapy/ Drug Delivery:

A multidisciplinary method was developed for the targeted distribution and release of drugs. This method aims to maximize the effectiveness of the Drug Delivery System (DDS). Drug delivery and targeting systems are now being developed to lower the probability of side effects and to enhance medicine availability at the point of disease. Even though the process of developing new pharmaceuticals and their discovery has advanced significantly, numerous drugs still have undesirable side effects because they interact with parts of the body that are not the target of the treatment.

MNPs are the preferred choice for drug delivery activity because they are effective in targeting diseased cells and tissues, hence termed as conventional drug delivery vehicles. To increase the efficacy of targeted drug administration and enable programmed distribution of therapeutic agents, it is possible to take one step further by coupling several moieties responsive to appropriate environmental stimuli like temperature and radiation. IONPs have received a lot of interest in the field of drug delivery because of their unique features and biocompatibility. Iron oxide has the following functions in drug delivery:

- Magnetic Targeting: IONPs may be magnetized, enabling the precise administration of drugs. MNPs may be guided to certain parts of the body, such as tumor spots, using an external magnetic field. This tailored administration improves treatment efficacy while reducing off-target consequences.
- 2. Drug Encapsulation: IONPs are capable of carrying a wide range of drugs. They can be functionalized with various surface coatings to enhance drug loading and encapsulation effectiveness. Drugs can be entrapped within the core of nanoparticles or attached to their surface, giving degradation resistance and allowing for controlled release.
- 3. Controlled Drug Release: IONPs can be configured to release drugs in a regulated manner. Through modifications in their surface properties or by incorporating stimuli-responsive materials, such as pH-sensitive or temperature sensitive polymers, the release of drugs can be triggered by specific physiological conditions, such as the acidic environment of tumors.
- 4. Imaging and Tracking: IONPs possess inherent magnetic properties that enable them to be visualized by MRI. This imaging capability allows for real-time monitoring of the distribution and accumulation of nanoparticles in the body, providing valuable information on drug delivery efficiency and biodistribution.

5. Theranostics: Theranostics is the ability of IONPs to perform both therapeutic and diagnostic activities. They can be loaded with therapeutic and imaging contrast agents, permitting the administration of drugs and therapeutic monitoring. This integrated approach enables individualized therapy and the creation of more effective treatment options.

Gonzalez-Rodriguez et al. [5] combine Graphene Oxide (GO) with Magnetite- Fe₃O₄ NPs to enhance its performance as an MRI contrast agent and biocompatible magnetic drug delivery additive. When the Doxorubicin (DOX) drug is non-covalently bound to GO-Fe₃O₄ conjugates, it delivers drug into cells efficiently.

2.3.2.1 Targeted Drug Delivery:

Certain targeting strategies are necessary to specifically target the drug in the intended tissue or organ to decrease effectiveness and dose-related toxicity because very few drugs bind to the intended therapeutic target. In 1960 Paul Ehrlich proposed the idea of targeted drugs as a "magic bullet," but the use at the clinical level is difficult [7]. NPs have the potential to transport active pharmaceuticals and may resemble a "magic bullet" due to enhanced therapeutic index and efficacy, ability to entrap hydrophilic and lipophilic drugs, the capacity to repeatable sizes with surface functionalization, the enhanced drug stability against enzymatic degradation, the ability to deliver intact drugs entrapped in different tissues and cells for site-specific targeted delivery, and the decreased toxicity of drugs to healthy cell [7]. To ensure the successful delivery of drugs, drug targeting techniques need to fulfil two fundamental needs. Once administered, drugs have to reach their intended locations with the least amount of dose loss and blood circulation activity. Secondly, drugs have to just affect the intended cells, avoiding any negative consequences on healthy cells. Drug targeting has been approached from two perspectives: passive targeting and active targeting as shown in Fig.2.2 [7].

a) Passive Targeting:

Passive targeting enables the drug to reach its target site by utilizing the intrinsic qualities of the organ or tissue of interest. The pathophysiological features of tumor veins, such as their leaky vasculature with holes ranging from 100 to 800 nm, are exploited by passive targeting, to allow nanodrugs to concentrate in tumor tissues. Tumor arteries are often extremely disorganized, dilated, and packed with holes, which causes poor lymphatic outflow and increases the gaps that exist between endothelial cells. Leaky vascularization and poor lymphatic drainage make it easier for NPs to enter and remain inside the tumor site. This is referred to as Enhanced Permeability and Retention (EPR) effect. The phenomenon known as

EPR refers to passive targeting, in which the NPs attach themselves to specific areas via the leaky vasculature of tumor. This approach is unsuccessful when used on tumors that are poorly perfused or have an irregular structure. In such circumstances, insufficient MNP dispersion might result in tumor heating or tissue overload.

Tumor tissue preferentially receives drug-loaded NPs over healthy cells because their tiny size, rather than any binding, and also the tight connections keep the NPs in place. As a result, compared to free drug delivery, a passive targeting helps to deposit more drug in solid tumors [7].

The TME differs from that of healthy cells, which allow passive targeting. In order to sustain their high metabolic rate, rapidly proliferating cancer cells require more oxygen and nutrients. As a result, an acidic environment is formed, and glycolysis is boosted to obtain additional energy. Chemotherapy medicines can target tumor cells with this advantage. Therapeutic chemicals are released when pH-sensitive NPs break down at the acidic pH of a tumor, as they are stable at an average physiological pH of 7.4. To optimize circulation time and targeting capabilities in cancer treatment, it is important to correctly regulate the size and surface properties of NPs to limit absorption by the Reticulo Endothelial System (RES).

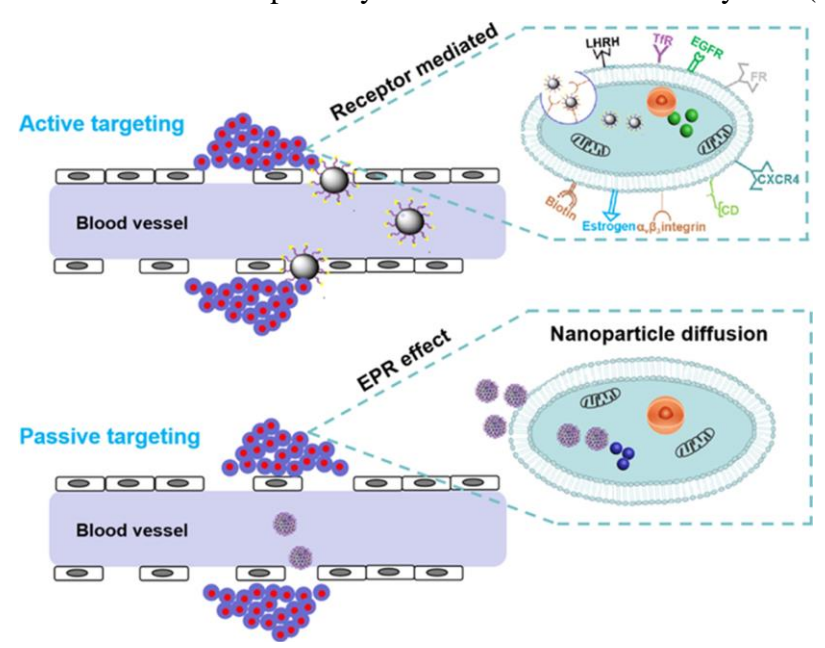


Fig.2.2: Mechanisms of passive and active targeting in drug delivery: EPR effect and receptor-mediated approaches [8].

b) Active Targeting:

By employing a range of conjugation techniques that selectively bind to certain cell surface receptors, ligands like as antibodies, peptides, vitamins, aptamers, or small molecules can be affixed to the surface of nanocarriers in order to overcome the limitations of passive

targeting. The receptors must be substantially expressed on cancer cells as opposed to healthy cells in order to get high specificity. A technique called receptor-mediated endocytosis is used to internalize the targeted conjugates. When targeting ligands attach to the receptors, endosomes are formed to surround the ligand-receptor complex and the plasma membrane. The endosome is then sent to certain organelles, where enzymes or an acidic pH are used to release the drug [7].

Mechanism for Targeted Drug Delivery:

Magnetically targeted therapy entails binding cytotoxic medicines to a biocompatible MNPs carrier. These drug/carrier combinations are often delivered to the patient through the circulatory system as a biocompatible ferrofluid. Once the particles are concentrated at a specific location within the body by high-gradient external magnetic fields. The medication may be released by enzymatic activity or by changing physiological parameters like temperature, osmolality, or pH [8]. Theoretically, this technique offers significant benefits over standard, non-targeted cytotoxic drug treatment. DDS sensitive to ionic microenvironment, pH, enzymes, and redox are examples of endogenous stimuli with biological and chemical origins. These DDS control the microenvironment of tissues, overexpress certain enzymes, interact with antibodies and antigens, and identify host-guest moieties in a particular state to initiate the release of drugs.

2.3.3 Hyperthermia Therapy:

Researchers faced the difficulty of treating cancer without causing harm to the rest of the body. Some medical procedures are expensive, and some have side effects. For example, chemotherapy can cause hair loss, a drop in white blood cells, and radiation therapy can destroy healthy cells and tissues. Among the available options for cancer treatment, hyperthermia seems to be the most promising therapy. The idea of using heat to cure particular diseases or tumors is not new; it has a long history. In ancient times, the Greeks, Romans, and Indians employed heat to cure different tumors.

2.3.3.1 Modes of Hyperthermia:

The classification of hyperthermia modes is based on the kind of heating source and the type of heated target. There are three main types of heating sources:

- a. Use of hot liquid,
- b. Contactless applicator (e.g. infrared devices, ultrasound radiation, and microwave radiofrequency), and
- c. Insertion of the heating source (like probes, antennas, laser fiber, and mediators).

Due to the lack of target specificity, heating with an external liquid or contactless applicator is not recommended. The inability of these strategies to effectively deliver heat energy to tumors located deep within normal tissues without causing damage led to the development of technologies utilizing internal heating sources. Therefore, it appears that using magnetic micro- or nanoscale mediator devices where particles are injected as particle dispersions that when exposed to an electric or magnetic field, transform electromagnetic energy into heat. The most recent methods for treating Magnetic Hyper Thermia (MHT) rely on injectable colloidal dispersions of magnetic particles, which act as micro-or nanoscale mediators. These methods can be used in three different ways [9]:

- i. Arterial Embolization Hyperthermia (AEH),
- ii. Direct Injection Hyperthermia (DIH), and
- iii. Intracellular Hyperthermia (IH).

Because of their improved temperature uniformity, these techniques show the most promise for cancer therapy. For isolated malignant cells in any part of the body, the most effective way to selectively overheat tumor cells is through the intracellular approach, which is based on delivering MNPs for selective absorption. The fundamental property of MHT is the absorption of energy from the oscillating magnetic field by one or more of the following processes, which results in the transformation of energy into heat.

- 1. Eddy currents are generated in a material with low electrical resistance.
- 2. Magnetization is reversed inside a magnetic material.
- 3. Rotation of the magnetic moment with respect to its surroundings

Each of them is described briefly in **Section 2.4.** (1-3).

Hyperthermia treatment using nanoparticles in an alternating current magnetic field began in the late 1950s. However, therapeutic applications remained well behind the horizon due to weak field parameters and inexact thermotherapy [10].

Two forms of heating treatments are currently available: (a) thermos ablation, which involves heating to temperatures above 46 °C (up to 56 °C) to directly destroy tumors through cell necrosis, coagulation, or carbonization; and (b) mild hyperthermia, which is performed at temperatures between 41 and 46 °C to elicit an immune response for non-specific cancer immunotherapy. When MNPs are exposed to a high-frequency alternating current magnetic field, they are heated to a temperature range of 41 to 46 °C. The heating is caused by the fluctuation of their magnetic moment. Thus, the temperature of malignant tissue increases from 41 to 43 °C, where cancer cells often die [11]. Magnetic heating via inductive mediators is

mostly determined by the size and magnetic properties of the particles [12]. Gilchrist et al. [13] conducted the first experimental studies in 1957 to destroy tumor cells through heating using magnetic particles under the effect of Alternating Magnetic Field (AMF) as shown in **Fig.2.3** [14].



Fig.2.3: Schematic of the first prototype of the Magnetic Fluid Hyperthermia (MFH) therapy System (MFH Hyperthermie systeme GmbH, Berlin, Germany): Highlights include an alternating current magnetic field magnetic field axis that is perpendicular to the patient couch (1), a ferrite-core applicator that operates at 100 kHz (2), an adjustable vertical aperture (3), an air-cooling system (4), and a manual control unit (5). Fluoro-optic probes are used in an intrusive manner to measure temperature [14].

They used Maghemite- γ-Fe₂O₃ nanoparticles with sizes ranging from 20 to 100 nm with a magnetic field of 1.2 MHz to heat several tissue samples. In the past 50 years, there have been notable advancements in the field of MHT. Numerous magnetic materials and techniques for energizing and delivering them to the cancer site have been tested and documented. Currently, it is one of the most significant secondary treatment modalities to be utilized in combination with chemotherapy and radiation. Cancer treatment often makes use of ferromagnetic and superparamagnetic NPs to achieve desired heating for lower external magnetic fields.

2.4 Magnetic Hyper Thermia (MHT) Therapy:

Jorden et al. [14] introduced the idea of Magnetic Fluid Hyperthermia (MFH) in 1999. A fluid with MNPs was introduced directly into a tumor to cause MFH. Compared to laser, microwave, and ultrasound therapies, hyperthermia is less invasive. Magnetic fluids are made

by dispersing MNPs in water or hydrocarbon fluid. They are heated through Neel or Brownian relaxation, hysteresis loss, and frictional losses in viscous suspension. The surrounding tumor absorbs the heat generated by the MNPs. Principle of MHT is depicted in **Fig.2.4**.

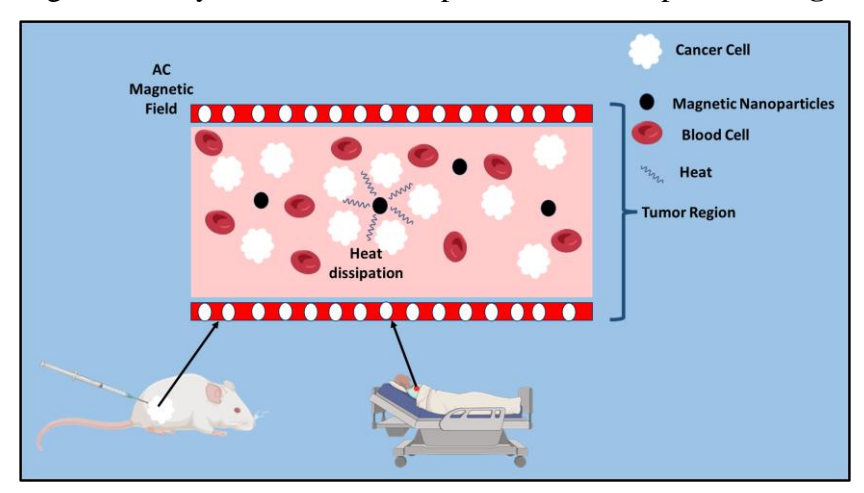


Fig.2.4: Magnetic Hyper Thermia (MHT) using MNPs.

The generation of heat depends on the amount of MNPs used and the applied AMF. Some of the requirements of MNPs for effective hyperthermia are,

- 1) At room temperature, it must exhibit the superparamagnetic properties [15].
- 2) The particle should have an organic or inorganic polymer coating and a core diameter between 10 to 20 nm.
- 3) It must work properly in the frequency range that corresponds human body tolerance [16].
- 4) It should produce a stable aqueous suspension in water-based fluids without agglomerating and is biocompatible, and less toxic [15].
- 5) The size and saturation magnetization values greatly affect the efficiency of hyperthermia [17].

The TME, specifically the facts that hypoxic (low-oxygen) cancer cells are considerably more radiation-resistant than euoxic (well-oxygenated) cancer cells, and cancer cells in hypoxia are more susceptible to heat than those in euoxia, the radiation and hyperthermia therapies can be combinedly used to kill the cancer cells [18].

For MHT, applied field frequencies in the low radiofrequency range (100-400 kHz) are used to achieve the therapeutic threshold [19]. Maier-Hauff et al. [20] conducted clinical trials of MHT in brain tumor patients under an AMF of frequency 100 kHz by monitoring the hyperthermic temperature within 42-49 °C. It was found that this temperature limit has not harmed any patients and hence this temperature window and the applied magnetic field frequency can be used for MNPs based MHT with minimal side effects [21]. MNPs are also being used as drug carriers when combined with MHT to achieve enhanced drug release and

thermotherapy in a single platform [22].

Magnetically induced hyperthermia also termed as Magnetic Hyper Thermia (MHT) is a tool to increases temperature by magnetization and demagnetization of MNPs. AMF applied causes magnetic energy to dissipate as thermal energy [23]. Eddy current, hysteresis, and relaxation losses are responsible for the conversion of heat [24]. The heating is made localized by inserting MNPs well within the tumor area so that healthy cells are sparely affected.

2.4.1 Eddy Current Loss:

Eddy Currents (ED) are formed as a result of the induction law. It does not apply only to magnetic materials, but to any macroscopic conducting materials. ED loss is also defined as the Joule loss, i.e. generation of ED by an AMF and is influenced by the electrical resistance of the material. **Equation 2.1** provides the heat loss caused by ED.

$$ED = \frac{(\mu \pi df H)^2}{20\rho}$$
 (2.1)

where,

 μ = permeability of a material,

d = diameter of the particle, and

 ρ = resistivity of the material.

Under AMF, hysteresis loss and residual loss (Neel and Brownian relaxations) are major contributor for heating effect compare to ED [25].

2.4.2 Hysteresis Loss:

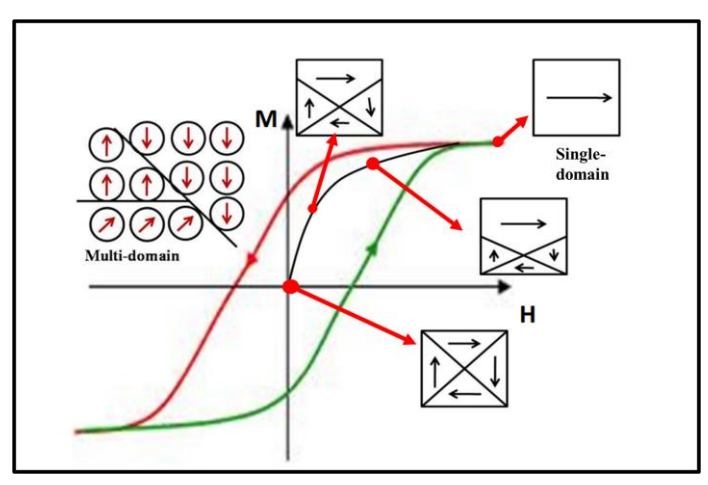


Fig.2.5: Hysteresis loop of a multi-domain ferromagnetic materials [23].

Ferromagnetic materials have a multi-domain system with hysteresis loss, which is the amount of energy converted into heat in each cycle of the magnetization and demagnetization process. Because the external magnetic field forces the magnetic moments to align in external

field direction which cause domain walls to move in a multi-domain system. To modify the direction of spins inside a particular domain, the walls must shift. The displacement of domain walls (shown in **Fig.2.5**) depends upon structural faults of the atomic arrangements (defects, dislocations, vacancies, etc.), known as the Barkhausen effect, and is an irreversible process.

Equation 2.2 gives dissipated power per unit volume [23].

$$P_{FM} = \mu_0 f \int H. dM \qquad \dots (2.2)$$

2.4.3 Relaxation Loss:

Heat is produced in single-domain MNPs due to super spin alignment in the direction of the applied magnetic field. When the energy barrier prevents the rearrangement of magnetic moments, the magnetic energy is transformed into thermal energy [23]. One of the main aspects of Superparamagnetic Iron Oxide Nanoparticles (SPIONs) is the characteristic time scale for thermally activated switching of magnetic moments. Heat is produced due to the delay in the magnetic moment relaxation via either Brownian or Neel relaxation when the field reversal time is less than the particle relaxation time after exposure to AMF.

2.4.3.1 Neel Relaxation Mechanism:

The critical domain size is the precise volume at which a drop in particle size results in the near vicinity of several domain barriers. Within this single magnetic domain, the atomic magnetic moments are magnetized in the same direction, resulting in a superparamagnetic or huge magnetic moment. The anisotropy constant (K) and magnetic volume (V) are the energy barriers that spinning magnetic moments must overcome with the assistance of an external AMF. This energy is released as the particle moment relaxes to its equilibrium orientation (Neel Relaxation).

Louis Neel created the Neel relaxation mechanism theory in 1949 to explain magnetic viscosity, a time-dependent magnetic phenomenon [23,26-28]. As seen in Fig.2.6 (a), super spins orient to the direction parallel to the applied magnetic field when the physical location of MNPs is maintained fixed. At this instance, magnetic anisotropy energy dissipates magnetic energy and prevents super spins from reorienting. Neel relaxation time (τ_N) is the relaxation time for the magnetic moment to flip in parallel and antiparallel directions and calculated using $\tau_N = \tau_{\circ} e^{\Delta E/k_B} = 1/2\pi v_N$ [29].

Where v_N is maximum frequency of heating via Neel relaxation.

Equation 2.3 gives maximum magnetic susceptibility, $\chi''(v)$.

$$\chi''(\nu) = \frac{\chi_0 \Phi}{(1 + \Phi^2)}$$
 (2.3)

where,

$$\Phi = \nu t_N \tag{2.4}$$

$$\chi_0 = \frac{\mu_0 M_S^2 V}{kT}$$
 (2.5)

where M_S is saturation magnetization.

2.4.3.2 Brownian Relaxation Mechanism:

The Brownian motion of particles inside a carrier liquid may also be the cause of heating for both single-domain and multi-domain. This is essentially explained by the torque that an external AMF applies to a magnetic moment, which causes the magnetic particles to rotate collectively as shown in **Fig.2.6** (b).

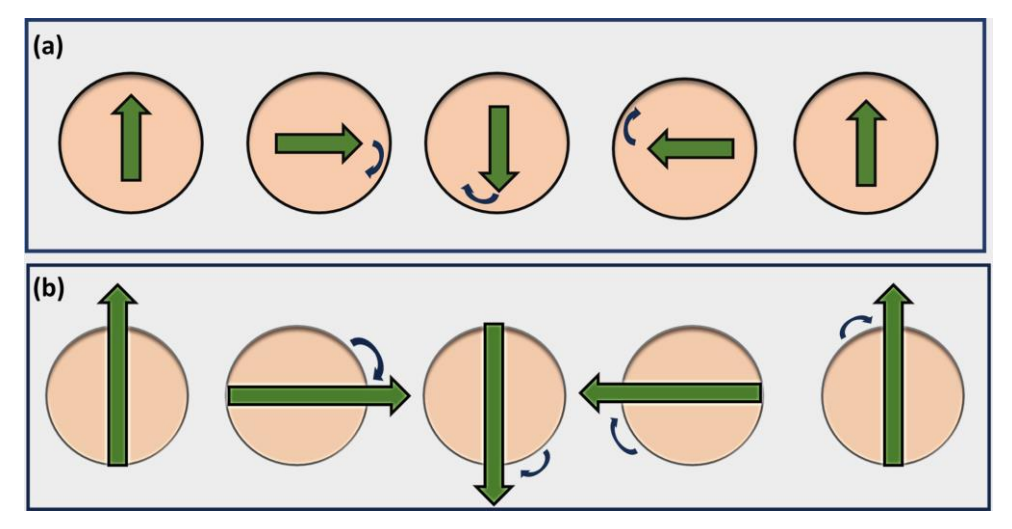


Fig.2.6: Magnetic loss mechanisms in single-domain magnetic nanoparticles: (a) Neel relaxation and (b) Brownian relaxation.

Energy must be provided in order to conquer the rotating friction caused by the surrounding liquid. Brownian relaxation is the term for the energy released during relaxing of particle moment. Similar to the Neel relaxation time, the Brown relaxation time (τ_B) calculated using equation $\tau_B = \frac{3\eta V_h}{k_B T} = 1/2\pi v_B$.

Single-domain nanoparticles are defined as those with a core diameter of less than 20 nm. As a result, the reciprocal internal (Neel) and exterior (Brownian) diffusion of the particle magnetic moment together control their magnetization relaxation [30]. If both Neel and Brownian motion exist, then the total effective relaxation time (τ) for heat dissipation is calculated using **Equation 2.6**:

$$\frac{1}{\tau} = \frac{1}{\tau_N} + \frac{1}{\tau_B}$$
 (2.6)

Theoretically, at a certain particle size, both relaxation times contribute equally to heat generation [23]. However, the Brownian process moves faster for larger particles and lower viscosity fluids, while the Neel mechanism generates heat for small particles and higher viscous

fluids. In hyperthermia, MNPs with ferromagnetic, ferrimagnetic, or superparamagnetic characteristics are injected near the tumor as a biocompatible suspension. When these MNPs are exposed to an oscillating magnetic field, heat is generated through a variety of mechanisms, including Neel relaxation (magnetic moment rotation, which occurs in superparamagnetic NPs), Brownian relaxation (particle rotation, which occurs in all types of NPs), hysteresis loss (which occurs in ferrimagnetism and ferromagnetic NPs), and eddy current [31].

2.4.4 Parameters for Efficient MHT Application:

2.4.4.1 Size and Nature of MNPs:

Particle size has a significant impact on heating efficiency. Specific Absorption Rate (SAR) is a measure of efficient heating. Controlling particle size in the transition region (approximately 20 nm) can shift particle characteristics from ferromagnetic to superparamagnetic resulting in greater SAR values [23]. It is reported that IONPs within the superparamagnetic transition size regime (15-22 nm) exhibit the highest SAR values [32,33]. Guardia et al. [34] observed the heating profile of Magnetite-Fe₃O₄ NPs with varying particle sizes spanning from 12 to 30 nm and observed an increased SAR value of 2277 W g⁻¹ corresponding to 19 nm particle size. Similarly, in another study of Maghemite- γ-Fe₂O₃ NPs with sizes varying from 5-16.5 nm with SAR values of 1650 W g⁻¹ was obtained, the highest value detected for 16.5 nm sized NPs [33]. As the size varies, magnetization also changes correspondingly leading to different SAR values under similar experimental conditions. Comparatively larger-sized (within superparamagnetic range) MNPs developed higher saturation magnetization (Ms) value and consequent higher SAR value. For a better heating effect, the needed particle size must be optimized within the smallest feasible distributions since the SAR value is more heavily reliant on magnetization and relaxation losses [35-37]. Size of MNPs should be adjusted accordingly to correlate with the suitable applied AMF for maximizing SAR value. The optimized size regimes responsible for higher magnetization and SAR values are also attributed to different synthesis routes employed apart from anisotropy and external magnetic factors. If the particle size is less than 20 nm, then the heating due to eddy current is not a concern. Mechanism of each relaxation time is influenced by particle size; the bigger the particle, the higher the Brownian and Neel relaxation times [38].

2.4.4.2 Uniform and Controlled Heating:

The complexity of medical operations will rise due to the non-uniform dispersion of particles, which generates zones with varying amounts of power absorption from AMF at varying rates of heating [39].

2.4.4.3 Biocompatibility:

The biocompatibility of MNPs is a prerequisite for their use in MHT application. So that the immune system does not identify them as foreign materials. If so, the particle is taken up by the Mononuclear Phagocyte System (MPS) by opsonization, which leads to phagocytosis. Shielding of NPs from phagocytosis is essential to achieve optimal performance. To achieve this goal, nanoparticles are coated with hydrophilic biocompatible materials such as Poly Ethylene Glycol (PEG), Poly (Vinyl Alcohol (PVA), Polyethylenimine (PEI), etc. To prevent acute adverse effects from these MNPs, the cytotoxicity of the administered substance should be tested in vitro prior to injection [38]. In vivo experiments in rats showed that with a substantial dosage of 3000 µM of iron-based NPs, no negative effects occurred even after 7 days [40]. Feridex as T₂-contrast agent was authorized by the FDA in 1996 to detect liver lesions. An aqueous colloid of dextran-coated superparamagnetic MNPs is called Feridex. Several dextran-coated MNPs, including Endorem and Resovist, were also authorized for use in clinics within the same time frame. However, in 2009, adverse effects and serious safety concerns led to the withdrawal of Feridex and a few additional contrast agents [41]. Although there are several magnetic materials available, the majority of them are unusable. Magnetic materials, such as spinel ferrites like Magnetite- Fe₃O₄ and Maghemite- γ-Fe₂O₃, are well tolerated by the human body.

2.4.4.4 Colloidal Stability:

To employ MNPs for MHT, they must be colloidally suspended in a biocompatible medium. The stability of MNPs in suspension is regulated by three major factors, namely, a) the type of MNPs (hydrophobic or hydrophilic), b) magnetic properties, and c) Van der Waals forces [8]. Because of the interactions between the sub-nanometer size particles which are hydrophobic, MNPs aggregate to form micron-sized clusters in suspension. Furthermore, magnetic dipole-dipole interactions cause these MNPs to congregate, and when a magnetic field is applied, neighboring clusters get magnetized. Additionally, attractive Van der Waals forces allow MNPs to combine in suspension, lowering the total surface or internal energy. Consequently, this kind of aggregation may lessen MNPs' efficacy in MHT [13].

Ionic strength has a significant impact on the colloidal stability of MNPs, which is crucial for effective biological applications. Colloidal stability in physiological conditions, such as Phosphate Buffer Solution (PBS), can help to assess coating strength. The zeta potential (ζ -potential) and Dynamic Light Scattering (DLS) approach are used to investigate the stability of uncoated MNPs and coated MNPs. Good chemical stability at physiological pH ~7 is

necessary for the use of nanoparticles in biomedicine. Hydrodynamic size regulates the NPs concentration profile in the blood vessel and affects the permeability of NPs out of the vasculature, both of which have an impact on the NPs clearance process.

The ζ -potential of the particles may be used to measure the variation in surface charges, which can be used to control the electrostatic interaction of the nanoparticles. A crucial factor in the biomedical application of nanoparticles as nanomedicine is the determination of ζ -potential. For biomedical applications, the stability of nanoparticles in physiological media such as water, PBS, and ethanol is crucial. The suspension is stable for greater values of ζ -potential. The fact that NPs with high surface charge form stable solutions more easily. For example, the ζ -potential of bare Magnetite- Fe₃O₄ nanoparticles is typically between -30 and +30 mV, depending on the synthesis method, pH, and ionic strength of the medium [42].

2.4.4.5 High Specific Absorption Rate (SAR):

The amount of heat energy lost by the NPs per unit mass of particles per unit time is known as the Specific Loss Power (SLP), or SAR. As a result, the SAR measurement suggests that the temperature of nanoparticles increased in response to the applied field, indicating an increase in their hypothermic efficiency. Such MHT therapy relies on heating the canceraffected area, which may be accomplished by employing MNPs in an AMF to raise the temperature to 42 to 46 °C. MHT can eradicate cancer cells while having little effect on healthy tissues, suggesting that it may be utilized in targeted, cost-effective, and side-effect-free therapies. MHT requires magnetic materials with high SAR values. It takes a lot of MNPs to raise the temperature when SAR values are low, which might lead to further toxicity issues. Reducing MNPs cytotoxicity will increase the efficiency, which is necessary to increase SAR value of MNPs [38,43]. Equation 2.7 is used to calculate the SAR value,

$$SAR = C \times \frac{1}{m} X \frac{\Delta T}{\Delta t} \qquad \qquad \dots (2.7)$$

where, $\Delta T/\Delta t$ = temperature gradient,

C =Specific heat capacity of suspension, and

m =mass of material in suspension.

The SAR data cannot be compared to other systems data due to the tight connection between frequency and magnetic field intensity. While an increase in SAR is associated with a decrease in Intrinsic Loss Power (ILP). Consequently, it makes more sense to talk about heat dissipation in terms of ILP calculated using **Equation 2.8.**

$$ILP = \left(\frac{SAR}{fH^2}\right) \tag{2.8}$$

where, $\Delta T/\Delta t$ = temperature difference,

C =Specific heat capacity of suspension,

m = Mass of material in suspension,

f = Frequency, and

H = Magnetic field intensity.

2.4.4.6 Frequency of Applied AMF:

The amplitude and frequency of the applied AMF also affect the heat loss for MHT. In reality, it is very difficult to raise frequency and amplitude concurrently, therefore one has to choose which of the factors in the limiting product $(H_0.f)$ is preferable. The combination of AC field amplitude and frequency that should be employed depends largely on the type of particles that are available for therapy. Both the magnetic field (H) and the frequency (f) need to be within the medically acceptable and biologically safe ranges. It is believed that the useful field range is when f < 1.2 MHz and H < 15 kAm⁻¹. An adequate value has been reported for fields with H x f smaller than 4.85×10^8 Am⁻¹ s ⁻¹ (Atkinson criterion), which would be acceptable even if the exact limit has not yet been examined [44].

SAR is the amount of heat dissipated by MNPs in an AMF. The heat is generated by the thermal fluctuations of the magnetic moment. An external AMF supplies energy that excites the magnetic moment fluctuations, and this magnetic energy is converted into thermal energy. D. Soto-Aquino and C. Rinaldi [44] explain the Rosensweig analytical equations for power dissipation in a suspension of MNPs. In summary, the magnetization (M_B) of the suspension does not synchronize with the time-varying magnetic field (H_B) due to the thermal fluctuations of the magnetic moment in particles. This phase lag converts magnetic work (M_B x H_B) into internal energy. The average volumetric power dissipation for $f = \omega/2\pi$ of field cycles per second is given by: $P = \mu_0 \pi H_0^2 f \chi''$. The SAR value is given as $SAR = \frac{P}{\rho \phi}$ where *P* is power dissipation, ρ is the mass per unit volume of iron oxide, and φ the volume fraction of particles in the suspension. Hence, as magnetic field intensity and frequency increase, it leads to an increase in heat generation which directly affects the SAR value [44]. The heat generation is affected by permeability and retention impact of the tumor site [45].

2.5 Literature Review on MNPs used for MHT and Chemotherapy:

MNPs can be used in different biological applications with surface modifications. The literature review on the use of MNPs in MHT and Chemotherapy is given in **Table 2.1**.

Carvallho et al. [46] synthesized a biocompatible organic coating layer of MION@CMC where Carboxy Methyl Cellulose (CMC) is a natural cellulose derivative used as a stabilizing ligand, to create ultra-small iron oxide-based superparamagnetic nanoparticles

in an aqueous solution via one-pot green synthesis method. Then MION@CMC nano colloids and the anticancer drug DOX were covalently bonded to form MION@CMC-DOX, which forms magneto polymerases with a hybrid core-shell structure. These nanohybrids were successfully used for in vitro chemotherapy and MHT against brain cancer cells.

Khaledian et al. [47] studied the PLA (Poly (Lactic Acid)) -PEG-FA (Folic Acid) SPIONs loaded with DOX to deliver SPIONs and DOX to tumor cells. Using MTT (3-[4,5-dimethylthiazol-2-yl]-2,5 diphenyl tetrazolium bromide) and flow cytometry assay, the cytotoxicity, cellular uptake, and apoptotic impact of DOX-loaded PLA-PEG-FA SPIONs were quantitatively assessed on two cell lines, HeLa and CT26. Additionally, in vitro hyperthermia study with PLA-PEG-FA SPIONs loaded with DOX was carried out.

Song et al. [48] describe a drug-loaded ferrimagnetic micelle with a flowable core which is used in conjunction with chemotherapy to achieve efficient MHT. Ferrimagnetic iron oxide nanocrystals in the form of cubes coated with Poly Ethylene Glycol-Poly (2-Hexoxy-2-oxo-1,3,2 dioxaphospholane) (mPEG-b-PHEP) were chosen as MHT mediators due to their superior magnetic performance.

Serio et al. [49] studied biodegradable and biocompatible polymer-coated (PCL) electro spun fibers co-loaded with magnetic iron oxide nano cubes (IONCs), which exhibit remarkable thermal properties, to facilitate their activation under MHT of clinical use. Additionally, the anticancer drug DOX was included in the polymer fiber for combined hyperthermia and heat-enhanced drug release.

Mirzaghavami et al. [50] conducted a study on PEG/PCL based synthesis of a triblock copolymer coupled with FA ligand, a nano-micelle was formed for a delivery of 5-FU (Fluorouracil) drug. Using the MTT assay, cell viability was studied against a range of colon cancer cell lines (HT29, Caco-2, SW480, and HCT116) and human umbilical vein endothelial cells (HUVEC). Subsequently, the most 5-FU resistant colon cancer cell line HT29 was selected for additional studies. The cellular absorption of nanoparticles in two distinct cell lines (HT29 and HUVEC) and colon tumor tissues was assessed to examine the function of folic acid as a targeting ligand.

Mai et al. [51] studied Photo Induced Copper Mediated Radical Polymerization (PI-CMRP) by synthesizing cubic nanoparticles. IONC coated with PEG were synthesized using standard Schlenk line method and conjugated with DOX, which was placed within the thermoresponsive shell for MHT treatment. An in vivo xenograft tumor model was formed using A431 epidermoid carcinoma cells.

Alkhayal et al. [52] synthesized Magnetite- Fe₃O₄ nanocomposites using a simple microwave hydrothermal synthesis process for MHT. The Reduced Graphene Oxide (r-GO) and PEG were used to make the synthesized nanoparticles biocompatible. The cell cytotoxicity against human kidney and breast cancer cells reveals survival of >70% demonstrating their suitability for in vivo investigations. The performance of nano composites in different dispersion media was examined for their potential use in MHT.

Eskandani et al. [53] designed a smart DDS for cancer chemotherapy using MHT, a new folate-conjugated pH- and thermal-responsive magnetic hydrogel made of PVA, Poly(N-isopropylacrylamide) (PNIPAAm), and folate-conjugated Poly (Acrylic Acid) (PAA-FA). Drug DOX was added to the DDS, and the drug loading efficiency and the drug release profiles were studied at different values of pH and temperature. Using the MTT test, the anti-cancer efficacy of the produced DDS was assessed in chemotherapy alone and with hyperthermia also.

Liao et al. [54] suggested a magnetic nanoparticle-based ferroptosis-inducing nanoplatform using Magnetite-Fe₃O₄ nanoparticles loaded with Lonidamine (LND) drug. The Magnetite-Fe₃O₄ -LND again modified with PEG and coupled with Bis [3- (Tri Ethoxysilyl) propyl] Tetra Sulfide (BTES) containing disulfide linkages as the organosilica precursor. When these magnetic nanoparticles, along with Lithium Manganese Iron Phosphate (LFMP) were administered, the disulfide bonds in the nano platform experienced a sulfhydryl-disulfide exchange reaction that depleted GSH and rendered GPX4 inactive. When disulfide bonds break, the nanoparticle breaks down and releases LND. Moreover, under an AMF, synergistic effect was observed.

Lan et al. [55] synthesized Poly (Methacryloyloxyethyl Phosphoryl Choline) (MPC) based platform with DOX (FA- β -Cyclodextrin (β -CD)/DOX@Cu²⁺@ Gum Arabic (GA)@ Fe₃O₄) to release therapeutic drugs by pH/GSH stimulation, resulting in effective tumor-specific chemotherapy/Chemo Dynamic Therapy (CDT).

 Table 2.1: Literature review of MNPs for MHT and chemotherapy.

Sr. No	MNPs	Surface Modifier	Method	Application	Ref.
1.	Magnetite- Fe ₃ O ₄	Carboxy Methyl Cellulose (CMC)	One-pot green process	Magnetic Hyperthermia and Chemotherapy	[46]
2.	Magnetite- Fe ₃ O ₄	Poly (Lactic Acid) (PLA), Poly Ethylene Glycol (PEG), Folic Acid (FA)	Co- precipitation	Combined Thermotherapy and Chemotherapy	[47]
3.	Magnetite- Fe ₃ O ₄	Poly Ethylene Glycol-Poly (2-Hexoxy-2-oxo-1,3,2 dioxaphospholane) (mPEG-b-PHEP)	Schlenk line Method	Combined Magnetic Thermotherapy and Chemotherapy	[48]
4.	Iron Oxide Nanocubes (IONCs)	Poly Capro Lactone (PCL)	One pot synthesis	Combined Magnetic Hyperthermia and Drug delivery	[49]
5.	Magnetite- Fe ₃ O ₄	Folic Acid-conjugated PEG-PCL-PEG	Double emulsion solvent evaporation method	Drug Delivery	[50]
6.	IONCs	PEG	Schlenk line techniques	Drug delivery and Magnetic hyperthermia	[51]
7.	Magnetite- Fe ₃ O ₄	Reduced Graphene Oxide (RGO), PEG	Microwave Hydrothermal synthesis	Magnetic Hyperthermia	[52]
8.	Magnetite- Fe ₃ O ₄	Poly (Vinyl Alcohol) (PVA), Poly (N-Iso Propyl Acryl Amide) (PNIPAAm), folate- conjugated Poly (Acrylic Acid) (PAA-FA)	Reflux Method	Chemotherapy and Magnetic hyperthermia	[53]
9.	Magnetite- Fe ₃ O ₄	Lonidamine (LND), PEG- Modified Magnetic Organic Mesoporous Nanoparticles (MONs- PEG), Bis [3- (Tri Ethoxy Silyl) propyl-tetra sulfide (BTES)	Soft- Templating Methodology	Magnetic Hyperthermia	[54]
10	Magnetite- Fe ₃ O ₄	Gum Arabic (GA), β- Cyclodextrin (β-CD), Folic Acid (FA)	Co- precipitation	Chemo Dynamic Therapy	[55]

References:

- 1. Wilt T, MacDonald R, Rutks I, Shamliyan T, Taylor B, Kane R. Ann. Intern. Med. 148 (6) (2018) 435-48.
- 2. Kelly K, Jacobson J, Kennedy D, Braudt S, Mallick M, Weiner M. Journal of Pediatric Hematology/Oncology. 22 (5) (2000) 412-6.
- 3. De Visser K and Joyce J. Cancer cell. 41 (3) (2023) 374-403.
- 4. Mo R and Gu Z. Mater. Today. 19 (5) (2016) 274-83.
- 5. Gonzalez-Rodriguez R, Campbell E, Naumov A. PLoS One. 14 (6) (2019) e0217072-90.
- 6. Estelrich J and Busquets M. Mol. 23 (7) (2018)1567-93.
- 7. Laracuente M, Marina H, McHugh K. J. Control. Release. 327 (2020) 834-56.
- 8. Tian H, Zhang T, Qin S, Huang Z, Zhou L, Shi J, Nice E, Xie N, Huang C, Shen Z. J. Hematol. Oncol. 15 (1) (2022) 132-72.
- 9. Moroz P, Jones S, Gray B. Int. J. Hyperth. 18 (4) (2002) 267-84.
- 10. Mornet S, Vasseur S, Grasset F, Duguet E. J. Mater. Chem. 14 (14) (2004) 2161-75.
- 11. Lu A, Salabas E, Schüth F. Angew. Chem. Int. Ed. 46 (8) (2007) 1222-44.
- 12. Zhou X. Magnetism in medicine: a handbook, Medical Physics. 34 (12) (2007) 4978-80.
- 13. Gilchrist R, Medal R, Shorey W, Hanselman R, Parrott J. Taylor. Ann. Surg. 146 (4) (1957) 596-606.
- 14. Jordan A, Scholz R, Maier-Hauff K, Johannsen M, Wust P, Nadobny J, Schirra H, Schmidt H, Deger S, Loening S, Lanksch W. J. Magn. Magn. Mater. 225 (1-2) (2001) 118-26.
- 15. Kim D, Nikles D, Johnson D, Brazel C. J. Magn. Magn. Mater. 320 (19) (2008) 2390-96.
- 16. Ghosh Chaudhuri R and Paria S. Chem. Rev.112 (4) (2012) 2373-433.
- 17. Andreu I and Natividad E. Int. J. Hyperth. 29 (8) (2013) 739-51.
- 18. Chen Z, Han F, Du Y, Shi H, Zhou W. Signal Transduct. Target. Ther. 8 (1) (2023) 70-94.
- 19. Wu K and Wang J. AIP Advances. 7 (5) (2017) 056327-35.
- 20. Maier-Hauff K, Ulrich F, Nestler D, Niehoff H, Wust P, Thiesen B, Orawa H, Budach V, Jordan A. J. Neuro-Oncol. 103 (2) (2011) 317-324.
- 21. Zhao, S, Yu, X, Qian, Y, Chen W, and Shen J. Theranostics. 10 (14) (2020) 6278-309.
- 22. Liu W, Pei W, Moradi M, Zhao D, Li Z, Zhang M, Xu D, Wang F. ACS Appl. Mater. Interfaces. 14 (16) (2022) 18794-805.
- 23. Fortin J, Wilhelm C, Servais J, Menager C, Bacri J, Gazeau F. J. Am. Chem. Soc. 129 (9) (2007) 2628-35.
- 24. Hergt R and Dutz S. J. Magn. Magn. Mater. 311 (1) (2007) 187-92.
- 25. Aharoni A. Introduction to the Theory of Ferromagnetism. Clarendon Press; 109 (2000) 1-315.
- Goldman A. Handbook of modern ferromagnetic materials. Springer Science & Business Media.
 505 (2012) 1-643.
- 27. Dobson J. Gene Therapy. 13 (4) (2006) 283-87.

- 28. Gavilan H, Avugadda S, Fernandez-Cabada T, Soni N, Cassani M, Mai B, Chantrell R, Pellegrino T. Chem. Soc. Rev. 50 (20) (2021) 11614-67.
- 29. Attaluri A, Ma R, Qiu Y, Li W, Zhu L. Int. J. Hyperth. 27 (5) (2011) 491-502.
- 30. Hergt R, Dutz S, Muller R, Zeisberger M. J Phys Condens Matter. 18 (38) (2006) S2919-34.
- 31. Hergt R, Dutz S, Roder M. J Phys Condens Matter. 20 (38) (2008) 385214-26.
- 32. Yamamoto Y, Horiuchi K, Takeuchi M, Tanaka N, Aihara R, Takeuchi N, Fujita S. J. Appl. Phys. 116 (12) (2014)123906-13.
- 33. Lima E, Torres T, Rossi L, Rechenberg H, Berquo T, Ibarra A, Marquina C, Ibarra M, Goya G. J. Nanoparticle Res. 15 (1654) (2013) 1-11.
- 34. Guardia P, Di Corato R, Lartigue L, Wilhelm C, Espinosa A, Garcia-Hernandez M, Gazeau F, Manna L, Pellegrino T. ACS nano. 6 (4) (2012) 3080-91.
- 35. Manohar A, Vijayakanth V, Vattikuti S, Manivasagan P, Jang E, Chintagumpala K, Kim K. ACS Appl. Mater. Interfaces. 5 (4) (2022) 5847-56.
- 36. Obaidat I, Narayanaswamy V, Alaabed S, Sambasivam S, Muralee Gopi C. Magnetochemistry. 5 (4) (2019) 67-107.
- 37. Vassallo M, Martella D, Barrera G, Celegato F, Coisson M, Ferrero R, Olivetti E, Troia A, Sozeri H, Parmeggiani C, Wiersma D. ACS omega. 8 (2) (2023) 2143-54.
- 38. Mohapatra J, Xing M, Liu J. Materials. 12 (19) (2019) 3208-38.
- 39. Throat N, Shinde K, Pawar S, Brick K, Betty C, Ningthoujam R. Dalton trans. 41 (10) (2012) 3060-71.
- 40. Guo C, Weber R, Buckley A, Mazzolini J, Robertson S, Delgado-Saborit J, Rappoport J, Warren J, Hodgson A, Sanderson P, Chipman J. Int. J. Mol. Sci. 22 (2) (2021) 556-80.
- 41. Petrov K and Chubarov A. Encyclopedia. 2 (4) (2022) 1811-28.
- 42. Veiseh O, Gunn J, Zhang M. Adv Drug Deliv Rev. 62 (3) (2010) 284-304.
- 43. Hamley I. Chem. Int. Ed. 42 (15) (2003)1692-712.
- 44. Soto-Aquino D and Rinaldi C. J. Magn. Magn. Mater. 393 (2015) 46-55.
- 45. Neuberg T, Schopfa B, Hofmann H, Hofmann M, Rechenberg B. J. Magn. Magn. Mater. 293 (1) (2005) 411-18.
- 46. Carvalho S, Leonel A, Mansur A, Carvalho I, Krambrock K, Mansur H. Biomater. Sci. 7 (5) (2019) 2102-22.
- 47. Khaledian M, Nourbakhsh M, Saber R, Hashemzadeh H, Darvishi M. Int J Nanomedicine. 15 (2020) 6167-82.
- 48. Song Y, Li D, Lu Y, Jiang K, Yang Y, Xu Y, Dong L, Yan X, Ling D, Yang X, Yu S. Natl. Sci. Rev. 7 (4) (2020) 723-36.
- 49. Serio F, Silvestri N, Avugadda S, Nucci G, Nitti S, Onesto V, Catalano F, D'Amone E, Gigli G, Del Mercato L, Pellegrino T. J. Colloid Interface Sci. 607 (1) (2022) 34-44.
- 50. Mirzaghavami P, Khoei S, Khoee S, Shirvalilou S. Cancer Nanotechnol. 13 (1) (2022) 12-20.

- 51. Mai B, Balakrishnan P, Barthel M, Piccardi F, Niculaes D, Marinaro F, Fernandes S, Curcio A, Kakwere H, Autret G, Cingolani R. ACS Appl. Mater. Interfaces. 11 (6) (2019) 5727-39.
- 52. Alkhayal A, Fathima A, Alhasan A, Alsharaeh E. Nanomaterials. 1 (9) (2021) 2398-412.
- 53. Eskandani M, Derakhshankhah H, Jahanban-Esfahlan R, Jaymand M. Drug Deliv Sci Technol. 84 (2023) 104449.
- 54. Liao Z, Wen E, Feng Y. J. Nanobiotechnology. 22 (1) (2024)147-64.
- 55. Lan Z, Tan X, Chen C, Cao Y, Wan Y, Feng S. J. Biomater. Sci. Polym. Ed. 34 (15) (2023) 2041-59.

CHAPTER-03 EXPERIMENTAL TECHNIQUES

INDEX

Sr.No			Title	Page No.
3.1	Introdu	ction		49
3.2	Synthes	50		
	3.2.1	3.2.1 Steps Involved During Precipitation		
	3.2.2	Factors Influencing Co-Precipitation Process		52
		3.2.2.1	Effect of Solvent	52
		3.2.2.2	Effect of Precursor	53
		3.2.2.3	Effect of Concentration	53
		3.2.2.4	Effect of pH	53
		3.2.2.5	Effect of Temperature	54
		3.2.2.6	Effect of Stirring Speed	54
		3.2.2.7	Effect of Reaction Time	54
3.3	Surface	54		
3.3	3.3.1	.1 Introduction		
	3.3.2	Need for	56	
	3.3.3	Stabilizir	60	
		3.3.3.1	Core Shell Configuration	62
		3.3.3.2	Organic Materials	62
		3.3.3.3	Small Molecules and Surfactants	63
		3.3.3.4	Polymers	64
		3.3.3.5	Biomolecules	65
		3.3.3.6	Inorganic Materials	66
		3.3.3.7	Carbon	67
		3.3.3.8	Metals	67
		3.3.3.9	Metal Oxides	68
		3.3.3.10	Metal Sulfides and Selenides	69
		3.3.3.11	Bimagnetic Materials	69
		3.3.3.12	Ternary Structure and Multilayer Core-Shell Structure	70
		3.3.3.13	Organic-Inorganic Composite Structure	70

3.4	Charac	71		
	3.4.1	Introduct	71	
	3.4.2	Structural/Phase Analysis		71
		3.4.2.1	X-Ray Diffraction (XRD)	71
		3.4.2.2	Transmission Electron Microscopy (TEM)	73
		3.4.2.3	Fourier Transforms Infrared Spectroscopy (FTIR)	73
	3.4.3	Morphol	ogical Study	74
		3.4.3.1	Scanning Electron Microscopy (SEM)	74
	3.4.4	Function	alization and Particle Size Study	76
		3.4.4.1	Zeta Potential	76
		3.4.4.2	Dynamic Light Scattering (DLS)	76
	3.4.5	Magnetic Characterization		77
		3.4.5.1	Magnetic Induction Heating	77
		3.4.5.2	Vibrating Sample Magnetometer (VSM)	78
3.5	Biocon	79		
	3.5.1	Cell Vial	80	
	3.5.2	Hemolysis Assay		82
	Refere	83		

3.1 Introduction:

Synthesis of nanomaterials is generally categorized using physical, chemical, biological, or hybrid methods. The physical method, often known as the top-down or destructive approach, begins with bulk matter and progresses to smaller particles until nanoscale size is reached [1,2]. Chemical synthesis involves combining materials in a wet condition and adjusting reaction parameters to produce nanomaterials. This method is also known as the bottom-up approach, which starts with atoms, molecules, or ions in solution. Initiate with nucleating and then aggregating to produce nano-size particles [1]. Solvothermal, pyrolysis, microwave irradiation, chemical co-precipitation, sol-gel, microemulsion, and thermal decomposition all are included in this approach [1]. Biological synthesis uses microorganisms or plant extracts as a precursor to synthesize the required nanomaterials [3].

Different methods have been employed for the synthesis of Magnetic Nanoparticles (MNPs), including co-precipitation, chemical vapour deposition, thermal decomposition, laser pyrolysis, microwave-assisted, sonochemical. solvothermal, microemulsion, combustion, and carbon arc. Various innovative and efficient methods have been employed to synthesize Magnetite- Fe₃O₄ nanoparticles with different sizes and shapes (nanorods, nanotubes, and hierarchical superstructures) [4]. Co-precipitation is the most effective synthesis method among all those listed for synthesizing MNPs with regulated sizes and magnetic properties [5]. However, a detailed analysis of synthesized MNPs is necessary for the application-based study [6]. Using different characterization, one can analyze the shape, dimensions, size, orientation, crystallinity, magnetic properties, dispersion and intercalation of nanoparticles, zeta potential, wettability, adsorption potential, aggregation, etc [7]. Techniques such as Powder X-ray Diffraction (XRD), Transmission Electron Microscopy (TEM), Scanning Electron Microscopy (SEM), Fourier Transform Infrared Spectroscopy (FTIR), Dynamic Light Scattering (DLS), Zeta (ζ) potential, and Vibrating Sample Magnetometer (VSM) used to ascertain the properties of synthesized nanoparticles [7].

It is important to discuss tumor toxicity, pharmacokinetics, bio-distribution, and other biological characteristics of MNPs in addition to their biocompatibility with normal tissues. This study is important due to the diverse therapeutic applications of MNPs in cancer treatment, including drug delivery, cancer immunotherapy, Magnetic Hyper Thermia (MHT), and photodynamic therapy [8].

3.2 Synthesis of MNPs by Chemical Co-Precipitation Method:

The methods used for the synthesis of MNPs affect the physicochemical properties of synthesized nanoparticles such as size, shape, aggregation state, and surface chemistry. MNPs made by physical methods like mechanical milling have a broad size distribution (10-1000 nm), which renders them unsuitable for in vivo applications [9]. Consequently, chemical methods overcame the limitations of physical methods because of their high yield and efficacy in regulating nanoparticle size, which is necessary to prevent opsonization and subsequent clearance by the Reticulo Endothelial System (RES) [9]. Moreover, particles of a diameter between 10 to 40 nm are required for continuous blood circulation [10].

Precipitation from soluble liquids, which produces an insoluble solution by dissolving metal precursors in a common solvent, such as water, was one of the earliest methods to synthesize nanoparticles. Massive particle production is one advantage of precipitation procedures. To form uniform particles, a homogeneous precipitating process that separates nucleation from nuclei growth is commonly used [11]. In the process of synthesis of Magnetite- Fe₃O₄ nanoparticles, a 1:2 ratio of salts (such as Fe²⁺ and Fe³⁺) is dissolved in water. To precipitate the starting material while keeping the temperature below 100°C, a base solution [usually, KOH, NH₃OH, NaOH, or N(CH₃)₄OH] is added to a salt solution and constantly stirred [12].

Equation 3.1 depicts the general process that occurs when iron oxide (Magnetite) is formed.

$$Fe^{2+} + Fe^{3+} + 80H \rightarrow Fe_3O_4 + 4H_2O$$
 (3.1)
Magnetite

The final reaction product is obtained by filtering the precipitation of the relevant metal oxide and then annealing it. The co-precipitation approach offers several benefits, including good product purity, repeatability, minimal cost, and maximum yield. The morphology, size, composition, and form of the generated particles are highly influenced by the reaction circumstances (temperature, pH, ionic strength, type of base solution, etc). This method produces iron oxide particles that are often unstable, therefore they need to be functionalized with surfactants or polymers until they stabilize [12].

3.2.1 Steps Involved During Precipitation:

Nucleation, growth, coarsening, and agglomeration all occur simultaneously during chemical co-precipitation (Fig.3.1). Smaller-sized particles formed at the initial step of

precipitation, known as nucleation. All of the monomers present must develop simultaneously in a process called nuclei growth, whereby these precipitates tend to merge to create bigger, thermodynamically more stable particles. A detailed discussion of the precipitation process is given below.

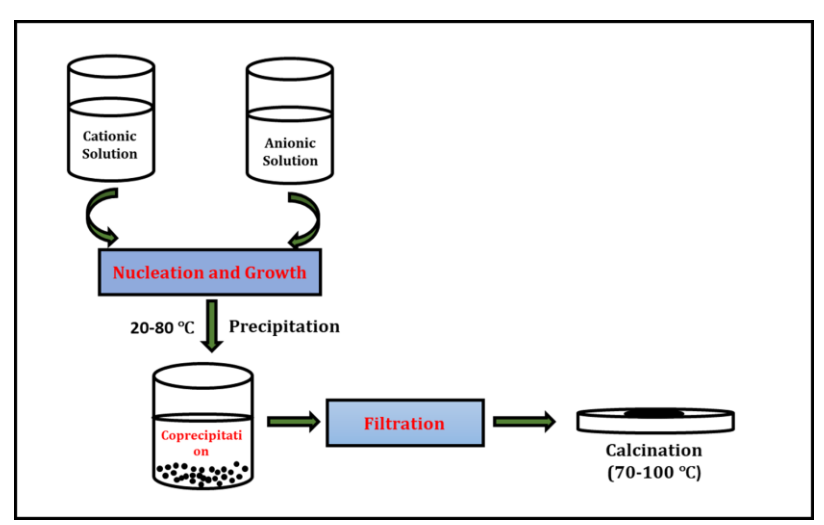


Fig.3.1: Synthesis of nanoparticles by coprecipitation method.

a) Liquid Mixing/Supersaturation:

Precipitation largely depends on how the constituent parts of the solution are mixed initially. Effective mixing can yield more homogeneous byproducts in co-precipitation. Also, the agglomeration is influenced by stirring rate. The nucleation process is more affected by the stirring rate than that of growth. Adjustments to the stirring rate and mixing technique can impact the aggregate size. Within a supersaturated zone, particles can form by nucleation or growth [13].

b) Nucleation and Growth:

Nucleation cannot take place unless the solution is supersaturated. In the supersaturated area, precipitation occurs with even a small disturbance because the system is not stable. During precipitation, a nucleus that can expand on its own is formed. A nucleus is the smallest collection of atoms, molecules, or ions in a solid phase. Nuclei are formed and precipitation starts when the concentration rises over a threshold point.

Once the nucleation process stops, the formation of clusters starts, and more monomers are added, which can develop on their own until a certain size is attained. Larger clusters continue to expand, whereas smaller clusters typically disintegrate again. When the concentration falls below the critical threshold due to the consumption of precursors by nucleation or growth processes, only the growth of pre-existing particles continues. Ions are

adsorbed onto the surface of seeded particles, causing growth to begin. Temperature, pH, and concentration affect this growth characteristic. If nucleation proceeds more quickly than growth, a narrow dispersion of tiny particles is produced by the system. While rapid growth causes the distribution of big particles to become narrower [13].

c) Aggregation of the Primary Particles:

One important stage that results in larger, more numerous, but still porous particles is agglomeration. Clusters of nanometre sized particles agglomerate to form secondary particles of micrometer size. Chemical and physical interactions can bind these particles together. The porosity of the spaces between primary particles is determined by particle stacking. When carbonates or metal hydroxides are used as a base they precipitate at extremely high supersaturation; therefore, nucleation happens spontaneously leading to aggregation [13]. The nucleation, growth, and aggregation mechanism in the coprecipitation method is shown in Fig.3.2 using the La Mer model [14].

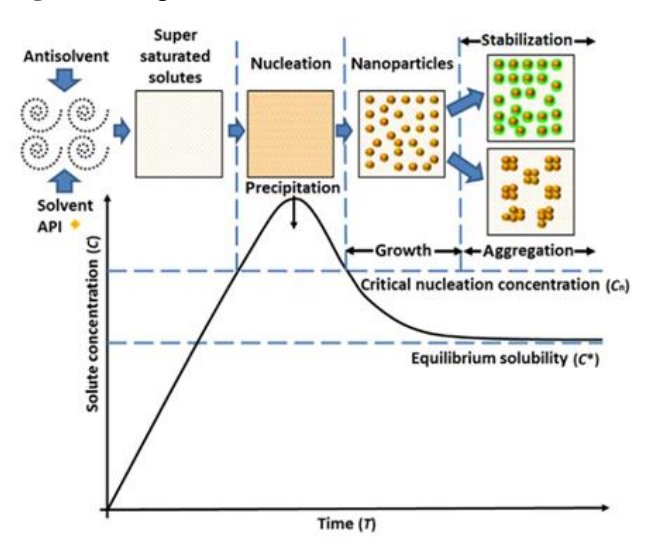


Fig.3.2: Nucleation and growth of MNPs based on the La Mer model [14].

3.2.2 Factors Influencing Co-Precipitation Process:

Several variables (shown in **Fig.3.3**) affect the purity, particle size, surface area, pore size, and pore volume of synthesized MNPs. These variables include pH, temperature, stirring speed, type of solvent, reaction time, etc.

3.2.2.1 Effect of Solvent:

Water is always used as a solvent in material synthesis because it is cost-effective. The use of organic solvents (Tetrahydrofuran (THF), acetonitrile, Dimethyl Sulfoxide (DMSO), acetone, Dimethyl Formamide (DMF), and ethanol) comes with a significantly higher cost.

Moreover, the majority of metal salts that are utilized as precursors dissolve in organic solvents poorly. Organic solvents have limited applications because of their negative environmental effects but they improve the quality of the results [13].

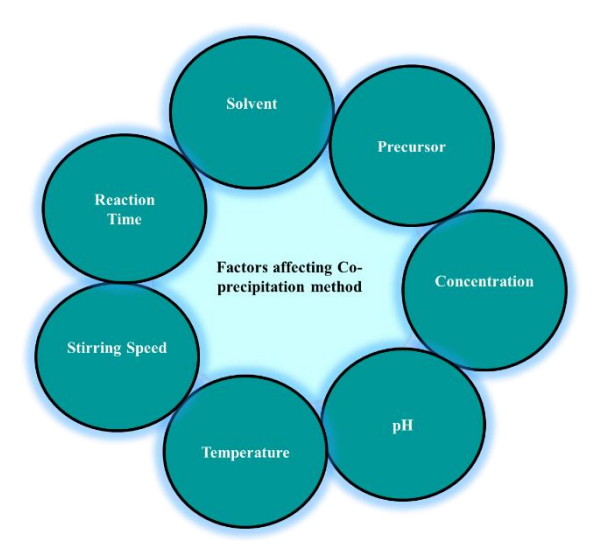


Fig.3.3: Factors affecting the coprecipitation method.

3.2.2.2 Effect of Precursor:

Precursors containing counter ions that quickly break down into volatile products are frequently used. Ammonia, sodium carbonate, and hydroxides are utilized as precipitants, while metal precursors such as chlorides, nitrate, and sulphate salts are selected as reactants. Repeated washing is required to remove the loosely bonded ions from the precipitate [13].

3.2.2.3 Effect of Concentration:

Precipitation occurs at high metal ion concentrations, which is obtained by decreasing the vessel volume, which increases the space-time yields. More supersaturation also causes precipitation to occur more quickly. Higher concentration levels lead to greater surface areas and smaller particle sizes due to an enhanced rate of nucleation [13].

3.2.2.4 Effect of pH

pH influences the degree of supersaturation which alters the outcomes [13]. As the base quantity or pH increases, the size of the nanoparticles reduces slightly. The reduction in particle size with increased pH value is due to the increased nucleation overgrowth and higher supersaturation rate [15]. Research has also demonstrated that controlling the final pH and ionic strength of non-complexing salt solutions influences nanoparticle size. The results show that when pH and ionic strength increase the average particle size decreases [16]. The addition of the basic solution to the mixed Fe²⁺ and Fe³⁺ ion solution, whether done slowly or quickly,

affects the size of the final product. The quick addition promotes continual nucleation regarding growth, allowing the production of small-size particles [15]. Particle sizes are also influenced by the kind of precipitating base. Under the following sequence, a reduction in magnetite size may be ascertained by the precipitating nature of the base: $(C_2H_5)_4NOH < KOH < NaOH$ [15].

3.2.2.5 Effect of Temperature:

The exact kind and degree to which precipitation temperature influences is still unpredictable, therefore the selection process normally involves trial and error. The initial size of the crystallite, surface area, and phase development of the precipitate are all dependent on the temperature of the precipitation. For example, for particles with a size of 9 nm, the time needed for full oxidation of Fe²⁺ ions was 3 h at 80°C, compared to almost 3 months at room temperature [17]. A temperature rise might lead to a larger crystallite. This might be because, temperature rise improves solubility, which lowers solvent supersaturation and eventually accelerates growth to produce larger-sized particles.

3.2.2.6 Effect of Stirring Speed:

The stirring speed influences the particle size of MNPs for crystallization and solid-catalyzed processes. The dispersed phase must be uniformly spread throughout the liquid, necessitating higher stirring rates. In addition, when the stirring rate increases, the homogeneity of the reaction solution improves, resulting in smaller particles and narrower size dispersion [18].

3.2.2.7 Effect of Reaction Time:

The size and magnetic characteristics of precipitated particles are affected by the rate of alkali addition and the reaction time. According to the literature, it is observed that 300 s is needed for the digestion process to finish the development of magnetite nanoparticles and achieve a state of thermodynamic equilibrium. It has been observed that the particle size grows from 6.7 to 8.2 nm during the development stage (22-300 s). Above 300 s, agglomeration is possible [19].

3.3 Surface Functionalization:

3.3.1 Introduction:

Surface functionalization is also referred to as surface engineering of nanoparticles. When modifying the magnetic core particles to incorporate coatings, it offers steric and/or electrostatic repulsive interactions. The NPs coating needs to be non-toxic in addition to

stable. During synthesis, Iron Oxide Nanoparticles (IONPs) are coated with either inorganic or organic compounds to inhibit oxidation and aggregation [20].

However, by covering the surface of nanoparticles, the toxicity of the particles can be decreased. In general, surface coatings have a quicker rate of circulation and can lessen typical tissue toxicity. It also stabilizes nanoparticles and prevents harmful ion leakage from NPs. For example, Serum protein optonin shortens circulation time and improves phagocytosis by adhering to the surface of hydrophobic nanoparticles [21]. Unnecessary RES absorption decreases the bioavailability of nanodrugs and increases their toxicity to the patient. The hydrophobicity of nanoparticles brings about the process of phagocytic internalization and particle clearance as shown in Fig.3.4 (1). In Fig.3.4 (1), (A) shows the hydrophobic nanoparticles in blood circulation are recognized as foreign bodies; (B) and (C) show phagocytosis by phagocytes leading to nanoparticle elimination. Therefore, covering the hydrophobic surface of nanoparticles with a layer of hydrophilic materials increases the possibility of targeting cells while decreasing the ability of the immune system to identify it as given in Fig.3.4 (2) which increases the circulation period of targeted nanocarrier in the blood and creates steric repulsive forces against plasma proteins. In Fig.3.4 (2), (A) shows hydrophilic polymer-coated nanoparticles circulating in the bloodstream; (B) and (C) illustrate endocytosis by target cells [22]. A hydrophilic, non-ionic, flexible, and biocompatible polymers that serve as surface protectors are used for surface functionalization, such as Poly Ethylene Glycol (PEG), and Poly Vinyl Pyrrolidone (PVP), etc [23].

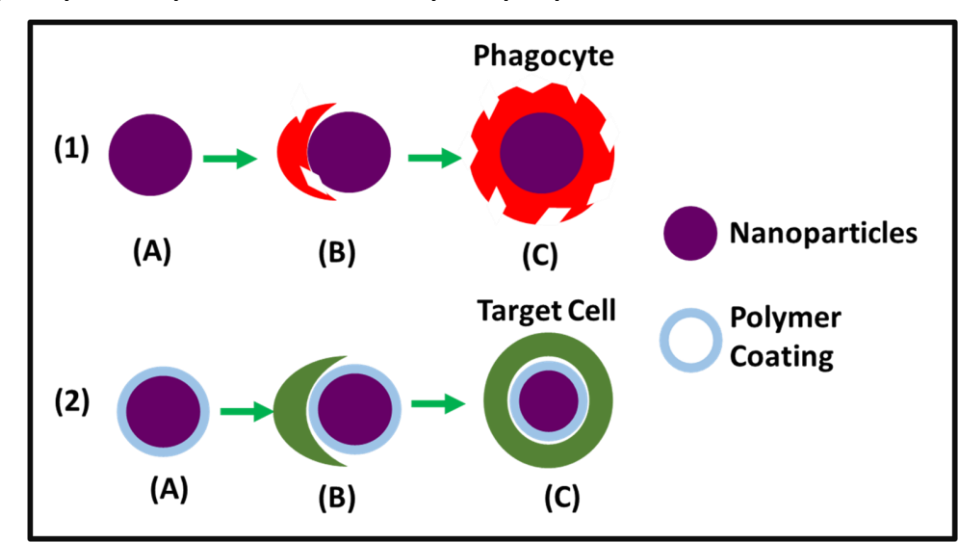


Fig.3.4: (1) Elimination of hydrophobic nanoparticles and (2) Coated hydrophilic nanoparticles in blood circulation.

It has been observed that the half-life of PEG-coated nanoparticles is more than 7 h, but in the absence of PEG, it is less than a minute [24]. Additionally, blood circulation time is accelerated by increasing the PEG content on nanoparticles. PEG is used in tablets as lubricants and binders, is nontoxic and antimicrobial, and is extremely soluble in water and not absorbed by humans [25].

3.3.2 Need for Surface Functionalization:

Functionalization of MNPs is necessary for their efficient use in biological applications. As illustrated in **Fig.3.5**, the optimal surface functionalization should prevent MNPs from aggregating, provide guidance to improve water compatibility, enhance colloidal stability, stabilize the surface, and render nanoparticles biocompatible.

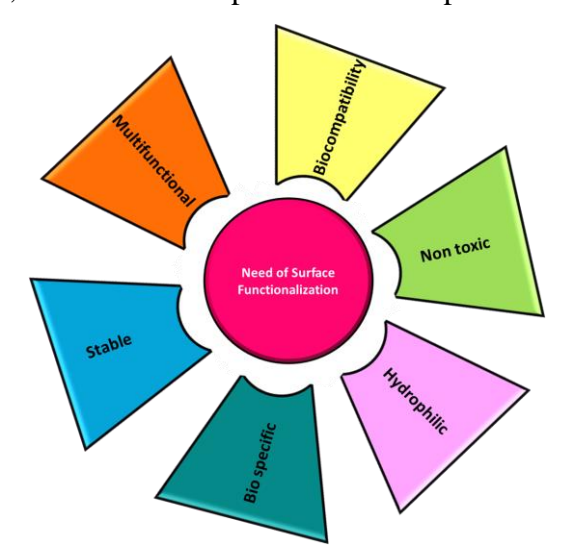


Fig.3.5: Need of surface functionalization for biomedical applications.

a) Stabilization Against Aggregation:

The primary benefits of using particles smaller than 100 nm: the enhanced tissular diffusion, decreased sedimentation rates (high stability in suspension), and increased effective surface areas, which facilitate ligand attachment. Particles must be tiny (less than 100 nm) to be able to pass through the RES. After injection, they need to stay in the bloodstream and can flow via organs and tissue capillary networks without causing a vascular embolism. IONPs are highly magnetic and tend to aggregate due to strong magnetic dipole-dipole interaction. Due to this tendency of MNPs, large clusters are obtained having a size of a few microns. Surface functionalization of MNPs creates a non-magnetic layer on the surface which lowers magnetic dipole-dipole interaction and prevents the formation of large aggregates. Depending on the particle system and the right selection of surfactants, particles get dispersed in aqueous

media [26].

Using organic solvents, ligand molecules can be applied to the surface of MNPs to stop the particles from aggregating. Dynamic binding and unbinding processes are caused by interactions between the surface of nanoparticles and an electron-donating group of a ligand molecule [27,28]. To reduce the agglomeration of nanoparticles, two primary techniques are employed: steric and electrostatic stabilization.

Steric Stabilization:

For MNPs to remain colloidal stable throughout a wide pH range and at high salt concentrations, steric stabilization is required. It depends on the polymeric material used on the surface of MNPs and can be achieved by functionalizing MNPs with ligand shells or embedded polymeric matrix. The resulting repulsive potential may be tracked using the polymer density, polymer molar mass, solvent quality, and binding. When the central core of two sterically stable base materials moves towards one another. The polymer layer prevents the aggregation/dipole-dipole moment. It promotes colloid stability by increasing the osmotic pressure between MNPs and decreasing the entropy of polymers [29,30].

Electrostatic Stabilization:

The formation of clusters of colloidal suspension can be accompanied by experimentation and electrostatic stability by varying the salt content [31]. The stability factor is determined by turbidimetric measurements or light scattering, and parameters linked to colloidal stability as a function of salt concentration. At this concentration, it is possible to inhibit electrostatic layers.

According to the Derjaguin, Landau, Verwey, and Overbeek (DLVO) theory, the absence of a steric stabilizing layer explains the interaction of the MNPs. According to DLVO theory, the aggregation of aqueous dispersion quantifies the force between charged surfaces interacting through a liquid medium. The phenomenon known as the "double layer of counterions" combines electrostatic repulsion with van der Waals attraction. Stabilization works well in electrostatic nanoparticles with low salt concentrations and pH levels at or below the isoelectric point [32,33].

b) Estimation of Surface Charge with Colloidal Stability:

MNPs must be functionalized in liquid media for biomedical applications. Particles covered with specific shells of surfactants or polymers are used to stabilize magnetic fluids. While there are now several methods for stabilizing water-based ferrofluids, aggregation

cannot be prevented when it comes to biological media [34]. In the biological environment, the formation of aggregation has adverse consequences such as the difficulty of removing nanoparticles from organisms, the possibility of blood clots, and a loss in therapeutic efficacy. Thus, for magnetic fluids to be developed for use in biological applications, an understanding of their aggregation regimes is essential.

Drug delivery techniques involving colloidal NP-based carriers, show promise in cancer treatment, owing to the fast advancement of nanotechnology. Micelles, liposomes, dendrimers, and polymers are some of the several macromolecular forms proposed for drug delivery. Superparamagnetic Iron Oxide Nanoparticles (SPIONs) surface functionalized with various polymers and linkers are as shown in **Fig.3.6**. There are several methods by which the drug is encapsulated, adsorbed, linked, or trapped in nano-matrices. Ideally, they could carry a drug in bulk or on their surface that could be delivered to the intended organ by being driven there. The first preclinical trials using magnetic albumin microspheres loaded with Doxorubicin (DOX) to treat rat cancer were carried out by Widder et al. [35]. The size, charge, and surface chemistry of magnetic particles are crucial for these applications because they affect the capacity of body to absorb the particles and the rate at which blood circulates. For example, after systemic injection, bigger particles with diameters higher than 200 nm are often retained by the spleen by mechanical filtration before being removed by phagocyte cells, resulting in shorter blood circulation period [36,37].

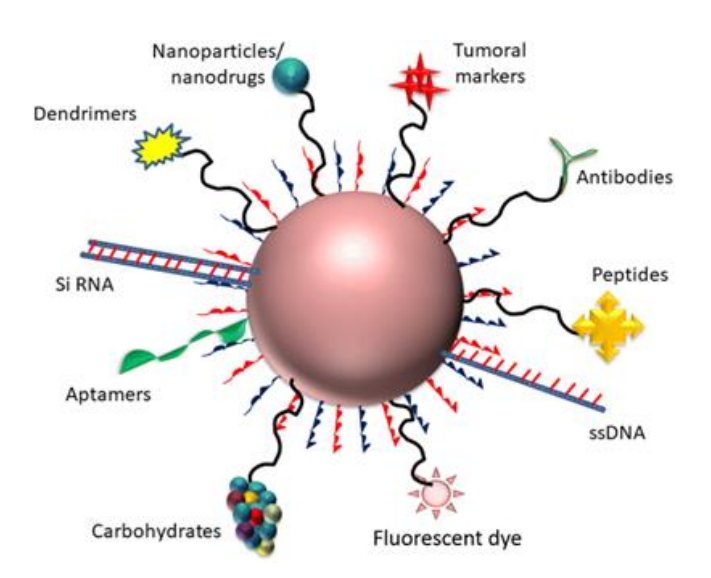


Fig.3.6: Surface functionalization of MNPs [38].

The dispersibility and stability of NPs are the primary issues in biomedicine, which

depend on their surface chemistry. The dispersion depends on the net surface charge and stability. The coulombic interaction between the charged groups and hydrophilic ionic group inhibits aggregation.

Zeta potential (ζ -potential) is typically used to show the colloidal stability of system. Capping ligand molecules that can give charge or steric hindrance is a typical approach of stabilizing the particle surface in nanoparticle dispersion. The liquid layer that surrounds the particles is divided into two regions: an inner area, also known as the Stern layer, and an outer or diffuse region. Ions are weakly bonded in the outer region with a wider layer of mostly opposite charge, and strongly linked at the inner region due to a small coating of positive charge that accumulates around the negatively charged particle. While ions outside the diffuse layer stay in the bulk dispersant, ions traveling with particles inside the diffuse layer form a stable entity. The zeta potential is the definition of potential at this plane. The schematic representation of Zeta potential is given in **Fig.3.7**.

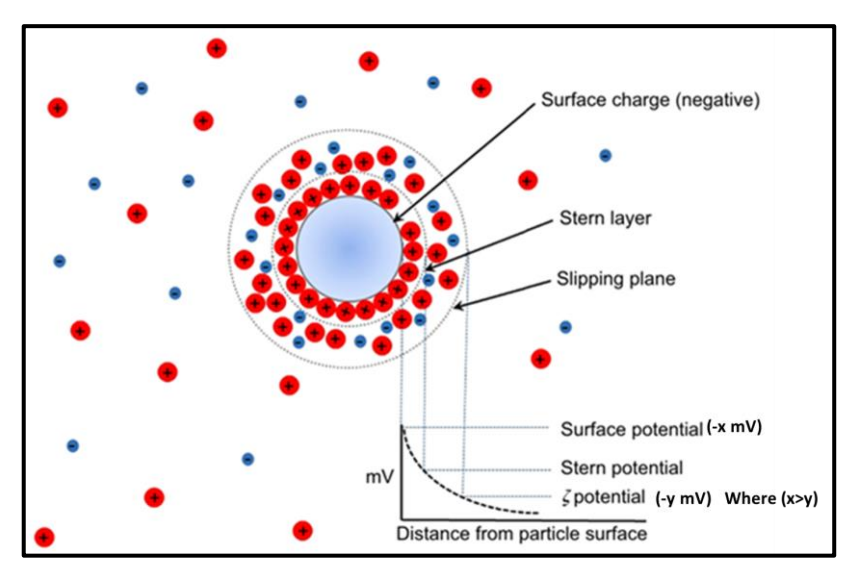


Fig.3.7: Schematic representation of Zeta potential [39].

The stability of the particle dispersion is indicated by the amplitude of the ζ -potential. Particles in dispersion medium are stable between -30 mV to +30 mV. When particles are significantly positively or negatively charged along the edge of a diffuse plane, electrostatic repulsion can keep the particles apart and avoid agglomeration. This is shown by a greater absolute value of the ζ -potential. Lower ζ -potential, on the other hand, suggests that there are less repulsive interactions between the particles, which means that they are more likely to combine and form an unstable colloidal dispersion [39].

c) Particle Size and Size Distribution:

To achieve controlled biodistribution, bio-elimination, and contrast effects, the majority of MNPs used in biomedicine must be monodisperse, which means that each nanoparticle must have almost identical physical and chemical properties. To produce biocompatible MNPs for biomedicine, the synthesis methodologies have also given rise to several surface modification procedures [40,41]. MNPs exhibit a multitude of remarkable new phenomena, including superparamagnetism, high field irreversibility, high saturation field, extra anisotropy contributions, and shifted loops upon field cooling. The magnetic behaviour of individual NPs is dominated by surface and finite size effects, which give rise to these phenomena [42].

d) Biocompatibility and Toxicity of MNPs:

Development and the conversion of fundamental research into treatments that apply to clinical practice have benefited greatly from nanotechnology. MNPs have been specifically used to target, track, and activate stem cells, as well as for cell labelling and targeting. There is a continual focus on safety, with particular attention on toxicity. The therapeutic efficacy of the drug may eventually be restricted by any signs of toxicity. The key factors that determine toxicity are the dose and planned usage of the MNPs, in addition to their own physical, chemical, and structural properties. According to certain in vitro research, MNPs at therapeutic dosages have been shown to have negative effects on cells. Yet, there hasn't been as much coverage of long-term in vivo research [43].

It is imperative to chemically stabilize the uncoated MNPs to prevent oxidation (corrosion) and acid erosion-related deterioration [44,45]. Coating the nanoparticles with organic species (such as polymers or surfactants) or an inorganic layer (like silica or gold) is a few of potential agents to improve biocompatibility. Concerns about the impact of nanoparticle size and coated nanoparticle cytotoxicity persist despite the widespread usage of MNPs in biological applications. Yu et al. [44] investigated dextran and the polymer PEG coated nanoparticles (5-30 nm) uptake and cytotoxicity by exposing porcine aortic endothelial cells. Bare nanoparticles caused a more than 6-fold increase in cell mortality at the maximum dose (0.5 mg mL⁻¹) and considerable cell elongation, but functionalized nanoparticles maintained cell viability and morphology.

3.3.3 Stabilizing Agent:

During MNP synthesis, stabilizers such as surfactants or polymers are often added to

stabilize the newly synthesize surfaces and avoid aggregation. The type of surface coating and how it is applied to the magnetic core influence not only the overall size of the colloid, but also its biological destiny. Nonpolymeric stabilizers based on organic monomers with functional groups are commonly used for surface stabilization. like carboxylate, phosphate, or sulphate, e.g., alkane sulphonic and alkane phosphonic acids, lactobionic acid, lauric acid, dodecyl phosphonic and hexadecyl phosphonic acids, or phosphonates; or polymeric stabilizers, such as dextran, PEG, Poly Vinyl Alcohol (PVA), alginate, chitosan, pullulan, or Poly Ethylene Imine (PEI). When polymeric materials are used as stabilizers, the adsorption of polymers onto MNPs provides protective steric repulsion and functions as a barrier to particle contact, keeping the particles apart. Amphiphilic copolymers with a hydrophilic segment that disperses into the aqueous medium and a hydrophobic segment that anchors to the particle surface provide the most effective protection.

Polymeric coatings can alter the surface properties of MNPs (chemical functionality and surface charge) while simultaneously functioning as an efficient aggregation barrier, resulting in physically and chemically stable magnetic nano formulations. The polymer coatings reduce the average density of the magnetic cores. Hence, the gravitational settling of MNPs in the blood flow can be regarded as minimal after vascular administration [intravenous (IV) or intra-arterial]. However, before contemplating biomedical applications, three crucial properties of the polymer must be taken into account: chemical structure (biodegradability and hydrophobic/hydrophilic character), length and molecular weight, attachment mechanism to the particle surface (covalent, hydrophobic, or ionic binding, and degree of surface coverage.

The polymer conformation on the nanoparticle surface adds to their effective hydrodynamic size and antifouling capabilities, both of which are essential factors in reducing the fast blood clearance of nanoparticles following IV injection due to immunological recognition. To assist the effective attachment of the polymers onto the surface of the MNPs, numerous functional compounds, such as bisphosphonates or alkoxysilanes, may be utilized [46]. This is done to ensure that the MNPs continue to operate properly. Researchers have used a variety of ways to create several types of magnetic iron oxide nanocomposites. Fig.3.8 depicts the possible core-shell configuration of MNPs.

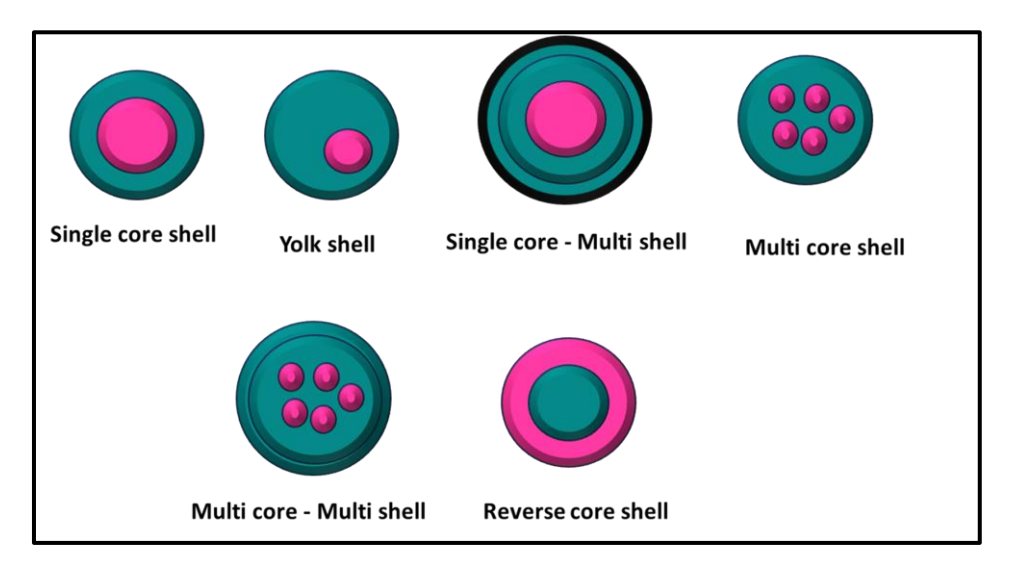


Fig.3.8: Core-shell configuration of magnetic composite nanomaterials.

3.3.3.1 Core Shell Configuration:

a) Core-Shell Structure:

Core-shell structure and reverse core-shell structure:

The core of iron oxide was covered with either inorganic or organic compounds that may act as a support for biomolecules. This was done to make MNPs stable and biocompatible. A structure is referred to as having a yolk structure when the core of MNPs is not situated in the center after functional coating. If MNPs are capable of coating the surface of either organic or inorganic materials, then the structure has an inverse core. Nanomaterials made of magnetic composites not only increase the stability of materials but also introduce new physical and biological features [46,47].

b) Multilayer Core-Shell Structure (Matrix Dispersed Structure):

The formation of a multilayer core-shell structure is accomplished by coating a large number of nanoparticles of iron oxide with other substances. The magnetic property of MNPs is dependent on the size of the magnetic iron oxide core when the structure is multilayered and organized in a core-shell fashion. By distributing MNPs throughout the matrix, it is possible to prevent the nanoparticles from clumping together to form massive ferromagnetic species [48].

3.3.3.2 Organic Materials:

To avoid aggregation, biocompatible MNPs with an organic material layer may be used to stabilize for a wide variety of in-vitro and in-vivo applications, such as electromagnetic shielding, Magnetic Resonance Imaging (MRI), drug targeting, magnetic cell

separation, and so on. This is because the organic material layer protects the aggregation of MNPs. MNPs have coatings made of a variety of organic substances, including dextran, starch, PEG, Poly (Lactic) Acid (PLA), PEI, and others.

3.3.3.3 Small Molecules and Surfactants:

MNPs functionalized using special groups -OH, -COOH, -NH₂, -SH with proper surface modification. These groups are suitable for further modification when they are attached to different bioactive molecules for various applications. The main advantage of small molecules or surfactants functionalized on MNPs is to maintain a small dynamic radius on its surface. The surfactant bound to the surface controls the growth of nanoparticles during synthesis and also prevents the MNPs from aggregating. A surfactant becomes soluble in polar or aqueous solvents based on its interactions with the solvent. On the other hand, nonpolar organic solvents like hexane, toluene, or chloroform contain a nonpolar surfactant, such as a hydrocarbon chain [49]. This is because nanoparticles that include a nonpolar surfactant, such as a hydrocarbon chain, are insoluble in polar organic solvents.

The addition of a high number of tiny compounds, such as silane and dopamine, has a typical strategy of modifying the properties of MNPs [50].

a) Silane:

The -OH group at the surface of MNPs may form a connection with the -Si group, which allows silane to be connected covalently to the surface of the MNPs. Additional cross-linking processes result in the formation of a thin layer of inorganic silica that surrounds the particle. This is done to produce a variety of terminal groups, comprising alcohol (CH₃OH), amine (-NH₂), carboxyl (-COOH), and thiol (-SH), all of which are helpful in terms of increasing biological activity and applications. P-amino phenyl trimethoxy silane meracaprtrophyl and 3-Amino Propyl Triethyloxy Silane (APTES), triethyloxysilane, Meracaprtrophyl Triethyloxy Silane (MPTES), and 2- (carboxy methythio) ethyl trimethyl silane are used for silane surface functionalization. For maintaining the morphology of Magnetite- Fe₃O₄ nanoparticles, APTES is advantageous than MPTES, as MPTES coating decreases the overall saturation magnetization (Ms) value of Magnetite- Fe₃O₄ nanoparticles [51]. Sun et al. [52] reported an innovative one-pot synthesis of adaptable monosilane-coated MNPs with surface amine groups. One approach that may be utilized to perform the conversion of a surface functional group to carboxylic acid is the conjugation of PEG diacid to -NH₂ isopropyl groups.

b) Thiol-Glutathione:

Glutathione (GSH, γ -Glutamyl-Cysteinyl-Glycine) is one of the most significant tripeptides among thiols, impacting nearly all physiological processes and directly linked to the environment of malignant cells. According to reports, GSH protects healthy cells, engages a wide range of cellular processes, and is crucial in controlling different cell physiological processes. GSH is one of the most significant redox species in the human body and has the greatest capacity to cause carriers to release anticancer medications. It has been observed that the inclusion of free GSH increases cellular mortality and drug release effectiveness. Despite this, there is very less scientific literature documenting the use of GSH-coated nanoparticles for the release of anticancer drugs [53].

3.3.3.4 Polymers:

Polymer functionalization provides a multifunctional group and more colloidal stability and biocompatibility as compared to the small molecule and surfactant. Polymer plays a significant role in biological application, as polymer coating increases repulsive forces which help in balancing the magnetic interaction and van der Waals attractive force between MNPs also increases. A variety of man-made and natural polymers are employed to functionalize surfaces of MNPs. Natural polymers can be taken from the environment and are naturally occurring. Typical examples of natural polymers are gelatin, cellulose, protein, starch, chitosan, and dextran. Scientists and engineers create synthetic polymers, or they can be made from petroleum oil. PEI, PVA, Poly (acrylic acid) (PAA), and PEG are examples of conventional synthetic polymers. Polymer coating on MNPs decreases saturation magnetization (Ms) value but makes them biocompatible and water soluble [54].

Several strategies have been examined for combining MNPs with polymers, including physical adsorption, self-assembly, self-association, Atom Transfer Radical Polymerization (ATRP), and Reverse Addition-Fragmentation Chain Transfer Polymerization (RAFTP) [55,56]. In the current chapter, we highlight some polymers such as PEG, PVA, chitosan, and dextran since these polymeric materials were most extensively utilized in prior studies.

a) Polyethylene Glycol (PEG):

PEG is a synthetic polymer that is widely employed in nanoparticle functionalization because it dissolves in water, this polymer is hydrophilic and biocompatible. PEG was accepted by the US Food and Drug Administration (FDA) as biocompatible [57]. Additionally, it increases the time period of MNPs in blood circulation, which might be highly

helpful for applications involving drugs delivery. The effectiveness of nanoparticle uptake in cells is enhanced by PEG coating [58]. Apart from its high solubility and stability in aqueous solutions, it also demonstrates stability in physiological saline solutions. The one drawback of PEG coating is that it is not known how long it will take for PEG to be cleared from the body. Kievit et al. [59] explored safe gene delivery using PEI-PEG-Chitosan copolymer-coated iron oxide nanoparticles.

b) Polyvinyl Alcohol (PVA):

PVA has minimal toxicity, is hydrophilic and biocompatible, and inhibits the aggregation of nanoparticles in biological environments [58,59]. PVA-based synthesis processes result in monodispersed particles. Furthermore, PVA has improved crystallinity as a result of its multi-hydroxyl structure, which gives it excellent thermomechanical qualities for bio-related applications such as crystallinity, high elastic modulus, and tensile strength [58].

c) Chitosan:

Chitosan, a cationic polymer resembling the cellulose structure, comprises glycosidic connections and 2-amino-2-deoxy-h-d-glucan. It is mostly used in pharmaceutical applications because of its mucoadhesive quality, positive charge, and amino group. Chitosan is insoluble in water at basic or neutral pH levels; however, it becomes soluble in water at acidic pH levels when amino groups are protonated. Chitosan does not cause allergic reactions due to its biocompatible nature. It is also biodegradable, with harmless amino sugars serving as the breakdown products [60].

d) Dextran:

Dextran, a key chemical for coating MNPs, has been employed in fundamental medical procedures such as MRI, cancer diagnosis, and treatment [57,58]. It is a polymer approved for therapeutic use, which prevents nanoparticles from clumping. Even though dextran is biocompatible, the enzyme that breaks down the material, called dextranase, cannot be produced in human cell lines [61]. One of the primary drawbacks of dextran coating is its poor connection with the MNPs surface, which may harm applications.

3.3.3.5 Biomolecules:

Biomolecule-functionalized MNPs have lately acquired appeal as an efficient and common technique for biological separation, detection, sensing, and other applications. Their biocompatibility is much improved when compared to small molecules or polymers. Direct

production of iron oxide/biomolecule composite nanoparticles is frequently accomplished by physical adsorption. Bovine/human serum, enzymes, biotin, proteins, avidin, albumin, and polypeptides are examples of biomolecules. The primary barrier to coat biomolecules in current applications is their poor conjugation efficiency to MNPs. Hence, it requires a high quantity of biomolecules, prohibitively high prices, and multidisciplinary characterization, which is not always carried out for every material investigation [62,63]. Wiogo et al. [64] performed adsorption of serum protein onto IONPs surface by dissolving the serum proteins in an RPMI-1640 (Roswell Park Memorial Institute) solution containing varying amounts of fetal bovine serum.

3.3.3.6 Inorganic Materials:

Non-polymeric coating materials have been used in addition to polymers to achieve colloidal stability and avoid aggregation of MNPs. This is done in conjunction with the use of polymers. There is a lot of interest in using inorganic materials that have been functionalized to MNPs as composites for developing improved hybrid magnetic nanomaterials. They are utilized extensively to enhance the efficiency of semiconductors, optoelectronics, catalysts, and quantum dot information storage, such as in optical bioimaging, biological labeling, and other similar applications. The synthesis of such MNPs with many functions presents a challenge to the nucleation of one phase on the surface of another phase [65].

a) Silica:

One of the most often utilized inorganic materials to functionalize MNPs is silica. Silica is utilized in catalysis, biolabeling, bio separation, and some commercial ferrofluids because it inhibits nanoparticle aggregation [66]. The main challenge associated with silica coating is to achieve uniform silica shell thickness. Unequal thickness causes uneven heating in hyperthermia application due to the irregular magnetic field [67]. A silica covering aids in preventing a biological medium and an internal active ingredient from coming into contact. It increases the biocompatibility of particles by enhancing their chemical stability and lowering their toxicity [68,69]. Due to hydrophilic nature of silica, it aids in the binding of a variety of biological ligands while also enhancing stability, dispersibility, and the absence of adverse responses. To create iron oxide@SiO₂ composite nanoparticles, the two easiest methods are the Stober synthesis and the reverse microemulsion approach. The most widely utilized silanes that attach to surface of MNPs readily through the OH group are Tetraethoxysilane

(TEOS), Vinyltriethoxysilane (VTEOS), and Octadecyltrimethyloxy silane [70,71].

3.3.3.7 Carbon:

Carbon shows more stability at high temperatures and pressure in a variety of physical and chemical conditions. Carbon-coated MNPs have lately spurred a great deal of research interest because of their excellent chemical and thermal stability as well as their high electrical conductivity. MNPs with carbon covering inhibit oxidation and stop corrosion in the magnetic core material. Better dispersibility and stability than those demonstrated by bare IONPs are provided by a hydrophilic carbon coating on MNPs cores [71].

Carbon-functionalized MNPs may be synthesized using a variety of techniques. To make carbon-coated MNPs, glucose is normally dissolved in water as part of the preparation process. This makes it challenging to get significant quantities of high-quality iron oxide/carbon for prospective use. **Chart 3.1** depicts a two-step technique for carbon coating on MNPs. The polymer layer was transformed into a carbon layer by annealing or another heat treatment after the surface of MNPs was covered with polymer to create MNPs/carbon composite nanoparticles.

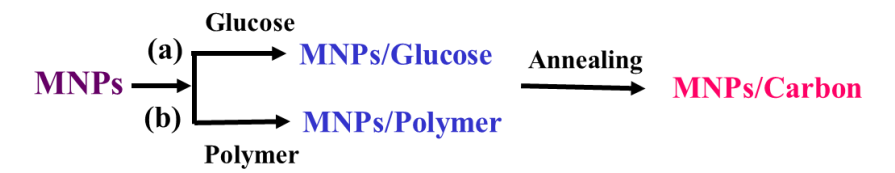


Chart 3.1: Two-step approach for the synthesis of MNPs/ carbon nanomaterials.

Graphene, a novel class of carbon compounds, has been exploited in biological applications such as targeted drug delivery and MRI. Iron oxide/Graphene hybrid nanomaterials have been created using a variety of synthesis methods, which may be broadly classified as in situ and ex-situ [72]. When MNPs are coated with graphene, the charge transfer behavior in graphene changes, making it feasible to deliver tiny drugs or nucleic acids to a target cell (cancer or stem cell). Biomedical applications such as targeted drug delivery and MRI have made use of Magnetite- Fe₃O₄/graphene hybrid materials [73-75]. The composites of Graphene Oxide (GO) and Magnetite- Fe₃O₄ nanoparticles coated with amino dextran were discovered by Chen et al. [76] to study cellular MRI.

3.3.3.8 Metals:

The combination of metallic NPs and physicochemical properties of MNPs and their potential as catalysts has piqued the curiosity of material scientists in biotechnology and

biomedicine. Localized Surface Plasmon Resonance (LSPR) and Surface-Enhanced Raman Spectroscopy (SERS) are two intriguing characteristics of metallic (Au, Ag, Cu, Pd, Co, Pt) nanoparticles [77]. Numerous anisotropic metallic nanoparticles are used in contrast imaging [78], catalysis [79], medicine [80], and sensing [81]. It is challenging to coat metal directly on the surface of MNPs using the thermal decomposition approach [82]. Nevertheless, noble metals including Au, Ag, Pt, and Pd exhibit corrosion resistant qualities, making perfect functional materials for MNPs. Nonetheless, it is observed that hybrid MNPs/metal structures form aggregated, multilayer, core-shell, and dumbbell structures using microemulsion and thermal degradation techniques. Additives and surfactants can change the surface properties and stability of metallic nanoparticles [83]. The Magnetite- Fe₃O₄@Au structure, which is a core-shell structure, is the most often described in literature [84]. As common base metals, MNPs are combined with metal particles (e.g., Fe, Ni, Cu, and Co) via various synthesis methods. The dispersibility of MNPs is improved by certain metal coatings, which also increase saturation magnetization (Ms) value.

a) Gold:

Lin et al. [85] reported on gold-coated MNPs for the first time in 2001. Iron oxide cores have been protected from oxidation by coating with gold, also the colloidal stability is enhanced using gold coating. The gold coating is beneficial because of the well-known optical properties, also it has high functionalization capability and is biocompatible [85]. One disadvantage is that the magnetic properties of MNPs coated with gold are attenuated, and the interaction of two different surfaces makes coating maintenance problematic. Nonetheless, it has been shown that gold-coated MNPs are stable in neutral and acidic pH environments [86].

3.3.3.9 Metal Oxide:

Recent developments have made significant progress in the synthesis of iron oxidemetal oxide nanocomposite [87]. The findings show that combining MNPs with semiconductors permits the exploration of novel functionalities derived from metal oxides. Various metal oxides are used to form a composite with IONPs, such as TiO₂ [88], ZnO [89], SnO₂ [90], MgO [91], Y₂O₃ [92], WO₃ [93], Cu₂O [94] and Al₂O₃ [95]. The stability of iron oxide significantly increased when composite was combined with semiconductors to explore novel functional derivatives from metal oxide. Coating MNPs with semiconductor materials is a standard method of producing bifunctional composites. Recently, iron oxide-metal composite nanoparticles have been synthesized using the sonochemical, spray pyrolysis, and

ion implantation methods.

3.3.3.10 Metal Sulfides and Selenides:

Minerals containing metal sulfides and selenides, such as chalcocite (Cu₂S), bismuthinite (Bi₂S₃), pyrite (FeS₂), and clausthalite (PbSe) are common and inexpensive. Due to the significance of magnetic iron oxide/metal sulfide in understanding the quantum size effect and its many applications, significant advancements have been made in this field [96]. Examples of MNPs/metal sulfides are γ-Fe₂O₃/PbSe, Fe₃O₄/ZnS, CdSe@Fe₂O₃, and Fe₃O₄/CdS [97-101]. Iron oxide with Layered Transition Metal Dichalcogenides (LTMDs) (Except MoS₂) has not yet been reported. The study of the relative properties of these composites should be increased in the future.

3.3.3.11 Bimagnetic Materials:

The use of MNPs in conjunction with a variety of magnetic inorganic materials is known as a bimagnetic. By adjusting the materials, their combination, volume ratio, and phase between the core and the shell, bimagnetic NPs show a rational style capacity for managing the blocking temperature and coercivity in MNPs [102]. This can be accomplished by controlling the blocking temperature and the coercivity of the MNPs. Co_3O_4 and MFe_3O_4 , where M = Mn, Co, Zn, Ni, Fe, and Pt, are two examples of the most significant and commonly magnetic hard and soft materials that have been coupled with IONPs to generate bimagnetic nanoparticles [103].

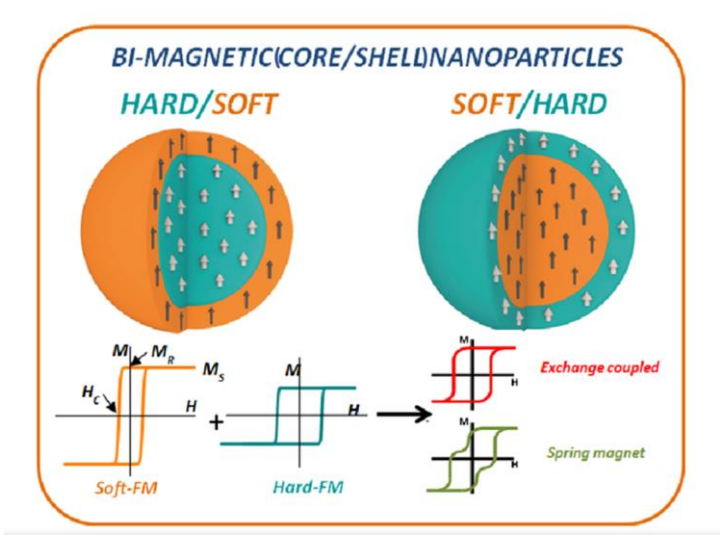


Fig.3.9: Hysteresis loop for soft and hard magnetic materials [102].

As seen in **Fig.3.9**, the secondary magnetic materials that are coated on MNPs typically have a dramatic effect on the magnetic properties. In particular, they generate the

exchange coupling effect between soft-phase and hard-phase magnetic materials. The exchange interaction between hard and soft magnetic materials produces an exchange spring magnet, which is a magnetic material with high coercivity and high saturation properties [102].

3.3.3.12 Ternary Structure and Multilayer Core-Shell Structure:

One common method for building ternary and multilayer core-shell structures is Layer by Layer (LBL) assembly. It offers an excellent chance to control the characteristics of the core and many functional shells. To hold the assembly of these nanostructures electrostatic force and hydrogen bonding interaction is responsible. This approach is relatively controllable and therefore promises to incorporate MNPs and various functional layers into the nanostructure. One flexible approach to creating ternary and multilayer core-shell nanostructures is to use a sequential deposition procedure such as $Fe_3O_4@SiO_2@Au$ [104], $Fe_3O_4@SiO_2@TiO_2$ [105], α - $Fe_2O_3/SiO_2/SnO_2/TiO_2$ [106], and α - $Fe_2O_3/Ag/SiO_2/SnO_2$ [107].

3.3.3.13 Organic-Inorganic Composite Structure:

It will be beneficial to employ hybrid materials, which comprise both organic and inorganic subcomponents for coating. Within the framework of this composite structure, the outermost layer of the iron oxide is concurrently coated with at least one organic component which offers novel options for the creation of novel materials and chemicals for research, and also has enhanced peculiar features that show excellent applicability in various fields.

Nowadays a wide variety of functional inorganic materials are being manufactured and connected with MNPs. Polyoxometalates, Metal-Organic Frameworks (MOF), and Upconversion (UC) materials are a few examples of materials that fall under this category. UC materials are mostly used in biomedical applications due to their ability to employ a two-photon multiphoton process to convert longer wavelength photons into shorter wavelength [108]. Fe₃O₄@LaF₃:Yb³⁺: Er³⁺ are some examples of organic-inorganic composite structures, which are more commonly referred to as UC [109]. NaYF₄: Yb, BaTiO₃ [110], Ag₂WO₄ [111] are the other examples of organic-inorganic composite materials.

3.4 Characterization of Magnetic Nanoparticles:

3.4.1 Introduction:

Chemical, physical, and biological techniques are used to characterize the synthesized MNPs. Phase, composition, surface, microstructure, and structural analysis are all important components of characterization. The different techniques used to analyze the physicochemical, magnetic and biological properties of synthesized nanoparticles are listed in **Chart 3.2**.

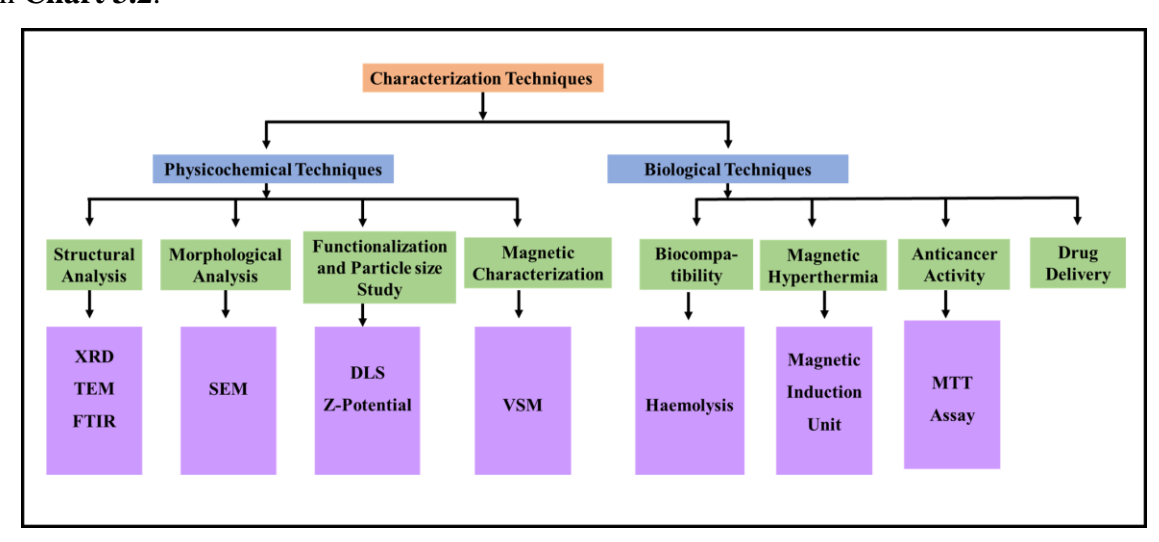


Chart 3.2: Different techniques used for characterization of MNPs.

The structure or phase analysis was studied using XRD and TEM, the morphological analysis was analyzed using SEM. The magnetic characterization was carried using VSM technique.

3.4.2 Structural / Phase Analysis:

3.4.2.1 X-Ray Diffraction (XRD):

A schematic of an X-ray diffractometer is shown in **Fig.3.10** (a). In most cases, diffraction occurs when the distance between scattering centres and the wavelength of incident radiation are of equal magnitude [112]. In crystalline material atoms are arranged in a unit cell, which is a repeating pattern with interatomic spacing between atoms is comparable to the wavelength of X-rays (0.5-2.5 Å). Hence, the crystal acts as 3D grating for X-rays.

Bragg conducted systematic studies on diffraction from crystalline materials and developed the formula known as Bragg's law (**Equation 3.2**),

$$2dsin\theta = n\lambda \qquad \qquad \dots (3.2)$$

where,

d =Interplanar spacing,

- θ = Diffraction angle,
- λ = Wavelength of X-ray, and
- n =Order of diffraction.

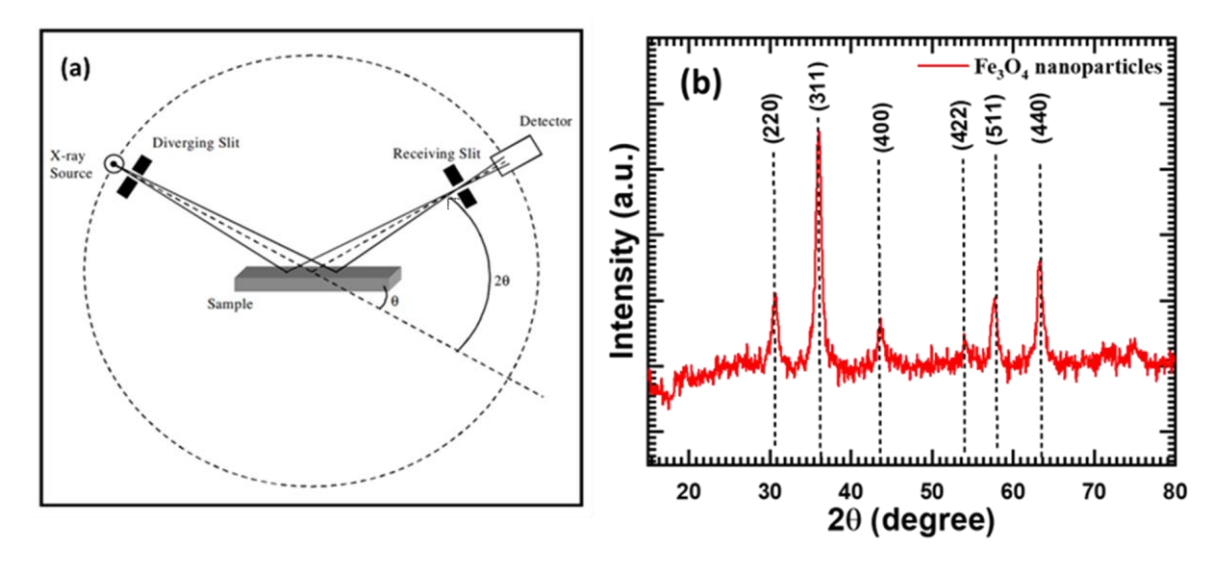


Fig.3.10: (a) Schematic of X-ray diffractometer [113] and (b) XRD pattern of Magnetite-Fe₃O₄ nanoparticles.

XRD experiments are commonly used to confirm crystal structure and phase formation. During the experiment, λ or θ must be continuously adjusted to satisfy Bragg's criterion. Phases in a sample may be identified using the standard Joint Committee on Powder Diffraction Standards (JCPDS) file based on d-spacing, and reflections can be indexed using Miller indices. If the diffracting crystal is small, then destructive interference does not occur at $\theta \pm d\theta$. In proportion to the size of the small crystal, it widens the peak that corresponds to the diffracted beam. Particle size may be ascertained by observing the broadening of the diffraction peak. The Scherrer formula as given in **Equation 3.3** is used to calculate the crystallite size of nanoparticles using XRD data [113,114].

$$D_{xrd} = \frac{0.9\lambda}{\beta \cos \theta} \qquad \dots (3.3)$$

where,

 D_{xrd} = Particle size,

 λ =Wavelength of X-rays,

 β =Line broadening at Full Width at Half Maxima (FWHM), and

 θ = Diffraction angle.

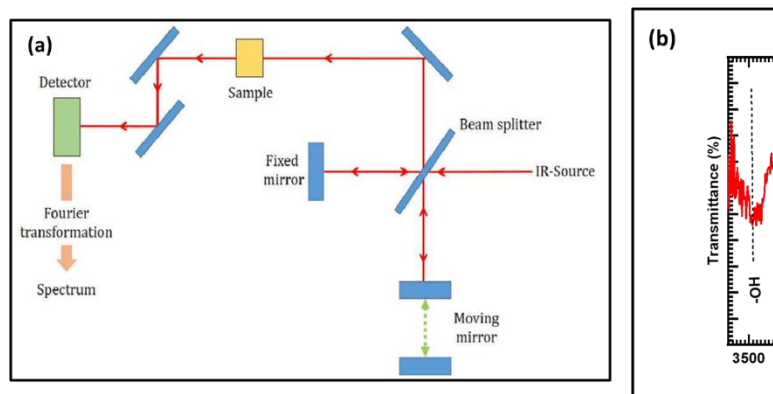
An example of an XRD pattern of Magnetite- Fe₃O₄ nanoparticles is provided in Fig.3.10 (b) to demonstrate the analysis of XRD data obtained from the XRD study.

3.4.2.2 Transmission Electron Microscopy (TEM):

Transmission Electron Microscopy (TEM) uses a high-energy electron beam in a vacuum to create images of a sample. Electrons passing through the sample are detected to form detailed images. TEM allows to see atomic structures in crystals and molecular components. It provides visualization from the microscale (1 μ m = 10⁻⁶ m) to the nanoscale (1 nm = 10⁻⁹ m). TEM reveals details beyond light microscopy by using focused electrons for high-resolution imaging. It helps to examine microstructures, tissues, cells, proteins, and crystalline materials. Additionally, it provides insights into crystal orientations and elemental compositions, except for the lightest elements.

3.4.2.3 Fourier Transforms Infrared Spectroscopy (FTIR):

Technique that is frequently used to analyse both organic and certain inorganic compounds is Fourier Transform Infrared (FT-IR) spectroscopy. According to the fundamental principles of molecular spectroscopy, some molecules absorb light energy at certain wavelengths known as resonance frequencies [115]. For example, the H₂O molecule resonates at 3450 cm⁻¹ in the infrared part of the electromagnetic spectrum. The equipment is separated into three categories: near (12,500 to 4000 cm⁻¹), mid (4000 to 400 cm⁻¹), and far-IR (400 to 10 cm⁻¹). The mid-IR range (4000 to 400 cm⁻¹) is the most important since it contains the majority of fundamental vibrations. **Fig.3.11 (a)** shows a schematic representation of FTIR and **Fig.3.11 (b)** shows FTIR spectrum of Fe₃O₄ nanoparticles.



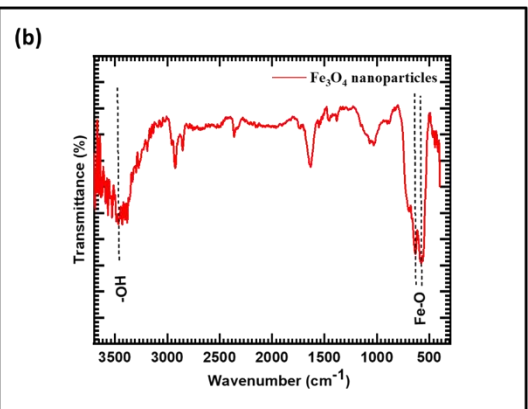


Fig.3.11: (a) Schematic of an FTIR spectrometer [115] and (b) FTIR spectrum of Magnetite-Fe₃O₄ nanoparticles.

The choice of material for the beam splitter depends on the area being studied. Materials such as iron oxide or germanium are placed on top of an infrared-transparent substrate (such as potassium bromide or caesium iodide) to produce beam splitters in the infrared region. Force constant, shape, and relative masses of the atoms control the absorption

wavelength. Every band in a spectrum represents the distinct functional groups and bonds. The source of radiation enters the interferometer and passes to the detector. The signal is amplified and converted to a digital signal by the analog-to-digital (A/D) converter and amplifier before being delivered to the computer. A portion of the infrared radiation in the 10,000-100 cm⁻¹ range is absorbed by the sample, while the rest continues to pass. The radiation is converted by the sample into vibrational or rotational energy. The signal that appears at the detector is usually a spectrum representing the chemical fingerprint of the material ranging from 4000 to 400 cm⁻¹. FTIR is a crucial tool for chemical identification as every molecule has a unique fingerprint [116].

FTIR is mostly used for phase confirmation in inorganic oxides, or ferrites, based on the existence of octahedral and tetrahedral molecular vibrations. It is necessary to cover produced nanoparticles with organic, inorganic, or biocompatible compounds to expand their potential usage in biomedical applications. Considering this, FTIR spectroscopy provides insight into the effective adhesion of the coating agent to the surface of the magnetic core.

3.4.3 Morphological Study:

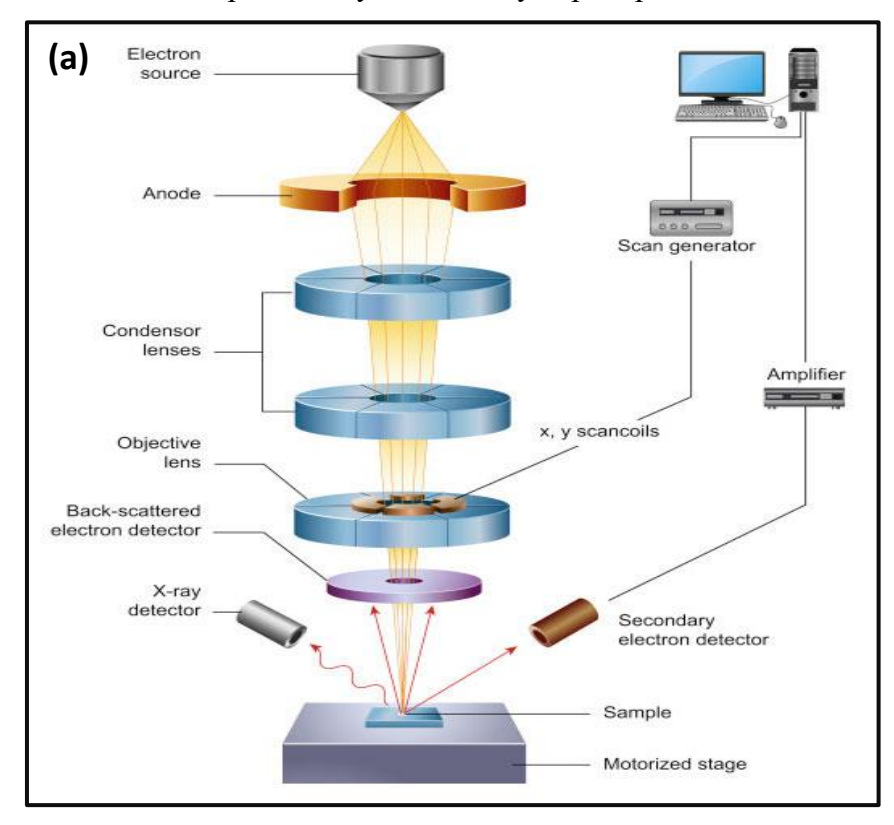
3.4.3.1 Scanning Electron Microscopy (SEM):

Scanning Electron Microscopy (SEM) is used to analyze the morphology of sample and surface topography. Selective point locations on the sample can be analyzed using the SEM; this technique is especially useful for qualitative or semi-quantitative identification of crystalline structures, crystal orientations, and chemical composition. The SEM shows incredibly detailed two-dimensional images at a magnification higher than that of a light microscope. The SEM may also be used with an Energy-Dispersive X-ray spectrometer (EDX) to do quantitative and qualitative chemical analysis.

In SEM the electron beam produces an electron column above the sample chamber. Electrons can be produced by a field emission cathode or a thermal emission source, such as a heated tungsten filament. Depending on the evaluation goals, the incident electron energy can range from 100 to 30 keV. The electrons are focused into a very small area by use of a sequence of magnetic lenses that this beam passes through as it descends. The focused beam is moved over the object by a series of scanning coils toward the bottom.

When an electron beam strikes a sample surface, electrons are released as a result of elastic and inelastic scattering. Backscattered electrons are high-energy electrons ejected by elastic scattering having equivalent energy to incident electrons. Secondary electrons are low-

energy electrons released as a result of inelastic scattering with an energy of 50 eV or less. An amplifier receives the findings from a detector that counts the electrons. The final image is the total amount of electrons produced by every point on the sample [117]. Fig.3.12 (a) shows a schematic of a scanning electron microscope and Fig.3.12 (b) shows an example of SEM images of Magnetite- Fe₃O₄ nanoparticles synthesized by coprecipitation method.



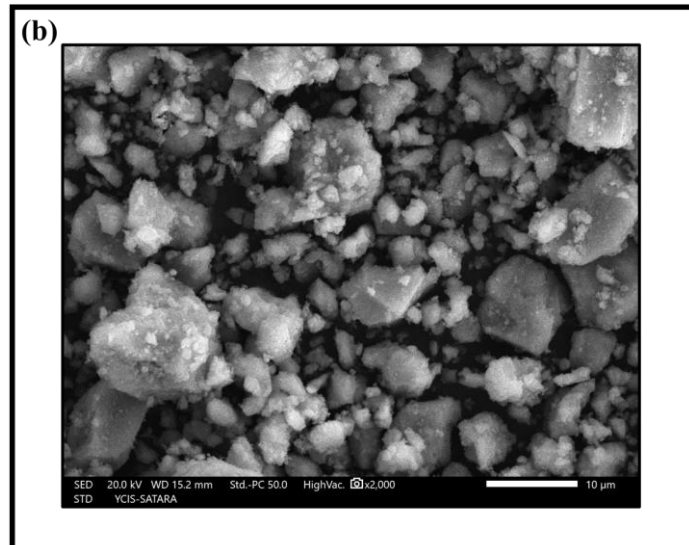
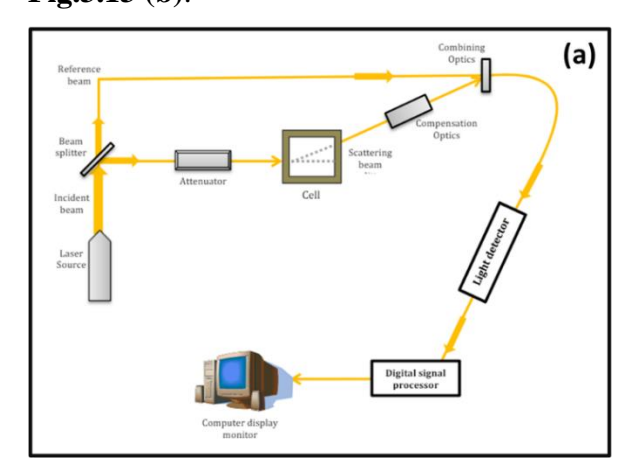


Fig.3.12: (a) Schematic of scanning electron microscope [117] and (b) SEM image of Magnetite- Fe₃O₄ particles.

3.4.4 Functionalization and Particle Size Study:

3.4.4.1 Zeta Potential:

It is necessary to disperse synthesized MNPs in an appropriate base fluid (such as water) for biological uses. A zeta potential (ζ -potential) analyzer was used to investigate dispersion stability, aggregability, and sedimentation qualities. The ζ -potential and pH values of the produced suspension were measured using a Zetasizer (Malvern Instruments Ltd). The potential difference between the stationary fluid layer attached to the dispersed particles and the dispersion medium is known as the ζ -potential. Although the ζ -potential cannot be observed directly, it is calculated by the use of theoretical models and observations of electrophoretic or dynamic electrophoretic mobility [118]. An optical setup of ζ -potential detection is shown in Fig.3.13 (a) with an example of Magnetite- Fe₃O₄ nanoparticles in Fig.3.13 (b).



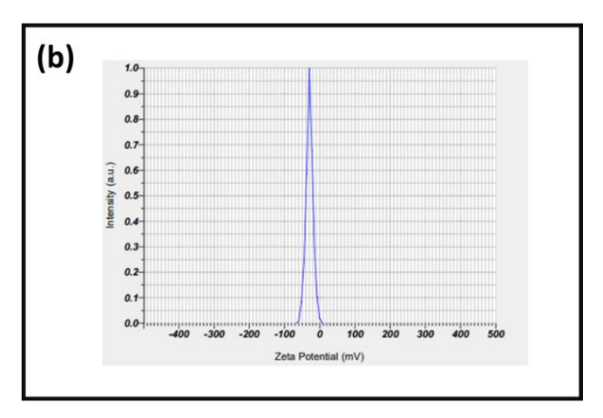


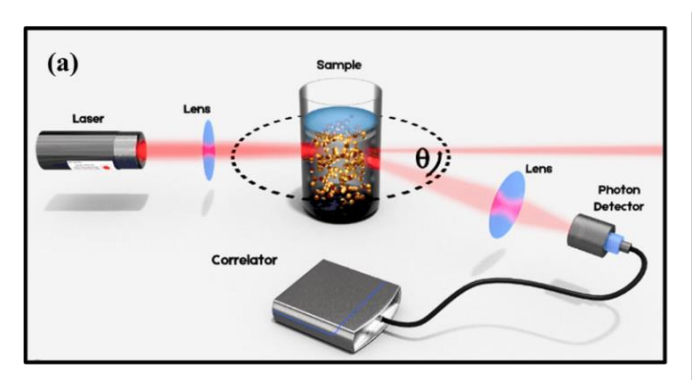
Fig.3.13: (a) Optical configuration of the Zetasizer [118] and (b) Zeta potential for Magnetite-Fe₃O₄ nanoparticles.

3.4.4.2 Dynamic Light Scattering (DLS):

Dynamic Light Scattering (DLS) is used to estimate the hydrodynamic size of particles (pristine or coated). DLS measurements were performed using a Malvern 4800 Autosizer with a 7132 digital correlator and a 632.8 nm He-Ne laser beam. Every measurement was done with water circulation at 25.0 ± 0.1 °C. A cylindrical cell of diameter 10 mm was used in all light scattering investigations. For every sample, five measurements of the scattered light intensity were made at 130° . A photon correlator with 192 channels was used to determine the autocorrelation function.

Semi-classical light scattering theory states that an oscillating polarization of electrons in molecules occurs when light strikes matter. After that, the molecules emit (scatter) light,

functioning as secondary sources of light. The frequency variations, angular distribution, polarization, and intensity of scattered light are all influenced by the size, shape, and molecular interactions of the scattering medium. DLS is one of the methods of light scattering. A schematic of the DLS device is shown in **Fig.3.14** (a). The hydrodynamic size of Magnetite-Fe₃O₄ nanoparticles measured using DLS technique, as given in **Fig.3.14** (b) using water as solvent as an example. The following presumptions underpin the operation of the DLS [119]: The dispersed particles or macromolecules suspended in a liquid medium experience Brownian motion; in this case, the probability density function, which is given by: P (r, t|0,0) = $(4\pi \text{ D t})^{-3/2} \exp(-r^2 4\text{ D t})$, where D is the diffusion constant. This generates variations in particle concentration, resulting in local inhomogeneities of the refractive index. This causes changes in the intensity of the dispersed light.



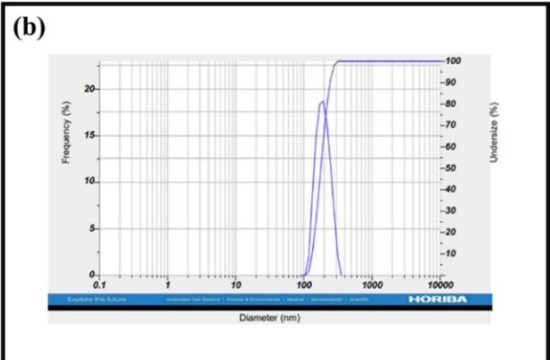


Fig.3.14: (a) Optical configuration of Dynamic Light Scattering (DLS) [119] and (b) DLS of Magnetite- Fe₃O₄ nanoparticles.

The Stokes-Einstein formula (**Equation 3.4**), gives the relationship between the particle size, viscosity and diffusion coefficient.

$$D = \frac{k_B T}{6\pi \eta a} \tag{3.4}$$

Where,

a =Radius of the beads,

 $k_B = \text{Boltzmann constant},$

T= temperature in Kelvin, and

 η = coefficient of viscosity of the solvent.

3.4.5 Magnetic Characterization:

3.4.5.1 Magnetic Induction Heating:

Heating of MNPs can be studied using a magnetic induction heating effect under application of an Alternating Magnetic Field (AMF) of appropriate strength. This is called

Magnetic Hyper Thermia (MHT). The key factor in MHT is the heating of MNPs, which is expressed in terms of the Specific Absorption Rate (SAR) value, defined as the capacity of MNPs to convert magnetic energy into heat. Generally, temperatures between 42-44 °C are considered to be useful for killing cancer cells. In present study, nanoparticles were self-heated in water at various amplitudes of AMF. The temperature rise for each sample after 10 minutes is observed for a fixed frequency of 278 kHz. The 100% conversion of magnetic energy into heat is not possible, this power loss in IONPs is due to residual loss, eddy current loss, and hysteresis loss. The hysteresis loss is minimal for superparamagnetic IONPs. The experimental setup for magnetic induction heating is shown in **Fig.3.16**.

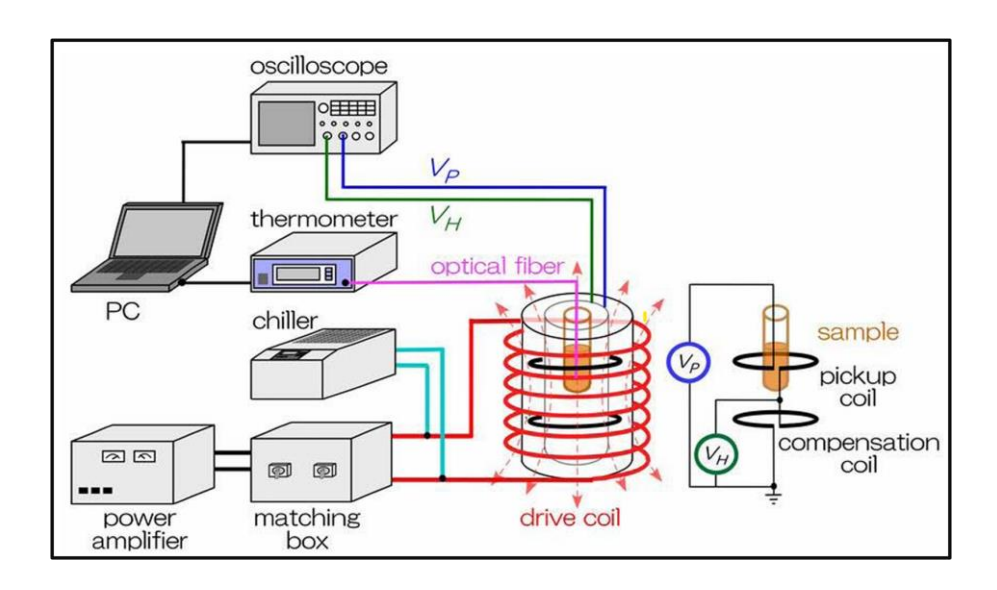


Fig.3.16: Experimental setup for MHT [120].

3.4.5.2 Vibrating Sample Magnetometer (VSM):

Superparamagnetic behaviour is one of the key requirements for MNPs to be eligible for in vivo biological applications. For superparamagnetic MNPs, remanence and coercivity are negligible. This method was developed in 1956 by physicist Simon Foner at MIT Lincoln Laboratory. They work well in manufacturing, process control, testing, and research & development where a constant AMF is applied to the MNPs under study.

A magnetic field known as the magnetic stray field is created around the MNPs by the magnetic dipole moment. A set of pick-up coils measures the variation in the magnetic stray field over time that occurs as the sample is moved up and down on a long rod as shown in **Fig.3.17** (a). VSM analysis of superparamagnetic IONPs as an example is shown in **Fig.3.17**

(b). Induced current is produced in the coils due to oscillatory motion of the MNPs during magnetization and demagnetization. A trans-impedance amplifier is used to increase the induced current. Using controlling and monitoring software, the gadget can provide data on the magnetization-demagnetization of MNPs with time (hysteresis curve) [121].

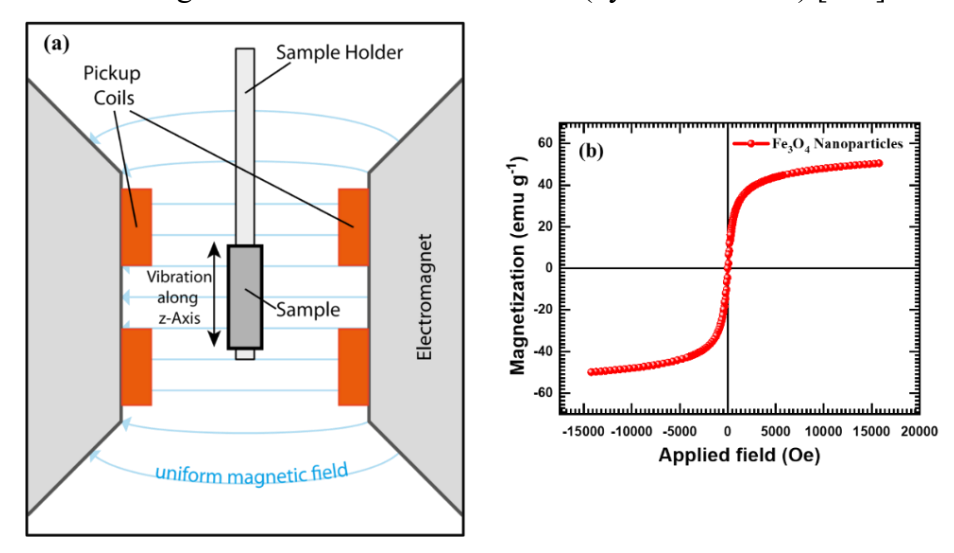


Fig.3.17: (a) Principle of VSM [121] and (b) VSM analysis of IONPs.

3.5 Biocompatibility Study:

As nanotechnology advances, concerns regarding the adverse effects of nanomaterials particularly on human health are becoming more and more prevalent. Hence an investigation on biocompatibility of nanoparticles has become an essential area of study. It is beneficial to run many tests to achieve a reliable conclusion. The samples will be sent for in vivo testing on animals that are similar to the human model. Based on several in vivo experiments for MNPs conducted on animals, histology and serologic blood tests revealed no adverse effects following a seven-day therapy at a high dosage of 3,000 µmol nanoparticles per kg of body weight [122]. When the biocompatibility tests show negligible or no effects for the concentrations of MNPs used on human clinical studies then it is sent to FDA for approval.

Hydrophilic substances, such as water or physiological brine, are needed as solvents for the suspension of MNPs. The pH level of the suspension is kept at a nearly neutral (7.4). The cytotoxicity of every new sample is investigated thoroughly before in-vivo use. biocompatibility can be assessed with variety of methods shown in **Fig.3.18**.

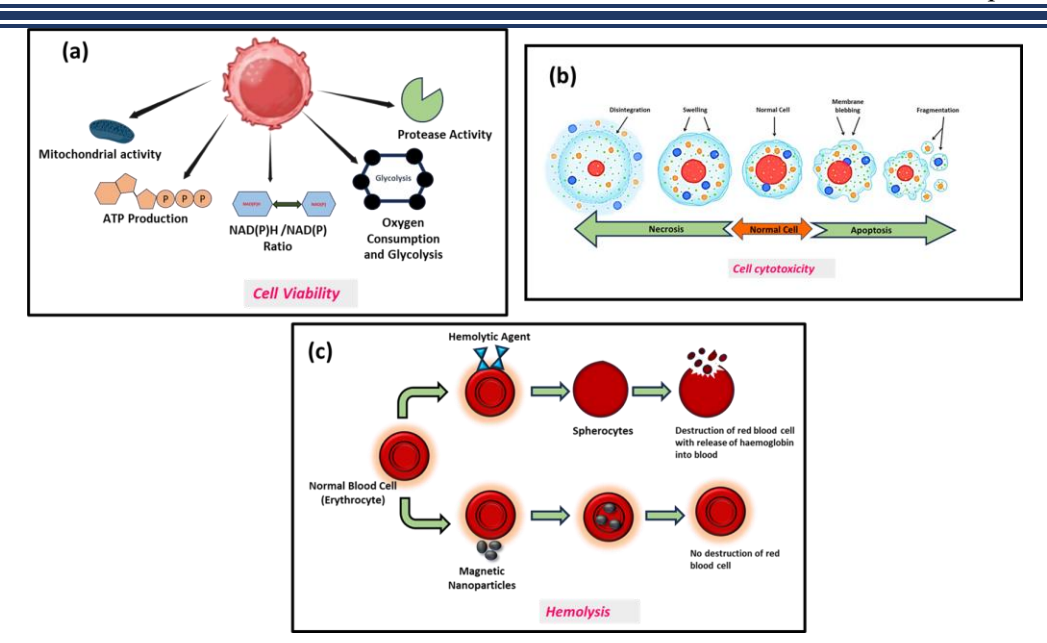


Fig. 3.18: Various assays (methods) to assess biocompatibility: **(a)** Cell Viability, **(b)** Cytotoxicity, and **(c)** Hemolysis.

3.5.1 Cell Viability /Cytotoxicity Assays:

Chart 3.3 shows classification of cell viability and cytotoxicity tests, these assays are categorized according to the types of endpoints that are measured (e.g., color changes, fluorescence, luminescence, and so on).

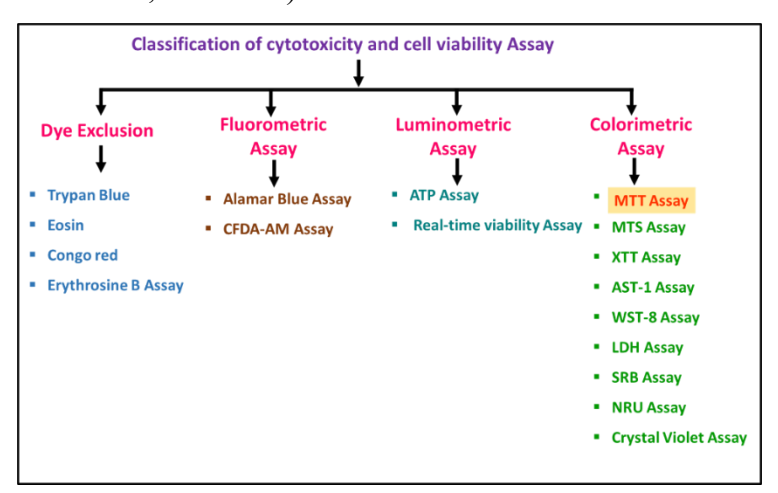


Chart 3.3: Different types of cytotoxicity and cell viability assays.

Chemical cytotoxicity studies and drug screening frequently involve in-vitro cell viability and cytotoxicity assays with cultured cells. To assess chemical toxicity and limit tumor cell proliferation throughout the drug development process, these assays are now being used in oncological investigations. They are efficient and don't require the usage of animals.

An extensive variety of sample materials may also be tested using them. For cell viability and cytotoxicity investigations, a variety of cell activities are utilized, including co-enzyme creation, Adenosine Tri Phosphate (ATP) production, cell adhesion, membrane permeability, enzyme activity, and nucleotide absorption activity. Studies using human cells may be more pertinent than some in vivo animal investigations, and in vitro cytotoxicity or cell viability tests provide a number of benefits, including time, cost savings, and automation. They do not have the technical advancement to fully replace animal testing, which is a major disadvantage [12].

Fig.3.19: MTT assay to study cell viability and cell toxicity of nanoparticles.

In the present study cell viability /cytotoxicity of IONPs were studied using MTT assay (3-(4, 5-dimethythiazol-2-yl)-2, 5-diphenyl tetrazolium bromide). The MTT assays are used for in-vitro cell viability and cytotoxicity of nanoparticles. The MTT assay is significantly better than other kinds as it is simple to apply, safe, highly reproducible, and often used to assess cytotoxicity and cell viability [122]. The MTT test measures the viability, proliferation, and cytotoxicity of cells by assessing their metabolic activity. This colorimetric test yields data based on metabolically active cells reducing a yellow tetrazolium salt (3-(4,5-dimethylthiazol-2-yl)-2,5-diphenyltetrazolium bromide, or MTT) to purple formazan crystals (refer Fig.3.19). Live cells include enzymes called NAD(P)H-dependent oxidoreductases, which convert MTT into formazan. The insoluble formazan crystals are dissolved using a solubilization solution, such as dimethyl sulfoxide (DMSO). The absorbance of the obtained coloured solution is then measured at a wavelength of 400-600 nm using a multi well spectrophotometer. The more stimulated the cells are, the deeper the colour. In this study, the cytotoxicity of nanoparticles was evaluated using MDA-MB-231 human breast cancer cell lines and L929 mouse fibroblast cell lines.

The following **Equations 3.5** and **3.6** were used to calculate the percentage of cell viability and cytotoxicity of IONPs after treating with cell lines.

% Cell viability =
$$\frac{Absorbance\ of\ test\ sample}{Absorbance\ of\ control}X100 \qquad (3.5)$$

% Cytotoxicity =
$$100 - \%$$
 Cell viability (3.6)

3.5.2 Hemolysis Assay:

The entry of foreign particles into the body can have a variety of and sometimes conflicting effects, so determining their effects on the body is a critical step in their applicability. Because the injected nanoparticles come into direct touch with blood tissue and its components, an evaluation of their hemocompatibility is essential for further study. Hemolysis percentage is calculated using **Equation 3.7**.

Percentage hemolysis =
$$\frac{[OD(test) - OD(negative control)]}{[OD (positive control) - OD (negative control)]}X100 \qquad (3.7)$$
where OD = Optical density at 540 nm.

References:

- 1. Sagadevan S, Imteyaz S, Murugan B, Anita Lett J, Sridewi N, Weldegebrieal G, Fatimah I, Oh W. Green Process. Synth. 11 (1) (2022) 44-63.
- 2. Joudeh N and Linke D, J. Nanotechnol. 20 (1) (2022) 262-91.
- 3. Macchione M, Biglione C, Strumia M. Polymers. 10 (5) (2018) 527-61.
- 4. Majidi S, Sehrig F, Farkhani S, Goloujeh M, Akbarzadeh A. Artif. Cells Nanomed. Biotechnol. 44 (2) (2016) 722-34.
- 5. Sandler S, Fellows B, Mefford O. Anal. Chem. 91 (22) (2019) 14159-69.
- Patra J, Das G, Fraceto L, Campos E, Rodriguez-Torres M, Acosta-Torres L, Diaz-Torres L, Grillo R, Swamy M, Sharma S, Habtemariam S. J. nanobiotechnol. 16 (71) (2018) 1-33.
- 7. Mukherjee S, Liang L, Veiseh O. Pharmaceutics. 12 (2) (2020) 147-67.
- 8. Fitzgerald W, Lamborg C, Hammerschmidt C. Chem. Rev. 107 (2) (2007) 641-62.
- 9. Cornell R and Schwertmann U. Weinheim: Wiley-vch. 15 (3-4) (2003) 1-572.
- 10. Friák M, Schindlmayr A, Scheffler M. New J. Phys. 9 (1) (2007) 5-21.
- 11. Kianfar E. J. Supercond. Nov. Magn. 34 (7) (2021) 1709-35.
- 12. https://edurev.in/t/114593/Precipitation-and-co-precipitation--Catalyst-Scien.
- 13. Mascolo M, Pei Y, Ring T. Materials (Basel). 6 (12) (2013) 5549-67.
- 14. Tao J, Chow S, Zheng Y. Acta Pharm. Sin. B. 9 (1) (2019) 4-18.
- 15. Vayssieres L, Chanaec C, Tronc E, Jolivet J. J. Colloid Interf. Sci. 205 (2) (1998) 205-12.
- 16. Hachem K, Ansari M, Saleh R, Kzar H, Al-Gazally M, Altimari U, Hussein S, Mohammed H, Hammid A, Kianfar E. BioNanoScience. 12 (3) (2022) 1032-57.
- 17. Valenzuela R, Fuentes M, Parra C, Baeza J, Duran N, Sharma S, Knobel M, Freer J. J. Alloys Compd. 488 (1) (2009) 227-31.
- 18. Khan I, Saeed K, Khan I. Arab. J. Chem. 12 (7) (2019) 908-31.
- 19. Gnanaprakash G, Philip J, Jayakumar T, Raj B. J. Phys. Chem. B. 111 (28) (2007) 7978-86.
- 20. Waheed S, Li Z, Zhang F, Chiarini A, Armato U, Wu J. J. nanobiotechnol. 20 (1) (2022) 395-421.
- 21. Mundekkad D and Cho W. Int. J. Mol. Sci. 23 (3) (2022) 1685-715.
- 22. Yoo J, Chambers E, Mitragotri S. Curr. Pharm. Des. 16 (21) (2010) 2298-307.
- 23. Zhu N, Ji H, Yu P, Niu J, Farooq M, Akram M, Udego I, Li H, Niu X. Nanomaterials. 8 (10) (2018) 810-40.
- 24. Anbarasu M, Anandan M, Chinnasamy E, Gopinath V, Balamurugan K. SpectrochimActa A Mol. Biomol. Spectrosc. 135 (2015) 536- 539.

- 25. Hao R, Xing R, Xu Z, Hou Y, Gao S, Sun S. Adv. Mater. 22 (25) (2010) 2729-42.
- 26. Weisbecker C, Merritt M, Whitesides G. Langmuir. 12 (16) (1996) 3763-72.
- 27. Love J, Estroff L, Kriebel J, Nuzzo R, Whitesides G. Chem. Rev. 105 (4) (2005) 1103-70.
- 28. Fritz G, Schädler V, Willenbacher N, Wagner N. Langmuir. 18 (16) (2002) 6381-90.
- 29. Napper D. J.Colloid Interface Sci. 32 (1) (1970) 106-14.
- 30. Ji X, Copenhaver D, Sichmeller C, Peng X. J. Am. Chem. Soc. 130 (17) (2008) 5726-35.
- 31. Kobayashi M, Skarba M, Galletto P, Cakara D, Borkovec M. J. Colloid Interface Sci. 292 (1) (2005) 139-47.
- 32. Ortega-Vinuesa J, Martin-Rodriguez A, Hidalgo-Alvarez R. J. Colloid Interface Sci. 184 (1) (1996) 259-67.
- 33. Liese A and Hilterhaus L. Chem. Soc. Rev. 42 (15) (2013) 6236-49.
- 34. Salunkhe A, Khot V, Pawar S. Curr. Top. Med. Chem. 14 (5) (2014) 572-94.
- 35. Widder K, Senyei A, Ranney D. Adv. Pharmacol. 16 (1979) 213-71.
- 36. Hao R, Xing R, Xu Z, Hou Y, Gao S, Sun S. Adv. Mater. 22 (25) (2010) 2729-42.
- 37. Gupta A and Gupta M. Biomater. 26 (18) (2005) 3995-4021.
- 38. Kumar Y, Sinha A, Nigam K, Dwivedi D, Sangwai J. Nanoscale. 15 (13) (2023) 6075-104.
- 39. Xu C and Sun S. Polym. Int. 56 (7) (2007) 821-26.
- 40. Lu A, Salabas E, Schüth F. Angew. Chem. Int. Ed. 46 (8) (2007) 1222-44.
- 41. Markides H, Rotherham M, El Haj A. J. Nanomater. 2012 (1) (2012) 614094-105.
- 42. Shenoy D, Amiji M. Int. J. Pharm. 293 (1-2) (2005) 261-70.
- 43. Horcajada P, Gref R, Baati T, Allan P, Maurin G, Couvreur P, Férey G, Morris R, Serre C. Chem. Rev. 112 (2) (2012) 1232-68.
- 44. Yu M, Huang S, Yu K, Clyne A. Int. J. Mol. Sci. 13 (5) (2012) 5554-70.
- 45. Wang C, Xu C, Zeng H, Sun S. Adv. Mater. 21 (30) (2009) 3045-52.
- 46. Reddy L, Arias J, Nicolas J, Couvreur P. Chem. Rev. 112 (11) (2012) 5818-78.
- 47. Xu F, Geiger J, Baker G, Bruening M. Langmuir. 27 (6) (2011) 3106-12.
- 48. Sperling R and Parak W. Philos. Trans. R. Soc. A. 368 (1915) (2010) 1333-83.
- 49. Wu W, Jiang C, Roy V. Nanoscale. 8 (47) (2016) 19421-74.
- 50. Tartaj P, Gonzalez-Carreno T. Serna C. Adv. Mater. 13 (21) (2001)1620-4.
- 51. Xu C, Xu K, Gu H, Zheng R, Liu H, Zhang X, Guo Z, Xu B. J. Am. Chem. Soc. 126 (32) (2004) 9938-39.
- 52. Sun Z, Yathindranath V, Worden M, Thliveris J, Chu S, Parkinson F, Hegmann T, Miller D. Int J Nanomedicine. 8 (1) (2013) 961-70.

- 53. Quarta A, Curcio A, Kakwere H, Pellegrino T. Nanoscale. 4 (11) (2012) 3319-34.
- 54. Boyer C, Whittaker M, Bulmus V, Liu J, Davis T. NPG Asia Materials. 2 (1) (2010) 23-30.
- 55. Oh J and Park J. Prog. Polym. Sci. 36 (1) (2011) 168-89.
- 56. Caner N, Tugba I, Yasemin Y, Havva Y, Seda K. Int J Nanomedicine. 7 (2012) 1903-20.
- 57. Mahmoudi M, Sant S, Wang B, Laurent S, Sen T. Adv. Drug Deliv. Rev. 63 (1-2) (2011) 24-46.
- 58. Laurent S, Forge D, Port M, Roch A, Robic C, Vander Elst L, Muller R. Chem. Rev. 108 (6) (2008) 2064-110.
- 59. Kievit F, Veiseh O, Bhattarai N, Fang C, Gunn J, Lee D, Ellenbogen R, Olson J, Zhang M, Adv. Funct. Mater. 19 (14) (2009) 2244-51.
- 60. Bahavarnia F, Hasanzadeh M, Bahavarnia P, Shadjou N. RSC Adv. 14 (19) (2024) 13384-412.
- 61. Petrovici A, Pinteala M, Simionescu N. Molecules. 28 (3) (2023)1086-103.
- 62. Yang H, Park C, Woo M, Kim M, Jo Y, Park H, Kim J. Biomacromolecules. 11 (11) (2010) 2866-72.
- 63. Ren Y, Rivera J, He L, Kulkarni H, Lee D. Messersmith P. BMC Biotechnol. 11 (63) (2011) 1-8.
- 64. Wiogo H, Lim M, Bulmus V, Yun J, Amal R. Langmuir. 27 (2) (2011) 843-50.
- 65. He W, Cheng L, Zhang L, Liu Z, Cheng Z, Zhu X. ACS Appl. Mater. Interfaces. 5 (19) (2013) 9663-69.
- 66. Ding H, Zhang Y, Wang S, Xu J, Xu S, Li G. Mater. Chem. 24 (23) (2012) 4572-80.
- 67. Brollo M, Pinheiro I, Bassani G, Varet G. Merino-Garcia D, Guersoni V, Knobel M, Bannwart A, van der Geest C, Muraca D. ACS omega. 8 (36) (2023) 32520-5.
- 68. Wu W, He Q, Jiang C. Nanoscale Res. Lett. 3 (397) (2008) 397-415
- 69. Zhu Y, Ikoma T, Hanagata N, Kaskel S. Small. 6 (3) (2010) 471-78.
- 70. Cao Z, Yang L, Ye Q, Cui Q, Qi D, Ziener U. Langmuir. 29 (22) (2013) 6509-18.
- 71. Bae H, Ahmad T, Rhee I, Chang Y, Jin S, Hong S. Nanoscale Res. Lett. 7 (1) (2012) 1-5.
- 72. Fan H, Niu R, Duan J, Liu W, Shen W. ACS Appl. Mater. Interfaces. 8 (30) (2016) 19475-83.
- 73. Fan X, Jiao G, Zhao W, Jin P, Li X. Nanoscale. 5 (3) (2013) 1143-52.
- 74. Li X, Huang X, Liu D, Wang X, Song S, Zhou L, Zhang H. JPC C. 115 (44) (2011) 21567-73.
- 75. Georgakilas V, Otyepka M, Bourlinos A, Chandra V, Kim N, Kemp K, Hobza P, Zboril R, Kim K. Chem. Rev. 112 (11) (2012) 6156-214.

- 76. Chen W, Yi P, Zhang Y, Zhang L, Deng Z, Zhang Z. ACS Appl. Mater. Interfaces. 3 (10) (2011) 4085-91.
- 77. Henry A, Bingham J, Ringe E, Marks L, Schatz G, Van Duyne R. J. Phys. Chem. C. 115 (19) (2011) 9291-305.
- 78. Yen C, Mahmoud M, El-Sayed M. J. Phys. Chem. A. 113 (16) (2009) 4340-45.
- 79. Ju-Nam Y and Lead. Sci. Total Environ. 400 (1-3) (2008) 396-414.
- 80. Dreaden E, Alkilany A, Huang X, Murphy C, El-Sayed M. Chem. Soc. Rev. 41 (7) (2012) 2740-79.
- 81. Zhang J, Thurber A, Hanna C, Punnoose A. Langmuir. 26 (7) (2010) 5273-78.
- 82. Gu H, Zheng R, Zhang X, Xu B. J. Am. Chem. Soc. 126 (18) (2004) 5664-65.
- 83. Kim D, Yu M, Lee T, Park J, Jeong Y, Jon S. Nanotechnology. 22 (15) (2011) 155101-08.
- 84. Zhai Y, Zhai J, Wang Y, Guo S, Ren W, Dong S. J. Phys. Chem. C. 113 (17) (2009) 7009-14.
- 85. Lin J, Zhou W, Kumbhar A, Wiemann J, Fang J, Carpenter E, O'connor C. J. Solid State Chem. 159 (1) (2001) 26-31.
- 86. Shubayev V, Pisanic II T, Jin S. Adv. Drug Deliv. Rev. 61 (6) (2009) 467-77.
- 87. Wu W, Jiang C, Roy V. Nanoscale. 7 (1) (2015) 38-58.
- 88. Wu W, Xiao X, Zhang S, Li H, Zhou X, Jiang C. Nanoscale Res. Lett. 926 (4) (2009) 926-31.
- 89. Ahadpour Shal A and Jafari A. J. Supercond. Novel Magn. 27 (2014) 1531-38.
- 90. Liu J, Cheng J, Che R, Xu J, Liu M, Liu Z. J. Phys. Chem. C. 117 (1) (2013) 489-95.
- 91. Shinde G and Thakur J. Res. Chem. Intermed. 50 (2) (2024) 817-38.
- 92. Gowd G, Patra M, Mathew M, Shukla A, Songara S, Vadera S, Kumar N. Opt. Mater. 35 (9) (2013) 1685-92.
- 93. Xi G, Yue B, Cao J, Ye J. Chem. Eur. J. 17 (18) (2011) 5145-54.
- 94. Li Z, Wen Y, Shang J, Wu M, Wang L, Guo Y. Chin Y. J Chem. 25 (2) (2014) 287-91.
- 95. Chen C and Chen Y. J. Biomed. Nanotechnol. 4 (1) (2008) 73-79.
- 96. Lai C, Lu M, Chen L. J. Mater. Chem. 22 (1) (2012) 19-30.
- 97. Liu X, Fang Z, Zhang X, Zhang W, Wei X, Geng B. Cryst. Growth Des. (1) (2009) 197-202.
- 98. Etgar L, Lifshitz E, Tannenbaum R. J. Phys. Chem. C. 111 (17) (2007) 6238-44.
- 99. Liu D, Tong L, Shi J, Yang X, Yang H. J. Mater. Sci.: Mater. Electron. 23 (2012) 464-67.
- 100. Zedan A, Abdelsayed V, Mohamed M, El-Shall M. J. Mater. Sci. Mater. Electron. 1312 (15) (2013) 1-8.

- 101. Zhan F and Zhang C. J. Mater. Chem. 21 (13) (2011) 4765-67.
- 102. Lopez-Ortega A, Estrader M, Salazar-Alvarez G, Roca A, Nogues J. Physics Reports. 553 (2015) 1-32.
- 103. Gonzales M and Krishnan K. J. Magn. Magn. Mater. 311 (1) (2007) 59-62.
- 104. Jiang H, Zeng X, Xi Z, Liu M, Li C, Li Z, Jin L, Wang Z, Deng Y, He N. J.Biomed. Nanotechnol. 9 (4) (2013) 674-84.
- 105. Wang Z, Shen L, Zhu S. Int. j. photoenergy. 2012 (1) (2012) 202519-25.
- 106. Chen J, Chen C, Liu J, Xu R, Qiao S, Lou X. Chem Commun. 47 (9) (2011) 2631-33.
- 107. Sun L, Wu W, Yang S, Zhou J, Hong M, Xiao X, Ren F, Jiang C. ACS Appl. Mater. Interfaces. 6 (2) (2014) 1113-24.
- 108. Yao W, Tian Q, Liu J, Wu Z, Cui S, Ding J, Dai Z, Wu W. Mater. Chem C. 4 (26) (2016) 6327-35.
- 109. Zhang L, Wang Y, Yang Y, Zhang F, Dong W, Zhou S, Pei W, Chen H, Sun H. Chem Commun. 48 (91) (2012) 11238-40.
- 110. Huo X, Li W, Zhu J, Li L, Li Y, Luo L, Zhu Y. J. Phys. Chem. C. 119 (46) (2015) 25786-91.
- 111. Shen J, Lu Y, Liu J, Yang X. J. Mater. Sci. 51 (2016) 7793-802.
- 112. Jenkins R. X-ray techniques: overview. Encyclopedia of analytical chemistry. (2000) 1-20.
- 113. Bunaciu A, UdriȘTioiu E, Aboul-Enein H. X-ray diffraction: instrumentation and applications. Critical reviews in analytical chemistry. 45 (4) (2015) 289-99.
- 114. Le Troedec M, Sedan D, Peyratout C, Bonnet J, Smith A, Guinebretiere R, Gloaguen V, Krausz P. Compos. A: Appl. Sci. Manuf. 39 (3) (2008) 514-22.
- 115. Griffiths P. Fourier transform infrared spectrometry. Science. 222 (4621) (1983) 297-302.
- 116. Alonzo D, Gao Y, Zhou D, Mo H, Zhang G, Taylor L. J. Pharm. Sci. 100 (8) (2011) 3316-31.
- 117. Inkson B, Scanning electron microscopy (SEM) and transmission electron microscopy (TEM) for materials characterization. Materials characterization using nondestructive evaluation (NDE) methods, Woodhead publishing. (2016) 17-43.
- 118. Lunardi C, Gomes A, Rocha F, De Tommaso J, Patience G. The Canadian Journal of Chemical Engineering. 99 (3) (2021) 627-39.
- 119. Aleandri S, Vaccaro A, Armenta R, Völker A, Kuentz M. Pharmaceutics. 10 (3) (2018) 94-104.

- 120.Tonthat L, Yamamoto Y, Aki F, Saito H, Mitobe K. IEEE Transactions on Magnetics. 54 (6) (2018) 1-4.
- 121. "Magnetic Property Measurement System", SQUID VSM User's Manual (2009).
- 122. Hayyan M, Hashim M, AlNashef I. Chem. Rev. 116 (5) (2016) 3029-85.

CHAPTER-04 SYNTHESIS, CHARACTERIZATION, AND MAGNETIC HYPERTHERMIA STUDY OF MAGNETITE- Fe₃O₄ NANOPARTICLES

INDEX

Sr.No		Page No.		
4.1	Introdu	Introduction		
4.2	Experi	mental	90	
4.3	Results	91		
	4.3.1	Structural/ Phase Analysis	91	
	4.3.2	Morphological Analysis	93	
	4.3.3	Chemical Signature	94	
	4.3.4	Particle Size and Zeta Potential Study	95	
	4.3.5	Vibrating Sample Magnetometer (VSM) Analysis	96	
	4.3.6	Magnetic Hyper Thermia (MHT) Study	98	
	4.3.7	Biocompatibility	99	
4.4	Conclu	isions	102	
	Referen	104		

4.1 Introduction:

Physical, optical, magnetic, and electrical properties show unique transformations when the particle size is less than 100 nm. Thus, a nanomaterial is a fundamental of agglomerated particles whose size is below 100 nm. When the size is lower than Bohr's exciton radius (quantum dot), quantum confinement effects are observed. These properties are quite different from bulk materials [1]. Nanocrystalline spinel ferrites have potential applications in microwave absorbers, recording systems, chemical sensors, imaging, permanent magnets, ferrofluid technology, and biomedical applications [2]. Spinel ferrite exhibits Tetrahedral (A) and Octahedral (B) sublattices in cubic space group. In the compound (MFe₂O₄), M²⁺ (M = Fe, Co, Mg, Ni, Mn, etc.) and Fe³⁺ are organized at two different crystallographic sites with tetrahedral and octahedral oxygen coordination. Normal spinel is the structure that results when 16 B sites are filled by Fe³⁺ cations, and M²⁺ cations fill 8 A sites. In inverse spinel structure, M²⁺ ions occupy the B site whereas Fe³⁺ ions randomly occupy both A and B sites [3]. Hydrophilic ferrofluids are mostly employed in medical applications for therapy and detecting medical problems. The hydrophobic ferrofluids are used in applications like rotating shaft seals and loudspeakers [4]. Ferrite nanoparticles exhibit spin canting, metastable cation distribution, core/shell structure, and superparamagnetism when the particle size is below 20 nm. These properties are contingent upon several variables, including anisotropy, surface morphology, composition, grain size, and interparticle interactions. The electrical and magnetic properties of ferrites can be affected by the distribution of cations between tetrahedral and octahedral sites. This distribution can be regulated by the synthesis methods and synthesis parameters [5].

Hematite- α -Fe₂O₃, Maghemite- γ -Fe₂O₃, and Magnetite- Fe₃O₄ are the most common phases of iron oxide among various ferrite materials. The most prevalent type of iron oxide utilized in biomedical applications is Magnetite-Fe₃O₄, which has a greater saturation magnetization (Ms) value, is less toxic, biocompatible, easy to tag biomolecules, and simple to synthesize. Because of these special qualities, Magnetite- Fe₃O₄ nanoparticles have been authorized for use in clinical human trials [6,7].

The reaction mechanism has significant influence on the physicochemical properties of synthesized nanoparticles such as magnetic properties, solubility, and crystal structure. These characteristics have been shown to change when the $[Fe^{2+}]$ / $[Fe^{3+}]$ ion ratio changes. Magnetite-Fe₃O₄ nanoparticles have an inverse spinel crystal structure where Fe²⁺ ions are found in the B site, whereas Fe³⁺ ions are evenly distributed throughout the A and B sites. The

dominant factor behind the magnetic properties of these ferrites is the super exchange interaction between cations occupying the A- and B-sites in conjunction with oxygen ions [2,8,9].

In the present study, chemical co-precipitation method was used to synthesize Iron Oxide Nanoparticles (IONPs) by varying the molar ratio of iron salts, providing Fe^{2+} and Fe^{3+} ions.

4.2 Experimental:

Materials:

Materials used to synthesize IONPs: Iron (III) chloride hexahydrate (FeCl₃·6H₂O, ≥99%); Iron (II) chloride tetrahydrate (FeCl₂·4H₂O, ≥99%); and Sodium hydroxide (NaOH, ≥99%) -Sigma-Aldrich.

A) Synthesis of IONPs:

To synthesize IONPs the molar concentration ratio Fe^{2+} : Fe^{3+} ions was taken 0.5:2.5, 1:2, 1.5:1.5, and 2:1, labelled as I_1 , I_2 , I_3 , and I_4 , respectively.

FeCl₂·4H₂O and FeCl₃·6H₂O were separately dissolved in Double Distilled Water (DDW) for the given molar ratio with constant stirring. In this mixture, 80 mM of NaOH was added dropwise to bring the pH of the iron salt solution to 13 from the initial acidic pH 3.2. The precursor was maintained at 70±5 °C for 60 min and then cooled to room temperature. Using magnetic decantation process, precipitate was collected and washed with DDW, and desiccated in an oven at a temperature of 70 °C. The samples thus obtained were labelled as I_1 , I_2 , I_3 , and I_4 .

Numerous studies have been conducted on the co-precipitation method employing Fe²⁺ and Fe³⁺ ions interacting in an alkaline condition. In the co-precipitation method, if the percent of Fe³⁺ ions exceeds 2, then ferric hydroxide is formed quickly [8] as seen for sample I₁. Following reaction mechanism is proposed for the synthesis of Magnetite-Fe₃O₄ (IONPs) via coprecipitation method:

In the first stage, ferric and ferrous hydroxides are formed:

$$FeCl_3 = Fe^{3+} + 3Cl^-$$

 $Fe^{3+} + 3OH^- = Fe(OH)_3$ (4.1)
 $FeCl_2 = Fe^{2+} + 2Cl^-$
 $Fe^{2+} + 2OH^- = Fe(OH)_2$ (4.2)

In the second stage, ferric hydroxide decomposes to Ferric-oxyhydroxide (FeOOH):

$$Fe(OH)_3 = FeOOH + H_2O$$
 (4.3)

Finally, reaction between Ferric-oxyhydroxide (FeOOH) and Ferrous hydroxides (Fe (OH)₂) takes place to form Magnetite- Fe₃O₄ particles:

$$2FeOOH + Fe(OH)_2 = Fe_3O_4 + 2H_2O \qquad (4.4)$$

The overall reaction is as follows:

$$2Fe^{3+} + Fe^{2+} + 80H^{-} = 2Fe(0H)_3 Fe(0H)_2 \rightarrow Fe_3O_4 + 4H_2O$$
 (4.5)

For sample I_1 Ferrous hydroxide is oxidized to Ferric hydroxide and then to Hematite- α -Fe₂O₃[8]:

$$2Fe(OH)_3 = Fe_2O_3 + 3H_2O \qquad (4.6)$$

Various factors, like initial concentration, molar ratios of ferrous and ferric salts, concentration of base solution, reaction temperature, stirring rate, etc, were optimized.

B) Characterization:

X-ray Diffraction (XRD) patterns of powder samples I_1 , I_2 , I_3 , and I_4 were recorded with CuK α radiation (λ =1.546 Å). Scanning Electron Microscopy (SEM) (JEOL, JSM-IT200 (Japan)) was used to observe the morphology. Fourier Transform Infrared Spectroscopy (FTIR) spectra were recorded on Alpha (II) Bruker device operating in a range of 400-4000 cm⁻¹. Hydrodynamic particle size and zeta (ζ)-potential were recorded using (HORIBA SZ-100) with water as a dispersant. Vibrating Sample Magnetometer (VSM) (EV X) was used to study magnetic properties at room temperature. Magnetic Hyper Thermia (MHT) study for all the samples was carried using an EasyHeat 8310 (Ambrell, UK) assembly. Based on MHT outcome, the anticancer efficacy of the Magnetite- Fe₃O₄ (sample I_2) nanoparticles was made using (3-[4,5-dimethylthiazol-2-yl]-2,5 diphenyl tetrazolium bromide) (MTT) assay and evaluated against L929 fibroblast cell line and MDA-MB-231 breast cancer cell line. The hemolysis assay was used to assess the effect of synthesized particles on red blood cells, i.e. to check the hemocompatibility of Magnetite- Fe₃O₄ (sample I_2) nanoparticles.

4.3 Results and Discussion:

4.3.1 Structural/Phase Analysis:

X-Ray Diffraction (XRD):

The XRD patterns for samples I_1 , I_2 , I_3 , and I_4 are shown in **Fig.4.1**. All the samples show polycrystalline structure. Sample I_1 shows rhombohedral spinel crystal structure revealing Hematite- α -Fe₂O₃ phase. Samples I_2 , I_3 , and I_4 reveal cubic inverse spinel crystal structure of Magnetite- Fe₃O₄ phase. The average lattice constant for samples I_2 , I_3 , and I_4 is 8.33 Å. The XRD patterns perfectly match with the JCPDS card nos. 00-33-0664 for Hematite- α -Fe₂O₃ (I_1) and 00-019-0629 for Magnetite- Fe₃O₄ (I_2 , I_3 , and I_4). The average

crystallite size calculated using the Scherrer formula (**Equation 3.3** (**Chapter-03**)) for the prominent peaks is found to be 25 ± 4 nm for Sample I₁ and 10.5 ± 1.3 nm for samples I₂, I₃, and I₄.

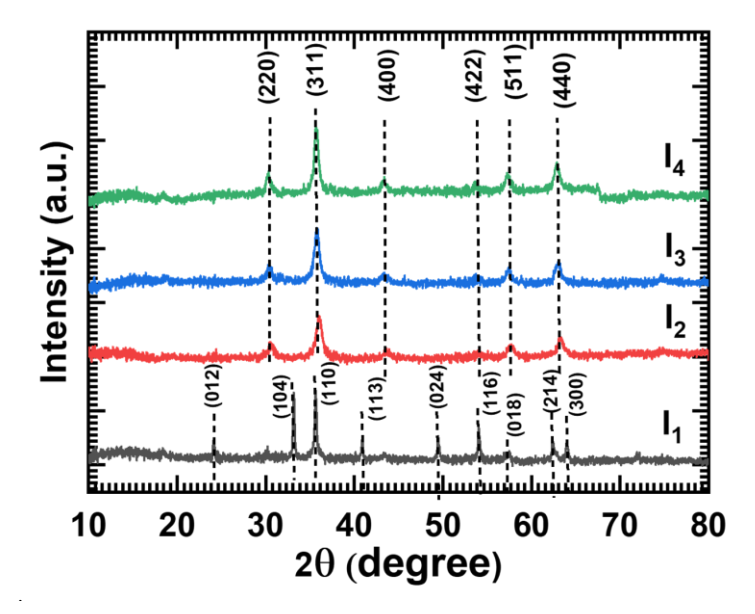


Fig.4.1: XRD patterns of Hematite- α -Fe₂O₃ (sample I₁) and Magnetite- Fe₃O₄ (samples I₂, I₃, and I₄) nanoparticles.

The increase in crystallite size for sample I_1 may be due to a higher concentration of Fe^{3+} ions compared to Fe^{2+} ions.

Transmission Electron Microscopy (TEM):

The particle size was further evaluated using Transmission Electron Microscope (TEM) (JEOL, JEM 2100). The Transmission Electron (TE) micrographs for three different magnifications are shown in **Fig.4.2** for Magnetite- Fe₃O₄ (sample I₂). The average particle size is found to be 10± 0.5 nm, which matches with that calculated from XRD study.

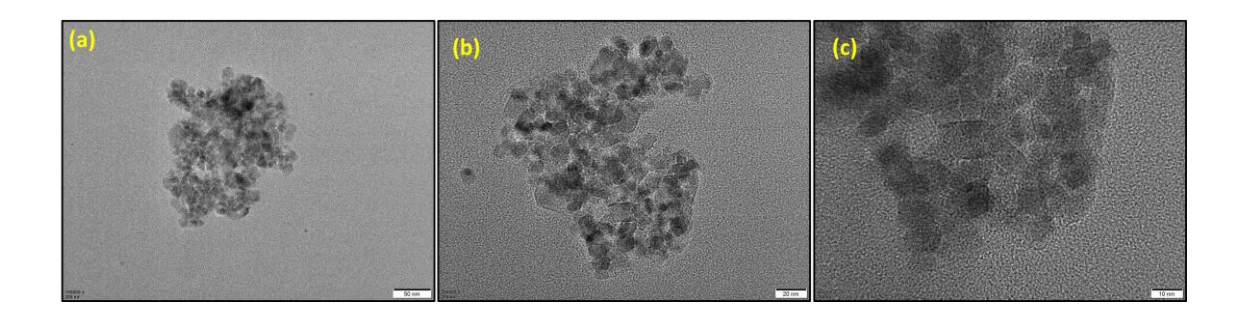


Fig.4.2: TE micrographs of Magnetite- Fe₃O₄ (sample I₂) nanoparticles at different magnifications.

4.3.2 Morphological Analysis:

Scanning Electron Microscopy (SEM):

The surface morphology of the synthesized IONPs were studied using SEM. The Scanning Electron (SE) micrographs at two different magnifications are shown in **Fig.4.3**.

Granular surface morphology of agglomerated IONPs is seen with an average grain size of 32.38 nm, 38.42 nm, and 43.21 nm for samples I₂, I₃, and I₄, respectively.

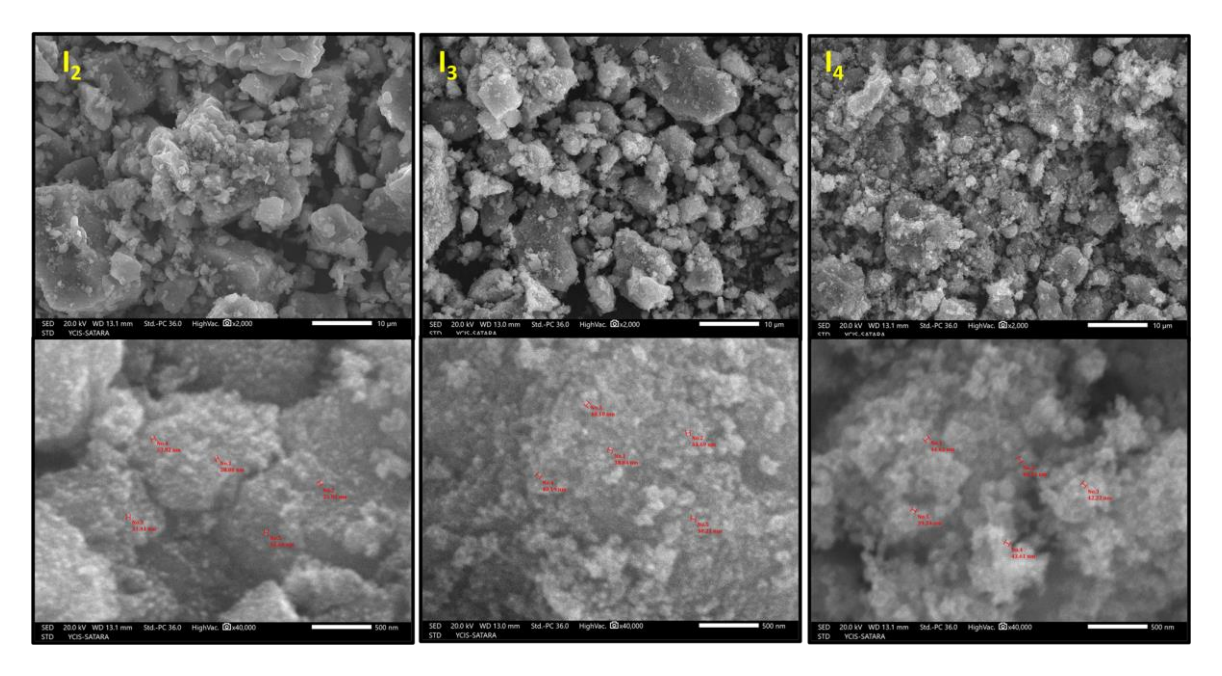


Fig.4.3: SE Micrographs of samples I₂, I₃, and I₄ at 2000X and 40000X.

Energy Dispersive X-Ray (EDX/EDAX) Analysis:

The elemental composition in terms of atomic weight percentage was analyzed using EDX technique to evaluate stoichiometry of the IONPs. The EDX profile for samples I₂, I₃, and I₄ is shown in **Fig.4.4**.

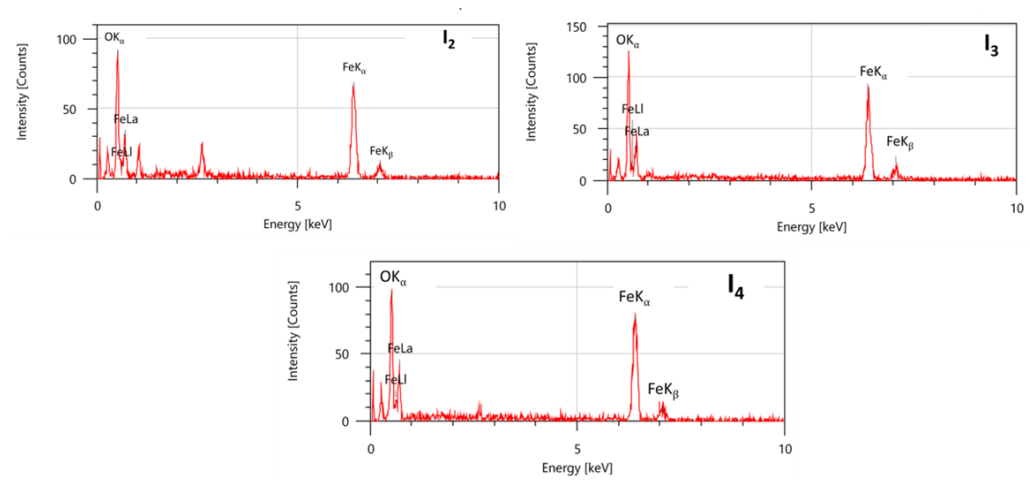


Fig.4.4: EDX profile of samples I₂, I₃, and I₄.

The atomic weight percentage of Fe and O elements present in the samples I_2 , I_3 , and I_4 is given in **Table 4.1**. The EDX analysis of samples I_2 , I_3 , and I_4 shows close agreement with theoretical value.

Table 4.1: Weight percentages of the Fe and O atoms in the samples I₂, I₃, and I₄ from EDX profile.

Sample name	Atomic V	Weight %	Fe ₃ O ₄ stoichiometry	
	Fe	0	2.61 (theoretical)	
I ₂	70.90	29.10	2.43	
I 3	69.70	30.30	2.30	
I ₄	72.56	27.44	2.64	

4.3.3 Chemical Signature:

Fourier-Transform Infrared Spectroscopy (FTIR):

The chemical bonds existing in Magnetite- Fe₃O₄ is studied using FTIR spectroscopy in which the incident infrared radiation is absorbed at a resonant frequency of bending, stretching, or vibrating chemical bonds that exist between the atoms within the compound.

The FTIR absorption spectra of samples I_2 , I_3 , and I_4 within the wavenumber range of $4000 \text{ to } 300 \text{ cm}^{-1}$ are shown in **Fig.4.5**.

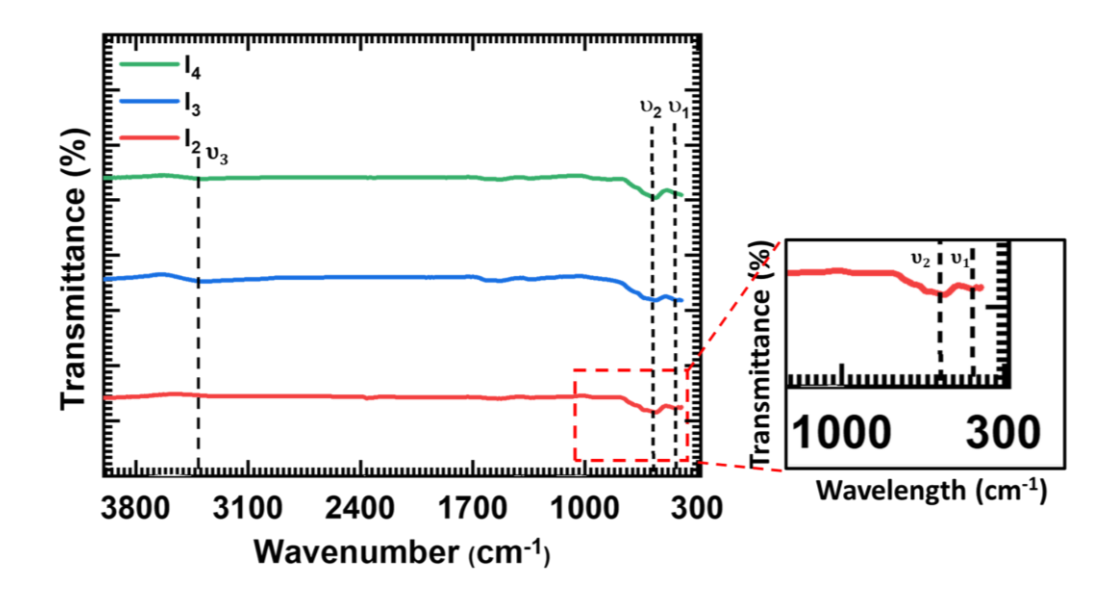


Fig.4.5: FTIR Spectra of samples I₂, I₃, and I₄.

An FTIR study revealed the presence of vibrating stretching bond Fe-O (υ_1 = 431.17 to 454.82 cm⁻¹) at the octahedral site and Fe-O (υ_2 =556.36 to 561.18 cm⁻¹) at the tetrahedral site. The presence of Fe-O stretching bonds at tetrahedral and octahedral sites indicates formation of inverse spinel ferrite phase.

The absorption band at 1600 cm⁻¹ is attributed to the bending vibration of the O-H bond, while the absorption band at 3400 cm⁻¹ (υ_3) is due to the stretching vibration of the O-H bond; both are characteristic of a hydroxyl group which can cause the broadness of the peak around 3400 cm⁻¹ (υ_3) [10,11].

4.3.4 Particle Size and Zeta Potential Study:

Dynamic Light Scattering (DLS):

Good chemical stability at physiological/neutral pH \sim 7 is necessary for the use of nanoparticles in biomedicine. Veiseh et al. [12] studied that the physicochemical characteristics of nanoparticles seem to have a major impact on their biodistribution. The hydrodynamic size influences the permeability of nanoparticles out of the vasculature and controls the nanoparticles concentration profile in the blood vessel, which in turn influences the nanoparticle's clearance process.

The DLS study was performed for sample I₂ to investigate the hydrodynamic diameter of nanoparticles with the average size distribution at room temperature using DDW at pH value of 7.2. The observed hydrodynamic diameter of IONPs is 113.7 nm (**Fig.4.6**). The hydrodynamic size of IONPs is more compared to actual size of the nanoparticles due to solvation layer of water molecules and ions around the particles, along with the little aggregation [12].

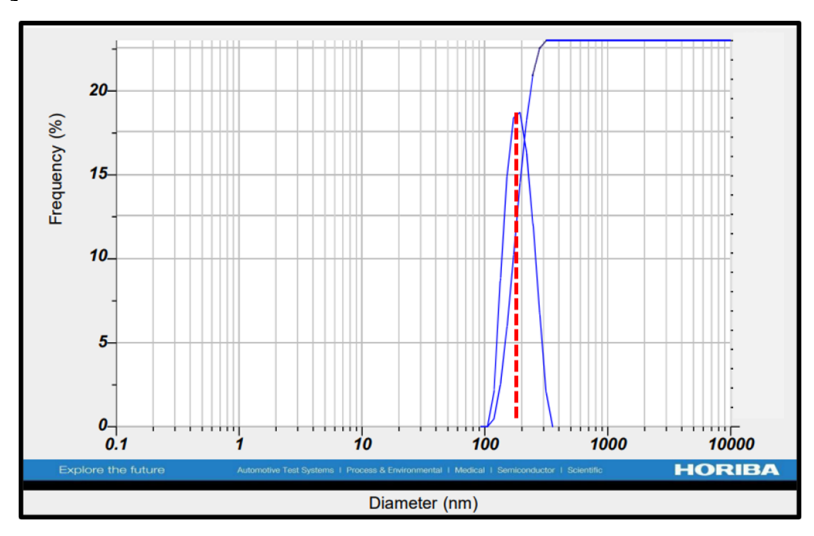


Fig.4.6: Hydrodynamic diameter of IONPs.

Zeta potential (ζ -potential):

The ζ - potential is used to measure the variation in surface charges of particles, which is used to control the electrostatic interaction of the nanoparticles. The stability of nanoparticles is investigated using ζ - potential measurements in water (pH \sim 7). The standard value of ζ - potential of MNPs to be used for biomedical applications is ± 30 mV [13]. The ζ -potential of IONPs varies in the range of -70 to 0 mV with a peak value at -30 mV as shown in **Fig.4.7**. The repulsive forces between negatively charged sheath around the IONPs cause the increase in hydrodynamic size as indicated in DLS study.

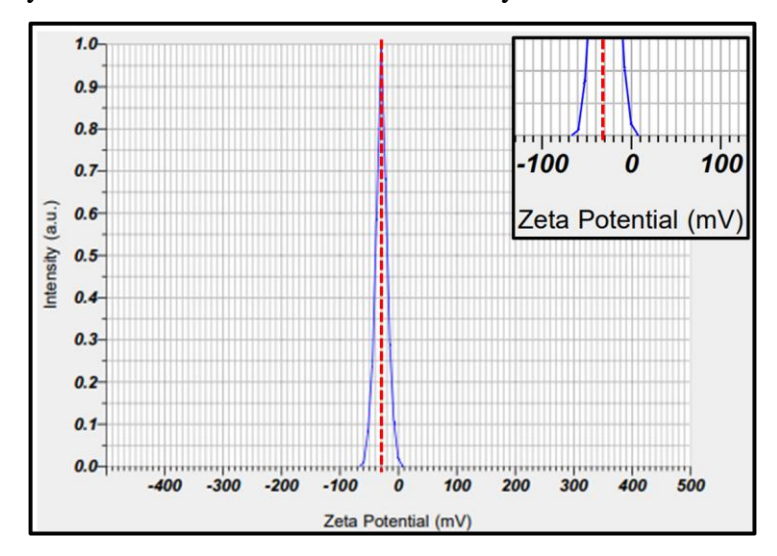


Fig.4.7: Zeta potential value of IONPs (Inset: enlarge view of zeta potential scale from -70 to +10 mV).

4.3.5 Vibrating Sample Magnetometer (VSM) Analysis:

The magnetic parameters, namely type of magnetism, saturation magnetization (Ms), coercivity (Hc), and retentivity, can be evaluated with the help of VSM, which generates a hysteresis loop of IONPs. The hysteresis loops for IONPs (samples I₂, I₃, and I₄) were obtained with the external magnetic field window of ±17 kOe at room temperature, which are shown in **Fig.4.8**.

The observed values of saturation magnetization (Ms) and coercivity (Hc) for samples I₂, I₃, and I₄ are given in **Table 4.2**. The obtained saturation magnetization (Ms) values are smaller than the saturation magnetization (Ms) value of bulk Magnetite- Fe₃O₄ i.e. 92 emu g⁻¹. The decrease in saturation magnetization (Ms) value of IONPs is caused by spin canting and the presence of irregular spins on the surface of nanoparticles. The variation in saturation magnetization (Ms) and coercivity (Hc) values may be due to an increase in particle size [13].

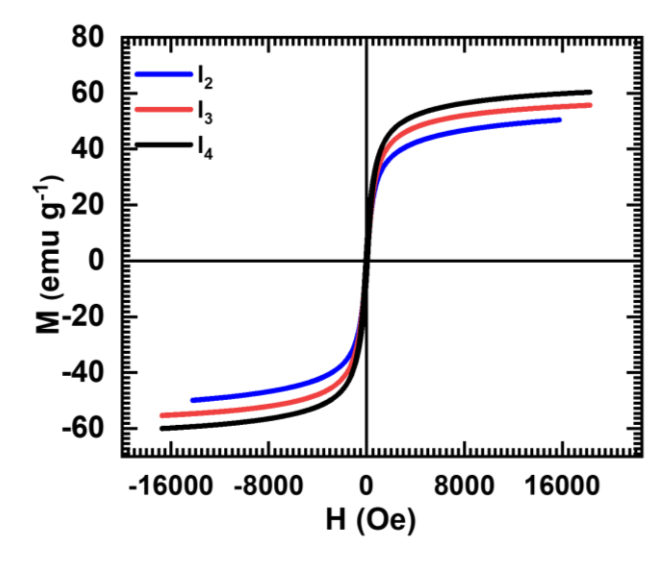
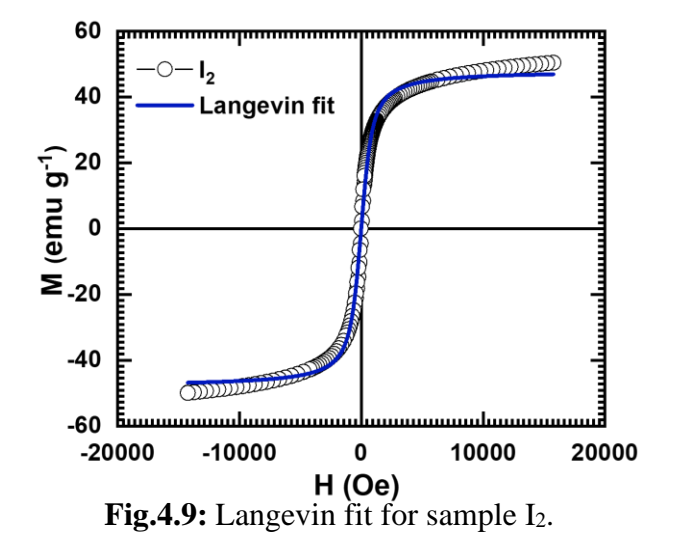


Fig.4.8: Magnetization versus magnetic field curves of samples I₂, I₃, and I₄.

Table 4.2: Saturation magnetization (Ms) and Coercivity (Hc) values of samples I₂, I₃, and I₄.

Sample	Ms (emu g ⁻¹)	Hc (Oe)	
I ₂	50.20	32.83	
I 3	55.54	35.99	
I ₄	60.21	61.45	

All the synthesized IONPs (samples I₂, I₃, and I₄) displayed Super Paramagnetic characteristics, exhibiting a S-shaped hysteresis curve. For the Super Paramagnetic IONPs field-dependent magnetization curves were fitted using the Langevin function. The exact fit was observed for sample I₂ as shown in **Fig.4.9** while samples I₃ and I₄ showed deviation for Langevin fit



4.3.6 Magnetic Hyper Thermia (MHT) Study:

When an Alternating Magnetic Field (AMF) is applied, the magnetization and demagnetization of IONPs produce heat due to hysteresis loss, Eddy current, and residual losses, this is called MHT. The MHT of samples I₂, I₃, and I₄ were studied using a magnetic induction heating device for 600 s. The heating ability of MNPs is expressed in terms of the Specific Absorption Rate (SAR) value which is defined as the capacity of MNPs to convert magnetic energy into heat. Generally, temperatures between 42-45°C are suitable to kill cancer cells. Thus, the MHT cancer therapy basically requires a suitable amount of MNPs to be inserted into cancer tumor and application of external AMF of appropriate strength to increase the temperature to kill the cancer cells. The efficacy of the treatment can be more effective when drugs are used along with MNPs.

Samples I₂, I₃, and I₄ with concentrations of 1, 2, and 3 mg mL⁻¹ were kept in a 3 mL cuvette containing 1 mL of DDW. This cuvette was kept in a MHT device and external AMF of fixed frequency (278 kHz) was applied for 600 s. The change in temperature was recorded for three different AMF strengths (13.3, 20.0, and 26.7 kA m⁻¹). **Fig.4.10** shows the temperature vs time curves of all the samples.

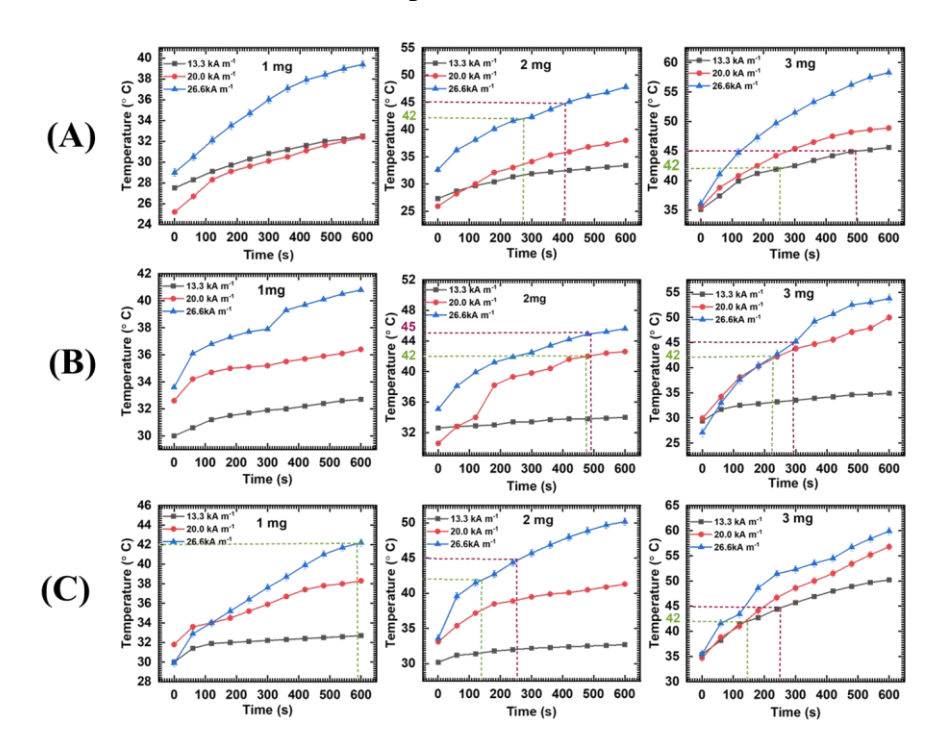


Fig.4.10: Temperature Vs Time variation for: (A) I₂, (B) I₃, and (C) I₄.

It is observed that with increase in the concentration of IONPs, there is increases in the temperature. Samples I_2 , I_3 , and I_4 show therapeutic temperature rise (beyond 42 °C) at the field strengths of 20.0 and 26.7 kA m⁻¹ for the 2 and 3 mg mL⁻¹ concentrations of magnetic

suspension. The therapeutic temperature is attained within 300 to 500 s for samples I_2 , I_3 , and I_4 when concentrations are 2 or 3 mg.

The SAR and Intrinsic Loss Power (ILP) values calculated using **Equations 2.7** and **2.8** (**Chapter-02**) as a function of magnetic field strength for samples I₂, I₃, and I₄ for different concentrations are shown in **Table 4.3**.

Table 4.3: SAR and ILP values for samples I_2 , I_3 , and I_4 for different magnetic field strengths.

Sampl	Applied Field	SAR (W g ⁻¹)			ILP (nHm² kg-¹, n=1)		
e	(kA m ⁻¹)	1	2	3	1	2	3
		mg mL ⁻¹	mg mL ⁻¹	mg mL ⁻¹	mg mL ⁻¹	mg mL ⁻¹	mg mL ⁻¹
	13.6	55.86	48.43	53.64	1.09	0.94	1.04
I_2	20	104.74	79.56	100.29	0.94	0.72	0.90
	26.7	125.69	124.53	137.62	0.63	0.63	0.69
	13.6	41.89	30.32	20.75	0.81	0.59	0.40
I_3	20	111.72	76.97	76.1	0.11	0.69	0.68
	26.7	174.57	116.62	103.77	0.88	0.59	0.52
	13.6	97.76	34.59	65.31	1.90	0.67	1.27
I_4	20	125.69	79.56	95.63	1.13	0.72	0.86
	26.7	209.49	207.55	142.28	1.06	1.05	0.72

It is seen that with increase in field strength SAR value increases and ILP values decreases as required for efficient MHT similarly no specific trend is observed for different concentrations [14-16].

Samples I₂, I₃, and I₄ show Magnetite- Fe₃O₄ phase with particle size less than 20 nm, which is suitable for MHT study. Based on the results of the physicochemical and magnetic characterization, it is noted that **sample I₂**, which corresponds to the Magnetite- Fe₃O₄ phase of IONPs with average crystallite size of 9.73 nm is most suitable for further biological studies such as biocompatibility (cell viability/toxicity) and MHT towards normal cell lines and breast cancer cell lines.

4.3.7 Biocompatibility:

Pristine, PEG coated and GSH coated Magnetite- Fe₃O₄ nanoparticles of different concentrations were subjected for biocompatibility tests. This topic gives results for pristine Magnetite- Fe₃O₄ nanoparticles (sample I₂).

(a) Cell Viability/Cytotoxicity Assay:

3-(4, 5-dimethylthiazol- 2-yl)-2,5-diphenyltetrazolium bromide (MTT) Assay:

Due to wide applications of iron oxide in the field of biomedical, cell viability and cell toxicity are the primary steps to check their biocompatibility. To study the toxicity, Magnetite- Fe₃O₄ nanoparticles were mixed with fibroblast cell line (L929) and cancer cell line (MDA MB 231).

The 96-well flat-bottom microplate was used to seed the cells in an incubator maintained at 37°C with 95% humidity and 5% CO₂ for 12 h. After seeding the cell lines for 12 h, different concentrations of 100, 50, 25, 12.5, 6.25, and 3.125 μg mL⁻¹ of Magnetite-Fe₃O₄ nanoparticles were mixed and the resulting mixture is incubated for further 48 h. After two rounds of Phosphate buffered saline (PBS) washing, each well is stained with 20 μL of MTT staining solution, followed by incubation at 37 °C. After 4 h, 100 μL of Dimethyl Sulfoxide (DMSO) was given to each well to dissolve the formazan crystal, and the absorbance at 570 nm was measured using a microplate reader.

Equations 3.5 and **3.6** (Chapter-03) were used to calculate the percentage of cell viability/ toxicity of Magnetite- Fe_3O_4 nanoparticles.

For L929 fibroblast cell line, the Magnetite- Fe₃O₄ nanoparticles show decrease in cell viability from 97 to 92 % with increase in the concentration of Magnetite- Fe₃O₄ nanoparticles from 3.125 to 100 µg mL⁻¹ as shown in **Fig.4.11 (a)**. The microscopy pictures of untreated and treated L929 fibroblast cell line for 100 µg mL⁻¹ of Magnetite- Fe₃O₄ nanoparticles is shown in **Fig.4.11 (b)**.

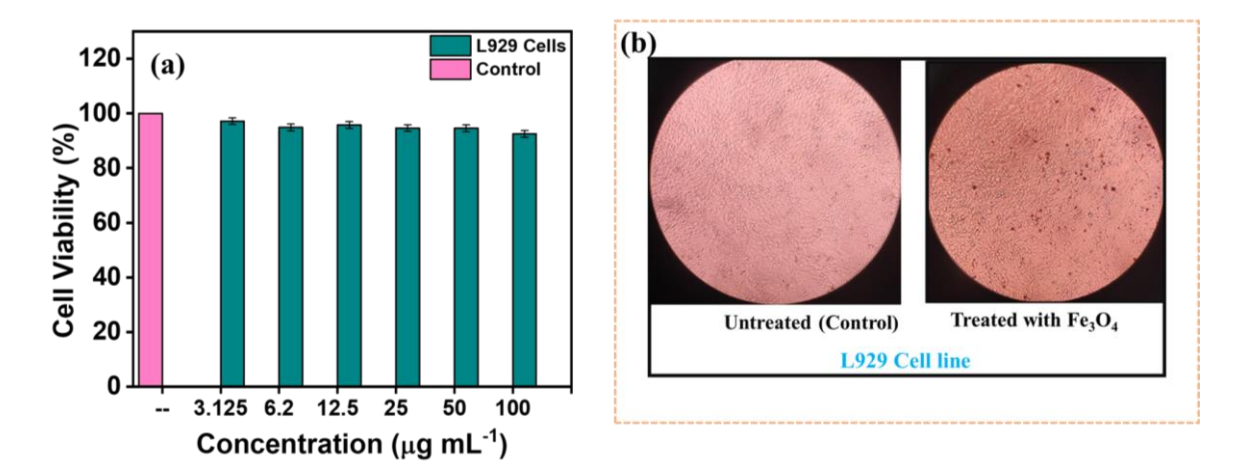


Fig.4.11: (a) Histogram of cell viability percentage and (b) The microscopy pictures of the L929 cell line.

For MDA-MB-231 breast cancer cell line, the Magnetite- Fe₃O₄ nanoparticles show increase in cell toxicity from 10 to 78% with increase in concentration from 3.125 to 100 μg mL⁻¹. Thus, the cell toxicity (killing of cancer cells) increases with concentration of Magnetite- Fe₃O₄ nanoparticles [17] as shown in Fig.4.12 (a). The microscopic picture of breast cancer cell line (MDA MB 231) for concentration of 100 μg mL⁻¹ of IONPs is shown in Fig.4.12 (b).

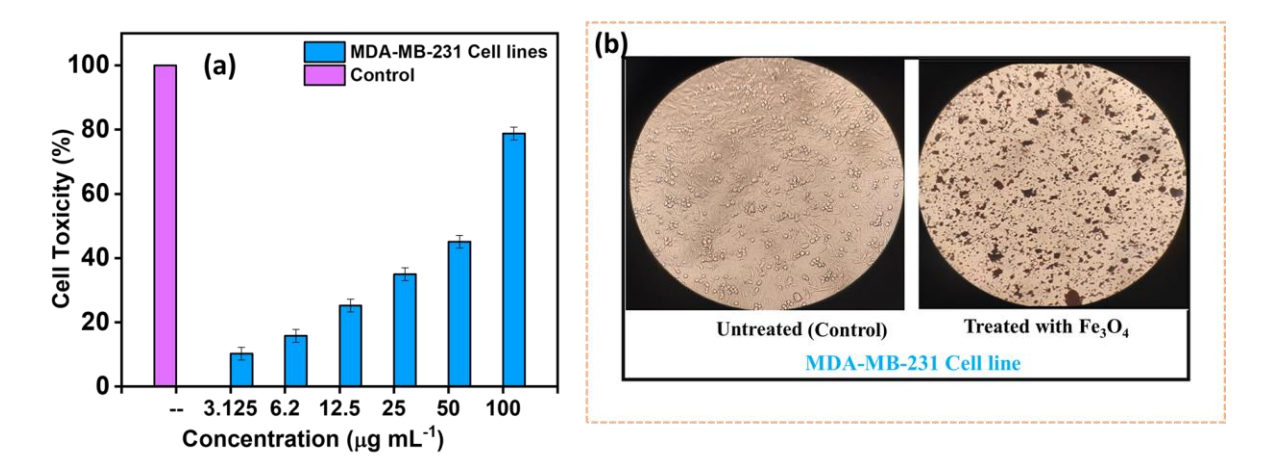


Fig.4.12: (a) Histogram of cytotoxicity percentage and (b) The microscopy pictures of the MDA MB 231 cell line.

As the concentration of nanoparticles increases, more Fe-ions are available to interact with cancer cells in Tumor Micro Environment (TME) which leads to increase in cell toxicity. The generation of Reactive Oxygen Species (ROS) by Magnetite- Fe₃O₄ nanoparticles is toxic to cancer cells and is the cause of cell death. This may be described as follows: in the cell, Magnetite- Fe₃O₄ nanoparticles break down into Fe²⁺ and Fe³⁺ ions at a pH of 4-5 (TME). The resulting ions play an important role in ROS formation by converting mitochondrial H₂O₂ into hydroperoxyl (HOO•) and hydroxyl (HO•) radicals via Fenton reaction. Another possibility is ferroptosis or iron metabolism caused by lipid peroxidation [13].

(b) Hemolysis Assay:

The entry of foreign particles into the body can have a variety of and sometimes conflicting effects, so determining their effects on the body is a critical step in their applicability. Because the injected nanoparticles come into direct touch with blood tissue and its components, an evaluation of their hemocompatibility is essential for further study.

For this study fresh human blood (10 mL) was collected in heparinized centrifuge tubes, rotated at 3000 rpm for 10 min, and washed three times with an equivalent volume of normal saline. The blood volume was measured and reconstituted as a 10% v/v solution in normal saline. The reaction mixture included 1 mL of 10% red blood cell suspension. Triton X-100 was used as a standard drug (positive control), saline as a negative control, and test sample with different concentrations of Magnetite- Fe₃O₄ nanoparticles were then incubated at 56°C for 30 min, and centrifuged at 2500 rpm for 5 min. The absorbance of the supernatant was measured at 560 nm. Hemolysis percentage was calculated using **Equation 3.7** (**Chapter-03**).

The concentration of the Magnetite- Fe₃O₄ nanoparticles was varied from 0.5 to 2.0 mg mL⁻¹. The change in hemolysis percentage is shown in **Fig.4.13** (a). The photographs of RBC suspensions of 1) Positive control (Triton x-100), 2) Negative Control (saline), and 3) Test sample are shown in **Fig.4.13** (b).

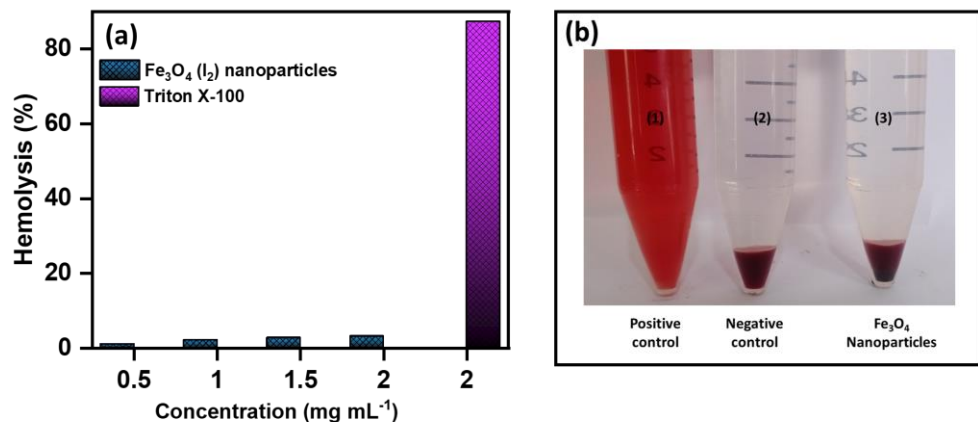


Fig.4.13: (a) Hemolysis percentage of Magnetite- Fe₃O₄ nanoparticles and (b) the photographs of RBC suspensions (1) Positive control (Triton x-100), (2) Negative Control (saline), and (3) Test sample.

The percentage of hemolysis is between 1 to 3 which is well below 5% as per ISO 10993-5 guidelines [18].

4.4 Conclusions:

Chemical coprecipitation method can be used to synthesize Magnetite- Fe₃O₄ nanoparticles with crystallite size well below 20 nm. The XRD study reveals inverse spinel crystal structure of Magnetite- Fe₃O₄ phase of IONPs with relevant tetrahedral and octahedral positions of ferrous and ferric ions. Sample I₂ with average crystallite size of 9.73 nm shows prominent magnetic properties and is found useful for MHT. The magnetization of 50.20 emu g⁻¹ and coercivity of 32.83 Oe confirm the superparamagnetic regime of

Magnetite- Fe₃O₄ nanoparticles. The toxicity of Magnetite- Fe₃O₄ nanoparticles against MDA-MB-231 breast cancer cell lines provides significant anticancer results where cell toxicity increases with an increase in the concentration of Magnetite- Fe₃O₄ nanoparticles. The Magnetite- Fe₃O₄ nanoparticles exhibit hemolysis below 5% which is permissible for biomedical applications. The highest values of SAR and lowest values of ILP can be obtained at physiologically safe ranges of external magnetic field strength and frequency, which makes synthesized Magnetite- Fe₃O₄ nanoparticles suitable for MHT cancer therapy.

References:

- 1. Jiang W, Lai K, Hu H, Zeng X, Lan F, Liu K, Wu Y, Gu Z. J. Nanoparticle Res. 13 (10) (2011) 5135-45.
- 2. Alibeigi S and Vaezi M. Chem. Eng. Technol: Industrial Chemistry-Plant Equipment-Process Engineering-Biotechnology. 31 (11) (2008) 1591-96.
- 3. Dojcinovic M, Vasiljevic Z, Pavlovic V, Barisic D, Pajic D, Tadic N, Nikolic M. J. Alloys Compd. 855 (1) (2021) 157429-66.
- 4. Kim J, Kim S, Kim Y. J. Nanosci. Nanotechnol. 14 (11) (2014) 8739-44.
- 5. Khot V, Salunkhe A, Phadatare M, Thorat N, Pawar S. J. Phys. D: Appl. Phys. 46 (5) (2012) 055303-13.
- 6. Ali A, Zafar H, Zia M, ul Haq I, Phull A, Ali J, Hussain A. Nanotechnol Sci Appl. 9 (9) (2016) 49-67.
- 7. Gnanaprakash G, Mahadevan S, Jayakumar T, Kalyanasundaram P, Philip J, Raj B. Mater. Chem. Phys. 103(1) (2007) 168-75.
- 8. Nejabat S, Ranaei Siadat S, Tahmasian Z, Mirzajani F, Fatemi F, Hosseinkhani S, Abedi M. Phys. Chem. Res. 9 (2) (2021) 241-52.
- 9. Jiang C, Yang S, Gan N, Pan H, Liu H. J. Magn. Magn. Mater. 439 (2017) 126-34.
- 10. Thorat N, Townely H, Brennan G, Parchur A, Silien C, Bauer J, Tofail S. ACS Appl. Bio Mater. 5 (6) (2019) 2669-87.
- 11. Singh A, Kumar P, Pathak S, Jain K, Garg P, Pant M, Mahapatro A, Rath D, Wang L, Kim S, Maurya K. J. Alloys Compd. 968 (2023) 171868-81.
- 12. Veiseh O, Gunn J, Zhang M. Adv. Drug Deliv. Rev. 62 (3) (2010) 284-304.
- 13. Shagholani H, Ghoreishi S, Mousazadeh M. Int. J. Biol. Macromol. 78 (2015) 130-6.
- 14. Patel N, Mulla N, Khot V, Patil R. Emerg. Mater. 7 (3) (2024) 1071-80.
- 15. Hergt R and Dutz S. J. Magn. Magn. Mater. 311 (1) (2007) 187-92.
- 16. Kalaiselvan C, Thorat N, Sahu N. ACS omega. 6 (8) (2021) 5266-75.
- 17. Bhavikatti S, Zainuddin S, Ramli R, Nadaf S, Dandge P, Khalate M, Karobari M. Sci. Rep. 14 (1) (2024) 11878-98.
- 18. Verde E, Landi G, Gomes J, Sousa M, Bakuzis A. J. Appl. Phys. 111 (12) (2012) 123902-11.

CHAPTER-05

SYNTHESIS, CHARACTERIZATION,
MAGNETIC HYPERTHERMIA, AND
CHEMOTHERAPY STUDY OF PEG COATED
MAGNETITE - Fe₃O₄ NANOPARTICLES

INDEX

Sr.No		Title	Page No.	
5.1	Introdu	Introduction		
5.2	Experin	nental	106	
	5.2.1	Surface Functionalization of Magnetite- Fe ₃ O ₄ Nanoparticles with PEG	107	
	5.2.2	Characterization	108	
5.3	Results	and Discussion	109	
	5.3.1	Structural/ Phase Analysis	109	
	5.3.2	Morphological Analysis	110	
	5.3.3	Chemical Signature	111	
	5.3.4	Particle Size and Zeta Potential Study	112	
	5.3.5	Vibrating Sample Magnetometer (VSM) Analysis	114	
	5.3.6	Magnetic Hyper Thermia (MHT) Study	115	
	5.3.7	Drug Loading and Drug Release Study	117	
	5.3.8	Biocompatibility	120	
5.4	Conclu	sions	122	
	Referen	nces	124	

5.1 Introduction:

In 1990, the new interdisciplinary term "nanomedicine" was introduced in the medical field. It was described as the application of nanoscopic or fine-structured materials in medicine that have distinctive biological effects due to their fascinating properties [1]. For example, Iron Oxide Nanoparticles (IONPs) have a physicochemical feature that are beneficial for many biomedical applications such as Magnetic Resonance Imaging (MRI) [2], drug delivery, cell tracking, Magnetic Hyper Thermia (MHT) [3], biosensors, and cell labelling [4], etc. Among different forms of iron oxide (Goethite, Wustite, Magnetite- Fe₃O₄, Maghemite- γ -Fe₂O₃, and Hematite- ∞ -Fe₂O₃), the main attention has been placed on Magnetite- Fe₃O₄ nanoparticles due to less toxicity, biocompatibility, injectability, chemical stability, high saturation magnetization (Ms) value, superparamagnetic properties, interaction with biomolecules, biomolecule dispersions, and ease of synthesis [5].

However, the coating is essential to make IONPs biocompatible, as pristine IONPs have a substantial specific surface area and significant interaction between dipoles. Also, the chemical stability and magnetic properties were affected, due to intense chemical activity leading to surface oxidation [6]. To improve the stabilization of Magnetite- Fe₃O₄ nanoparticles, relevant and biocompatible surfactants/polymers such as Poly Ethylene Glycol (PEG), chitosan, Poly Acrylic Acid (PAA), dextran, Poly Vinyl Alcohol (PVA), citric acid, Cetrimonium Bromide (CTAB), silica, etc are required on the surface of nanoparticles [7-9]. Among all, the foremost utilized agent for surface coating is PEG, due to extremely high biocompatibility, affinity with water, capacity to extend the period that Magnetite- Fe₃O₄ nanoparticles circulate in blood circulation, increased dispersibility, improved colloidal stability, non-toxicity, and low-cost [10].

Adding PEG to Magnetite- Fe₃O₄ nanoparticles significantly improves their biocompatibility, stability, and cellular absorption. PEG binding, frequently enhances the in vivo half-life of small drug molecules, decreases enzyme degradation, reduces toxicity, increases water solubility, increases dispersibility, and decreases agglomeration. These effects are commonly exploited in a variety of biomedical applications [11]. Thus, Magnetite- Fe₃O₄ nanoparticles coated with PEG become important for different biomedical applications.

Along with the nature of the surfactant, the size, shape, morphology, and dispersibility of Magnetite- Fe₃O₄ nanoparticles affect biomedical applications. As a result, the researcher concentrated on the various synthesis methods to monitor structure, morphology, and size with adaptable and intriguing features. To synthesize Magnetite- Fe₃O₄ nanoparticles, many

synthesis methods were discussed earlier in literature such as microwave, spray pyrolysis, laser pyrolysis, polyol, microemulsion, co-precipitation, sol-gel, thermal decomposition, sonochemical, solvothermal, and hydrothermal method [12-17] etc. The coprecipitation is one of these methods that is easy, quick, and efficient for the synthesis of both uncoated and PEG-coated Magnetite- Fe₃O₄ nanoparticles. For this method, the reaction medium must be basic with a Ferrous (Fe²⁺) to Ferric (Fe³⁺) ion ratio of 1:2 for the synthesis of Magnetite- Fe₃O₄ nanoparticles.

Two approaches were used for the synthesis of polymer-coated Magnetic Nanoparticles (MNPs) by coprecipitation method: in-situ and post-synthesis coating process. In the in-situ process, polymer coated MNPs can be obtained during the synthesis process by adding polymer directly into the reaction mixture, and post-synthesis process involves two steps, i.e. adding polymer separately once MNPs are completely synthesized in the first step of synthesis [18,19].

The European Medicines Agency (EMA) and Food and Drug Administration (FDA) approved some formulations based on IONPs, specifically on Magnetite- Fe₃O₄ and Maghemite- γ-Fe₂O₃, for diagnostic and therapeutic applications such as treatment for iron deficiency, MRI, and cancer therapy [20,21]. One of the prospective treatments for the death of cancerous cells is MHT, which is mediated by MNPs. In this therapy, MNPs can heat the local tumor area by elevating the temperature in the range of 42-45°C which is favourable for hyperthermia application under the influences of Alternating Magnetic Field (AMF). In this therapy, MNPs convert the magnetic energy into thermal energy via different mechanisms such as hysteresis loss, residual losses (Neel and Brownian relaxation), and eddy current [19].

In the present study, to synthesize PEG coated Magnetite- Fe₃O₄ nanoparticles a simple two-step (post synthesis coating process) coprecipitation method was used in which the weight percentage of PEG was varied and concentration of Magnetite- Fe₃O₄ nanoparticles was kept same for all variations.

5.2 Experimental:

Materials:

Materials used to synthesize PEG coated Magnetite- Fe₃O₄ nanoparticles: Iron (III) chloride hexahydrate (FeCl₃·6H₂O, ≥99%); Iron (II) chloride tetrahydrate (FeCl₂·4H₂O, ≥99%); Sodium hydroxide (NaOH, ≥99%); Poly Ethylene Glycol (PEG- 400MW)-Sigma-Aldrich, Phosphate Buffered Saline (PBS); Dimethyl Sulfoxide (DMSO); and Doxorubicin hydrochloride (DOX. HCl)- Sigma-Aldrich.

5.2.1 Surface Functionalization of Magnetite- Fe₃O₄ Nanoparticles with PEG:

A) Synthesis of Magnetite- Fe₃O₄ Nanoparticles:

FeCl₂·4H₂O and FeCl₃·6H₂O were separately dissolved in Double Distilled Water (DDW) at a molar ratio of 1:2 with constant stirring. In this mixture, 80 mM of NaOH was added dropwise to bring the pH of the iron salt solution to 13 from the initial acidic pH 3.2. The precursor was maintained at 70±5 °C for 60 min and then cooled to room temperature. Using magnetic decantation process, precipitate was collected and washed with DDW, and desiccated in an oven at a temperature of 70 °C. The preparative parameters for the synthesis of Magnetite- Fe₃O₄ nanoparticles are shown in **Table 5.1**.

Table 5.1: Optimized preparative parameters for the synthesis of Magnetite- Fe₃O₄ nanoparticles.

Chemicals used and optimized preparative parameters					
Name and concentration of	FeCl ₂ . 4H ₂ O (0.1 M), FeCl ₃ .6H ₂ O (0.2 M), NaOH (0.8 M)				
precursors					
Base addition rate	Dropwise (1 mL min ⁻¹)				
рН	3.2 (Before adding NaOH)				
	13 (after addition of NaOH)				
Reaction temperature	70 °C				
Recation Time	60 min				

B) Synthesis of PEG coated Magnetite- Fe₃O₄ Nanoparticles:

After obtaining powder of Magnetite- Fe₃O₄ nanoparticles, PEG-coating over Magnetite- Fe₃O₄ nanoparticles was done with a mass ratio variation of Fe₃O₄: PEG by varying the weight percentage of PEG. The variations of PEG concentrations used in the reaction bath are given in **Table 5.2**.

Table 5.2: Variation of PEG concentration with Magnetite- Fe₃O₄ nanoparticles.

Samples	Mass of Fe ₃ O ₄ NPs (g)	Mass of PEG (g)	Weight Percentage of PEG	
P0	0.5	0.0	0	
P1	0.5	0.25	33.33	
P2 0.5		0.5	50	
P3 0.5		1.0	66.66	
P4	0.5	1.5	75	

Initially, PEG was dissolved into 25 mL of DDW and stirred for 60 min at a temperature of 60°C. Then 0.5 g of Magnetite- Fe₃O₄ nanoparticles were added in PEG solution and stirred for further 60 min. The mixture of PEG- Magnetite- Fe₃O₄ nanoparticles was decanted with a permanent magnet and desiccated in an oven for 12 h at 40°C. The same procedure was carried out for PEG concentration variation (w/w %) of 0, 33.33, 50, 66.66, and 75% and labelled as P0, P1, P2, P3, and P4, respectively.

5.2.2 Characterization:

(A) Physicochemical Characterization:

X-ray Diffraction (XRD) patterns of powder samples P0, P1, P2, P3, and P4 were recorded with CuKα radiation (λ=1.546 Å). Scanning Electron Microscopy (SEM) (JEOL, JSM-IT200 (Japan)) was used to observe the morphology. Fourier Transform Infrared Spectroscopy (FTIR) spectra were recorded on Alpha (II) Bruker device operating in a range of 400-4000 cm⁻¹. Hydrodynamic particle size and zeta (ζ)-potential were recorded using (HORIBA SZ-100) with water as a dispersant. Vibrating Sample Magnetometer (VSM) (EV X) was used to study magnetic properties at room temperature. Magnetic Hyper Thermia (MHT) study of samples was carried out using an EasyHeat 8310 (Ambrell, UK) assembly. Based on MHT outcome, the anticancer efficacy of the Magnetite- Fe₃O₄ (sample P0) and PEG coated Fe₃O₄ nanoparticles (sample P1 and P4) was studied using MTT assay and evaluated against L929 fibroblast cell line and MDA-MB-231 breast cancer cell line. The hemolysis assay was used to assess the effect of synthesized particles on red blood cells, i.e. to check the hemocompatibility of PEG coated Magnetite- Fe₃O₄ nanoparticles (sample P1).

(B) Biological characterization:

(a) Cell Viability/Cytotoxicity Assay:

MTT (3-(4, 5-dimethythiazol-2-yl)-2, 5-diphenyl tetrazolium bromide) Assay:

For in vitro studies, fibroblast cell line (L929) and breast cancer cell line (MDA-MB-231) were mixed with Magnetite- Fe₃O₄ (P0) and PEG coated Magnetite- Fe₃O₄ (P1 and P4) nanoparticles and assessed using an MTT assay. The experiment was performed as discussed in Section 4.3.7 (a) (Chapter-04).

(b) Hemolysis Assay:

The hemocompatibility of PEG coated Magnetite- Fe₃O₄ (P1) nanoparticles was studied using hemolysis assay as discussed in **Section 4.3.7 (b) (Chapter-04)**.

5.3 Results and Discussion:

5.3.1 Structural/ Phase Analysis:

X-ray Diffractometer (XRD):

The XRD patterns for samples P0, P1, P2, P3, and P4 are shown in **Fig.5.1**. All the samples show polycrystalline structure. All samples reveal cubic inverse spinel crystal structure of Magnetite- Fe₃O₄ phase. Even after being coated with PEG, the crystal structure of Fe₃O₄ particles remained the same. The XRD patterns perfectly match with the JCPDS card 00-019-0629 for Magnetite- Fe₃O₄ [22]. The average crystallite size calculated using the Scherrer formula (**Equation 3.3 (Chapter-03)**) for the prominent peaks is found to be 9±0.7 nm for Sample P0 and 5±1.9 nm for samples P1, P2, P3, and P4. Thus, the particle size decreases after PEG coating.

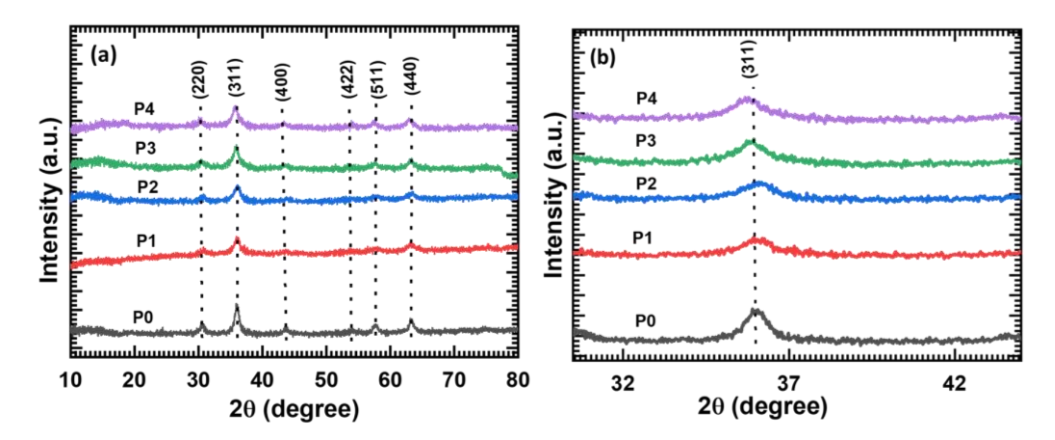


Fig.5.1: **(a)** XRD patterns of Magnetite- Fe₃O₄ (sample P0) nanoparticles and PEG coated Magnetite- Fe₃O₄ (samples P1, P2, P3, and P4) nanoparticles and **(b)** enlarged view of (311) peak.

Fig.5.1 (b) shows that with the addition of PEG in Fe₃O₄ particles, the intensity of characteristic diffraction peak (311) decreases and becomes wider, compared to pristine Magnetite- Fe₃O₄ nanoparticles revealing the decrease in crystallite size. The decreasing crystallinity with increasing PEG concentration is obvious as PEG concentration hinders particle growth and prevents nanoparticle aggregation [12].

Transmission Electron Microscopy (TEM):

The particle size was further evaluated using Transmission Electron Microscope (TEM) (JEOL, JEM 2100). The Transmission Electron (TE) micrographs for three different magnifications are shown in **Fig.5.2** (a-c) for PEG coated Magnetite- Fe₃O₄ (Sample P1) nanoparticle. The average particle size is found to be 13± 0.8 nm, which matches with that calculated from XRD study.

The particle size distribution curve plotted for the PEG coated Magnetite- Fe₃O₄ (Sample P1) using TE micrograph **Fig.5.2** (a) is as shown in **Fig.5.2** (d). The average particle size of 13± 0.8 nm was calculated from the TE micrographs using Image-J software, and by selecting approximately 30 particles from **Fig.5.2** (a) TE micrographs to plot the curve for particle size distribution.

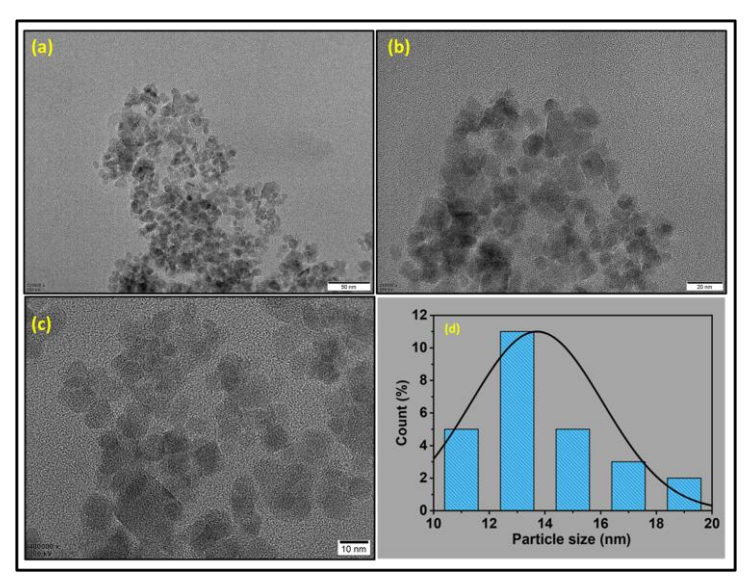


Fig.5.2: TE micrographs of PEG coated Magnetite- Fe₃O₄ (sample P1) nanoparticles at different magnifications.

5.3.2 Morphological Analysis:

Scanning electron microscopy (SEM):

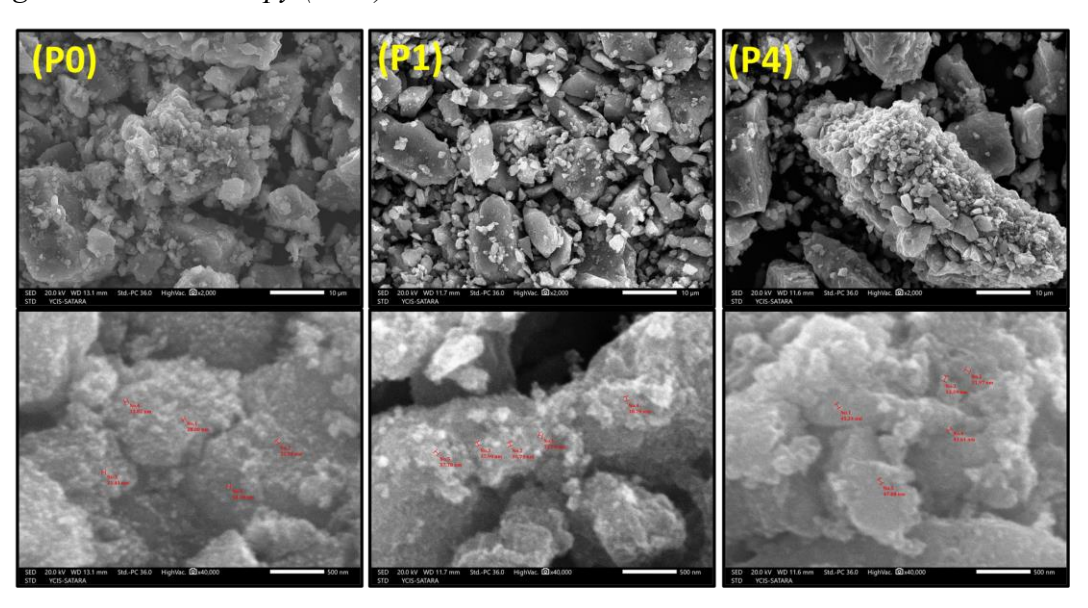


Fig.5.3: SE Micrographs of Magnetite- Fe₃O₄ nanoparticles (sample P0) and PEG-coated Magnetite- Fe₃O₄ nanoparticles (samples P1 and P4) at 2000X and 40000X magnifications.

The surface morphology of the synthesized Magnetite- Fe₃O₄ (P0) nanoparticles and PEG coated Magnetite- Fe₃O₄ (P1 and P4) nanoparticles were studied using SEM. The Scanning Electron (SE) micrographs at two different magnifications are shown in **Fig.5.3**. Granular surface morphology of agglomerated nanoparticles is seen with average grain size of 32 to 42 nm.

The increase in PEG ratio caused the higher particle size because it attached to Fe₃O₄ with PEG chains, preventing agglomeration. The nucleation rate per unit area is isotropic at the interface between Magnetite- Fe₃O₄ nanoparticles, leading to the formation of the granular shape [23]. Adding PEG can reduce aggregation by offering steric repulsion to aggregation, which weakens the strength of the Van der Waals forces [12]. On the other hand, there is still agglomeration of particles observed after PEG coating in Fig.5.3 (P1 and P4). This agglomeration is observed due to the inherent properties of MNPs, namely magnetic dipole-dipole, and Van der Waals forces interaction between nanoparticles.

5.3.3 Chemical Signature:

Fourier-Transform Infrared Spectroscopy (FTIR):

The chemical bonds existing in Magnetite-Fe₃O₄ are studied using FTIR spectroscopy in which the incident infrared radiation is absorbed at a resonant frequency of bending, stretching, or vibrating chemical bonds that exist between the atoms within the compound.

The FTIR absorption spectra of Magnetite- Fe₃O₄ (P0) nanoparticles and PEG coated Magnetite-Fe₃O₄ (P1 to P4) in the wavenumber range of 4000 to 400 cm⁻¹ are shown in Fig.5.4.

An FTIR study revealed the presence of vibrating stretching bond Fe-O (υ_1 = 574 cm⁻¹) [11]. In addition, several other peaks are also observed that correspond to PEG. The C-O-C absorption peak (υ_2) is observed at 1099 cm⁻¹ in pure PEG while in PEG coated Magnetite-Fe₃O₄ (P1, P2, P3, and P4) nanoparticles, it shifts to 1107 cm⁻¹. The absorption peak (υ_3) at 1631 cm⁻¹ is assigned to asymmetric C=O. With an increase in the PEG concentration, the C=O band shifts from 1631 to 1634 cm⁻¹ revealing the existence of PEG in the final product. The result shows that Magnetite-Fe₃O₄ nanoparticles coordinate with PEG by carbonyl group. A decrease in particle size and shifting of absorption reveal the interaction between Magnetite-Fe₃O₄ and PEG and the surface modification of Magnetite-Fe₃O₄ nanoparticles with PEG [23].

The band around 2861 cm⁻¹ (v₄) is due to the presence of the -C-H- stretching bands, showing evidence of PEG molecules in the samples. The absorption peak (v₅) at 3467 cm⁻¹ arises from the stretching vibration of the hydroxyl (-OH) group, which is adsorbed on the surface of Magnetite- Fe₃O₄ nanoparticles. The presence of the hydroxyl group allows the further surface functionalization of the material by replacing the -OH group with PEG.

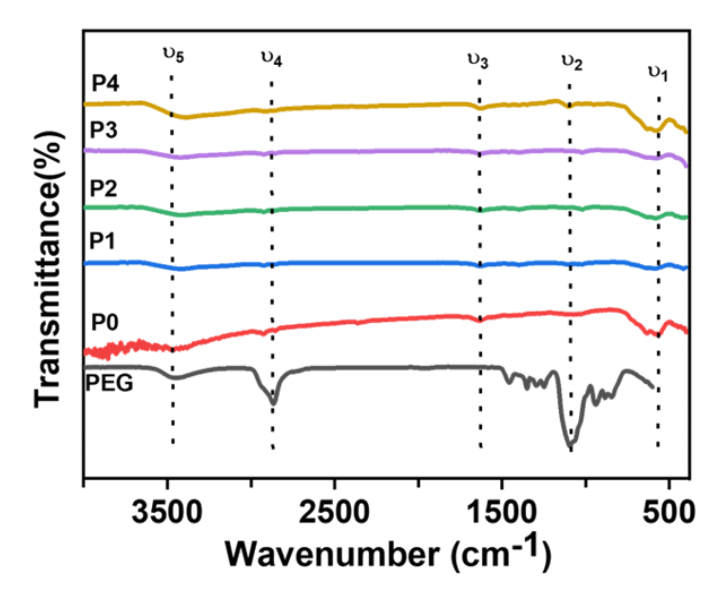


Fig.5.4: FTIR spectra of Magnetite- Fe₃O₄ (sample P0) nanoparticles, PEG, and PEG coated Magnetite- Fe₃O₄ (samples P1 to P4) nanoparticles.

5.3.4 Particle Size and Zeta Potential Study:

Dynamic Light Scattering (DLS):

Good chemical stability at physiological/neutral pH \sim 7 is necessary for the use of nanoparticles in biomedicine. DLS was used to assess the hydrodynamic characteristics of the MNPs in aqueous dispersions using water (pH-7) because of its biological relevance. The hydrodynamic size, and ζ -potential, of PEG coated Magnetite- Fe₃O₄ nanoparticles (sample P1) were assessed using DLS technique. The hydrodynamic diameter of Sample P1 is shown in Fig.5.5.

The DLS study was performed for PEG coated Magnetite- Fe₃O₄ nanoparticles (sample P1) to investigate the hydrodynamic diameter of nanoparticles with the average size distribution at room temperature using DDW at pH value of 7.2. The observed hydrodynamic diameter of PEG coated Magnetite- Fe₃O₄ nanoparticles (sample P1) is 95.1 nm (**Fig.5.5**). The obtained hydrodynamic size is more compared to actual size of the nanoparticles due to solvation layer of water molecules and ions around the particles along with the little aggregation [12].

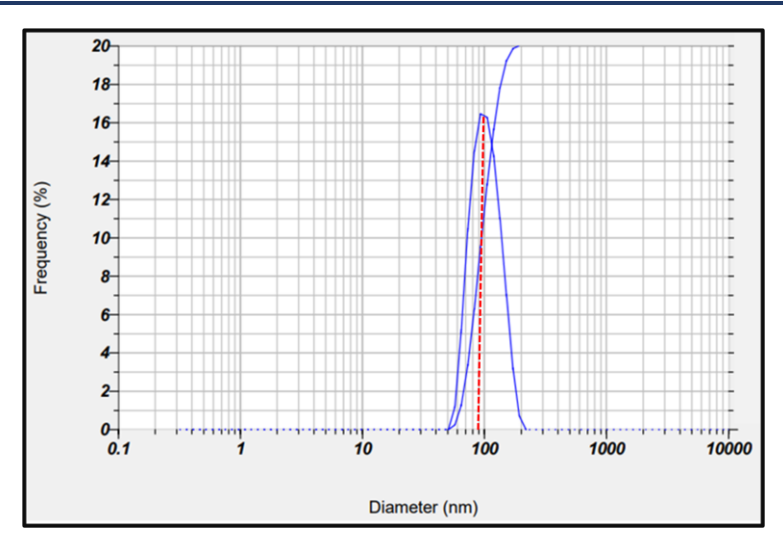


Fig.5.5: Hydrodynamic diameter of PEG coated Magnetite-Fe₃O₄ nanoparticles (Sample P1).

The hydrodynamic size observed for PEG coated Magnetite- Fe₃O₄ nanoparticles (sample P1) is less than that of Magnetite- Fe₃O₄ nanoparticles (sample P0) (113.7 nm). PEG coated nanoparticles have lower hydrodynamic diameter values, indicating a reduction in aggregation. If the polymer is thick enough, the Van der Waals attraction between particles is weaker than Brownian thermal energy. This is the origin of the word "steric" stabilization, which creates extra repulsive energy barriers. Therefore, a nonmagnetic coating of PEG or PVA on the surface of the nanoparticles provides steric or static repulsion, thereby balancing the attraction forces among the particles, resulting in a smaller hydrodynamic diameter [24].

Zeta potential (ζ -potential):

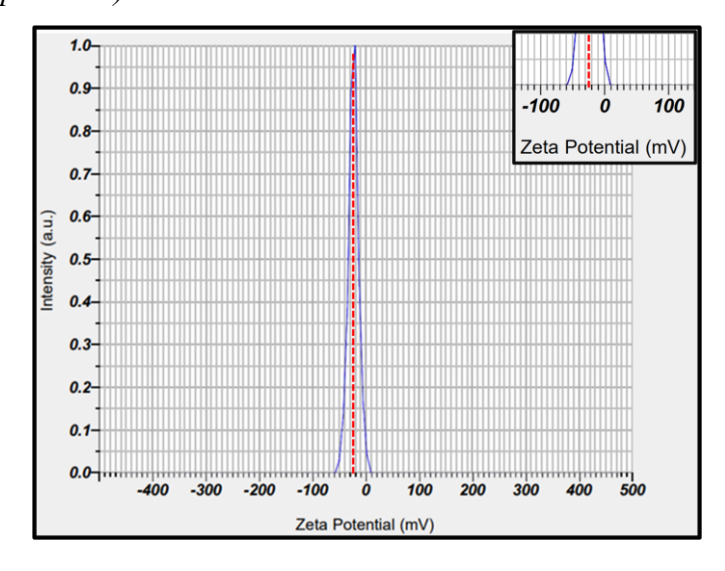


Fig.5.6: Zeta potential value of PEG coated Magnetite- Fe₃O₄ nanoparticles (sample P1) by DLS technique (Inset: enlarge view of zeta potential scale from -70 to +10 mV).

The ζ -potential is crucial for analysing the stability of colloidal suspensions since it determines the magnitude and kind of surface electric charge. The value of ζ - potential is -22 mV for PEG coated magnetite- Fe₃O₄ nanoparticles as shown in Fig.5.6. The ζ - potential of bare Magnetite- Fe₃O₄ nanoparticles is typically between -30 and +30 mV, depending on the synthesis method, pH, and ionic strength of the medium. PEG-coated Magnetite- Fe₃O₄ nanoparticles have a lower absolute value ζ - potential than bare Magnetite- Fe₃O₄ nanoparticles. This is because the PEG coating tends to hide the surface charge of nanoparticles, resulting in values generally ranging from -5 to -15 mV, or even closer to neutral, depending on the molecular weight and density of the PEG used for coating [25].

5.3.5 Vibrating Sample Magnetometer (VSM) Analysis:

The magnetic parameters, namely type of magnetism, saturation magnetization (Ms), coercivity (Hc), and retentivity, can be evaluated with the help of VSM which generates a hysteresis loop of IONPs.

The hysteresis loops for Magnetite- Fe₃O₄ (sample P0) nanoparticles and PEG-coated Magnetite- Fe₃O₄ (sample P1 and P4) nanoparticles were obtained in the external magnetic field window of ±16 kOe at room temperature, which are shown in **Fig.5.7**.

The saturation magnetization (Ms) value of Magnetite- Fe₃O₄ nanoparticles decreases from 50 to 30 emu g⁻¹ with increasing concentration of PEG from 0 to 75%. These results specify a higher saturation magnetization (Ms) value for larger particle size, which also resembles XRD analysis. The decrease in the magnetization value for PEG coated Fe₃O₄ nanoparticles is due to the adsorption of nonmagnetic polymer coating on the exterior of MNPs [26,27].

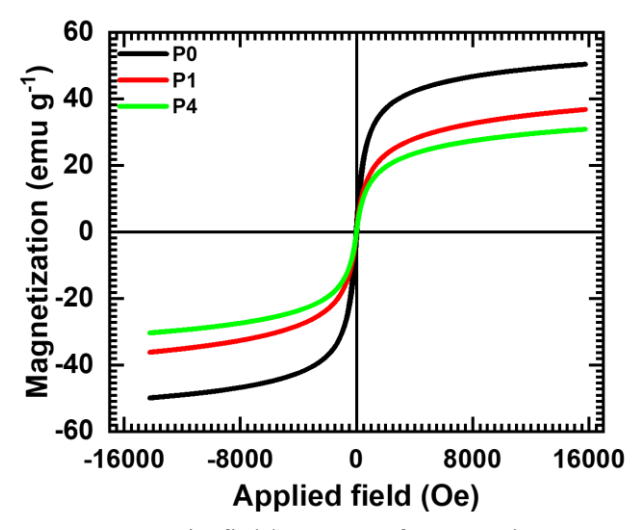


Fig.5.7: Magnetization versus magnetic field curves of Magnetite- Fe₃O₄ (sample P0) and PEG-coated Magnetite- Fe₃O₄ (samples P1 and P4) nanoparticles.

It has been reported that for biomedical applications saturation magnetization (Ms) value of 7-22 emu g⁻¹ is adaptable [28,29]. Hence, the level of saturation magnetization (Ms) obtained for Magnetite- Fe₃O₄ nanoparticles (P0) and PEG-coated Magnetite- Fe₃O₄ (P1 and P4) nanoparticles is adequate for the biomedical field. The values of magnetization parameters are shown in **Table 5.3**.

Table 5.3: Saturation magnetization (Ms) and Coercivity (Hc) of Magnetite- Fe₃O₄ (sample P0) nanoparticles and PEG coated Magnetite- Fe₃O₄ (samples P1 and P4) nanoparticles.

Sample	Ms (emu g ⁻¹)	Hc (Oe)
P0	50.2	32.83
P1	36.5	5.0
P4	30.6	4.7

Among all variations of PEG coating with Magnetite- Fe₃O₄ nanoparticles, sample P1 is carried out for further study due to its physicochemical and magnetic properties which are desirable for further biological study. For MHT, chemotherapy, and biological study sample P1 was used due to its moderate magnetic parameters.

5.3.6 Magnetic Hyper Thermia (MHT) Study:

When an Alternating Magnetic Field (AMF) is applied, the magnetization and demagnetization of IONPs produce heat due to hysteresis loss, Eddy current, and residual losses, this is called MHT. The MHT of PEG coated Magnetite- Fe₃O₄ (P1) nanoparticles were studied using a magnetic induction heating device for 600 s. The heating ability of MNPs is expressed in terms of the Specific Absorption Rate (SAR) value which is defined as the capacity of MNPs to convert magnetic energy into heat. Generally, temperatures between 42-45°C are suitable to kill cancer cells. Thus, the MHT cancer therapy basically requires a suitable amount of MNPs to be inserted into cancer tumor and application of external AMF of appropriate strength to increase the temperature to kill the cancer cells [30,31].

The DLS study was performed for PEG coated Magnetite- Fe₃O₄ nanoparticles (sample P1) to investigate the hydrodynamic diameter of nanoparticles with the average size distribution at room temperature using DDW at pH value of 7.2. The observed hydrodynamic diameter of PEG coated Magnetite- Fe₃O₄ nanoparticles (sample P1) is 95.1 nm (**Fig.5.5**). The obtained hydrodynamic size is more compared to actual size of the nanoparticles due to solvation layer of water molecules and ions around the particles along with the little aggregation [12].

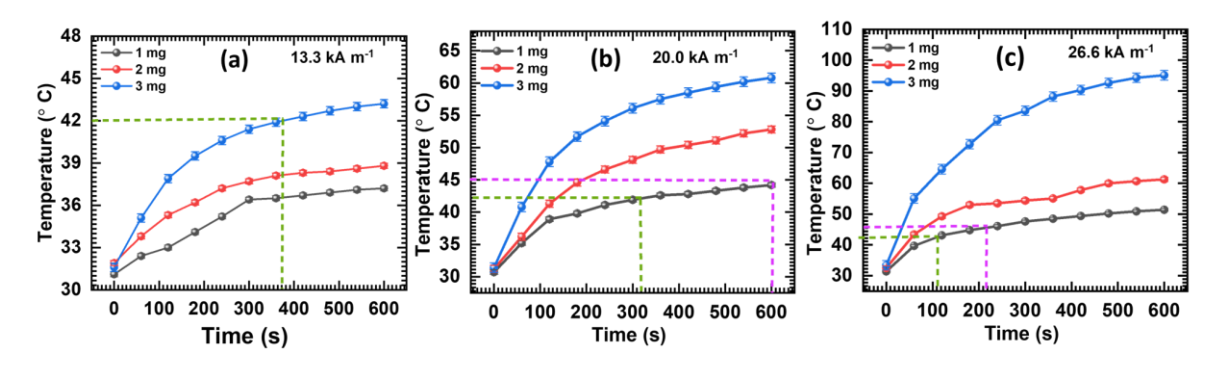


Fig.5.8: Temperature Vs Time variation for PEG coated Magnetite- Fe₃O₄ (P1) nanoparticles.

PEG-coated Fe₃O₄ (sample P1) nanoparticles with concentrations of 1, 2, and 3 mg mL⁻¹ were kept in a 3 mL cuvette containing 1 mL of DDW. This cuvette was kept in a MHT device and external AMF of fixed frequency (278 kHz) was applied for 600 s. The change in temperature was recorded for three different AMF strengths (13.3, 20.0, and 26.7 kA m⁻¹). **Fig.5.8** shows the temperature vs time curves of all the samples.

It is observed that with increase in the concentration of nanoparticles, there is increases in the temperature. PEG coated Magnetite- Fe₃O₄ (P1) nanoparticles show therapeutic temperature rise (beyond 42 °C) at the field strengths of 20.0 and 26.7 kA m⁻¹ for the 2 and 3 mg mL⁻¹ concentrations of magnetic suspension. The therapeutic temperature is attained within 100 to 600 s for PEG coated Magnetite- Fe₃O₄ (P1) nanoparticles when concentration is 2 or 3 mg.

The SAR and Intrinsic Loss Power (ILP) values calculated using **Equations 2.7** and **2.8** (Chapter-02) as a function of magnetic field strength for PEG coated Magnetite- Fe₃O₄ (P1) nanoparticles for different concentrations are shown in **Table 5.4**.

Table 5.4: SAR and ILP values for PEG coated Magnetite- Fe₃O₄ (sample P1) nanoparticles for different magnetic field strengths.

Concentration of MNPs (mg mL ⁻¹)	1	2	3	1	2	3
Field (kA m ⁻¹)		SAR (W g	1	ILP (n)	Hm kg ,	n=1)
13.6	30.32	26.65	24.64	0.59	0.52	0.48
20	104.98	70.15	66.17	0.95	0.64	0.60
26.7	193.63	152.92	152.76	0.98	0.78	0.78

It is seen that with increase in field strength SAR value increases and ILP values decreases as required for efficient MHT similarly SAR values decrease with increase in concentrations [32].

The increased heating ability of PEG-coated Magnetite- Fe₃O₄ (sample P1) nanoparticles than magnetite- Fe₃O₄ nanoparticles might be associated with PEG coating as it increased the dispersion in suspension, which leads to an increase in the heating efficiency of MNPs.

5.3.7 Drug Loading and Drug Release Study:

Preparation of standard calibration curve:

The stock solution was prepared by adding 1 mg Doxorubicin (DOX) in a volumetric flask containing 100 mL of PBS. Then the standard calibration curve of DOX was obtained at different concentration ranges (0.5-10 µg mL⁻¹) prepared from the stock solution and the absorbance was measured at a wavelength of 430 nm as shown in **Fig.5.9** (a). The calibration curve was plotted by taking absorbance on the Y-axis and the concentration of DOX on the X-axis as shown in **Fig.5.9** (b). A calibration curve is used to calculate the concentration of drugs in unknown samples by comparing the observed response to the reference curve. In **Fig.5.9** (b) the linear shift with an R² value of 0.99 reveals a good calibration.

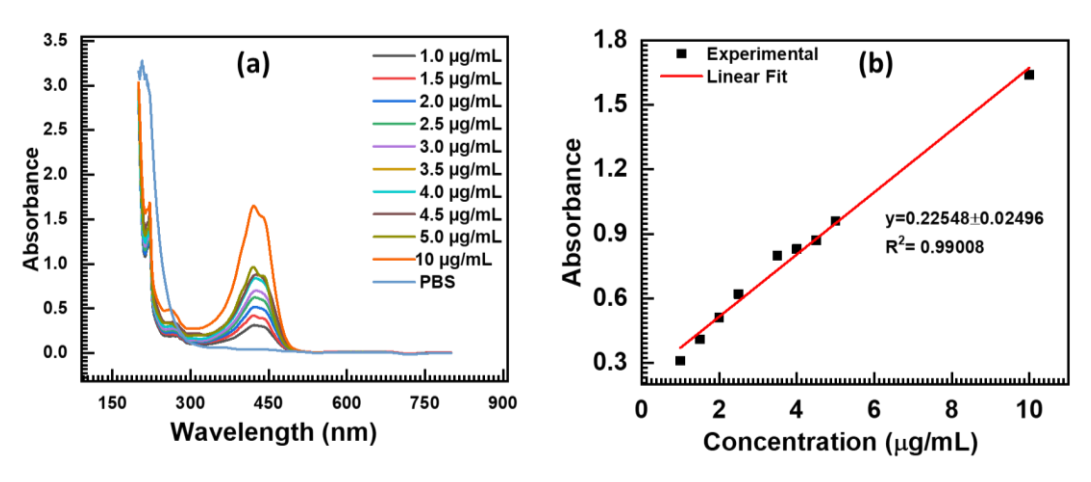


Fig.5.9: (a) Ultraviolet absorption spectroscopy of DOX and (b) Calibration curve of DOX. *Drug Loading*

The water-soluble anti-cancer drug DOX was selected as the model drug, which was conjugated to Magnetite- Fe_3O_4 (sample P0) nanoparticles and PEG coated Magnetite- Fe_3O_4 (sample P1) nanoparticles. The DOX loading procedure involves the dispersion of 50 mg of synthesized nanoparticles in 20 mL of aqueous DOX solution (drug concentration = 0.1 mg mL⁻¹) of PBS (pH-7.4). To promote DOX adsorption, the mixture of nanoparticles in DOX

was shaken for 48 h at 37°C using a 250 rpm rotary shaker. The magnetic particles were extracted using a permanent magnet at predetermined intervals, and a UV-vis spectrophotometer was used to detect the optical density of the remaining DOX in the supernatant at 480 nm. After a particular adsorption time (48 h), the concentration of DOX remained constant as the particle loading capacity neared saturation. The drug loading efficiency (DLE) was calculated using **Equation 5.1**.

$$DLE(\%) = \frac{c_{Dox_{in}} - c_{Dox_{fin}}}{c_{Dox_{in}}} X100 \qquad$$
 (5.1)

where,

 C_{Doxin} = Initial concentration of DOX, and

 C_{DoxFin} = Concentration of DOX in the supernatant.

The maximal drug DLE of 84% was obtained for PEG coated Magnetite- Fe₃O₄ nanoparticles after 48 h. The loading of the drug is due to the electrostatic attraction between the negatively charged PEG coated particle and the protonated drug (DOX) molecule as the drug is in its hydrochloride form. Therefore, the negative surface charge of PEG coated Fe₃O₄ was almost neutralized by a partially positively charged drug molecule. A neutral thin spherical coating was established over the coated Magnetite- Fe₃O₄ nanoparticles by the drug molecules. Additionally, it has been observed that π - π stacking and hydrophobic contact can effectively load drugs with aromatic rings onto the surface of nanoparticles by using the delocalized π electrons [9].

Drug Release

To simulate tumor and normal tissue conditions, 0.01 M of PBS (pH 4.5, 6.8, and 7.4) was formed. After dispersing 5 mg of DOX-loaded PEG coated Magnetite- Fe₃O₄ nanoparticles in 10 mL PBS, the solution was transferred to a dialysis bag submerged in 20 mL of the same medium and held in a shaker at 37 °C. At regular intervals (0.5, 1, 2, 3, 4, 5, 6, 7, 8, 9, 10, 11, 12, 24, and 48 h), 0.5 mL PBS was withdrawn from the dialysis bag and absorbance was measured at 480 nm and replaced with a fresh solution of the same volume. The release tests were carried out in triplicate. The drug release efficiency (DRE) was calculated by following **Equation 5.2.**

$$DRE(\%) = \frac{c_{Dox_0} - c_{Dox_t}}{c_{Dox_t}} \qquad$$
 (5.2)

where,

 C_{Dox0} = Initial concentration of DOX, and

C_{Doxt} = Concentration of DOX at a time (t).

The drug release profile was studied by varying the pH of physiological solution (PBS), i.e. 4.5, 6.8, and 7.4 as shown in **Fig.5.10**. The highest release was observed at pH 4.5 as shown in **Fig.5.10** (a). The drug release efficiency of DOX loaded Magnetite- Fe₃O₄ nanoparticles and DOX loaded PEG coated Magnetite- Fe₃O₄ nanoparticles is given in **Table 5.5**.

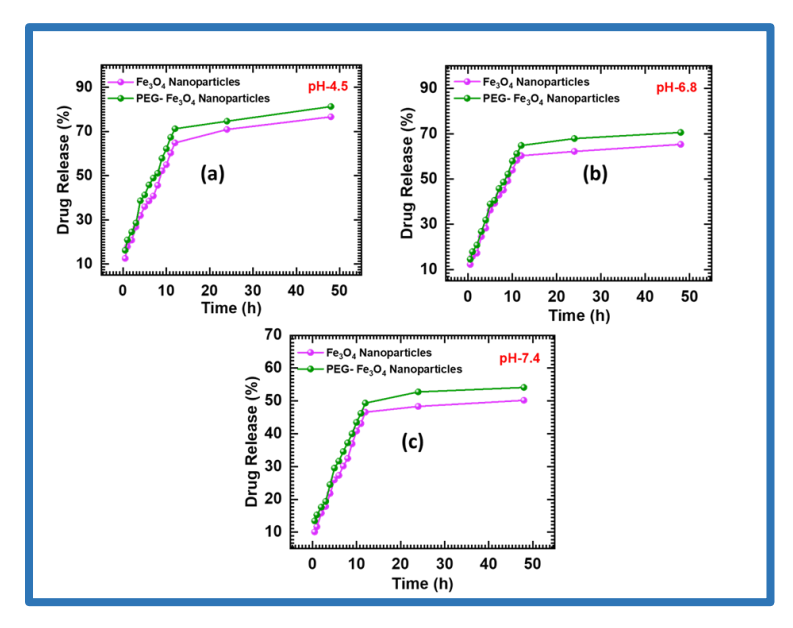


Fig 5.10: Drug release percentage of the DOX loaded Magnetite- Fe₃O₄ nanoparticles and PEG coated Magnetite- Fe₃O₄ nanoparticles at different pH: (a) pH-4.5, (b) pH-6.8, and (c) pH-7.4.

Table 5.5: Drug release percentage of DOX loaded Magnetite- Fe₃O₄ nanoparticles (sample P0) and PEG coated Magnetite- Fe₃O₄ nanoparticles (sample P1) at different pH values.

pH → NPs ↓	4.5	6.8	7.4
Fe ₃ O ₄	76.6%	65.32%	50.19%
PEG-Fe ₃ O ₄	81.26%	70.6%	54.11%

The in vitro release tests show that DOX-loaded Magnetite- Fe₃O₄ and DOX-loaded PEG-coated Magnetite- Fe₃O₄ nanoparticles are pH-sensitive and can potentially release their therapeutic payload in the acidic tumor microenvironment. In this study it is also observed that the drug release is more rapid for acidic medium (TME) as compared to physiological pH of 7.4.

Besides, it is observed that as pH increases, drug release efficiency decreases. In addition, a possible component contributing to increased drug release at acidic pH levels is

the potential decrease in the π - π stacking interaction between DOX molecules and a drop in pH, facilitating drug release at acidic pH levels. The current model provides an appropriate platform for DOX release to the tumor cells under pH-controlled circumstances, as the tumor cells have an acidic pH. Hence the addition of PEG greatly accelerates the DOX release from nanoparticles [9].

5.3.8 Biocompatibility:

(a) Cytotoxicity/ Cell Viability Assay:

3-(4, 5-dimethylthiazol- 2-yl)-2,5-diphenyltetrazolium bromide (MTT) Assay:

Due to wide applications of iron oxide in the field of biomedical, cell viability and cell toxicity are the primary steps to check their biocompatibility. To study the toxicity, PEG coated Magnetite- Fe₃O₄ nanoparticles were mixed with fibroblast cell line (L929) and cancer cell line (MDA MB 231).

Here, MTT assay was used for assessing the cell viability of fibroblast cell line (L929) and cell toxicity of breast cancer cell line (MDA-MB-231) at various concentrations (100, 50, 25, 12.5, 6.25, and 3.125 μg mL⁻¹) of Magnetite Fe₃O₄ nanoparticles (sample P0) and PEG-coated Magnetite- Fe₃O₄ nanoparticles (sample P1 and P4) after 48 h of incubation as discussed in **Section 4.3.7 (a) (Chapter-04)**. **Equations 3.5** and **3.6 (Chapter -03)** were used to calculate the percentage of cell viability/ toxicity of Magnetite- Fe₃O₄ nanoparticles.

For L929 fibroblast cell line it shows cell viability of 92.48, 93.07, and 94 % at a concentration of 100 mg L⁻¹ for samples P0, P1, and P4, respectively. as shown in **Fig.5.11** (a). The microscopy pictures of untreated and treated L929 cell line for 100 µg mL⁻¹ of IONPs is shown in **Fig.5.11** (b).

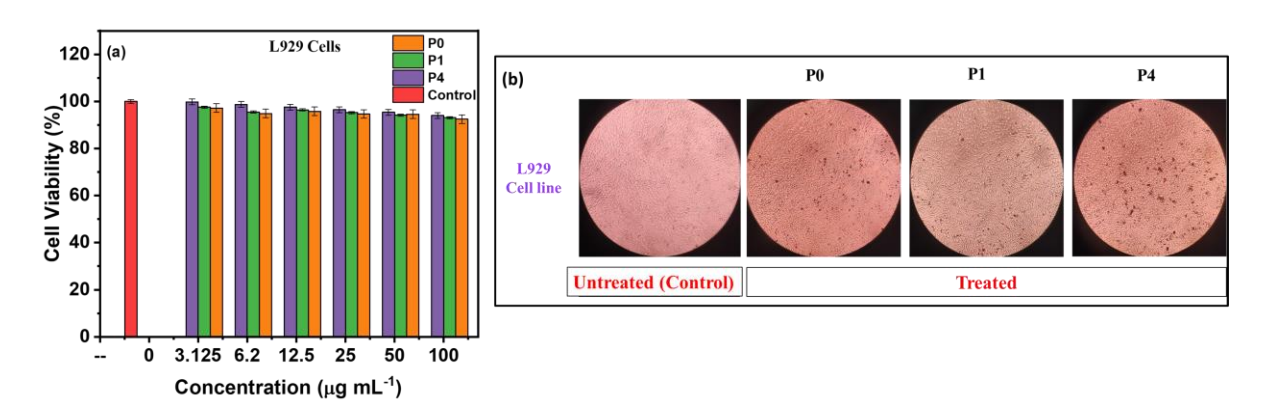


Fig.5.11: **(a)** Histogram of cytotoxicity percentage and **(b)** The microscopy pictures of the L929 cell line.

Hence the synthesized nanoparticles can be used for biomedical applications which do not harm healthy cells.

For MDA-MB-231 breast cancer cell line the Magnetite- Fe₃O₄ nanoparticles (sample P0) and PEG coated Magnetite- Fe₃O₄ nanoparticles (P1 and P4) show increase in cell toxicity with increase in concentration from 3.125 to 100 μg mL⁻¹. Thus, the cell toxicity (killing of cancer cells) increases with concentration of Magnetite- Fe₃O₄ nanoparticles [33] as shown in Fig.5.12 (a). The maximum cell toxicity of 84.46 % is observed for PEG coated Magnetite-Fe₃O₄ nanoparticles (sample P1) at a concentration of 100 μg mL⁻¹. The microscopic picture of breast cancer cell line (MDA MB 231) for concentration of 100 μg mL⁻¹ of IONPs is shown in Fig.5.12 (b).

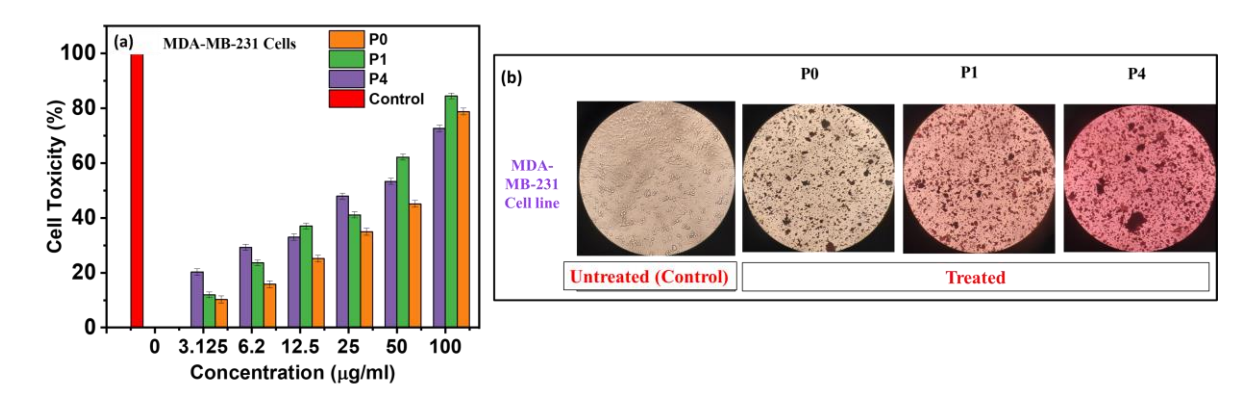


Fig.5.12: (a) Histogram of cytotoxicity percentage and (b) The microscopy pictures of the MDA MB 231 cell line.

In uncoated Fe₃O₄ nanoparticles, the iron ions can take part in the Fenton reaction and cause the tumor cell to undergo ferroptosis [34]. PEG-coated Fe₃O₄ nanoparticles have a considerably greater cytotoxic impact, which could be caused by a decrease in nanoparticle size that gives the particles a more specific surface area to interact with cells. Due to the surface functionalization of Fe₃O₄ nanoparticles with PEG, the ROS were significantly elevated and the matrix metalloproteinases were decreased. Additionally, the PEG coated Fe₃O₄ nanoparticles suppress the growth of the cancer cell due to the mitochondrial damage mechanism with activated tumor protein P53 resulting in apoptosis [2].

(b) Hemolysis Assay:

The entry of foreign particles into the body can have a variety of and sometimes conflicting effects, so determining their effects on the body is a critical step in their applicability. Because the injected nanoparticles come into direct touch with blood tissue and its components, an evaluation of their hemocompatibility is essential for further study.

For this study fresh human blood (10 mL) was collected in heparinized centrifuge tubes, rotated at 3000 rpm for 10 min, and washed three times with an equivalent volume of normal saline. The blood volume was measured and reconstituted as a 10% v/v solution in normal saline. The reaction mixture included 1 mL of 10% red blood cell suspension. Triton X-100 was used as a standard drug (positive control), saline as a negative control, and test sample with different concentrations of PEG coated Magnetite- Fe₃O₄ nanoparticles were then incubated at 56°C for 30 min, and centrifuged at 2500 rpm for 5 min, and the absorbance of the supernatant was measured at 560 nm. Hemolysis percentage was calculated using Equation 3.7 (Chapter-03).

The concentration of the PEG coated Magnetite- Fe₃O₄ nanoparticles was varied from 0.5 to 2.0 mg mL⁻¹. The change in hemolysis percentage is shown in **Fig.5.13**.

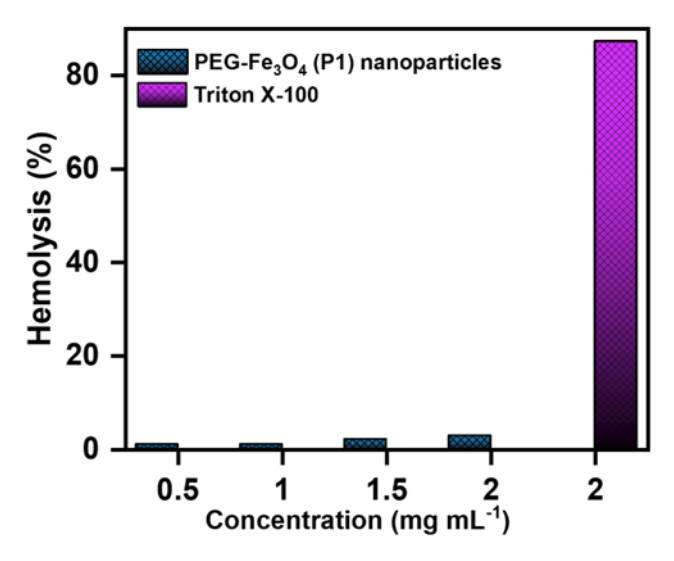


Fig.5.13: Hemolysis percentage of Triton X-100 (positive control) and PEG coated Magnetite-Fe₃O₄ nanoparticles.

The percentage of hemolysis is between 1 to 2.8 which is well below 5% as per ISO 10993-5 guidelines [35]. Hence it is observed that the PEG coated Magnetite- Fe₃O₄ nanoparticles does not show hemolytic activity and can be used for biomedical applications.

5.4. Conclusions:

PEG-coated Magnetite- Fe₃O₄ nanoparticles were successfully synthesized by the coprecipitation method. The structural, morphological, functional, and magnetic properties were examined using different characterization techniques. It is observed that the crystallite size decreases from 9.73 nm for pristine to average 6.9 nm for PEG coated Magnetite-Fe₃O₄ nanoparticles (sample P1). The synthesized quasi-spherical PEG-coated Magnetite- Fe₃O₄ nanoparticles show superparamagnetic behaviour with saturation magnetization (Ms) value

of 36.5 emu g⁻¹ and coercivity (Hc) of 5 Oe. Induction heating study showed the rise in temperature in the range of threshold temperature (42-45°C) under the influence of an external AMF, which is appropriate for MHT application for destruction of cancer tumor cells. In acidic pH, PEG-coated Magnetite- Fe₃O₄ shows a rapid drug release compare normal physiological pH. Hence the PEG-coated Fe₃O₄ nanoparticles can be used as carriers for drug delivery. MTT assay revealed the toxicity of 84.46 % towards the MDA-MB-231 breast cancer cell line and cell viability of 93.07 % towards L929 fibroblast normal cell line at 100 µg mL⁻¹. Thus, the PEG-coated Fe₃O₄ can be effectively used as an anticancer agent to kill cancerous cells with minimal side effects to normal cell lines. Hemolysis in PEG-coated Fe₃O₄ is less than 5%, which is acceptable to use in biomedical applications. Therefore, the resulting study reveals that PEG coated Fe₃O₄ nanoparticles is potential material for anticancer therapy.

References:

- 1. Wagner V, Dullaart A, Bock A, Zweck A. Nat. Biotechnol. 24 (10) (2006) 1211-17.
- 2. Salunkhe A, Khot V, Patil S, Tofail S, Bauer J, Thorat N. ACS Appl. Bio Mater. 3 (4) (2020) 2305-13.
- 3. Khot V, Salunkhe A, Ruso J, Pawar S. J. Magn. Magn. Mater. 384 (2015) 335-43.
- 4. Martinkova P, Brtnicky M, Kynicky J, Pohanka M. Adv. Healthc. Mater. 7 (5) (2018) 1700932-46.
- 5. Thapa B, Diaz-Diestra D, Beltran-Huarac J, Weiner B, Morell G. Nanoscale Res. Lett. 312 (12) (2017) 1-13.
- 6. Kadhim W, Nayef U, Jabir M. Surf. Rev. Lett. 26 (10) (2019) 1950079-105.
- 7. Nikam D, Jadhav S, Khot V, Bohara R, Hong C, Mali S, Pawar S. RSC Advances. 5 (13) (2015) 2338-45.
- 8. Salunkhe A, Khot V, Thorat N, Phadatare M, Sathish C, Dhawale D, Pawar S. Appl. Surf. Sci. 264 (2013) 598-604.
- 9. Szalai A, Manivannan N, Kaptay G. Colloids Surf. A: Physicochem. Eng. Asp. 568 (2019) 113-122.
- 10. Kumar P, Khanduri H, Pathak S, Singh A, Basheed G, Pant R. Dalton Trans. 49 (25) (2020) 8672-83.
- 11. Jafari A, Shayesteh S, Salouti M, Boustani K. J. Magn. Magn. Mater. 379 (2015) 305-12.
- 12. Antarnusa G, Jayanti P, Denny Y, Suherman A. Materialia. 25 (2022) 101525-37.
- 13. Rizzuti A, Dassisti M, Mastrorilli P, Sportelli M, Cioffi N, Picca R, Agostinelli E, Varvaro G, Caliandro R. J. Nanoparticle Res. 408 (17) (2015) 1-6.
- 14. Lungu I, Nistorescu S, Badea M, Petre A, Udrea A, Banici A, Fleaca C, Andronescu E, Dinischiotu A, Dumitrache F, Staicu A, Polymers. 12 (12) (2020) 2799-817.
- 15. Unni M, Uhl A, Savliwala S, Savitzky B, Dhavalikar R, Garraud N, Arnold D, Kourkoutis L, Andrew J, Rinaldi C. ACS nano. 11 (2) (2017) 2284-303.
- 16. Chacón, J, Picasso G., Félix L, Jafelicci J. Adv. Nat. Sci. 7 (1) (2016) 015014-22.
- 17. Aliramaji S, Zamanian A, Sohrabijam Z. Procedia Mater. Sci. 11 (2015) 265-69.
- 18. Antarnusa G and Suharyadi E. Mater. Res. Express. 7 (5) (2020) 056103-09.
- 19. Ghosh R, Pradhan L, Devi Y, Meena S, Tewari R, Kumar A, Sharma S, Gajbhiye N, Vatsa R, Pandey B, Ningthoujam R. J. Mater. Chem. 21 (35) (2011) 13388-98.
- 20. Khot V, Salunkhe A, Pricl S, Bauer J, Thorat N, Townley H. Drug Discov. Today. 26 (3) (2021) 724-39.
- 21. Loura N, Singh M, Dhull V. Emerg. Mater. 6 (5) (2023) 1415-40.
- 22. Joseph J, Nishad K, Sharma M, Gupta D, Singh R, Pandey R. Mater. Res. Bull. 47 (6) (2012) 1471-77.

- 23. Anbarasu M, Anandan M, Chinnasamy E, Gopinath V, Balamurugan K. Spectrochim. Acta A. 135 (2015) 536-39.
- 24. Namikuchi E, Gaspar R, da Silva D, Raimundo I, Mazali I. Nano Express. 2 (2) (2021) 020022-34.
- 25. Xie S, Zhang B, Wang L, Wang J, Li X, Yang G, Gao F. Appl. Surf. Sci. 326 (2015) 32-38.
- 26. Khashan S, Dagher S, Tit N, Alazzam A, Obaidat I. Surf. Coat. Tech. 322 (2017) 92-108.
- 27. Amini-Fazl M, Mohammadi R, Kheiri K. Int. J. Biol. Macromol. 132 (2019) 506-13.
- 28. Eivazzadeh-Keihan R, Radinekiyan F, Maleki A, Bani M, Hajizadeh Z, Asgharnasl S. Int. J. Biol. Macromol. 140 (2019) 407-14.
- 29. Hiergeist R, Andrä W, Buske N, Hergt R, Hilger I, Richter U, Kaiser W. J. Magn. Magn. Mater. 201 (1-3) (1999) 420-22.
- 30. Li Z, Kawashita M, Araki N, Mitsumori M, Hiraoka M, Doi M. Mater. Sci. Eng. C. 30 (7) (2010) 390-96.
- 31. Phalake S, Lad M, Kadam K, Tofail S, Thorat N, Khot V. ACS omega. 7 (48) (2022) 44187-198.
- 32. Nikam D, Jadhav S, Khot V, Phadatare M, Pawar S. J. Magn. Magn. Mater. 349 (2014) 208-13.
- 33. Rajaei H, Mofazzal Jahromi M, Khoramabadi N, Mohammad Hassan Z, Immunoregulation. 2(2) (2020) 89-102.
- 34. Kalaiselvan C, Thorat N, Sahu N, ACS Omega. 6(8) (2021) 5266-75.
- 35. Bhavikatti S, Zainuddin S, Ramli R, Nadaf S, Dandge P, Khalate M, Karobari M, Sci. Rep. 14(1) (2024) 11878-98.

CHAPTER-06

SYNTHESIS, CHARACTERIZATION,
MAGNETIC HYPERTHERMLA, AND
CHEMOTHERAPY STUDY OF GSH
COATED MAGNETITE -Fe₃O₄
NANOPARTICLES

INDEX

Sr.No		Page No.		
6.1	Introdu	127		
6.2	Experi	Experimental		
	6.2.1	Surface Functionalization of Magnetite- Fe ₃ O ₄ Nanoparticles with Glutathione (GSH)	129	
	6.2.2	Characterization	130	
6.3	6.3 Results and Discussion		130	
	6.3.1	Structural/ Phase Analysis	130	
	6.3.2	Morphological Analysis	132	
	6.3.3	Chemical Signature	132	
	6.3.4	Particle Size and Zeta Potential Study	133	
	6.3.5	Vibrating Sample Magnetometer (VSM) Analysis	135	
	6.3.6	Magnetic Hyper Thermia (MHT) Study	136	
	6.3.7	Drug Loading and Drug Release Study	138	
	6.3.8	Biocompatibility	139	
6.4	Conclu	sions	142	
	Referei	144		

6.1 Introduction:

Cancer has been recognized as a major health problem worldwide. Cancer is a disease caused by uncontrolled cell division and is also one of the most common causes of death in the world. Combining biomedicine with nanotechnology has led to amazing progress in cancer treatments. The use of nanoparticles is one of the most promising ways as it provides accurate targeting and strong cytotoxic effects against cancer cells without endangering healthy tissue. Among the wide range of nanoscale materials being studied for biomedical applications, Magnetic Nanoparticles (MNPs) attracted a great deal of attention because of their intrinsic, distinctive, and modifiable physiochemical properties such as their small size, high surface area, novel magnetic and optical effects, and quantum confinement, etc [1]. Among the several forms of MNP, Magnetite- Fe₃O₄ nanoparticles are of great interest because of their unique properties, which include ease to make them biocompatible and superparamagnetism [2]. Superparamagnetic iron oxide nanoparticles, or SPIONs, are Magnetite- Fe₃O₄ based nanocarriers actively used in targeted drug administration, Magnetic Resonance Imaging (MRI), and cancer treatment [3,4].

The primary benefit of a magnetic core for cancer treatment is that, it can be easily formed, modified and guided to the appropriate locations using an external Alternating Magnetic Field (AMF) [5,6]. However, weak factors like Van der Waals forces and magnetic dipole-dipole attractive interactions allow SPIONs to oxidize and aggregate, resulting in poor stability [7]. Developing functional coatings on SPIONs using biocompatible chemicals such as Poly Ethylene Glycol (PEG), Polyethylenimine (PEI), Poly Vinyl Alcohol (PVA), Glutathione (GSH), and so on helps to mitigate these restrictions to some extent [8,9]. Furthermore, functionalization of the surface of the nanoparticles may be significant for the conjugation of the nanoparticles with therapeutic agents for drug administration and/or diagnostic purposes [7].

One of the options to functionalize the core-shell nanoparticles with ligands, includes thiols [10]. Among various thiols, Glutathione (GSH, γ -glutamyl-cysteinyl-glycine) is a crucial tripeptide that directly impacts malignant cells and affects different physiological functions in the body. According to reports, GSH is important for regulating a variety of cell physiological processes as well as for protecting and participating in a wide range of cellular activities. GSH is one of the most significant redox species in the human body and is recognized to have the greatest capacity to cause anticancer drugs to be released from carriers. GSH can increase the efficacy of drug release and cellular mortality. GSH coated nanocomposites show very

promising activity for delivering drugs to specific cancerous tissue. These properties include improved systemic elongation time, enhanced aqueous solubility of anticancer drugs, and decreased associated systemic toxicities [11].

When treating cancer by chemotherapy, Doxorubicin (DOX) is the first line of defence, but it has several side effects on healthy cells. To regulate the drug release, the inclusion of conjugated GSH on the shell may help to decrease the adverse effects of DOX, resulting in improved anti-tumor activity [12].

Table 6.1 shows literature on the synthesis of surface functionalized Magnetite- Fe₃O₄ nanoparticles and their biomedical applications.

Table 6.1: Literature for the synthesis of surface functionalized Magnetite- Fe₃O₄ nanoparticles and their biomedical applications.

Sr. No	Nanoparticles	Coating Material	Method	Application	Reference
1.	Fe ₃ O ₄	GS-Au	Self-assembly method	Controlled DOX Release	[9]
2.	Fe ₃ O ₄	GSH and GSH/PEG	Coprecipitation	Nitric Oxide Delivery	[13]
3.	Fe ₃ O ₄	PEI /GSH	Coprecipitation	Targeted CUR Delivery	[14]
4.	Fe ₃ O ₄	GSH	Oxidative Polymerization	Catalysts for 2,4-DCP Degradation	[15]
5.	Fe ₃ O ₄	-	Solvothermal	Hyperthermia Therapy	[16]
6.	Fe ₃ O ₄	GSH /PEG/ PEI	Coprecipitation	Brain Researches	[17]
7.	Fe ₃ O ₄	GSH	Oxidative Polymerization	Magnetic Hyperthermia therapy, Drug Delivery	Present work

In the present study, GSH-coated Magnetite- Fe₃O₄ nanoparticles were synthesized. The coprecipitation method was used for the synthesis of the Magnetite- Fe₃O₄ nanoparticles,

and the oxidative polymerization method was used for coating tripeptide GSH on Magnetite-Fe₃O₄ nanoparticles.

6.2 Experimental:

Materials:

Materials used to synthesize GSH coated IONPs: Iron (III) chloride hexahydrate (FeCl₃·6H₂O, \geq 99%); Iron (II) chloride tetrahydrate (FeCl₂·4H₂O, \geq 99%); and Sodium hydroxide (NaOH, \geq 99%) -Sigma-Aldrich; Hydrogen peroxide (H₂O₂); Glutathione (GSH)-Hi-Media.

6.2.1 Surface Functionalization of Magnetite- Fe₃O₄ Nanoparticles with Glutathione (GSH):

A) Synthesis of Magnetite- Fe₃O₄ nanoparticles:

Magnetite-Fe₃O₄ nanoparticles were synthesized by coprecipitation method as mentioned in **Section 5.2.1** (A) (Chapter-05) as shown in **Fig.6.1** (a).

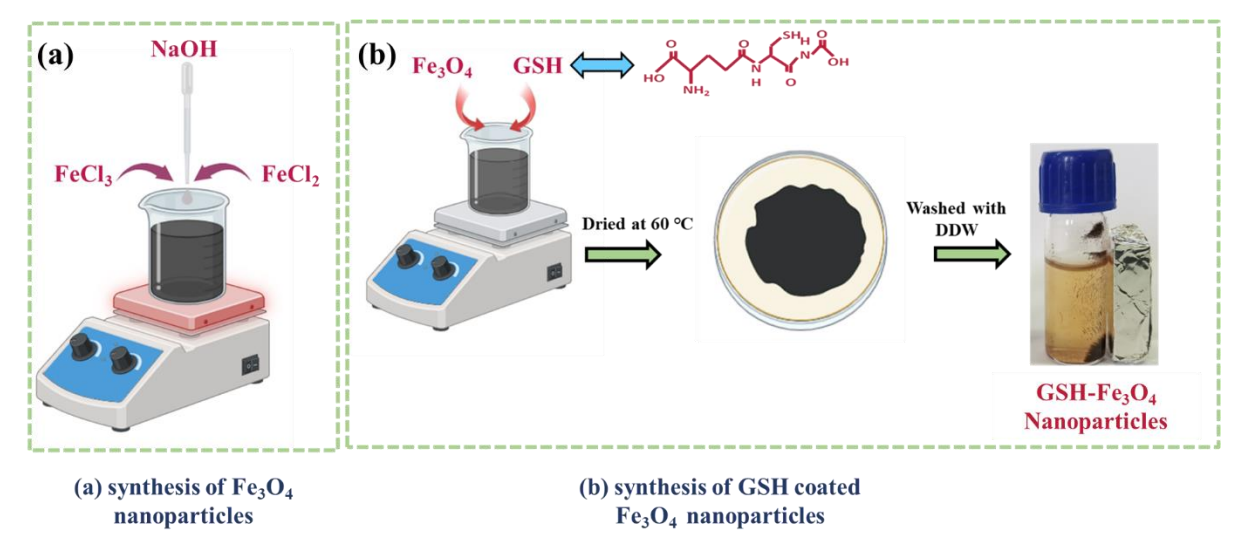


Fig.6.1: Synthesis of **(a)** Magnetite- Fe₃O₄ nanoparticles and **(b)** GSH-coated Magnetite-Fe₃O₄ nanoparticles.

B) Surface functionalization of Magnetite-Fe₃O₄ nanoparticles with GSH:

The oxidative polymerization method was used to synthesize GSH-coated Magnetite- Fe_3O_4 nanoparticles. Initially, 0.2 g of as-synthesized Magnetite- Fe_3O_4 particles were thoroughly dispersed in 25 mL Double Distilled Water (DDW), and then an equal molar mass of GSH was added to the above solution. After 30 minutes of vigorous stirring, the fully combined solution was heated to 70 °C and then 5mL H_2O_2 (H_2O_2 : $H_2O = 1:2$) was added dropwise for 1 h with continuous stirring. The product was then decanted, washed thrice using

DDW, and dried for 12 h at 60 °C. **Fig.6.1** depicts the schematic of synthesis: (a) Magnetite-Fe₃O₄ nanoparticles and (b) GSH coated Magnetite-Fe₃O₄ nanoparticles.

6.2.2 Characterization:

A) Physicochemical Characterization:

X-ray Diffraction (XRD) patterns of powder samples Magnetite- Fe_3O_4 and GSH coated Magnetite- Fe_3O_4 were recorded with $CuK\alpha$ radiation (λ =1.546 Å). Scanning Electron Microscopy (SEM) (JEOL, JSM-IT200 (Japan)) was used to observe the morphology. Fourier Transform Infrared Spectroscopy (FTIR) spectra were recorded on Alpha (II) Bruker device operating in a range of 400-4000 cm⁻¹. Hydrodynamic particle size and zeta (ζ)-potential were recorded using (HORIBA SZ-100) with water as a dispersant. Vibrating Sample Magnetometer (VSM) (EV X) was used to study magnetic properties at room temperature. Magnetic Hyper Thermia (MHT) study for all the samples was carried out using an EasyHeat 8310 (Ambrell, UK) assembly. The anticancer efficacy of the Magnetite- Fe_3O_4 , GSH, and GSH coated Magnetite- Fe_3O_4 was made using MTT assay and evaluated against L929 fibroblast cell line and MDA-MB-231 breast cancer cell line. The hemolysis assay was used to assess the effect of synthesized particles on red blood cells, i.e. to check the hemocompatibility of GSH coated Magnetite- Fe_3O_4 nanoparticles.

B) Biological Characterization:

(a) Cell Viability/Cytotoxicity Assay:

MTT (3-(4, 5-dimethythiazol-2-yl)-2, 5-diphenyl tetrazolium bromide) Assay:

For in vitro studies, fibroblast cell line (L929), and breast cancer cell line (MDA MB 231) were mixed with GSH coated Magnetite-Fe₃O₄ nanoparticles and assessed using an MTT cytotoxicity assay as discussed in **Section 4.3.7** (a) (Chapter-04).

(b) Hemolysis assay:

The hemocompatibility of GSH coated Magnetite-Fe₃O₄ nanoparticles was studied using hemolysis assay as discussed in **Section 4.3.7 (b) (Chapter-04)**.

6.3 Results and Discussion:

6.3.1 Structural/ Phase Analysis:

The XRD patterns for Magnetite- Fe₃O₄ particles and GSH coated Magnetite- Fe₃O₄ particles are shown in **Fig.6.2**. All the samples show polycrystalline structure revealing cubic inverse spinel crystal structure of Magnetite- Fe₃O₄ phase. The XRD patterns perfectly match with the JCPDS card no. 00-019-0629 for Magnetite- Fe₃O₄ particles and GSH coated Magnetite- Fe₃O₄ particles [18]. The average crystallite size calculated using the Scherrer

formula (**Equation 3.3** (**Chapter-03**)) for the prominent peaks is found to be 9±0.7 nm for Magnetite- Fe₃O₄ particles and 8±0.5 nm for sample GSH coated Magnetite- Fe₃O₄ particles.

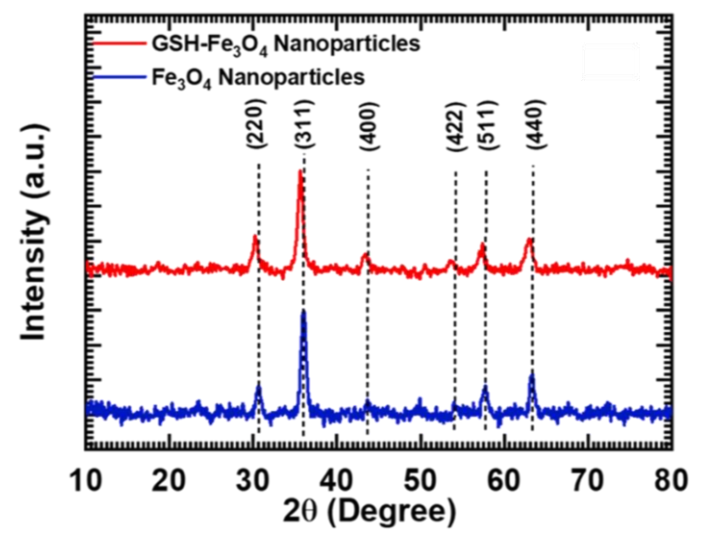


Fig.6.2: XRD patterns of Magnetite- Fe₃O₄ nanoparticles and GSH coated Magnetite- Fe₃O₄ nanoparticles.

A decrease in crystallite size is observed after GSH coating. The reduction in crystallite size with the addition of GSH is due to the GSH atoms occupying interstitial positions within the network of Magnetite- Fe₃O₄ particles, leading to the compression of the crystallite size in the case of anisotropic microdeformation [7].

Transmission Electron Microscopy (TEM):

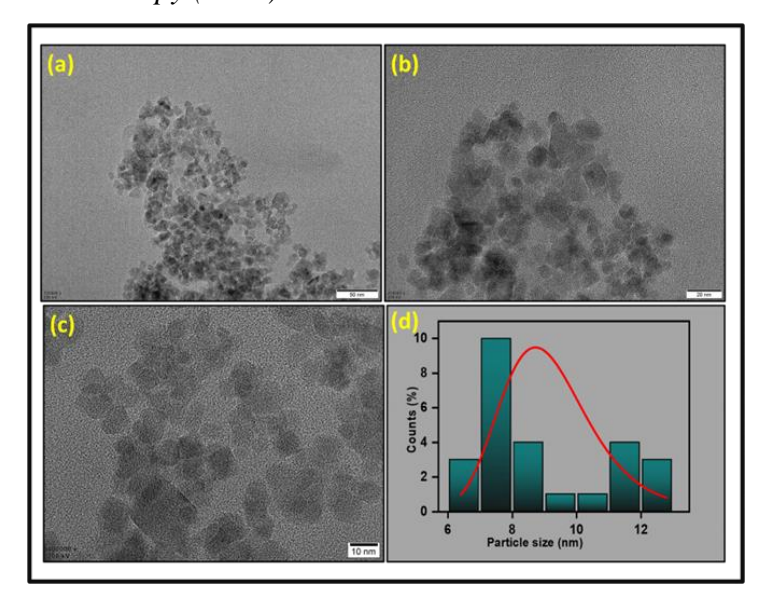


Fig.6.3: TE micrographs of GSH coated Magnetite-Fe₃O₄ nanoparticles at different magnifications.

The particle size was further evaluated using Transmission Electron Microscope (TEM) (JEOL, JEM 2100). The Transmission Electron (TE) micrographs for three different

magnifications are shown in **Fig.6.3** (**a-c**) for GSH coated Magnetite-Fe₃O₄ nanoparticles. The average particle size is found to be 8± 0.9 nm, which matches with that calculated from XRD study.

The particle size distribution curve plotted for the GSH coated Magnetite- Fe₃O₄ nanoparticles from the TE micrograph is as shown in **Fig.6.3** (**d**). The average particle size of 8± 0.9 nm was calculated from the TE micrographs using Image-J software, and by selecting approximately 30 particles from TE micrographs (**Fig.6.3** (**a**)) to plot the curve for particle size distribution.

6.3.2 Morphological Analysis:

Scanning Electron Microscopy (SEM):

The surface morphology of the synthesized GSH coated Magnetite-Fe₃O₄ nanoparticles was studied using SEM. The Scanning Electron (SE) micrographs at two different magnifications are shown in **Fig.6.4**. Granular surface morphology of agglomerated IONPs is seen with average grain size of 38 nm.

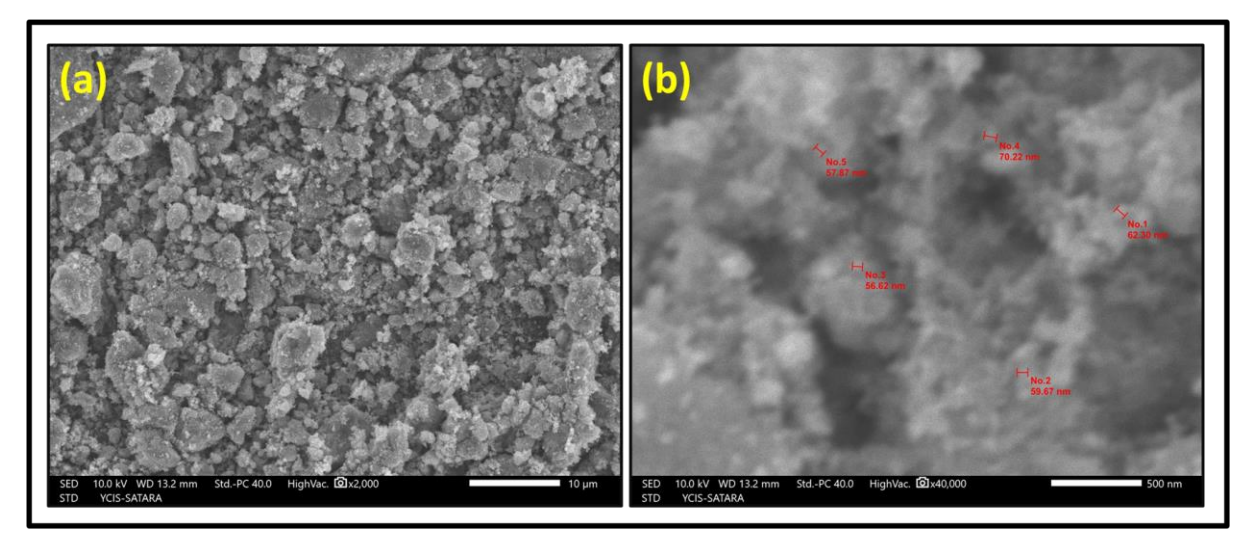


Fig.6.4: SE Micrographs of GSH coated Magnetite-Fe₃O₄ nanoparticles at 2000X and 40000X.

This increase in diameter is observed due to GSH coating on Magnetite- Fe₃O₄ nanoparticles. The agglomeration is observed because of intrinsic Van der Waals forces and magnetic dipole-dipole interactions between MNPs [14,19].

6.3.3 Chemical Signature:

Fourier-Transform Infrared Spectroscopy (FTIR):

The chemical bonds existing in Magnetite- Fe₃O₄ are studied using FTIR spectroscopy in which the incident infrared radiation is absorbed at a resonant frequency of bending,

stretching, or vibrating chemical bond that exists between the atoms within the compound [20]. The FTIR absorption spectra of Magnetite- Fe₃O₄ nanoparticles, GSH, and GSH coated Magnetite- Fe₃O₄ nanoparticles within the wavenumber range of 4000 to 300 cm⁻¹ are shown in Fig.6.5.

The absorption peaks at 579.19 and 424.93 cm⁻¹ in the crystal structure of Magnetite-Fe₃O₄ nanoparticles are attributed to Fe-O bonds, which correspond to the tetrahedral (Fe³⁺-O) and octahedral (Fe²⁺-O) sites, respectively [21]. Stretching vibration of hydroxyl (-OH) on the surface of Magnetite- Fe₃O₄ nanoparticles causes the absorption at 3434 cm⁻¹. The hydroxyl group allows the material to be further surface functionalized by replacing the -OH group with GSH.

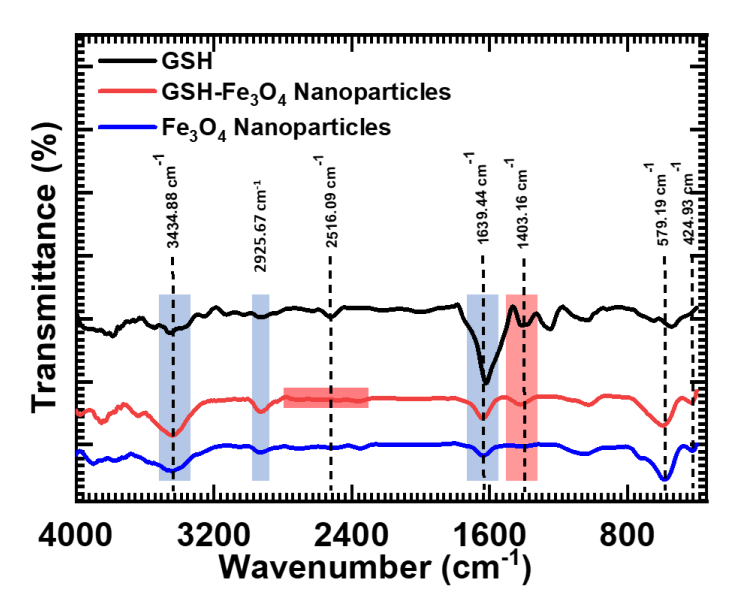


Fig.6.5: FTIR spectra of Magnetite- Fe₃O₄ nanoparticles, GSH, and GSH coated Magnetite- Fe₃O₄ nanoparticles.

The bands at 1639 cm⁻¹ (v_{assym} COO⁻) and 1403 cm⁻¹ (v_{sym} COO⁻) attributed to carboxylic groups demonstrate the presence of GSH [22]. The peptide bond at 3460 cm⁻¹ is a result of –NH stretching, a weak thiol band for S-H stretching at 2616 cm⁻¹, and vibrations related to C-S stretching come in between 650 and 700 cm⁻¹. Furthermore, bands corresponding to C-H sp³ bonds are seen at 2920 cm⁻¹ (v_{sym} C-H) [9]. Therefore, FTIR study confirms that the GSH coating is present on the surface of Magnetite-Fe₃O₄ nanoparticle.

6.3.4 Particle Size and Zeta Potential Study:

Dynamic Light Scattering (DLS):

Good chemical stability at physiological/neutral pH \sim 7 is necessary for the use of nanoparticles in biomedicine. DLS was used to assess the hydrodynamic characteristics of the

MNPs in aqueous dispersions using water (pH-7) because of its biological relevance. The hydrodynamic size, and ζ-potential, of GSH coated Magnetite- Fe₃O₄ nanoparticles were assessed using DLS technique.

The DLS study was performed for GSH coated Magnetite- Fe₃O₄ nanoparticles to investigate the hydrodynamic diameter of nanoparticles at room temperature using DDW at pH value of 7.2. The observed hydrodynamic diameter of GSH coated Magnetite- Fe₃O₄ nanoparticles is 112.5 nm (**Fig.6.6**). The obtained hydrodynamic size of GSH coated Magnetite- Fe₃O₄ nanoparticles is more compared to actual size of the nanoparticles due to solvation layer of water molecules and ions around the particles along with the little aggregation [12].

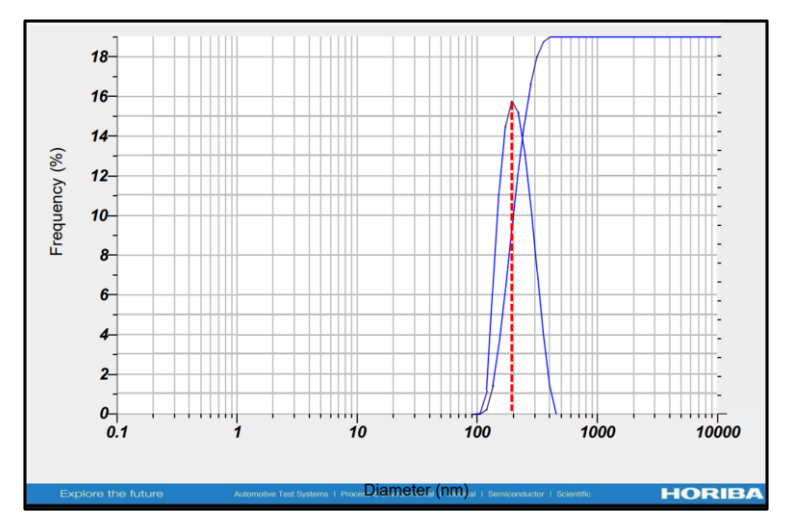


Fig.6.6: Hydrodynamic diameter of GSH coated Magnetite- Fe₃O₄ nanoparticles.

GSH coated Magnetite-Fe₃O₄ nanoparticles have a lower hydrodynamic diameter indicating a reduction in aggregation. If the coating is thick enough, the Van der Waals attraction between particles is weaker than Brownian thermal energy. This is the origin of the word "steric" stabilization, which creates extra repulsive energy barriers. Therefore, a nonmagnetic coating of PEG, PVA, or thiol (like GSH) on the surface of the MNPs provides steric or static repulsion, thereby balancing the attraction forces among the particles, resulting in a smaller hydrodynamic diameter [20].

Zeta potential (ζ *-potential*):

The ζ - potential is used to measure the variation in surface charges of particles, which is used to control the electrostatic interaction of the nanoparticles. The stability of nanoparticles is investigated using ζ - potential measurements in water (pH \sim 7). The standard value of ζ -potential of MNPs to be used for biomedical applications is ± 30 mV [13]. The ζ - potential of GSH coated Magnetite- Fe₃O₄ nanoparticles varies in the range of -60 to 10 mV with peak

value at -20 mV as shown in **Fig.6.7**. The repulsive forces between negatively charged sheath around the IONPs cause the increase in hydrodynamic size as indicated in DLS study.

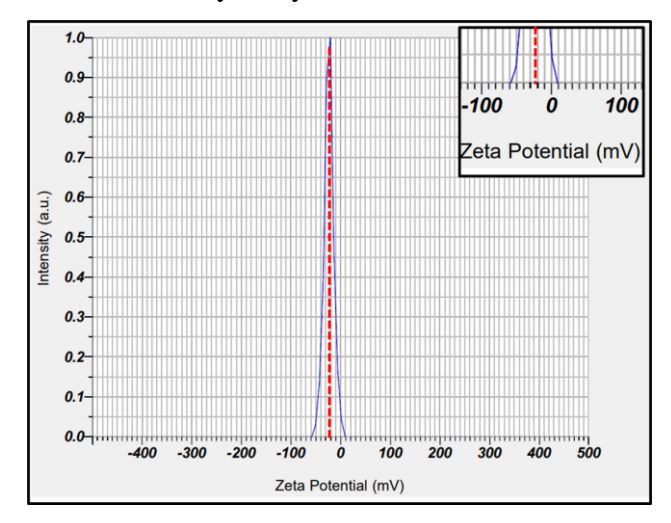


Fig.6.7: Zeta potential value of GSH coated Magnetite- Fe₃O₄ nanoparticles (Inset: enlarge view of zeta potential scale from -60 to +10 mV).

The negative ζ - potential value of GSH coated Magnetite- Fe₃O₄ nanoparticles is likely attributable to carboxylate anions on the surface. The significant interparticle repulsion between the negative charges keeps GSH-coated Magnetite- Fe₃O₄ nanoparticles from aggregating [20].

6.3.5 Vibrating Sample Magnetometer (VSM) Analysis:

The magnetic parameters namely type of magnetism, saturation magnetization, coercivity, and retentivity, can be evaluated with the help of VSM, which generates a hysteresis loop of IONPs.

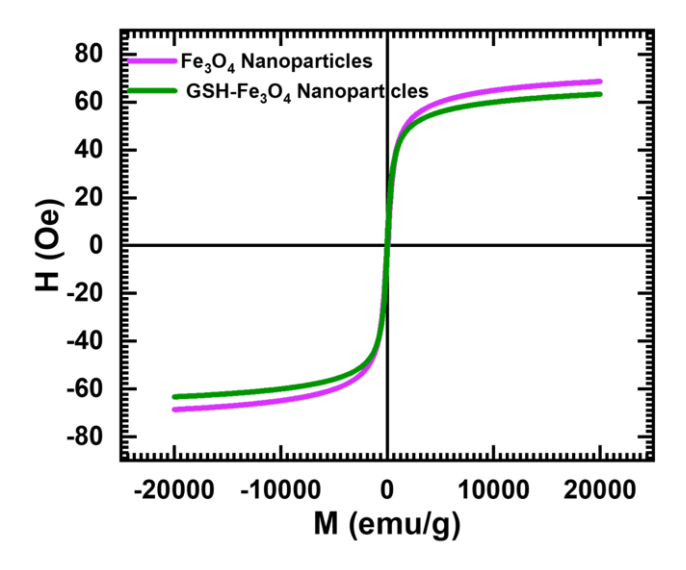


Fig.6.8: Magnetization versus magnetic field curves of Magnetite-Fe₃O₄ nanoparticles and GSH coated Magnetite- Fe₃O₄ nanoparticles.

The hysteresis loops for Fe₃O₄ and GSH coated Magnetite- Fe₃O₄ nanoparticles were obtained in the external magnetic field window of ±17 kOe at room temperature, which are shown in **Fig.6.8**.

The obtained saturation magnetization (Ms) value for Magnetite- Fe₃O₄ nanoparticles is 50.2 emu g⁻¹, and for GSH coated Magnetite- Fe₃O₄ nanoparticles is 48.3 emu g⁻¹, which is lower than that of the theoretically (92 emu g⁻¹) reported saturation magnetization (Ms) value of bulk Magnetite- Fe₃O₄ nanoparticles. The reduced magnetization value may result from spin pinning, the finite size effect, spin canting, crystal defects, the shape effect, and/or changes in the distribution of cations [23].

The decrease in saturation magnetization (Ms) value is observed after the GSH coating because the coating of nonmagnetic layers hinders the response of the applied magnetic field towards Magnetite- Fe₃O₄ nanoparticles, which results in a decrease in the magnetic moment. The obtained saturation magnetization (Ms) value of Magnetite- Fe₃O₄ and GSH-coated Magnetite- Fe₃O₄ nanoparticles is adaptable for biological applications, as according to reports, a saturation magnetization (Ms) value of 7–22 emu g⁻¹ is suitable for biomedical applications [18]. Table 6.2 shows the magnetization parameter values of synthesized nanoparticles.

Table 6.2: Magnetic properties of Magnetite- Fe₃O₄ and GSH coated Magnetite- Fe₃O₄ nanoparticles from VSM analysis.

Properties→ Nanoparticles↓	Ms (emu g ⁻¹)	Hc (Oe)	
Fe ₃ O ₄ Nanoparticles	50.2	32.83	
GSH coated Fe ₃ O ₄ Nanoparticles	49.22	18.23	

6.3.6 Magnetic Hyper Thermia (MHT) Study:

The heat produced by Magnetite- Fe₃O₄ nanoparticles in an AMF can potentially be used for cancer treatments. The Specific Absorption Rate (SAR), which measures the amount of heat generation per unit mass of Magnetite- Fe₃O₄ nanoparticles, and the local concentration of Magnetite- Fe₃O₄ nanoparticles, are the two key elements that affect the amount of heat generation that occurs locally.

Generally, temperatures between 42-45°C are suitable to kill cancer cells. Thus, the MHT cancer therapy basically requires a suitable amount of MNPs to be inserted into cancer

tumor and application of external AMF of appropriate strength to increase the temperature to kill the cancer cells.

GSH-coated Fe₃O₄ nanoparticles with concentrations of 3 mg mL⁻¹ were kept in a 3 mL cuvette containing 1 mL of DDW. This cuvette was kept in a MHT device and external AMF of fixed frequency (278 kHz) was applied for 600 s. The change in temperature was recorded for three different AMF strengths (13.3, 20.0, and 26.7 kA m⁻¹). **Fig.6.9** shows the temperature vs time curves of Magnetite- Fe₃O₄ and GSH coated Magnetite- Fe₃O₄ nanoparticles.

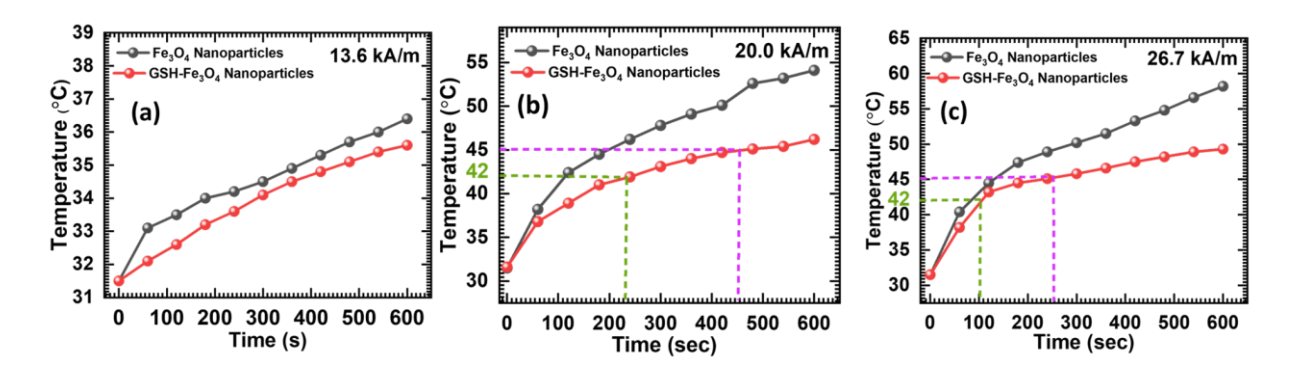


Fig.6.9: Temperature Vs Time variation for Magnetite- Fe₃O₄ and GSH coated Magnetite-Fe₃O₄ nanoparticles.

The SAR and Intrinsic Loss Power (ILP) values calculated using **Equations 2.7** and **2.8** (**Chapter-02**) as a function of magnetic field strength for GSH coated Magnetite- Fe₃O₄ nanoparticles for different concentrations are shown in **Table 6.3**.

Concentration (mg mL^{-1}) \rightarrow	3 mg mL ⁻¹					
Magnetic Strength (kA m ⁻¹) →		13.6	20.0		26.7	
MNPs	Fe ₃ O ₄	GSH coated Fe ₃ O ₄	Fe ₃ O ₄	GSH coated Fe ₃ O ₄	Fe ₃ O ₄	GSH coated Fe ₃ O ₄
SAR (W g ⁻¹)	37.32	13.99	156.31	121.31	207.63	156.31
ILP (nHm ² kg ⁻¹ , n=1)	0.77	0.27	1.4	1.09	1.04	0.07

Adding a GSH coating can lower the heating efficiency of Magnetite- Fe₃O₄ nanoparticles. The drop in temperature of the GSH-containing suspension is in good agreement with the magnetization value, indicating that the surface coating reduces the magnetic moment

of Magnetite- Fe₃O₄ nanoparticles, which leads to a decrease in the SAR value of GSH coated Magnetite- Fe₃O₄ nanoparticles. Compared to iron oxide nano agents available for therapeutic use, such as Feridex (115 W g⁻¹ and 0.16 nHm² kg⁻¹) and Resovist (104 W g⁻¹ and 0.21 nHm² kg⁻¹), the synthesized materials exhibited greater SAR and ILP values [24]. Hence the nanoparticles can be used as thermo-agent for MHT and drug delivery.

6.3.7 Drug Loading and Drug Release Study:

Drug Loading

UV-visible spectroscopy was used to assess the in-vitro drug loading process to quantify the adsorption of the drug onto the nanoparticle surface of GSH coated Magnetite-Fe₃O₄ nanoparticles as discussed in **Section 5.3.7** (**Chapter-05**). The DOX is used as a model drug for anticancer therapy to study the loading and release characteristics. Due to the electrostatic interaction between the positively charged amino and carbonyl groups of DOX and the negatively charged carboxylic group of GSH, the DOX may readily integrate into the nanoparticles. Furthermore, it has been shown that the delocalized π electrons in π - π stacking and hydrophobic contact may efficiently load drug that contain aromatic rings onto the surface of nanoparticles. The maximal drug loading capacity, or entrapment efficiency (EE), of 91% was calculated after 48 hours of drug loading using **Equation 5.1** (**Section 5.3.7** (**Chapter-05**)).

Drug Release:

The drug release profile of GSH coated Magnetite- Fe₃O₄ nanoparticles was studied as discussed in **Section 5.3.7** (**Chapter-05**).

The drug release performance of GSH coated Magnetite- Fe₃O₄ nanoparticles after 48 h and by varying the pH of physiological suspension i.e. at pH=4.5, 6.8, and 7.4 is shown in **Fig.6.10**. The drug release efficiency of DOX loaded Magnetite- Fe₃O₄ nanoparticles and DOX loaded GSH coated Magnetite- Fe₃O₄ nanoparticles is given in **Table 6.4**.

Table 6.4: Drug release percentage of DOX loaded Magnetite- Fe₃O₄ nanoparticles and GSH coated Magnetite- Fe₃O₄ nanoparticles at different pH values.

pH → NPs ↓	4.5	6.8	7.4
Fe ₃ O ₄	80.6%	79.32%	50.19%
GSH-Fe ₃ O ₄	87.75%	81.26%	58.49%

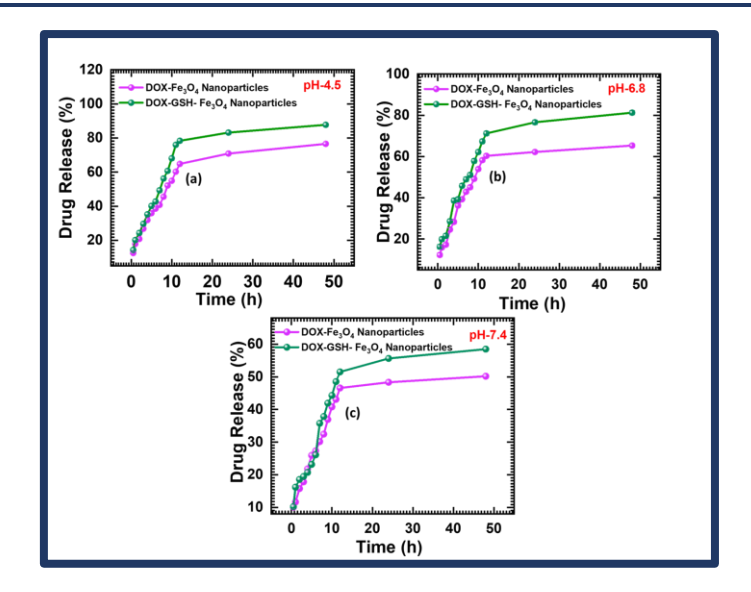


Fig.6.10: Drug release percentage of the DOX loaded Magnetite- Fe₃O₄ nanoparticles and GSH coated Magnetite-Fe₃O₄ nanoparticles at different pH: (a) pH-4.5, (b) pH-6.8, and (c) pH-7.4.

The in vitro release tests show that DOX-loaded Magnetite- Fe₃O₄ and DOX-loaded GSH-coated Magnetite- Fe₃O₄ nanoparticles are pH-sensitive and can potentially release their therapeutic payload in the acidic tumor microenvironment. In this study, it is also observed that the drug release is more rapid for acidic medium (TME) as compared to physiological pH of 7.4.

Hence, the study is appropriate for targeted therapy which is consistent with the acidic TME. While higher pH decreases the efficiency of drug release and lower pH probably increases drug release because of the reduced π - π stacking interaction. Therefore, the tumor-specific drug delivery is possible with the addition of GSH, which further speeds up DOX release in tumor acidic environment [9].

6.3.8 Biocompatibility:

(a) Cytotoxicity Assay:

3-(4, 5-dimethylthiazol- 2-yl)-2,5-diphenyltetrazolium bromide (MTT) Assay:

Due to wide applications of iron oxide in the field of biomedical, cell viability and cell toxicity are the primary steps to check their biocompatibility. To study the toxicity, GSH coated Magnetite- Fe₃O₄ nanoparticles were mixed with fibroblast cell line (L929) and cancer cell line (MDA MB 231).

Here, MTT assay was used for assessing the cell viability of fibroblast cell line (L929) and cell toxicity of breast cancer cell line (MDA-MB-231) at various concentrations (100, 50, 25, 12.5, 6.25, and 3.125 µg mL⁻¹) of Magnetite Fe₃O₄ nanoparticles, GSH, and GSH coated

Magnetite- Fe₃O₄ nanoparticles after 48 h of incubation as discussed in **Section 4.3.7** (a) (Chapter-04).

Equations 3.5 and **3.6** (**Chapter-03**) were used to calculate the percentage of cell viability/ toxicity of Magnetite- Fe₃O₄ nanoparticles.

For L929 fibroblast cell line, the GSH coated Magnetite- Fe₃O₄ nanoparticles show decrease in cell viability from 97 to 92 % with increase in the concentration of GSH coated Magnetite- Fe₃O₄ nanoparticles from 3.125 to 100 µg mL⁻¹ as shown in **Fig.6.11** (a). The microscopy pictures of untreated and treated L929 cell line for 100 µg mL⁻¹ of IONPs is shown in **Fig.6.11** (b).

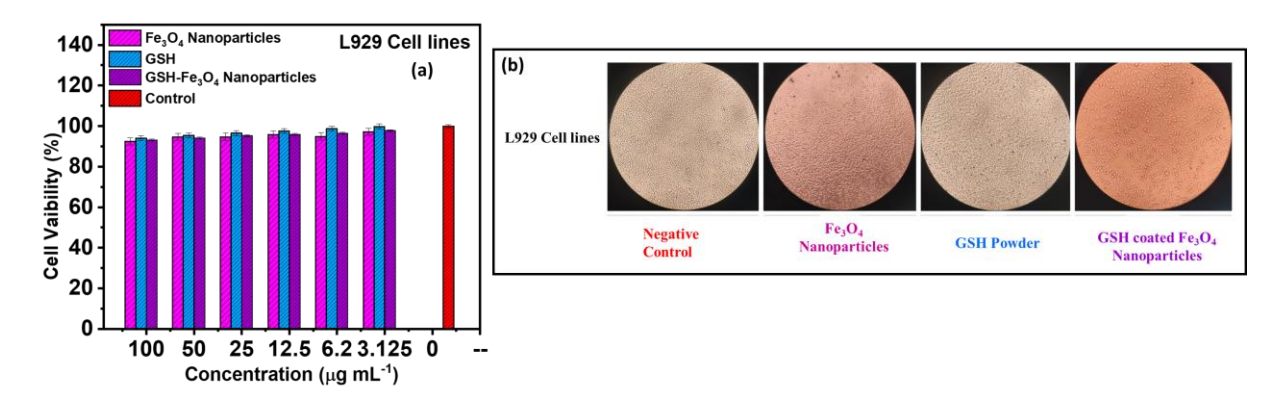


Fig.6.11: (a) Histogram of cell viability percentage and (b) The microscopy pictures of the L929 cell line.

For MDA-MB-231 breast cancer cell line, the GSH coated Magnetite- Fe₃O₄ nanoparticles show increase in cell toxicity from 21.47 to 80.73 % with increase in concentration from 3.125 to 100 μg mL⁻¹. Thus, the cell toxicity (killing of cancer cells) increases with concentration of Magnetite- Fe₃O₄ nanoparticles as shown in **Fig.6.12** (a). The microscopic picture of breast cancer cell line (MDA MB 231) for concentration of 100 μg mL⁻¹ of IONPs is shown in **Fig.6.12** (b).

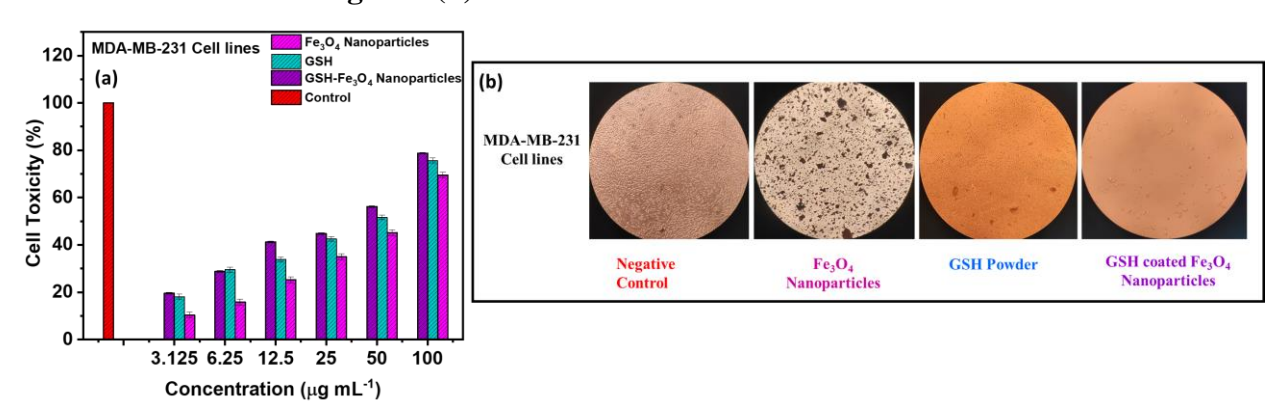


Fig.6.12: (a) Histogram of cell viability percentage and (b) The microscopy pictures of the MDA MB 231 cell line.

The activation of oxidative stress, which comprised lipid peroxidation and the generation of ROS, was demonstrated to be connected with cytotoxicity [25]. Cell toxicity increased more when MDA-MB-231 cell line were treated with GSH coated Magnetite-Fe₃O₄ nanoparticles than the cells treated with Magnetite-Fe₃O₄ nanoparticles.

Cell death mechanism

Magnetite- Fe₃O₄ produces ROS in large number, which is very harmful to cancer cells and may be the reason for cancer cell death. This might be explained as: At a pH of 4-5 (Tumor region), Magnetite- Fe₃O₄ may dissociate into Fe²⁺ and Fe³⁺ ions. Ferroptosis occurs in tumor cells when Magnetite- Fe₃O₄ nanoparticles penetrate cells, break down into Fe ions, and create ROS in mitochondria by converting H₂O₂ to free radicals. When this occurs, there is unregulated membrane lipid peroxidation, which leads to membrane permeability loss and, ultimately, cell death. The three processes involved in ferroptosis are, glutathione-dependent antioxidant mechanism, iron metabolism, and lipid peroxidation; small changes in these pathways lead to the death of cells. Modulating GSH levels may have therapeutic consequences due to its function in inducing apoptosis, necrosis, and ferroptosis. GSH is essential for maintaining intracellular oxidative equilibrium, serving as an antioxidant, and promoting metabolism and detoxification [26]. GSH serves as a substrate for GSH peroxidases (GPXs) and GSH-S-transferases (GSTs) and is involved in iron and sulphur metabolism. With increases in ROS as a result of ferroptosis, GSH reduces to balance it. The reduction in GSH inhibits GPX4, leading to lipid peroxidation and ROS accumulation, resulting in cell death [27].

GSH may also improve the way that nanoparticles interact with cells, which is another source of cell death. Furthermore, the superparamagnetic nature of both nanoparticles may be steered directly to the tumor location by applying an external magnetic field, boosting nanoparticle toxicity at the target region. Therefore, our findings indicate the potential applicability of Magnetite- Fe₃O₄ and GSH-coated Magnetite- Fe₃O₄ nanoparticles as powerful toxicants against tumorigenic cell lines [7].

(b) Hemolysis Assay:

The entry of foreign particles into the body can have a variety of and sometimes conflicting effects, so determining their effects on the body is a critical step in their applicability. Because the injected nanoparticles come into direct touch with blood tissue and its components, an evaluation of their hemocompatibility is essential for further study.

For this study fresh human blood (10 mL) was collected in heparinized centrifuge tubes, rotated at 3000 rpm for 10 min, and washed three times with an equivalent volume of normal

saline. The blood volume was measured and reconstituted as a 10% v/v solution in normal saline. The reaction mixture included 1 mL of 10% red blood cell suspension. Triton X-100 was used as a standard drug (positive control), saline as a negative control, and test sample with different concentrations of GSH coated Magnetite- Fe₃O₄ nanoparticles were then incubated at 56°C for 30 min, and centrifuged at 2500 rpm for 5 min, and the absorbance of the supernatant was measured at 560 nm. Hemolysis percentage was calculated using **Equation 3.7** (Chapter-03).

The concentration of the Magnetite- Fe₃O₄ nanoparticles was varied from 0.5 to 2.0 mg mL⁻¹. The change in hemolysis percentage is shown in **Fig.6.13**.

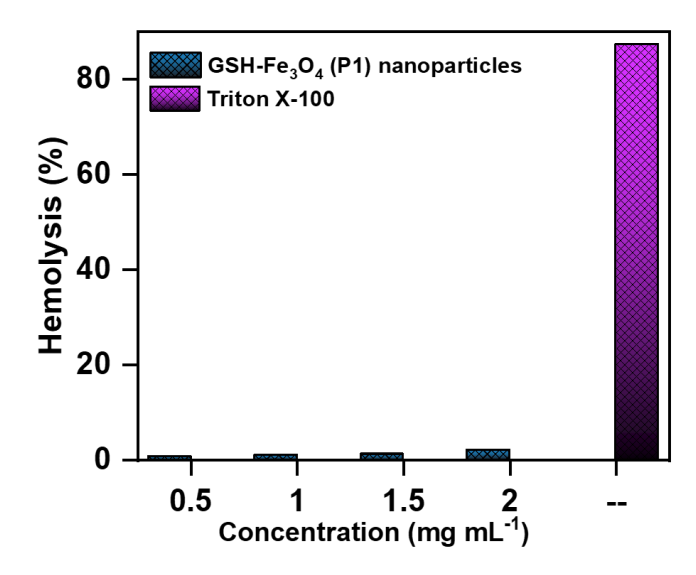


Fig 6.13: Hemolysis percentage of GSH coated Magnetite- Fe₃O₄ nanoparticles.

The percentage of hemolysis is between 1 to 2.1 which is well below 5% as per ISO 10993-5 guidelines [28]. Accordingly, it is observed that the GSH coated Magnetite- Fe₃O₄ nanoparticles are suitable for usage in biomedical applications and do not exhibit hemolytic activity.

6.4 Conclusions:

In the present study, Magnetite- Fe₃O₄ nanoparticles were successfully synthesized by a simple chemical coprecipitation method and surface modified with GSH via the oxidative polymerization method. The XRD analysis reveals there is no phase change of Magnetite- Fe₃O₄ after GSH coating. FTIR study confirms the composition of coated Magnetite- Fe₃O₄ nanoparticles with thiol (GSH). VSM studies showed the superparamagnetic behaviour of synthesized nanoparticles at room temperature with saturation magnetization (Ms) value 50.21 and 49.22 emu g⁻¹ for Magnetite- Fe₃O₄ and GSH coated Magnetite- Fe₃O₄ nanoparticles, respectively. The magnetic induction study reveals the synthesized nanoparticles

can potentially be used as thermoseeds for MHT. In acidic pH, GSH-coated Magnetite- Fe₃O₄ shows a rapid drug release compare normal physiological pH. Hence the GSH-coated Fe₃O₄ nanoparticles can be used as carriers for drug delivery. MTT assay revealed the toxicity of 80.73% towards the MDA-MB-231 breast cancer cell line and cell viability of 92 % towards L929 fibroblast cell line at 100 µg mL⁻¹. Thus, the GSH-coated Fe₃O₄ can be effectively used as an anticancer agent to kill cancerous cells with minimal side effects to normal cell lines. Hemolysis in GSH-coated Fe₃O₄ is less than 5%, which is acceptable to use in biomedical applications. Therefore, the resulting study reveals that GSH coated Fe₃O₄ nanoparticles is potential material for anticancer therapy.

References:

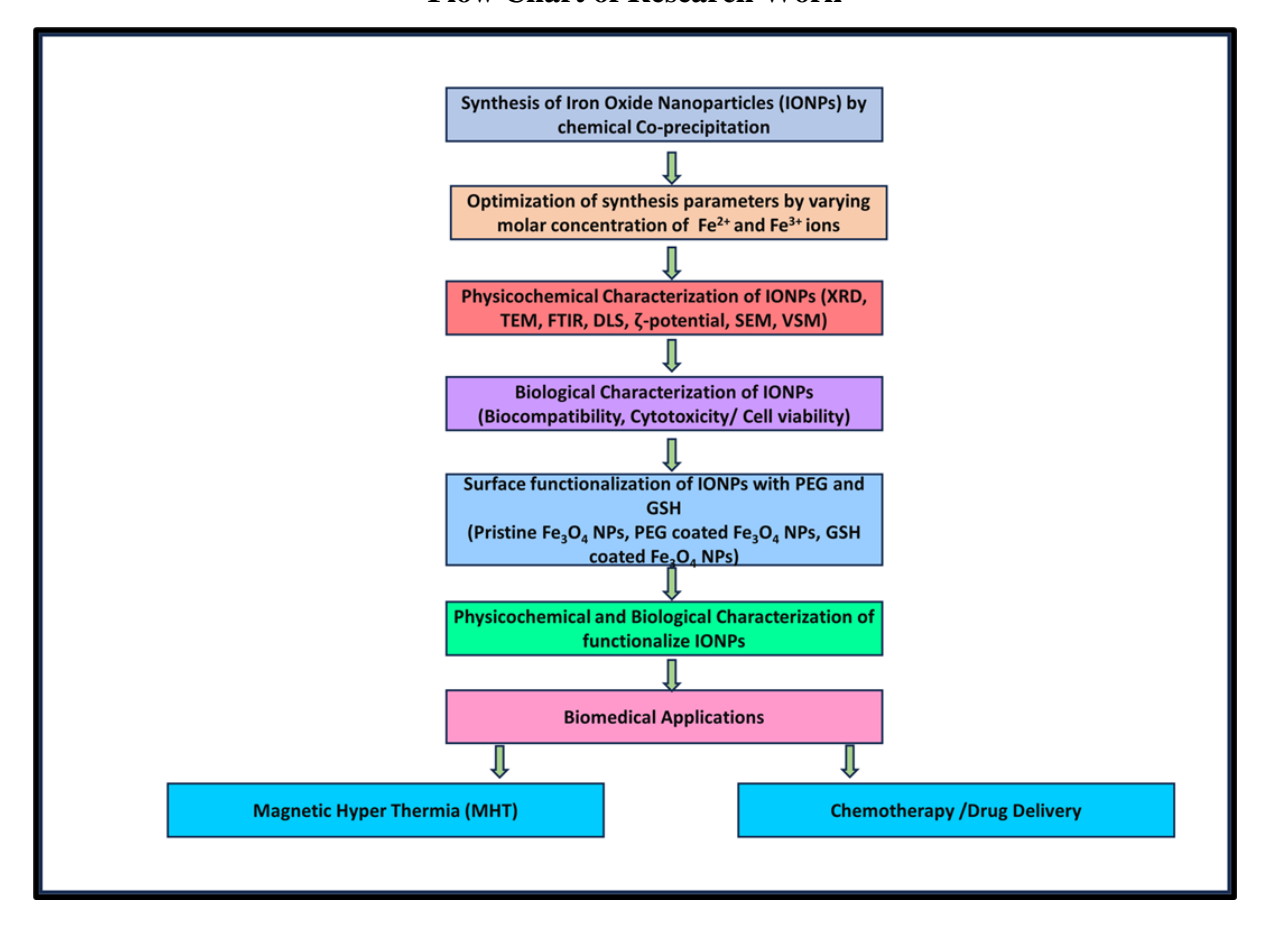
- 1. Pankhurst Q, Connolly J, Jones S, Dobson J. J. Appl. Phys. 36 (13) (2003) 167-83.
- 2. Patel N, Khot V & Patil R. Chem. pap. 78 (6) (2024) 3857-69.
- 3. Polavarapu L, Manna M, Xu Q. Nanoscale. 3 (2) (2011) 429-34.
- 4. Simpson C, Salleng K, Cliffel D, Feldheim D. Nanomedicine: Nanotechnology, Biology and Medicine. 9 (2) (2013) 257-63.
- 5. Jurgons R, Seliger C, Hilpert A, Trahms L, Odenbach S, Alexiou C. J. Phys. Condens. Matter. 18 (38) (2006) S2893-105.
- 6. Bourrinet P, Bengele H, Bonnemain B, Dencausse A, Idee J, Jacobs P, Lewis J. Invest Radiol. 41 (3) (2006) 313-24.
- 7. Haddad P, Santos M, de Guzzi Cassago C, Bernardes J, de Jesus M, Seabra A. J. Nanoparticle Res. 18 (369) (2016) 1-13.
- 8. Patel N, Mulla N, Khot V, Patil R. Emergent Materials. 7 (3) (2024) 1071-80.
- 9. Singh N, Nayak J, Sahoo S, Kumar. Mater. Sci. Eng. C. 100 (2019) 453-65.
- 10. Ganta S, Devalapally H, Shahiwala A, Amiji M. J. Control. Release. 126 (3) (2008) 187-204.
- 11. Kesavan M, Kotla N, Ayyanaar S, Kumar G, Rajagopal G, Sivaraman G, Webster T, Rajesh J. Nanomedicine: Nanotechnology, Biology and Medicine. 14 (5) (2018) 1643-54.
- 12. Smyth J, Bowman A, Perren T, Wilkinson P, Prescott R, Quinn K, Tedeschi M. Ann. Oncol. 8 (6) (1997) 569-73.
- 13. Santos M, Seabra A, Pelegrino M, Haddad P. Appl. Surf. Sci. 367 (2016) 26-35.
- Aeineh N, Salehi F, Akrami M, Nemati F, Alipour M, Ghorbani M, Nikfar B, Salehian F, Riyahi Alam N, Sadat Ebrahimi S, Foroumadi A. J. Biomater. Sci. Polym. Ed. 29 (10) (2018) 1109-25.
- 15. Zhou R, Shen N, Zhao J, Su Y, Ren H. J. Mater. Chem. A. 6 (3) (2018) 1275-83.
- 16. Jonak S and Borah J. Mater. Today Commun. 26 (2021) 101789-812.
- 17. Han G, Zhang B, Zhang H, Han D, Tan J, Yang B. J. Mater. Sci.: Mater. Med. 30 (5) (2019) 1-7.
- 18. Antarnusa G and Suharyadi E. Mater. Res. Express. 7 (5) (2020) 056103-09
- 19. Dutta A, Maji S, Mondal A, Karmakar B, Biswas P, Adhikary B, Sens. Actuators B: Chem. 173 (2012) 724-31.
- 20. Rajamanikandan R, Shanmugaraj K, Ilanchelian M. J. Clust. Sci. 28 (2017) 1009-23.
- 21. Jafari A, Shayesteh S, Salouti M, Boustani K. J. Magn. Magn. Mater. 379 (2015) 305-12.
- 22. Gonçalves L, Seabra A, Pelegrino M, De Araujo D, Bernardes J, Haddad P. RSC advances. 7 (24) (2017) 14496-503.
- 23. Upadhyay S, Parekh K, Pandey B. J. Alloys Compd. 678 (2016) 478-85.
- 24. Ding Y, Dai Y, Wu M, Li L. Chem. Eng. J. 426 (2021) 128880-931.

- 25. Dwivedi S, Siddiqui M, Farshori N, Ahamed M, Musarrat J, Al-Khedhairy A. Colloids Surf B. 122 (2014) 209-15.
- 26. Lu S and Ge J. American Journal of Physiology-Cell Physiology. 263 (6) (1992) 1181-9.
- 27. Valenti G, Tasso B, Traverso N, Domenicotti C, Marengo B. Redox Experimental Medicine. 2023 (1) (2023) e220023-35.
- 28. Bhavikatti S, Zainuddin S, Ramli R, Nadaf S, Dandge P, Khalate M, Karobari M. Sci. Rep. 14 (1) (2024) 11878-98.

CHAPTER-07 SUMMARY AND CONCLUSIONS

7.1 Summary

Flow Chart of Research Work



Chapter-01 includes fundamental description of nanoparticles (NPs), Magnetic Nanoparticles (MNPs), Iron Oxide nanoparticles (IONPs), and their related properties for biomedical applications. Chapter-02 describes biomedical applications of IONPs with description of Magnetic Hyper Thermia (MHT). Chapter-03 details experimental methods used for synthesis of IONPs, surface functionalization of IONPs, and physicochemical characterization techniques. Chapter-04 gives an account of synthesis of IONPs via chemical coprecipitation method. The optimization of synthesis parameters to obtain Magnetite- Fe₃O₄ nanoparticles by varying molar concentration of Fe²⁺ and Fe³⁺ ions. This is followed by the physicochemical characterization of pristine Magnetite- Fe₃O₄ nanoparticles. Chapter-05 includes method of surface functionalization of Magnetite- Fe₃O₄ nanoparticles with Poly Ethylene Glycol (PEG). The Physicochemical characterization (XRD, TEM, FTIR, SEM, DLS, ζ - potential, VSM), MHT, and biomedical studies like biocompatibility, cytotoxicity/ cell viability, hemolysis, and drug delivery studies are also reported. Chapter-06 includes method of surface functionalization of Magnetite- Fe₃O₄ nanoparticles with Glutathione (GSH). The

Physicochemical characterization (XRD, TEM, FTIR, SEM, DLS, ζ - potential, VSM), MHT, and biomedical studies like biocompatibility, cytotoxicity/ cell viability, hemolysis, and drug delivery studies are also reported. **Chapter-07** summarizes the present research works flow chart and conclusions while **Chapter-08** gives future scope for the present work and 80 recommendations.

7.2 Conclusions:

- IONPs of appropriate sizes were successfully synthesized by chemical coprecipitation method.
- Variation in the molar concentration of Fe²⁺ and Fe³⁺ ions affects the phase formation
 (Hematite and Magnetite) and shows different values of magnetic parameters.
- Magnetite- Fe₃O₄ nanoparticles obtained with molar ratio of Fe²⁺: Fe³⁺::1:2 show superparamagnetic behavior with the highest saturation magnetization value (Ms), and Lowest Intrinsic Loss Power (ILP), and these IONPs are used for biomedical application.
- Magnetite- Fe₃O₄ nanoparticles show suitable Magnetic Hyper Thermia (MHT) (42-45 °C) for concentrations of 2 mg mL⁻¹ and 3 mg mL⁻¹ under external Alternating magnetic Field (AMF) of 20 kA m⁻¹ and 26.7 kA m⁻¹.
- Magnetite- Fe₃O₄ nanoparticles were successfully functionalized with Poly Ethylene Glycol (PEG) and Glutathione (GSH). Their physicochemical and magnetic properties are found suitable for biomedical applications like MHT, biocompatibility, cytotoxicity/cell viability, and drug delivery.
- The maximum drug release in minimum time is achieved for GSH coated Magnetite-Fe₃O₄ nanoparticles in acidic conditions (pH<6.8) compared to PEG coated and pristine Magnetite-Fe₃O₄ nanoparticles.
- Cell toxicity and cell viability study of PEG coated and GSH coated Magnetite- Fe₃O₄ nanoparticles for L929 fibroblast cell line and MDA MB 231 breast cancer cell line shows average cell viability of 95% for fibroblast cell line and cytotoxicity of 85% for breast cancer cells using MTT assay.
- Thus, the goal of the viable synthesis method, optimization of synthesis parameters, physicochemical and biological characterization of IONPs reveals compatible results for PEG coated and GSH coated Magnetite-Fe₃O₄ nanoparticles.

CHAPTER-08 RECOMMENDATIONS

8.1 Recommendations

- In-vitro study of Pristine, Poly Ethylene Glycol (PEG) coated, and Glutathione (GSH) coated Magnetite- Fe₃O₄ nanoparticles for Magnetic Hyper Thermia (MHT) and drug carrier for chemotherapy was carried out. The same work can be extended for in vivo studies on animals.
- The extension of MHT study of Magnetite- Fe₃O₄ nanoparticles for clinical trials.
- The work of GSH coated Magnetite- Fe₃O₄ nanoparticles for biomedical applications (MHT) is reported first time and further study is recommended.
- The synergistic effect of MHT and chemotherapy might be efficacious for future research.



D. Y. Patil Education Society (Deemed to be University), Kolhapur. Re-accredited by NAAC with 'A+' Grade CGPA 3.48

Dr. Rakesh Kumar Sharma

MD, FMASG, MAMS Dean & Professor

Member, Governing Body Indian Council of Medical Research (ICMR), New Delhi

Dr. D. Y. Patil

Padmashree Awardee Founder President

Dr. Sanjay D. Patil Chancellor

President, DYP Group

Date: 01/01/2025

Ref No: DYPMCK/ IEC. 141/2025

INSTITUTIONAL ETHICS COMMITTEE, D. Y. PATIL MEDICAL COLLEGE, KOLHAPUR.

This is to certify that the research project titled,

"Glutathione-Responsive Superparamagnetic Iron Oxide (Fe304) Nanoparticles For The Magnetic Hyperthermia And Chemotherapy."

Submitted by

: Miss. Nadiya Niyazahmad Patel

Name of Guide

: Prof. R. S. Patil

Name of the Department

: Physics (Ph.D.)

Has been studied by the Institutional Ethics Committee (IEC) at its meeting held on 17th Dec 2024 and granted approval for the study with due effect with the following caveats:

- 1. If you desire any change in the protocol or standard recording document at any time, please submit the same to the IEC for information and approval before the change is implemented.
- 2. As per recommendations of ICMR, you must register your study with the Central Trials Registry- India (CTRI), hosted at the ICMR's National Institute of Medical Statistics (http://icmr-nims.nic.in). The registration details as provided by the website are to be submitted to the Institutional Ethics Committee within a period of 3 months from issue of this letter.
- 3. All serious and/or unexpected adverse events due to the drug/procedures tested in the study must be informed to the IEC within 24 hours and steps for appropriate treatment must be immediately instituted.
- 4. In case of injury/disability/death of any participant attributable to the drug/procedure under study, all compensation is to be made by the sponsor of the study.
- 5. The Chief investigator/Researcher must inform the IEC immediately if the study is terminated earlier than planned with the reasons for the same.
- 6. The final results of the study must be communicated to the IEC within 3 months of the completion of data
- 7. The researcher must take all precautions to safeguard the rights, safety, dignity and wellbeing of the participants in the study. Approved consent form is to be used modifications may be done with IEC permission approval.
- 8. The researcher must be up to date about all information regarding the risk/benefit ratio of any drug/procedure being used and any new information must be conveyed to the IEC immediately. The IEC reserves the right to change a decision on the project in the light of any new knowledge.
- 9. Before publishing the results of the study, the researcher must take permission from the Dean of the Institution.
- 10. Annual progress report should be submitted for all sponsored projects to the committee.
- 11. Unethical conduct of research in non-sponsored projects will result in withdrawal of the ethics approval and negation of all data collected till that date.

Ør. Mrs. Shimpa R. Sharma

(Member Secretary, IFC)

Little Committee

Jress: 869, 'E' Ward, D. Y. Patil Vidyanagar, Kasaba Bawada, Kolhapur - 416 006 (MS) India I Phone no.: (0231) 2601235-36

2601238 | Email: aypatilmedicalcollege@gmail.com | Website: www.dypatilmedicalkop.org

ECR/738/Inst/MH/2015/RR-21)

PATIENT CONSENT FORM

Center for Interdisciplinary Research, D Y Patil Education society (Deemed to be University), Kolhapur

I Miss. Nadiya Niyazahmad Patel, Ph.D. student working under the guidance of Prof. Raghunath S. Patil, Professor, Center for Interdisciplinary Research, has prepared the following consent form to be filled by patient, at the time of sample collection needed for my research work entitled "GLUTATHIONE-RESPONSIVE SUPERPARAMAGNETIC IRON OXIDE (Fe₃O₄) NANOPARTICLES FOR THE MAGNETIC HYPERTHERMIA AND CHEMOTHERAPY."

I, Mr/Mrs/Ms	Gender	Age:
Residing at		
D : 1 : 1 :		

Do hereby confirm that:

- (i) I have been asked by the Ph.D. student whether I wish to participate in a study under the aegis of Center for Interdisciplinary Research, D Y Patil Education Society (Deemed to be University).
- (ii) The nature of the study being undertaken by the student as well as the extent of my participation in it, have been duly explained to me in a language that I understand.
- (iii) The potential risks and consequences associated with this study have also been duly explained to me in a language that I understand.
- (iv) I also understand that my participation in this study is only for the benefit of advancement in the field of research and that at no point in time is my participation being solicited for any pecuniary gain by the student.
- (v) I have also been explained that I am in no way obliged to participate in the study and that, once I have agreed to participate in the study, I am still free to withdraw from participation in the study at any point in time upon notifying the Ph.D. student in writing in the prescribed form without assigning any reason.
- (vi)There will be no financial transaction between myself and Ph.D. student for my participation in that study;
- (vii) I have been explained that any data collected out of my participation in the study will only be used for research work.
- (viii) I have also been reassured that any publication of the data collected during the course of the study or any publication of its conclusions, shall be done on a 'no names' basis and shall under no circumstances reveal my personal identity. Any personal details likely to reveal my personal identity shall at all times remain confidential;
- (ix) The contents and effect of this consent form have also been duly explained to me in a language that I understand.

PATIENT CONSENT FORM

Center for Interdisciplinary Research, D Y Patil Education society (Deemed to be University), Kolhapur

By affixing my signature/thumb print hereto, I am therefore freely and voluntarily signifying my consent, intent and willingness to participate in the study of the student researcher for the purposes of the research work. I also certify that my right to privacy has not been infringed in any manner.

[SIGNATURE/THUMB PRINT OF PARTICIPANT] DATE:	
WITNESSED BY:	
(1) NAME:	
TITLE/CAPACITY:	
SIGNATURE:	
(2) NAME:	
TITLE/CAPACITY:	
SIGNATURE:	

PUBLICATIONS

ORIGINAL ARTICLE



Anticancer activity of surface functionalized magnetite (Fe₃O₄₎ nanoparticles—effect of polymer coating

Nadiya N. Patel¹ · Najiya R. Mulla¹ · Vishwajeet M. Khot¹ · Raghunath S. Patil¹

Received: 6 October 2023 / Accepted: 11 December 2023 © Qatar University and Springer Nature Switzerland AG 2023

Abstract

The two-step chemical coprecipitation method has been used to synthesize polyethylene glycol (PEG)-coated magnetite (Fe_3O_4) nanoparticles by varying the composition of Fe_3O_4 :PEG, with PEG as a stabilizer, dispersant, and to make Fe_3O_4 nanoparticles biocompatible. The inverse cubic spinel structure of Fe₃O₄ nanoparticles with 7.9 ± 0.1 and 6.9 ± 0.1 nm crystallite size was obtained for uncoated and PEG-coated nanoparticles respectively. The scanning electron microscopy (SEM) analysis revealed the Fe₃O₄ nanoparticles with quasi-spherical morphology and a decrease in aggregation with the addition of PEG. Fourier transform infrared spectroscopy (FTIR) results demonstrated that PEG is associated with Fe₃O₄ nanoparticles via carbonyl groups. The vibrating sample magnetometer (VSM) results showed that Fe_3O_4 and PEG-coated Fe_3O_4 nanoparticles both have superparamagnetic behavior with saturation magnetization (Ms) values of 50.3 and 36.5 emu g⁻¹ respectively at ambient temperature. Ms value decreases with an increase in PEG concentration, due to the addition of an extra non-magnetic polymer layer on the surface of Fe₃O₄ nanoparticles. The biotoxicity was tested against the MDA-MB-231 breast cancer cell line via MTT assay, showing a significant decrease in cell viability after PEG coating. Induction heating studies show the therapeutic temperature (42–45°C) reaches in the first 100 s once the alternating current (AC) magnetic field is applied to magnetic nanoparticle suspension. The calculated SAR value for Fe_3O_4 and PEG-coated Fe_3O_4 nanoparticles is in the range of 50-80 W g⁻¹. The overall assessment indicates that PEG functionalization has been successfully optimized for its application in magnetic hyperthermia therapy.

Keywords Antiproliferative activity · Coprecipitation · Cytotoxicity assay · MDA-MB-231 breast cancer cell lines · Magnetic hyperthermia · Magnetite · Polyethylene glycol · Superparamagnetic

- •Optimization of PEG on the surface of Fe₃O₄ nanoparticles is achieved by chemical coprecipitation.
- •The size and magnetization of the crystallites decreased as the concentration of PEG increased.
- •Optimized PEG concentration of 0.25-1.5 g coated on Fe₃O₄ nanoparticles exhibits inductive heating properties under the application of a physiological safe range of external alternating current magnetic field. (Temperature rises from 27 to 46 °C in 100 s.) PEG-coated Fe₃O₄ nanoparticles show promising results against anticancer activity and can be used for magnetic hyperthermia application to treat cancer.
- Raghunath S. Patil rsp17658@gmail.com

Published online: 20 December 2023

Centre for Interdisciplinary Research, D. Y. Patil Education Society (Deemed to be University), Kolhapur 416 006, India

1 Introduction

In 1990, the new interdisciplinary term "nanomedicine" was introduced in the medical field. It was described as the application of nanoscopic or fine-structured materials in medicine that have distinctive biological effects due to their fascinating properties [1]. Different nanomaterials have been put forward for theranostic applications in nanomedicine. For example, iron oxide nanoparticles (IONPs) are contemplated as incredibly covenanting physicochemical features that are beneficial for many biomedical applications such as magnetic resonance imaging (MRI) [2], drug delivery, cell tracking, magnetic hyperthermia (MHT) [3], and biosensors and cell labeling [4]. Among different forms of iron oxide (goethite, wustite, magnetite (Fe_3O_4), maghemite (γ - Fe_2O_3), and hematite (α -Fe₂O₃)), the main attention has been placed on Fe₃O₄ nanoparticles due to less toxicity, high level of biocompatibility, injectability, chemical stability, and high





ORIGINAL PAPER



Biological activities of iron oxide-based magnetic nanoparticles

Nadiya N. Patel¹ · Vishwajeet M. Khot¹ · Raghunath S. Patil¹

Received: 6 December 2023 / Accepted: 5 February 2024 © The Author(s), under exclusive licence to the Institute of Chemistry, Slovak Academy of Sciences 2024

Abstract

The anticancer and antibacterial potential of magnetite (Fe₃O₄) nanoparticles have been investigated using different biological assays. Also, an induction heating study was performed to check the magnetic hyperthermia application of synthesized Fe₃O₄ nanoparticles. An antimicrobial study was performed against gram-positive and gram-negative bacterial strains. Among them, the Staphylococcus aureus bacterial strain showed maximum antimicrobial activity with a 15 mm zone of inhibition for 500 μg/mL of Fe₃O₄ nanoparticles. The antioxidant activity was ascertained through a DPPH (1, 1-diphenyl-2, picrylhydrazyl) assay. Fe₃O₄ nanoparticles showed 30.57% free radical scavenging activity due to its antioxidative nature. The anticancer potential of Fe₃O₄ nanoparticles was evaluated against the breast cancer (MDA-MB-231) cell lines and fibroblast (L929) cell line using 3-(4, 5-dimethythiazol-2-yl)-2, 5-diphenyl tetrazolium bromide (MTT) cytotoxicity assay. Fe₃O₄ nanoparticles proved to be toxic to the MDA-MB-231 cell line even at a concentration of 3.125 µg mL⁻¹, and an increase in cytotoxicity to 89% from 20% was observed with the rise in Fe₃O₄ nanoparticles concentration to 100 μg mL⁻¹. The observed cytotoxicity for the L929 cell line is low revealing the biocompatible nature of synthesized Fe₃O₄ nanoparticles. Also, the biocompatibility for invitro application was examined using angiogenesis activity which does not show any antiangiogenics activity of synthesized Fe₃O₄ nanoparticles. Additionally, the inductive heating characteristic of Fe₃O₄ nanoparticles in an alternating current (AC) magnetic field was examined at a frequency of 278 kHz, and for the different magnetic fields of 13.3, 20.0, and 26.7 kA m⁻¹ for 600 s with different suspension concentrations of Fe₃O₄ nanoparticles as 0.5, 1.0, 2.0, 3.0, and 5.0 mg mL⁻¹. The highest rise in temperature of 60.63 °C was observed for 5 mg mL⁻¹ at a magnetic field of 26.7 kA m⁻¹ with a specific absorption rate (SAR) value of 85 Wg⁻¹ which makes them suitable for hyperthermia application. The study shows promising antimicrobial, antioxidative, anticancer, and induction heating properties. Herein, the present study reveals the potential of Fe_3O_4 nanoparticles for improved therapeutic applications and effective bactericidal propensity.

Published online: 06 March 2024



 [∀] Vishwajeet M. Khot wish.khot@gmail.com

Raghunath S. Patil rsp17658@gmail.com

Centre for Interdisciplinary Research, D. Y. Patil Education Society (Deemed to be University), Kolhapur 416006, India



www.chemistryselect.org

Optimization of Magnetite Nanoparticles for Magnetic Hyperthermia: Correlation with Physicochemical Properties and Cation Distribution

Nadiya N. Patel, [a] Vishwajeet M. Khot, *[a] and Raghunath S. Patil *[a]

The present study reveals the synthesis of Iron oxide nanoparticles (IONPs) by varying the molar ratio of ferric (Fe³+) to ferrous (Fe²+) ions via chemical coprecipitation method for the study of cationic distribution of Fe-ions and its potential application for magnetic hyperthermia therapy (MHT). X-ray diffraction (XRD), scanning electron microscopy (SEM), transmission electron microscopy (TEM), Fourier transform infrared spectroscopy (FTIR), and X-ray photoelectron spectroscopy (XPS), were used to characterize the physicochemical properties. Several structural parameters were estimated using the Rietveld refinement, resulting in structural modelling verified by magnetic characteristics. A vibrating sample magnetometer (VSM) assessed the magnetic hysteresis loop at room temperature in a field range of $\pm 15~\rm kOe$,

revealing superparamagnetic behavior for the ratio Fe^{2+}/Fe^{3+} 1:2. The saturation magnetization (Ms) of IONPs increased with the increasing Fe^{2+} concentration and attained a maximum value of 60.21 emu g^{-1} at a molar ratio of 2:1. The potential of the inductive heating capability of IONPs in an alternating current magnetic field (AMF) was studied to treat localized MHT. The changes in magnetic properties and inductive heating properties of IONPs are associated with the cationic distribution of Fe^{2+} at the tetrahedral (A) and octahedral (B) sites of crystal structure. The variation in cationic properties at the A and B sites may result in varying/tuneable magnetic properties, affecting the overall heating profiles of hyperthermia.

1. Introduction

Particles display unique optical, magnetic, or electrical characteristics when they go smaller than microns, particularly for nanoparticles (1-100 nm) which are quite different from those of fine particles or bulk materials.^[1] Nanocrystalline spinel ferrites have undergone extensive research owing to their potential applications in microwave absorbers, high-density recording systems, chemical sensors, imaging, permanent magnets, high-frequency devices, ferrofluid technology, and biomedical applications.^[2] In spinel ferrite complexes Oxygen atoms are packed closely together, exhibiting tetrahedral and octahedral sublattices. In the compound structure, M^{2+} (M = Fe, Co, Mg, Ni, etc.) and Fe³⁺ are organized at two different crystallographic sites with tetrahedral (A) and octahedral (B) oxygen coordination. Normal spinel is the structure that results when 16 B sites are filled by Fe^{3+} and M^{2+} cations fill 8 A-sites. In the inverse spinel structure, M²⁺ ions exclusively occupy the B-site whereas Fe³⁺ ions are randomly occupied at both A and B sites. Because M²⁺ and Fe³⁺ cations are present at both A-and B-sites and cation distribution is mixed, most spinel has a mixed (partially inverse) structure. The degree of inversion is characterized by an inversion parameter.^[3] Due to their possible use as ferrofluids, magnetic ferrite nanoparticles with inverted spinel structures have garnered much interest. Hydrophilic ferrofluids are mostly employed in medical applications, such as the treatment and detection of medical problems, whereas hydrophobic fluids with scattered magnetic nanoparticles (MNPs) are used as rotating shaft seals and loudspeakers.^[4] Ferrite nanoparticles exhibit spin canting, a metastable cation distribution, a core/shell structure, and superparamagnetic at the nanoscale. These phenomena are contingent upon several variables, including anisotropy, surface morphology, composition, grain size, and interparticle interactions. The electrical and magnetic properties of ferrites can be affected by the distribution of cations between tetrahedral and octahedral sites. The distribution can be regulated by the synthesis method.^[5]

Nanoparticles (NPs) play a crucial role in cancer research due to their versatility in diagnostic and therapeutic applications. Magnetic hyperthermia (MHT) uses MNP-mediated temperature increases in the therapeutic range of 42–46 °C under an alternating magnetic field (AMF) to destroy cancer cells. Specifically, superparamagnetic iron oxide (SPIONs) is in use to introduce into tumour for converting electromagnetic energy into heat under the influence of an AMF. The U.S. Food and Drug Administration (FDA) has started clinical studies to treat pancreatic cancer and prostate cancer using this approach. In MHT an important factor is the thermal performance of injected MNPs. The temperature rise caused by MNPs has direct thermal effects that favor cell death, it can also be used to advance other AMF-triggered treatment techniques (such as chemotherapy). MNPs can be used with other therapies to alter cell metabolic pathways, creating

Centre for Interdisciplinary Research, D. Y. Patil Education Society, (Deemed to be University), Kolhapur 416 0063, India

E-mail: wishkhot@gmail.com rsp17658@gmail.com

Supporting information for this article is available on the WWW under https://doi.org/10.1002/10.1002/slct.202403034

[[]a] N. N. Patel, V. M. Khot, R. S. Patil

\$ SUPER

Contents lists available at ScienceDirect

Journal of Alloys and Compounds

journal homepage: www.elsevier.com/locate/jalcom



Morphologically tuned MnO₂ thin film electrodes prepared by growth kinetic dependent SILAR approach for high-performance extrinsic pseudocapacitors

Najiya R. Mulla, Nadiya N. Patel, Shraddha B. Bhosale, Umakant M. Patil **, Raghunath S. Patil *

Centre for Interdisciplinary Research, D. Y. Patil Education Society, Kasaba Bawada, Kolhapur 416006, India

ARTICLE INFO

Keywords: Morphology tunning Marigold-like micro flower δ -MnO₂ thin film Extrinsic Pseudocapacitors

ABSTRACT

Rationally designed electrode materials that are morphologically tuned to attain large surface area can significantly possess the extrinsic pseudocapacitive charge-storing ability. Therefore, the current work approach focuses on synthesizing binder-free MnO₂ thin film electrodes with tuned morphology by the SILAR method through alteration in growth kinetics. The growth kinetics of SILAR are controlled by altering the precursor concentrations ratio among metal precursor (MnCl₂) and oxidizing agent (KMnO₄). The structural analysis confirmed the preparation of the δ -MnO₂ phase of manganese oxide. Moreover, alteration in growth kinetics resulted in a change in surface morphology with reduced nanowire size of marigold-like δ -MnO₂ microflowers. The MO-3 thin film electrode prepared at an optimum KMnO₄ and MnCl₂ precursor concentration ratio of 2:1 provides the maximum extrinsic pseudocapacitive conduct with the maximum specific capacitance of 774.5 F g $^{-1}$. Furthermore, the aqueous symmetric supercapacitor device exhibits the highest specific capacitance of 106 F g $^{-1}$ with a specific energy of 14.8 Wh kg $^{-1}$ at a high specific power of 1792 W kg $^{-1}$ and exhibits 83.2 % capacitive retention over 10,000 cycles. Furthermore, the symmetric aqueous device (MO-3//Na₂SO₄//MO-3) lights 5 red LEDs, demonstrating its commercial viability for energy storage systems. This research facilitated the scalable synthesis of binder-free δ -MnO₂ fine film electrodes with a desired morphology by facile SILAR method, ensuring their practical applicability in symmetric extrinsic pseudocapacitor devices.

1. Introduction

New and emerging renewable (non-conventional) energy sources are gaining popularity, such as wave, wind, geothermal, and solar energy, are being developed to replace fossil fuels and address environmental issues [1]. So, researchers are developing practical, long-term, and cost-effective energy storage technology that is environmentally conscious in response to the disruption and decreased continuity of non-conventional energy generation. Thus, electrochemical energy storage systems (ESSs), including batteries, supercapacitors, and fuel cells are highly desirable to stock created energy through non-conventional sources [2]. Supercapacitors are promising ESSs among the available energy storage devices (ESDs) since they have the ability to work in a well-organized and competent way with long cycle life performance, high specific energy (SE), high specific power (SP),

and low-cost, safe devices (non-flammable) energy storage [3].

Until now, various electrode materials, including phosphates, oxides, and sulfides, metal hydroxides, have been evaluated for use in pseudocapacitors [4] Generally, as per charge storage mechanisms, the maximum commonly exploited pseudocapacitive materials are regarded as extrinsic, intercalation, and intrinsic (renovated battery-type) pseudocapacitive [5]. Extrinsic pseudocapacitive materials are those with reduced particle size or crystallinity that can increase pseudocapacitive activity. However, excluding exceptional SP, extrinsic pseudocapacitive materials undergo low SE and poor stability. In insertion improving charge storage capacity of pseudocapacitors, the widely anticipated tactic to increase the storage capacity of electrodes by regulating the physical (i.e. crystallinity, conductivity, and hydrous nature) and morphological (i.e. surface area, porosity, and particle size) features of the storing materials [6]. Hence, developing gainful energy-storing

E-mail addresses: umakant.physics84@gmail.com (U.M. Patil), rsp17658@gmail.com (R.S. Patil).

 $^{^{\}ast}$ Corresponding author.

^{**} Co-corrosponding author.

CERTIFICATIES





This certificate is presented to

Ms. Nadiya Niyazahmed Patel

For his/her active participation in the 9-days Research Methodology Workshop

Organised by

Internal Quality Assurance Cell & Research Guidance Cell From 21st February to 5th March 2022.

Prof. Dr. Shimpa Sharma
Pro-VC & IQAC Coordinator

Prof. Dr. R. K. Sharma Dean, D.Y. Patil Medical College

Behasma

8

Prof. Dr. C. D. Lokhande Research Director & Dean, CIR



D. Y. PATIL EDUCATION SOCIETY,

(Institution Deemed to be University) Kolhapur Accredited NAAC with 'A' Grade

DNYANSHODH -2022

(Search For Knowledge)
On the occasion of National Science Day

Certificate

This is to certify that

WIMS. NADIYA NIYAZAHMAD PATEL

organized by Centre for Interdisciplinary Research (CIR), D. Y. Patil Education Society has presented a Poster on 28th February 2022, in Dnyanshodh -2022,

(Deemed to be University), Kolhapur - 416006.

Chairman
Prof. (Dr.) C. D. Lokhande
Dean.

Centre for Interdisciplinary Research

Dr. Arpita Pandey -TiwariAssociate Professor,
Department of Medical Biotechnology







SHIVAJI UNIVERSITY, KOLHPUR



of CIR, D.Y. Patil

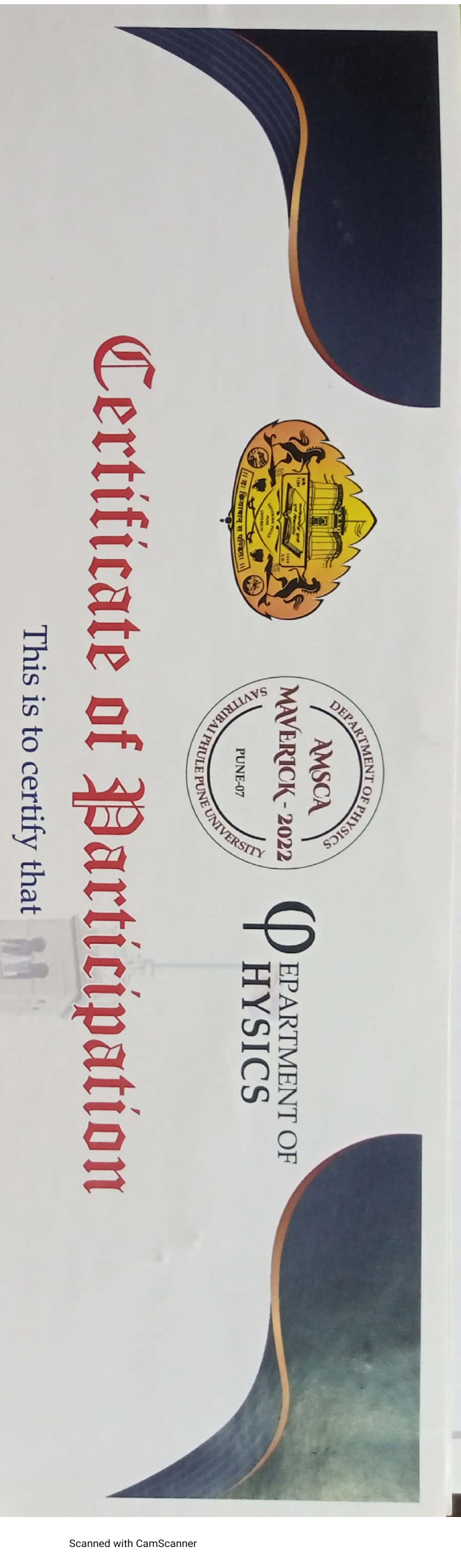
This is to certify that Ppfs/ph./ph./ms. Nadiya Niyazahmad Patel of CIR., D.Y. Pate to be University),

Education Society (Institution Deemed has worked as resource person/ participated/ worked as local Kolhapur.

Organizing committee member in the "Structural & Morphological Characterization using Sophisticated Instruments" under the Centre, Shivaji University, Kolhapur. His/Her contribution to the STUTI training program is highly appreciated of Science and Technology (DST), Ministry of Science & Technology, New Delhi from 12th to 18th September, 2022 held at SAIF-DST-CFC scheme Synergistic Training Program Utilizing the Scientific and Technological Infrastructure (STUTI) supported by Department







N. N. Patel

Synthesis, Characterization and Applications (AMSCA Maverick-2022) With Special Topic: New Education Policy held at the Department of Physics, Savitribai Phule Pune University, Pune-07, Maharashtra, India during Method from the Nanomaterials Theme made in the International Conference on Advanced Materials Participated and presented the Poster paper entitled Synthesis and Characterization of----- by Solvothermal D. Y. Patil Education Society, Institution Deemed to be University, Kolhapur

Convener

18th - 20th October, 2022.

(AMSCA Maverick-2022)

o-Convener

(AMSCA Maverick-2022)

(AMSCA Maverick-2022) Chairperson 0 कि मार्टिया



D. Y. PATIL EDUCATION SOCIETY,

Accredited NAAC with 'A' Grade (Deemed to be University) Kolhapur

DNYANSHODH-2023

(Search For Knowledge)

titicate

This is to certify that

Mr/Ms. Nadiya Niyazahmed Patel.

has presented a Poster on 9th March 2023, in Dnyanshodh -2023,

organized by Centre for Interdisciplinary Research (CIR), D. Y. Patil Education Society (Deemed to be University), Kolhapur - 416006.

Centre for Interdisciplinary Research Chairman
Prof. (Dr.) C. D. Lokhande
Dean,

Department of Medical Biotechnology. Dr. Arpita Pandey -Tiwari Associate Professor, Convener





"Education through self-help is our motto." - Karmaveer

Rayat Shikshan Sanstha's

RAJARSHI CHHATRAPATI SHAHU COLLEGE, KOLHAPUR

(Reaccredited 3rd Cycle by NAAC at 'A' Grade with CGPA 3.07)





Organizes Under G20 University Connect Program

One Day International Conference on



"Recent Trends in Fabrication of Nanomaterials and Their Applications (ICRTFNA-2023) "



This is to certify that, Dr. / Prof. / Mr. / Ms. / Mrs. Nadiya N. Patel

has participated / worked as Researce

Person/Chairperson/Organizing committee member in One Day International Conference on 'Recent Trends in Fabrication of Nanomaterials and Their Applications (ICRTFNA-2023) 'Organized by Department of Physics D. Y. P. kolhapur

and IQAC held on March 15, 2023. He/She has presented paper entitled Inductive heating of Magnetite Fezou nanoparticle for localized magnetic Hyperthermia

Coordinator

Organizing secretary

Principal

(ist prize-poster presentat

International Conference

"Advanced Materials Synthesis, Characterization and Applications - 2023"

ma Old ma

(AMSCA - 2023)

 $\phi_{\text{HYSICS}}^{\text{epartment of}}$

CERTIFICATE OF PARTICIPATION

This is to certify that,

Miss. Nadiya Patel, D. Y. Patil Education Society, Kolhapur has presented Poster on the topic The influence of the [Fe²⁺] /[Fe³⁺] molar ratio on the properties of superparamagnetic iron oxide nanoparticles (SPIONs) and Magnetic Hyperthermia study in the International Conference on AMSCA - 2023 held at the Department of Physics, Savitribai Phule Pune University, Pune, Maharashtra, INDIA during 21st to 24th November, 2023.

Convener AMSCA - 2023

Co-Convener AMSCA - 2023 Head Department of Physics, SPPU, Pune



D. Y. PATIL EDUCATION SOCIETY

NAAC 'A" Grade in 3rd Cycle

(Deemed to be University), KOLHAPUR

Certificate

Nanotechnology Addressing the Convergence of Materials Science, Biotechnology and Medical Science (IC-NACMBMdelivered invited talk/ chaired the session/ presented oral/ presented poster/ participated in the International Conference on Maharashtra, India during 12th to 14th February 2024. His/Hercontribution to the conference is highly appreciated 2024) held at the Centre for Interdisciplinary Research, D. Y. Patil Education Society (Deemed to be University), Kolhapur, This is to certify that Mr. /Ms. Patel Nadiya Niyaz Ahmad of Centre for Interdisciplinary Research, DYPES, Kolhapur has

Dr. Jayavant L. Gunjakar

Convener

Prof. Meghnad G. Joshi

Convener

Prof. Chandrakant D. Lokhande

Chairman



PM-USHA Sponsored **National Workshop**







Density Functional Theory for Material Scientists 2024 (NWDFTMS-2024)

September 23-24, 2024 Organized by

Department of Physics

(UGC-DRS-I & II, ASIST, DSA- I & II, DST FIST-I & II, PURSE)

Shivaji University, Kolhapur-416004, (M.S.), India

Certificate

This is to certify that Ms. Nadiya NiyazAhmad Patel of CIR, D. Y. Patil Education Society, Kolhapur has participated in the National Workshop on Density Functional Theory for Material Scientists 2024 (NWDFTMS-2024) held at Department of Physics, Shivaji University, Kolhapur-416004, (M.S.), India during September 23-24, 2024. His/her contribution to the workshop is highly appreciated.

> Convener NWDFTMS-2024

Chairman NWDFTMS-2024